N7728430

www.NTIS.gov
One Source. One Search. One Solution.

EFFECT OF TRANSIENT LIQUID FLOW ON RETENTION CHARACTERISTICS OF SCREEN ACQUISITION SYSTEMS

MCDONNELL-DOUGLAS ASTRONAUTICS CO.,
HUNTINGTON BEACH, CALIF

APR 1977

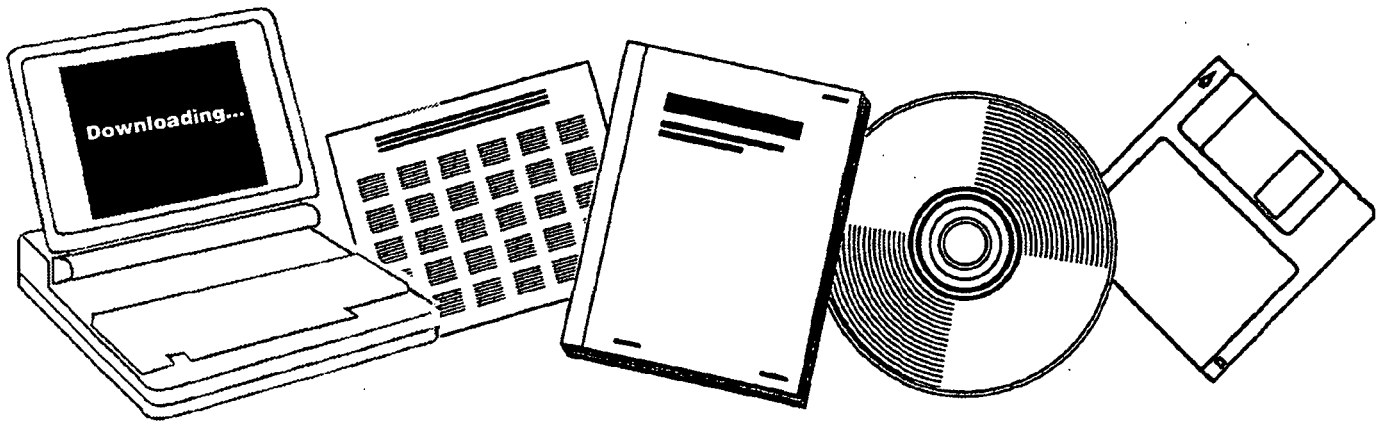

U.S. Department of Commerce
National Technical Information Service

Tailored to Your Needs!

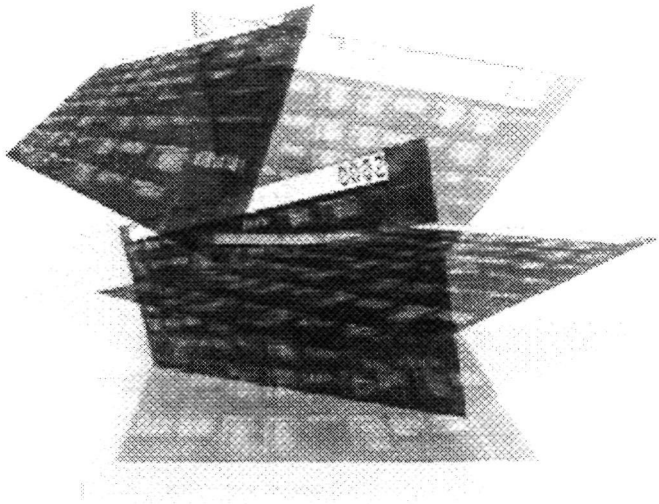

Selected Research In Microfiche

SRIM® is a tailored information service that delivers complete microfiche copies of government publications based on your needs, automatically, within a few weeks of announcement by NTIS.

SRIM® Saves You Time, Money, and Space!

Automatically, every two weeks, your SRIM® profile is run against all *new* publications received by NTIS and the publications microfiched for your order. Instead of paying approximately $15-30 for each publication, you pay only $2.50 for the microfiche version. Corporate and special libraries love the space-saving convenience of microfiche.

NTIS offers two options for SRIM® selection criteria:

Standard SRIM®–Choose from among 350 pre-chosen subject topics.

Custom SRIM®–For a one-time additional fee, an NTIS analyst can help you develop a keyword strategy to design your Custom SRIM® requirements. Custom SRIM® allows your SRIM® selection to be based upon *specific subject keywords*, not just broad subject topics. Call an NTIS subject specialist at (703) 605-6655 to help you create a profile that will retrieve only those technical reports of interest to you.

SRIM® requires an NTIS Deposit Account. The NTIS employee you speak to will help you set up this account if you don't already have one.

For additional information, call the NTIS Subscriptions Department at 1-800-363-2068 or (703) 605-6060. Or visit the NTIS Web site at *http://www.ntis.gov* and select SRIM® from the pull-down menu.

U.S. DEPARTMENT OF COMMERCE
Technology Administration
National Technical Information Service
Springfield, VA 22161 (703) 605-6000
http://www.ntis.gov

NASA CR-135218
MDC G6742

NATIONAL AERONAUTICS AND SPACE ADMINISTRATION

EFFECT OF TRANSIENT LIQUID FLOW ON RETENTION CHARACTERISTICS OF SCREEN ACQUISITION SYSTEMS

FINAL REPORT

April 1977

(NASA-CR-135218) EFFECT OF TRANSIENT LIQUID FLOW ON RETENTION CHARACTERISTICS OF SCREEN ACQUISITION SYSTEMS Final Report, Jun. 1975 - Mar. 1977 (McDonnell-Douglas Astronautics Co.) 206 p HC A01/MF A01 CSCL 20D G3/34

N77-28430

Unclas
39226

by E. C. Cady

MCDONNELL DOUGLAS ASTRONAUTICS COMPANY
5301 BOLSA AVENUE
HUNTINGTON BEACH, CALIFORNIA 92647

AUG 1977
RECEIVED
NASA STI FACILITY
INPUT BRANCH

prepared for

NATIONAL AERONAUTICS AND SPACE ADMINISTRATION
Lewis Research Center
21000 Brookpark Road
Cleveland, Ohio 44135

Contract NAS3-19719

1. Report No.	2. Government Accession No.	3. Recipient's Catalog No.
NASA CR-135218		

4. Title and Subtitle	5. Report Date
Effect of Transient Liquid Flow on Retention Characteristics of Screen Acquisition Systems	April 1977
	6. Performing Organization Code

7. Author(s)	8. Performing Organization Report No.
E. C. Cady	MDC G6742
	10. Work Unit No.

9. Performing Organization Name and Address	11. Contract or Grant No.
McDonnell Douglas Astronautics Company 5301 Bolsa Avenue Huntington Beach, California 92647	NAS 3-19719
	13. Type of Report and Period Covered

12. Sponsoring Agency Name and Address	13. Type of Report and Period Covered
NASA Lewis Research Center, Cleveland, Ohio	Final Report June 1975 to March 1977
	14. Sponsoring Agency Code

15. Supplementary Notes

Project Manager, John C. Aydelott, NASA Lewis Research Center, Cleveland, Ohio

16. Abstract

A comprehensive analytical and experimental program was performed to develop a design analysis, based on experimental data, to predict the effects of transient flow and pressure surges (caused either by valve or pump operation, or by boiling of liquids in warm lines) on the retention performance of screen acquisition systems. A survey of screen liquid acquisition system applications was performed to determine appropriate system environment and classification. A screen model was developed which assumed that the screen device was a uniformly distributed composite orthotropic structure, and which accounted for liquid inflow/outflow, gas ingestion quality, screen stress, and liquid spill. A series of 177 tests using 13 specimens (5 screen meshes, 4 screen device construction/backup methods, and 2 orientations) with three test fluids (isopropyl alcohol, Freon 114, and LH_2) provided data which verified important features of the screen model and resulted in a design tool which could accurately predict the transient startup performance of screen acquisition devices.

17. Key Words (Suggested by Author(s))	18. Distribution Statement
Transient effects Screen acquisition systems Cryogenic fluid surges Screen performance analysis	Unclassified-Unlimited

19. Security Classif. (of this report)	20. Security Classif. (of this page)	21. No. of Pages	22. Price*
Unclassified	Unclassified	206	

* For sale by the National Technical Information Service, Springfield, Virginia 22161

PREFACE

This report was prepared by McDonnell Douglas Astronautics Company under Contract NAS3-19719. The contract is administered by the National Aeronautics and Space Administration, Lewis Research Center, Cleveland, Ohio. The NASA Project Manager for the contract is Mr. John C. Aydelott. This final report describes technical efforts on the contract performed from June 1975 through March 1977.

Page
Intentionally
Left Blank

NOMENCLATURE

A	Area - m^2 (ft^2)
a, a'	Sound speed - m/sec (ft/sec)
CX	Water hammer constant in the direction of flow - m (ft)
CY	Water hammer constant moving against the flow - m (ft)
C_g	Gas sound speed - m/sec (ft/sec)
C_L	Liquid sound speed - m/sec (ft/sec)
C_1, C_2	Constant determined by pipe and screen restraining fixtures
D	Pipe diameter - m (in)
e	Pipe equivalent wall thickness - m (in)
E	Elastic modulus - N/m^2 (lbf/in^2)
f	Equivalent screen fraction
g	Gravitational acceleration - m/sec^2 (ft/sec^2)
g_c	9.8067 m/sec^2 (32.174 ft-lbm/lbf-sec^2)
H	Static pressure in equivalent feet of liquid - m (ft)
K	Liquid bulk modulus of elasticity - N/m^2 (lbf/in^2)
P	Pressure - N/m^2 (lbf/in^2)
Q	Volumetric rate - m^3/sec (ft^3/sec)
R	Pipe radius - m (in)
SX	Water hammer constant a/gA in direction of flow - sec/m^2 (sec/ft^2)
SY	Water hammer constant a/gA against flow - sec/m^2 (sec/ft^2)
t	Time - seconds
T	Temperature, °R or wave travel time - seconds
V	Velocity - m/sec (ft/sec)
X	Axial coordinate, gas volume fraction
γ	Ratio of specific heat
σ	Stress - N/m^2 (lbf/in^2)
μ	Poisson's ratio
ρ	Density - kg/m^3 (lbm/ft^3)

PRECEDING PAGE BLANK NOT FILMED

Subscripts

1	Axial direction
2	Circumferential direction
L	Liquid
P	Pipe
s	Screen
X	Traveling with the flow
Y	Traveling against the flow

CONTENTS

INTRODUCTION

As the nation progresses toward more routine space transportation operations, presently embodied by the development of the Space Shuttle, continuing technology improvement is required to increase payload and reduce in-orbit costs. As the Shuttle approaches the operational phase, renewed emphasis will be placed on improving the existing system by improving subsystems, such as using subcritical cryogen storage for life support and fuel cell reactant supplies to take advantage of significant weight savings and payload improvements. In addition, the Orbital Transfer Vehicle (OTV), as currently envisioned, requires orbital fueling, and plans for future manned orbiting stations include replenishment of fluid supplies. All of these systems have a common requirement: the ability to acquire and transfer subcritical fluids in low gravity.

Brute-force systems such as engine-accelerated fluid settling and transfer, and for some applications, supercritical fluid storage, can be used with attendant weight penalties. However, the potential of fine-mesh screen devices for low-gravity propellant acquisition and transfer is starting to be realized in some space vehicle systems, including the Shuttle orbital maneuvering system being developed by McDonnell Douglas Astronautics Company (MDAC).

These passive screen acquisition devices allow liquid flow while preventing gas flow through the screens by using the surface tension forces in the small pores of the screen. The bubble point (the pressure head of vapor which can be resisted by the screen) for even the finest-mesh screens is of the order of a few hundredths of an atmosphere. Consequently, the screen device must be designed for the worst expected combination of gravity head, dynamic head, and head losses due to friction. In addition, the device configuration and operating characteristics must be selected so the worst head combination imposed on the screen is below the bubble point by some defined safety factor. Further,

there are a variety of dynamic and transient effects which must be considered such as vibration, heat transfer, transient pressure surges at flow startup or shutdown caused by valve or pump operation, and surges from liquid boiling in warm feedlines.

In order to design screen devices which will operate reliably for both steady and dynamic operating conditions, realistic analyses, based on experimental data, are needed. Such analyses are available for steady operation of screen devices, accounting for real bubble point, flow losses, non-uniform flow, and heat-transfer effects (References 1-4). Analyses are in development for vibration effects (Reference 5) and through the program reported herein, for transient flow effects on screen retention devices.

The problem is the ability to analytically predict the effects on screen devices of pressure surges caused by the internal environment, configuration, and operating characteristics to ensure the successful operation of the unit. This requires an evaluation of current and potential screen system designs, and an understanding of the critical configurational and operational characteristics. A complete, versatile analysis of transient feed system dynamics is required which can predict pressure and flow transients anywhere within a specified feed system and can account for the interaction of components, screen device, and fluid. Further, and of considerable importance since the transient pressure surges may be several orders of magnitude above the screen device bubble point, the analysis must be able to define the pressure surge attenuation occurring in lines, fluid, junctions, attenuating components, and the screen device. A comprehensive experimental program is required which will verify the ability of the analysis to predict screen and feed system behavior, or define experimental factors required for successful system analysis.

Limited previous work attempted to define and understand this problem. Gluck, et al. (Reference 6) evaluated many of the fluid dynamic effects on screen devices of transient pressure surges from valve operation. However, this work did not consider the screen device application or potential environment, and did not evaluate the potential for complete device destabilization (failure). Further, the effects of pressure surges from liquid vaporization

in warm lines were not investigated. Although a complex and cumbersom compressible flow transient analysis was developed, the program was terminated before the experimental data could be used to verify the analysis and, therefore, produce a useful design tool. It was determined that significant gas ingestion at flow startup and liquid spillover at flow shutdown occurs. On the other hand, a limited program in which transient flow effects were studied (Reference 7) found no gas ingestion. However, to save cost, an existing screen device configuration was used in the latter program without evaluation or regard for how well the device simulated potential space acquisition systems. Also, pressure surges due to liquid vaporization were not evaluated. This work did not result in a comprehensive analytical tool, experimentally verified, which could be used for screen system design.

The objective of the program described herein is to develop a realistic design analysis, based on experimental data, to predict the effects of transient flow and pressure surges (caused either by valve or pump operation, or by boiling of liquids in warm lines) on screen device liquid retention performance. This will be accomplished by performing a survey of screen liquid acquisition system applications and determining the appropriate transient pressure and flow environment, analyzing the relations between transient flow effects and screen liquid retention characteristics, and experimentally verifying the analysis.

Page
Intentionally
Left Blank

ANALYTICAL PROGRAM

To ensure that the analysis to be developed would have the widest possible application and would reflect the design conditions for realistic systems, a comprehensive survey of current and potential space vehicle screen acquisition systems was performed. Following this, two existing MDAC computer codes, H672-Transient Effects Analysis, and P4557-Cryo-line Pressure Surge, were adapted to analyze the screen device effects. These codes were then used to simulate a representative surveyed system, and additional test cases run to determine the important parameters affecting screen device transient performance and aid in developing the experimental program plan.

SURVEY OF TRANSIENT EFFECTS

All current and potential space vehicle screen acquisition systems were surveyed and documented to determine, where available, data on systems involved, fluids, tankage, acquisition system and transfer line configuration, valve and pump operating characteristics, acceleration, vibration and thermal environment, and fluid quantity and mass flow requirements. A total of twelve systems were identified, and their salient characteristics are summarized in Table 1. Details on the configuration and characteristics of each system, where available, are contained in Appendix A.

The systems include currently developed devices, those in the preliminary stages of hardware development, and others which have been studied for potential applications, but which don't really exist in the form of hardware. The systems tabulated can be conveniently divided into two broad categories:

A. Small, localized screen devices used for engine restart. These devices (e.g., start baskets, start tanks, traps, etc.) are characterized by (1) having relatively large flow rates for a short period, and (2) experiencing relatively large g-levels (during which the device may fail, then refill).

PRECEDING PAGE BLANK NOT FILMED

Table 1

CURRENT AND POTENTIAL USES OF FINE-MESH WOVEN SCREEN IN LIQUID ACQUISITION SYSTEMS

No.	Application	Fluids	Acquisition System Configuration	Transfer Line Configuration	Valve and Pump Operating Characteristics	Ref.
•	CRYOGENIC TUG					
1	Cryogenic APS	LH_2, LO_2	Multiple channels	Valves, turbopump, heat exchanger, accumulator	TBD	4
2	Advanced Space Propulsion Module (ASPM) Concept	LH_2	Numerous screen cylinders within reservoir with containment screen	Valves, turbopump, accumulator		4
3	Centaur (Advanced)	LH_2, LO_2	Reservoir with containment screen	Subcooler, boost pump, engine pump	RL-10 Pump	3
4	LH_2 Tank Concept	LH_2	Annular cylindrical screen device in start tank	Valves, turbopump, accumulator		8
•	CRYOGENIC TANKER					
5	LO_2 Tanker for S-IIB	LO_2	Screen liner entire tank (5.54m sphere)			9
6	LH_2/LO_2 Tanker	LH_2, LO_2	Complete and partial wall screen liner	Valves, Q/D's, lines		2
7	S-IVC	LH_2 LO_2	Reservoir plus channels Reservoir with containment screen	Valves, turbopump Valves, turbopump		9, 10 10
•	SPACE SHUTTLE					
8	Space Shuttle OMS	N_2O_4, A-50	4 channels	Valves, lines	No Pump	11
9	Space Shuttle RCS	N_2O_4, A-50	4 channels	Valves, lines	No Pump	12
10	Space Shuttle Fuel Cell Reactant Supply	LH_2, LO_2	Complete pleated wall liner	Line, regulator	No Pump	2
•	OTHER					
11	Improved Agena Primary Propulsion Sys Secondary Propulsion Sys	 N_2O_4, A-50 N_2O_4, A-50	 Reservoir with several containment screens (common to both systems)	 Valves, lines, turbopump Valves, lines, pneumatic bellows pump	 8096 Mod Pump	 13
12	USAF Unmanned Satellite	N_2H_4	4 channels, 1.57m spherical tank	Valves, lines	No Pump	13, 14

B. Large distributed devices used for extended periods of liquid feed for auxiliary propulsion thrusters, life support system and fuel cell supply, or fluid transfer. These devices (e.g., distributed channels, screen liners, etc.) are characterized by (1) having relatively low flow rates for long durations under low-g, and (2) not usually allowing device failure or refill during use.

The systems tabulated are defined by number as shown in Appendix A. The systems in each category are shown in Table 2. In the first category, systems 2, 3, and 4 are Cryogenic Tug engine restart systems. System 3, the Centaur acquisition system, although conjectural at this time, is fairly well-defined. Because the LH_2/LO_2 propellants in this system have the potential for thermal pressure surges (as well as hydraulic surges), this system was initially recommended for further analytical study using the H672 code, as a system which is particularly representative of the Cryogenic Tug. System 7, for S-IVC engine restart, is also well-defined, but is a more conjectural system. However, because it represents a large-scale increase with LH_2/LO_2 over the Centaur system, it was also initially recommended for detailed analysis using H672. The Improved Agena (No. 11) is also a conjectural system which is not well-defined since development was halted in mid-program.

Table 2

SCREEN ACQUISITION SYSTEM CATEGORIES

Localized Engine Restart	Distributed Long-Term Transfer
2 ASPM	1 CSS/APS
*3 Centaur D-1S	5 S-IIB LO_2 Tanker
4 IDU	6 Tug Transfer Module
*7 S-IVC Stage	*8 Shuttle OMS
11 Improved Agena	*9 Shuttle RCS
	10 Advanced Fuel Cell Supply
	12 Satellite Orbit Adjust

*Initially recommended for further analysis

In the second category, System 1 is not as well-defined as other APS systems in this category and was not recommended for further analysis. Systems 5 and 6 are poorly defined with respect to valve and pump characteristics and downstream transfer line characteristics and could not be analyzed effectively. On the other hand, Systems 8 and 9, the Shuttle OMS and RCS systems, are very well-defined and differ by an order of magnitude in scale, and thus were both initially recommended for further detailed analysis with H672.

System 10, the Shuttle Fuel Cell Reactant Supply, was of current interest, but detailed investigation into the performance requirements for this system indicated the extreme likelihood that no transient problems could occur. The reasons for this are that the control valves are actuated when the Shuttle is on the launch pad and the tank and acquisition system are full. Further flow demand is accommodated through rather slow regulators on demand from rather large volume (high compliance) fuel cells. Thus the probability for large transient flow surges with this system appears minimal, and this system was not recommended for further analysis.

The final system, No. 12, the satellite orbit adjust system with the 1.57m (62-in) N_2H_4 tank, was the only currently operational screen system found. However, the system is used in a sensitive application and detailed system data is limited. Because this system was of the same general order for flow rate as the Shuttle RCS, it was not recommended for further analysis. The four systems initially recommended for further analysis, using the H672 code, included both cryogenic and storable, local and distributed, and large and small systems, and were thought representative of all applications for screen acquisition systems. However, the complexity of modeling of these systems, plus the limited utility of the data derived from their analysis, resulted in only one system, the Centaur D-1S, actually being modeled, as described further below.

TRANSIENT EFFECTS ANALYSIS

The analytical tool to be developed to analyze screen device response to transient pressure surges must also be able to handle the dynamic simulation of the entire feed system. This is because the pressure surges generated by downstream valves, pumps, or line boiling, will be attenuated as they travel

back toward the screen by the line material compliance, gas bubbles, if any, in the line, bends, constrictions, etc., and by the screen device itself. Our approach, therefore, was to use an existing feed system dynamic analysis computer code, modify it to include screen devices, and separately analyze the line boiling pressure surge, using it as an input to the dynamic analysis code.

MDAC had developed under its IRAD program a comprehensive computerized analysis of transient flow in propellant feed systems. This computer code, H672, is described in Appendix B, and is unique in that it uses a simple building block technique to model complex engine feed systems by retaining nonlinear descriptions of valves, tanks, and other engine components at discrete junctions in the total system, but solves the flow equations between components by an exact technique, using the method of characteristics. In this analysis, a propellant feed system is portrayed as variable sets of components located at discrete junctions within the system. Pressure and flow information is transmitted from component to component by characteristic waves, generated and modified by perturbations and boundary conditions at the components.

The simulations of feed system components which have been developed include feed tanks, valves, surge tanks, spring-loaded accumulators, bellows, pumps, and liquid injectors. The component simulations were designed to use the characteristic wave equations, together with the specified wave modification associated with each component, to determine the pressures and flows in the system. The simplicity with which the characteristic equations are developed for lines, junctions, and components is described in Appendix B.

This analysis has been used to analyze transient effects in actual launch vehicles, and has been correlated with flight data. For example, Figure 1 shows the H672 computer simulation of the MDAC Delta fuel pump inlet pressure transient, which compares well with the flight data.

In order to analyze screen device dynamic response using H672, it was necessary to develop new subroutines for inclusion in the H672 code. The

nomenclature employed is that used in H672, as described in Appendix B. The H672 code was written in British engineering units, as are the new analyses for the screen device performance, in order to be compatible with the existing code. The International System of Units (SI) are only used for the final results following complete system simulation. Mechanization of the screen device model described below consists of the creation of two new subroutines, plus the addition of suitable "common blocks" and instructions in the main program. The first new subroutine, SCRPRP, is a preparation routine for the actual screen system input. The SCRPRP routine takes the screen system input data, processes it for correct dimensions, manipulates it as required, and stores it for use in SR26. The SR26 routine performs the iterative calculations, and stores the solutions and characteristics of each model section of the screen device. Development of the SR26 screen model equations is described in detail in Appendix C. The important relations and features of the SR26 subroutine are described in the following section.

CR21

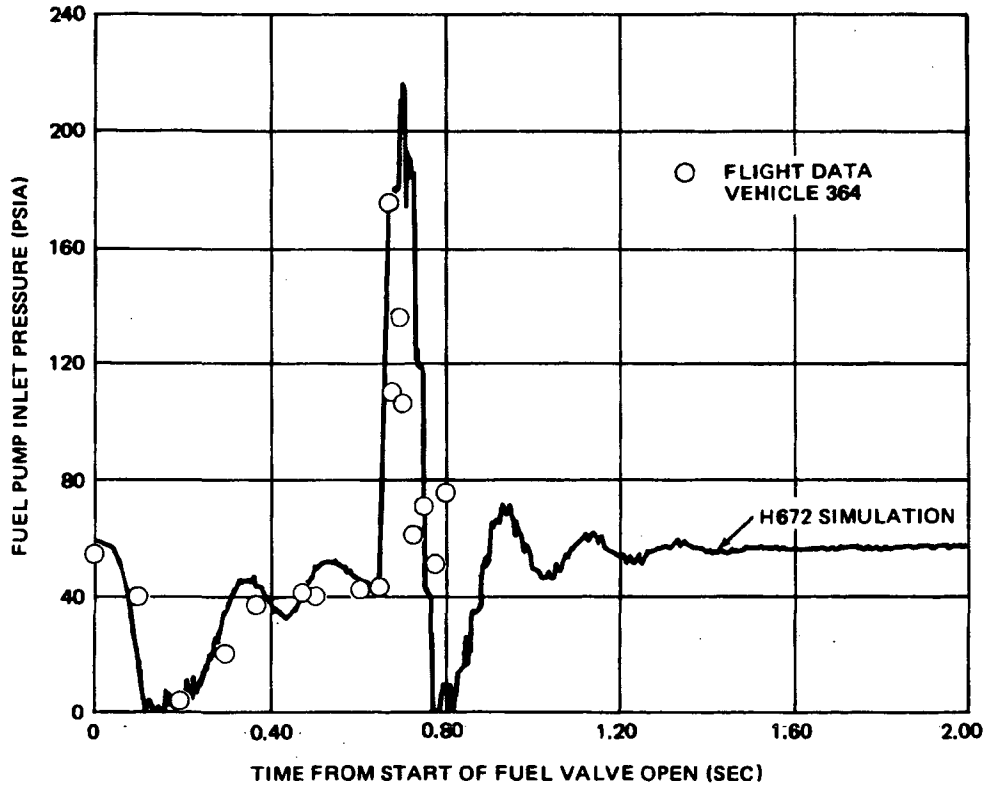

Figure 1. H672 Simulation of Delta Start Transient

SR26 SCREEN DEVICE MODEL DEVELOPMENT

A fine-mesh screen used on a propellant acquisition device exhibits characteristic behavior when subjected to a positive or negative pressure pulse in the liquid retained within the screen device. With a positive pressure pulse, liquid outflow occurs through the screen, which resists flow and also exhibits compliance in the direction of the flow through the screen. If the liquid outflow through the screen possesses sufficient kinetic energy to overcome the surface tension forces tending to hold the liquid to the screen, the liquid will leave the vicinity of the screen. This may be important to screen behavior when a negative pressure pulse arrives later. With a negative pressure pulse, and with liquid on both sides of the screen (including liquid which may have been pushed through the screen by a previous positive pressure pulse), liquid inflow will occur, again resisted by the screen which again exhibits compliance. With vapor on the outside of a screen experiencing a negative pressure pulse, vapor inflow through the screen will occur when the local pressure pulse magnitude exceeds the screen bubble point. Gas will continue to flow through the screen, resisted by the compliant screen, until the negative pressure pulse magnitude drops below the bubble point (assuming a wet screen) or to zero (assuming a dried screen). The pressure pulses are propagated along the screen device at a velocity determined by the bulk modulus of the liquid (modified by bubble ingestion) and the compliance of the screen.

The first step in the development of the screen-channel model was the determination of the equation for acoustic velocity in the screen device which included properties of the liquid, gas bubble, channel (supporting structure), and screen. It was assumed that initially the screen"pipe" was full of liquid. Fine-mesh twilled-weave screens are basically orthotropic in nature, i.e., they have different properties in the right angle directions of the weaving axes. As shown in Figure 2, the kind of screen-channel configuration which was amenable to analysis was a uniformly distributed screen-channel structure which could be characterized as a pipe having properties based on the proper combination of screen and channel properties.

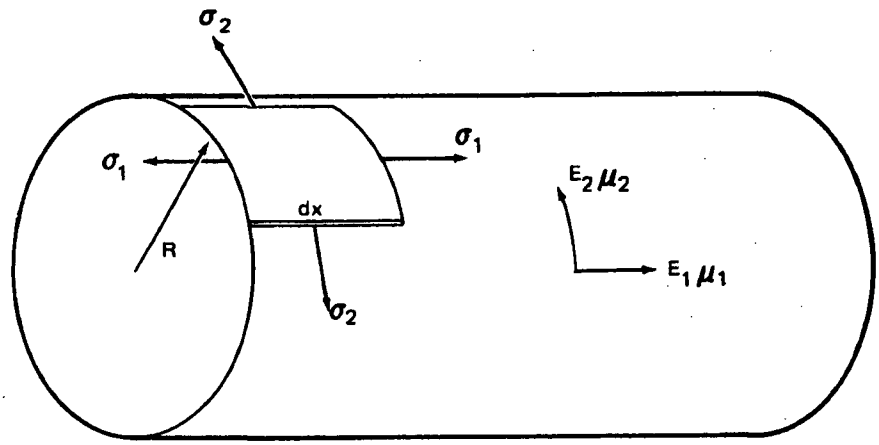

PIPE PROPERTIES	ELASTIC MODULUS, E_P
	POISSON'S RATIO, μ_P
	WALL THICKNESS, e_P
SCREEN PROPERTIES	ELASTIC MODULUS, AXIAL DIRECTION, E_{S_1}
	ELASTIC MODULUS, CIRCUMFERENTIAL, E_{S_2}
	POISSON'S RATIO, AXIAL, μ_{S_1}
	SCREEN THICKNESS, e_S

Figure 2. Orthotropic Structure Nomenclature

Following the usual derivation of the continuity equation for one-dimension, unsteady flow (shown in detail in Appendix C) and accounting for the elasticity of the fluid and pipe, and the effect of gas in the pipe, the final equation for the acoustic velocity in a liquid-gas mixture in a composite orthotropic pipe was:

$$a' = \left[\frac{x^2}{C_g^2} + \frac{(1-x)^2}{C_L^2} + x(1-x)\left(\frac{\rho_L}{\gamma P_A g} + \frac{\rho_g}{K g}\right) + \left\{(1-x)\frac{\rho_L}{g} + \frac{x\,\rho_g}{g}\right\}\left(\frac{D\,C_1}{e\,E_1} + \frac{D\,C_2}{e\,E_2}\right)\right]^{-1/2} \quad (1)$$

where x is the volume fraction of gas; C_g and C_L are the acoustic velocities in the gas and liquid, respectively; ρ_g and ρ_L are the corresponding densities; P_A is the absolute pressure in the pipe; γ is the ratio of specific heats for the

gas; g is the gravitational constant; K is the compressibility of the liquid; D and e are the pipe inside diameter and equivalent thickness; E_1 and E_2 are the orthotropic elastic moduli; and C_1 and C_2 are constants depending on the form of pipe constraint.

The complete screen device was divided into a series of sections, one of which is shown in Figure 3. The nomenclature used in Figure 3 is that used in the H672 analysis (see Appendix B and "Nomenclature") and the upstream conditions of head and flow, H1 and Q1, and downstream conditions H3 and Q5 are assumed known from the previous timestep so that the waterhammer constants can be defined:

$$CX = H1 + SX \cdot Q1$$

$$CY = H3 + SY \cdot Q5 \qquad (2)$$

CR21

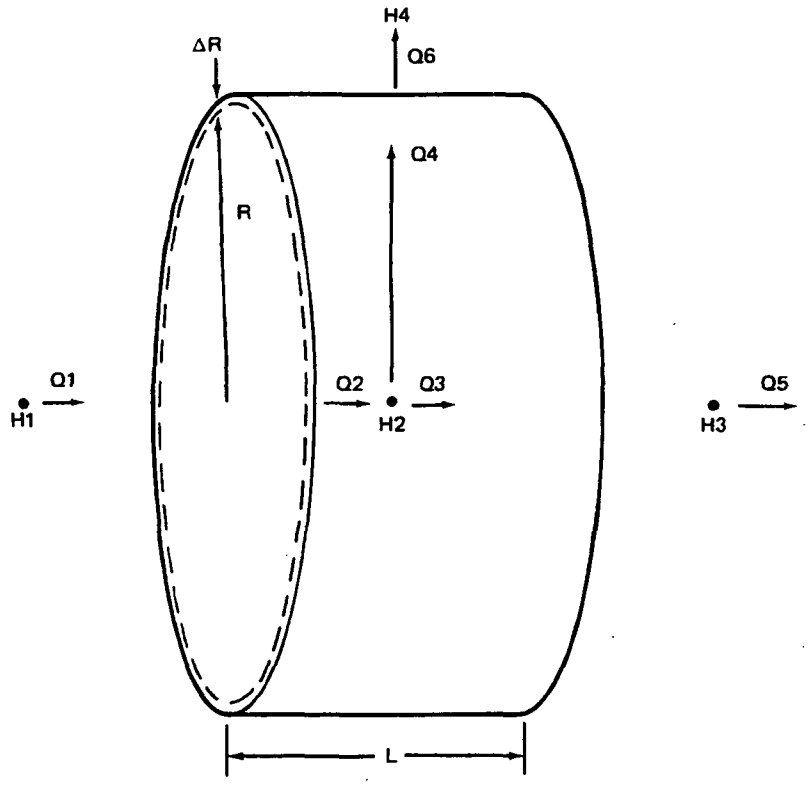

Figure 3. Screen Device Model

where

$$SX = \frac{a'}{g_c A_p}$$

$$SY = -\frac{a'}{g_c A_p}$$

With the waterhammer constants defined, the characteristic identities can be evaluated:

$$\begin{aligned} Q2 &= (CX - H2)/SX \\ Q3 &= (CY - H2)/SY \\ Q4 &= Q2 - Q3 \end{aligned} \tag{3}$$

Some of the Q4 flow, flows through the screen (Q6) because of the head difference:

$$H2 - H4 = \frac{A'Q6}{A_s} + \frac{B'(Q6)^2}{A_s^2} \tag{4}$$

where A' and B' are the experimentally determined liquid flow-loss coefficients for the screen, A_s is the screen area, and H4 is the tank pressure.

The rest of the flow, Q4 - Q6, expands the pipe slightly such that the change of volume is:

$$\Delta T\,(Q4 - Q6) = L\,2\pi R\,\Delta R \tag{5}$$

The above equations were combined and the outflow Q6 was solved explicitly (see Appendix C). The outflow Q6 could actually be liquid outflow, liquid inflow, or gas inflow, depending on the relative magnitudes of H2, H4, and the proper boundary conditions and flow-loss coefficients. For liquid outflow, Q6 is:

$$Q6 = \frac{2\left(H4 - \frac{1}{ZZ}\left(H4 + \frac{c \cdot CX}{SX} - \frac{c \cdot CY}{SY}\right)\right)}{-\left(a + \frac{c}{ZZ}\right) - \left(\left(a + \frac{c}{ZZ}\right)^2 - \left(4b\left(H4 - \frac{1}{ZZ}\left(H4 + \frac{c \cdot CX}{SX} - \frac{c \cdot CY}{SY}\right)\right)\right)\right)^{1/2}}$$

where

$$ZZ = 1 + \frac{c}{SX} - \frac{c}{SY}$$

$$a = A'/A_s$$

$$b = B'/A_s^2$$

$$c = 2e\, E_2/a'\, \rho_L\, \pi^2\, D^3\, (1 - P_o)\, f$$

From Q6, H2 is computed from Equation 4 and the flows from Equation 3. Q3 and H2 then become the upstream values used to compute the new conditions in the next section.

In order not to permanently deform the screen, the equivalent stress in the screen during the pressure pulse must be below some critical stress, e.g., the proportional limit of the screen. Another criterion which was checked when gas surrounds the screen device was whether liquid expelled through the screen by a pressure pulse would leave the screen.

Assuming negligible potential energy, the criterion for liquid breakaway was for the globule kinetic energy to exceed the surface tension energy. The critical velocity, V_{L_C}, which resulted in liquid globule breakaway was found to be:

$$V_{L_C} = \left[\frac{\sigma}{\rho_L} \cdot \frac{3}{4} g_c \frac{r_s^3}{r_L^4}\right]^{1/2} \tag{7}$$

If the liquid velocity was larger than V_{L_C} the liquid globule would leave the screen. In addition, if the quantity of liquid outflow was sufficient to wet the

entire screen surface, it was assumed that screen pore surface tension forces no longer existed, so that the liquid also left the screen. The quantity of liquid (QLSUM) held by the screen is kept current by correction (if any) in each time step. If QLSUM is positive, then inflow during a negative pressure pulse is liquid, until QLSUM goes to zero. This may retard gas ingestion for several time steps.

The model for gas ingestion and quality assumes that the quality in the device is uniform (i.e., the gas bubbles are not concentrated near the screen, but are distributed uniformly throughout the liquid in the screen).

The quality in the device is equal to the gas volume divided by the liquid volume (screen device volume minus gas volume. The gas volume (QSUM) is corrected in each time step by the amount of entrained gas that outflows (or inflows) from the screen device. The acoustic velocity a', from Equation 1 is updated in each time step by the quality from the preceding time step.

The most important boundary condition for the screen segment is whether gas or liquid surrounds it—this condition is input for the segment. The basic SR26 routine has three main branches as shown in the logic flow diagram in Figure 4. The code first checks if gas or liquid surrounds the screen—if liquid, it goes to Branch 1 which determines liquid inflow or outflow. If gas surrounds the screen, the code checks the previous time-step screen pressure-ullage pressure difference. If positive (screen pressure higher than ullage pressure) it goes to Branch 1 for liquid outflow. If negative, it checks whether the pressure difference exceeds the bubble point; if so, it goes to Branch 2, which determines gas ingestion. If the pressure difference is less than the bubble point, it goes to Branch 3, which sets the inflow (Q6) to zero.

In Branches 1 and 2, the screen stress based on the device section pressure difference is computed and compared to the maximum allowable stress (input), and if excessive, a warning message is printed. In addition, for liquid inflow/outflow the QLSUM is computed in Branch 1 (and Branches 2 and 3, if applicable). In all branches, the quality within the device section

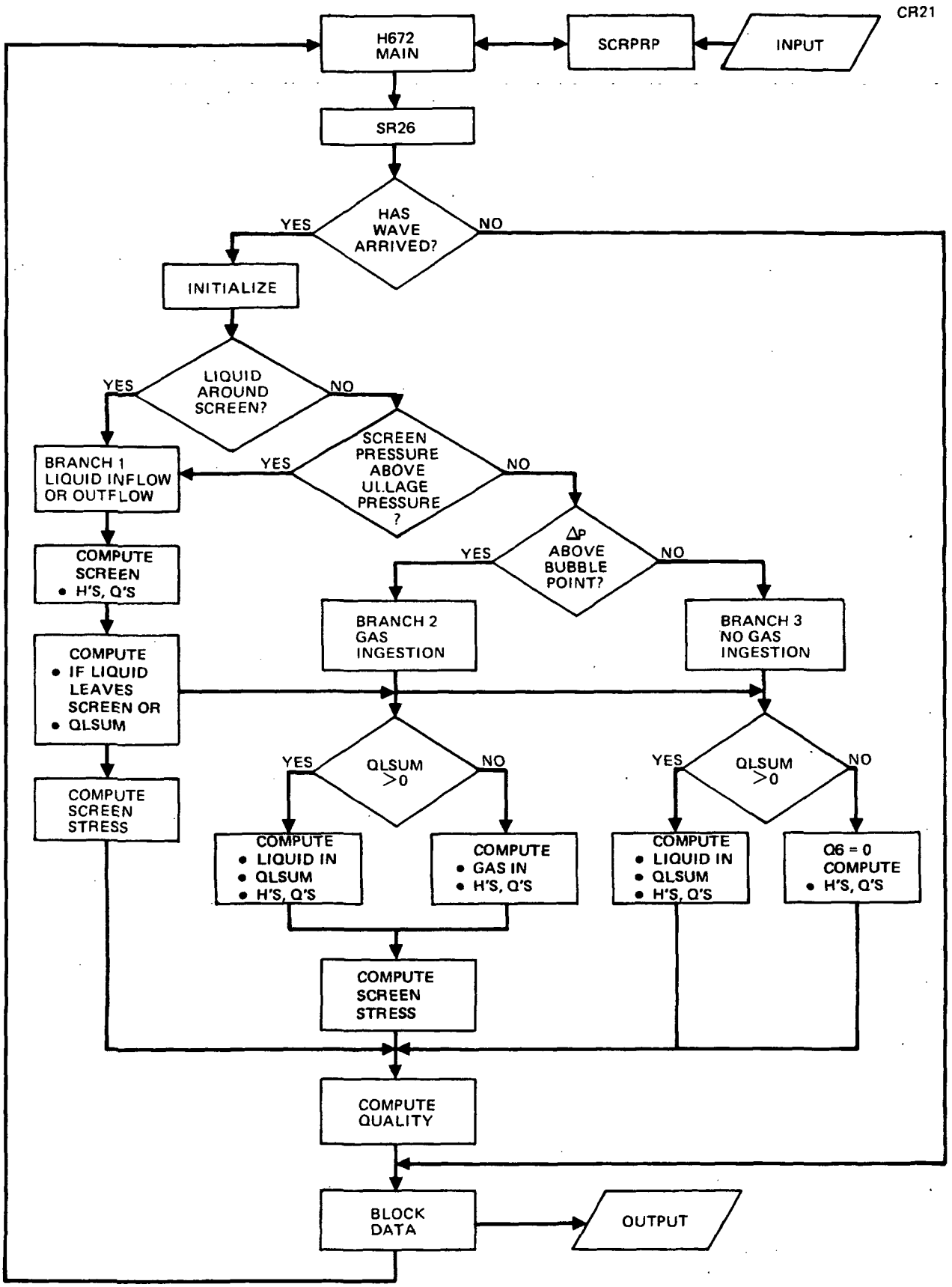

Figure 4. SR26 Logic Flow Diagram

is computed in each time step; if the quality exceeds 1.0, it is set to 1.0, and a warning message is printed.

The final configuration of the SCRPRP subroutine is shown in Appendix D. The data contained in SCRPRP is shown in Table 3. Parameters H1 through N must be input for each screen device section; SURX (17) through (20) are computed within the SCRPRP subroutine.

Table 3

DATA CONTAINED IN SURX BLOCK

H1	Screen Device Location	
SURX(1)	GAMMA	ullage gas γ
SURX(2)	RTGAS	ullage gas R· T (Ft/°R·°R)
SURX(3)	PGAS	initial ullage pressure (Psia)
SURX(4)	BPS	screen bubble point (Ft)
SURX(5)	EE	screen/pipe (eE_2/D^3) (Lb/In^4)
SURX(6)	STEM	maximum stress in screen (Psi)· equiv. screen thickness (In)
SURX(7)	AS1	screen flow-loss coefficient laminar-liquid (Sec)
SURX(8)	BS1	screen flow-loss coefficient turbulent-both (Sec^2/Ft)
SURX(9)	AS2	screen flow-loss coefficient laminar-gas (Sec)
SURX(10)	DPS	screen pore size (Ft)
SURX(11)	DS	screen channel diameter (In)
SURX(12)	DC	screen/pipe $\left(\frac{DC_1}{eE_1}+\frac{DC_2}{eE_2}\right)$ (In^2/Lb)
SURX(13)	PØ	screen fraction of open area
SURX(14)	F	screen/pipe screen fraction
SURX(15)	LS	screen/pipe length (In)
SURX(16)	PW	boundary code for screen/pipe 0.0 if dry 1.0 if wet
N		Propellant type 1 or 2
SURX(17)	RHØG	P/RT
SURX(18)	CG	$(\gamma g\ RT)^{1/2}$
SURX(19)		$\rho_L/\gamma Pg$
SURX(20)		ρ_G/Kg

In order to integrate the screen device section(s) into the total H672 feed system simulations, coded control numbers for head, flow, etc. must be input for each screen device section. These are called "J-BLOCK" and are shown in Table 4, where the nomenclature refers to that in Figure 3.

Table 4

J-BLOCK FOR SCREEN DEVICE

J-Block Location		
1	SPTY	Screen Device Identification Code (1 through 4)
2	H1	Pressure Head Control Number for station 1
3	H2	Control Number for pressure head at screen device junction, station 2
4	H3	Pressure head Control Number for station 3
5	Q1	Flow Control Number for station 1
6	Q2	Control Number for flow at screen device in branch 1 - 2
7	Q3	Control Number for flow at screen device in branch 2 - 3
8	Q5	Flow Control Number for station 3
9	TT	Total Time Control Number for screen device
10	T1	Control Number for wave travel time between stations 1 and 2
11	T2	Control Number for wave travel time between stations 2 and 3
12	SX	Control Number for pipe constant traveling with the flow between stations 1 and 2 (1 through 30 for system 1; 31 through 60 for system 2)
13	SY	Control Number for pipe constant traveling against the flow between stations 2 and 3 (1 through 30 for system 1; 31 through 60 for system 2)
14	A1	Pipe Type Control Number (1 through 30); the area corresponding to this pipe type is used to compute the static pressure at station 2
15	PRTY	Control Number for propellant type in screen device (1 or 2); this coincides with the system identification code
16	DAT	Datum Control Number for screen device
17	INFL	Initial Flow Control (1 or 2): 1 signifies that flow initialization at the screen device proceeds from station 1; 2 designates procession from station 3.
18	BYP	Bypass Flow Control (1 or 2): 1 signifies that the flow direction of Q5 follows the assumed convention; 2 designates that the direction of Q5 is opposite the assumed convention.

Five constants are carried by the H672 program, as shown in Table 5. The final configuration of the screen device subroutine SR26 is shown in Appendix E.

Table 5
H672 PROGRAM CONSTANTS

CNST	(1)	=	144.
CNST	(2)	=	576.
CNST	(3)	=	3.141593
CNST	(4)	=	32.174
CNST	(5)	=	12. *SQRT (62.4)

The BLOCK output is presently arranged to output screen device screen-ullage pressure differential, quality, local sonic velocity, screen inflow/outflow and QLSUM for up to four screen device sections, together with up to 20 heads (pressures) and 10 flows throughout the feed system, and other data such as time, valve position, outlet (sink) pressure, etc.

CRYOGEN BOILING PRESSURE SURGE ANALYSIS

Pressure surges caused by boiling liquids in warm lines is a significant problem which is not specifically modeled in the H672 code but which can be easily accommodated by the engine and injector subroutine. This subroutine allows a pressure pulse or ignition spike occurring in an engine to be transmitted to the rest of the feed system through the injector. Our approach was to use a zero-resistance injector and model the engine pulse to conform to the shape of the pulse generated by boiling fluid, which was predicted from the MDAC computer analysis, P4557, described below.

A number of analyses exist to determine the pressure and flow history which occurs with boiling of cold fluid in a warm line during flow, and to concurrently determine the line cooldown time. The most comprehensive was developed by Steward, et al. (Reference 15). The MDAC version of that analysis, P0734, is large, complex, and expensive to run, and also is much too comprehensive for the results needed for this study, which only requires the initial (worst) pressure surge and flow reversal. Steward earlier developed a much simpler analysis to determine initial pressure surge

(Reference 16), and under its IRAD program MDAC developed a computer code, P4557, based on this analysis which is simple, inexpensive to run, and has been correlated with Steward's experimental LN_2 data. The cryopressure surge analysis is described in detail in Appendix F. Important features of the analysis are:

- It accounts for any initial temperature distribution in the line.
- It accounts for the degree of subcooling of the entering liquid.
- It determines the pressure and flow history throughout the pipe.
- Heat-transfer mechanisms are forced convection until boiling occurs, then an empirical boiling heat flux.
- Fanno flow is used to determine the vapor flow characteristics.

The P4557 program was originally set up for LN_2 to correlate with the experimental data of Steward (Reference 16), The experimental configuration and operating parameters are shown in Figure 5. The major unknown in the correlation is the selection of an empirical boiling heat flux. It was found for LN_2 that the Breen-Westwater film boiling correlation shown in Reference 17 (3.2 Watt/cm^2 at ΔT = 220K) gave excellent correlation with the experimental data as shown in Figure 6. (The two solid lines represent extremes of several experimental tests.) Since use of the film boiling heat flux is reasonable from a physical sense, this heat flux, based on the Breen-Westwater correlation, was also used for the other fluids of interest to this program (LH_2-9 Watt/cm^2, LO_2-3 Watt/cm^2, Freon 114 - 1.5 Watt/cm^2), together with the appropriate physical properties. The pressure surges for these fluids with the same physical system are also shown for comparison in Figure 6. The LO_2, because of its higher density and inertia, peaks at a pressure slightly higher, and somewhat later than LN_2. Conversely, LH_2 with its very low viscosity, density, and inertia, peaks very rapidly and at a low pressure value. The Freon 114 was assumed to boil at the minimum film boiling heat flux, due to the small difference between the pipe and liquid temperatures. The pressure rises slowly toward the saturation pressure at the pipe wall temperature (26.2 N/cm^2 [38 psig]).

The P4557 code was used to predict the boiling pressure surge for both experiment planning and for experiment data correlation, as described in the following paragraphs.

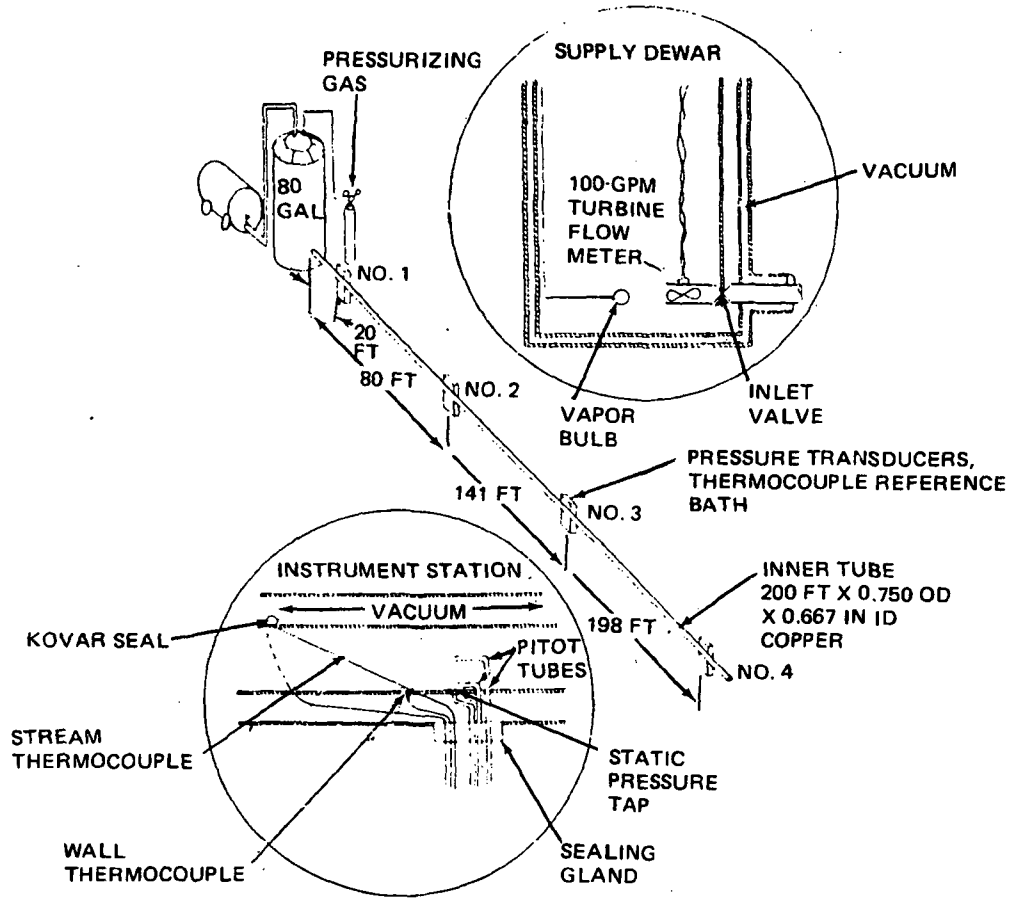

FLUID, LN_2
FLUID TEMPERATURE, 75.7°K
TANK (DRIVING) PRESSURE, 51.6 N/CM^2 (74.8 PSIA)
AMBIENT PRESSURE, 8.5 N/CM^2 (12.3 PSIA)
VALVE OPENING TIME, 0.5 SEC
EQUIVALENT COLD PIPE LENGTH, 127 CM
DISTANCE TO VALVE, 15 CM

Figure 5. NBS Experimental Configuration and Operating Parameters

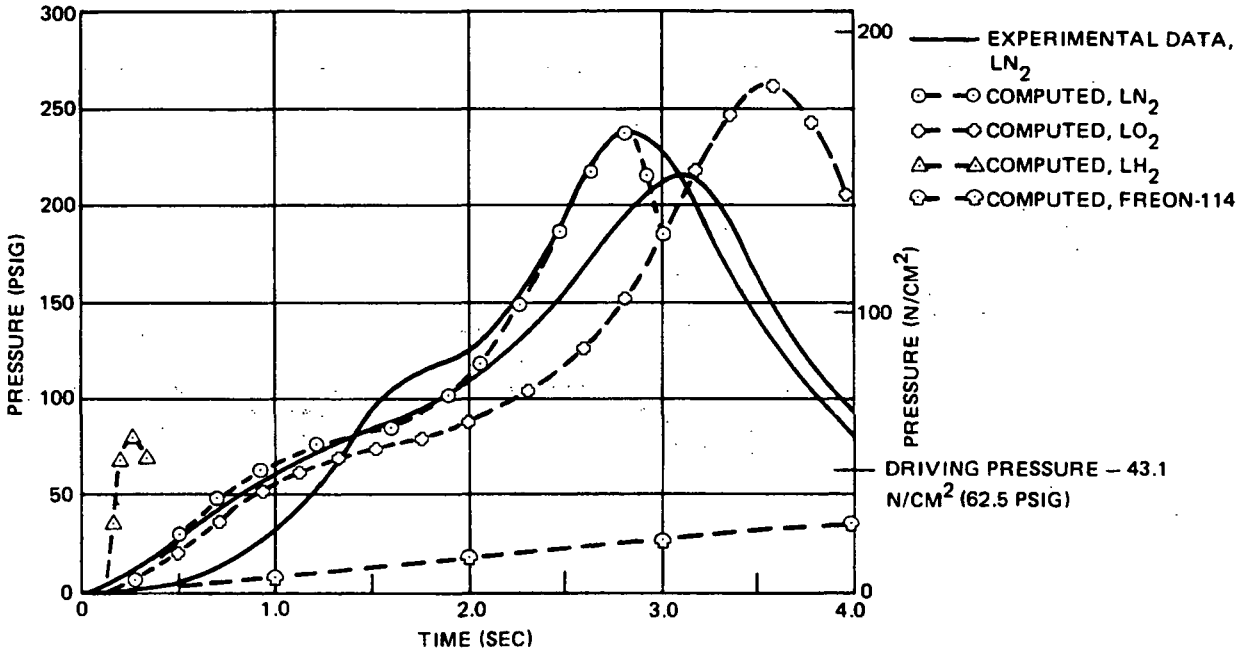

Figure 6. Correlation of Transient Pressure Surge

EXPERIMENTAL PROGRAM ANALYSIS AND PLANNING

The experimental program analysis and planning was accomplished in several steps. First, a simple test model was simulated using H672 (and P4557) to check out the SR26 subroutine and also determine the important influences on screen device transient behavior. Next, the Centaur D-1S system was analyzed in detail, and finally the results of the above simulations were used to develop a matrix of test conditions which would evaluate those effects with the strongest influence on screen device transient behavior, and provide data usable for realistic analytical correlation.

Two test cases were assumed, with conditions and configuration as shown in Figure 7. The fluid for both cases was LH_2, saturated at 10.34 N/cm^2 (15 psia). The first test case assumed a totally cold system (giving only hydrodynamic effects, no cryogenic boiling pressure surge). The system shown in Figure 7 consisted of a tank, a screen device, 0.61 m (2 ft) of 2.5-cm (1.0-in) diameter pipe, a valve, 3.05 m (10 ft) of 2.5-cm (1.0-in) diameter pipe, and an injector. The tank pressure was assumed constant at

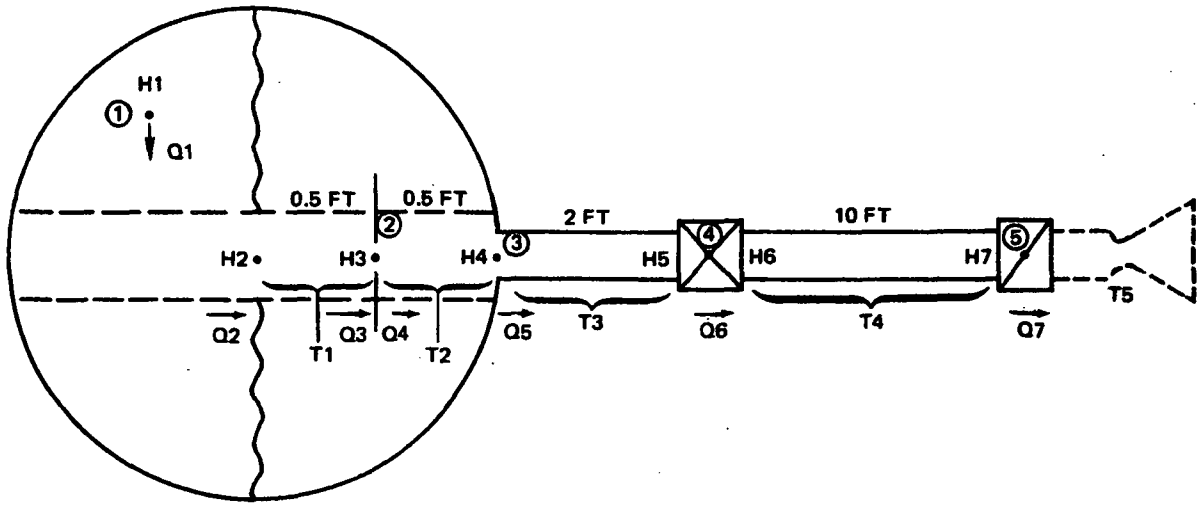

① SR05 TANK
② SR26 SCREEN
③ SR01 JUNCTION
④ SR11 VALVE
⑤ SR12 INJECTOR
(SR18 · PRESSURE SURGE)

FLUID: LH_2 SATURATED AT 15 PSIA
ρ = 4.4 LB/FT^3
K = 9750 PSI
σ = 1.32 X 10^{-4} LB/FT

ULLAGE GAS: GHe AT 40°R
γ = 1.67
RT = 1545/4 · 40 = 15,450 FT

TANK: 48-IN DIA SPHERE X 0.03 WALL VOLUME = 33.51 FT^3
ULLAGE HEIGHT, 1 FT. ULLAGE PRESSURE, 25.0 PSIA

SCREEN: 2.0-IN DIA X 1.0 FT LONG 325 X 2,300 BPS = 2.42 FT
AS1 = 1.44 BS1 = 2.27 AS2 = 0.297 DPS = 0.00001 FT
DS = 2.0 IN Pϕ = 0.060 DC = 0.0936 IN^2/LB LS = 1.0 FT
EE = 2.45 LB/IN^4 STEM = 15.75 PSI-IN F = 0.999 PW = 0.0

PLUMBING: PIPES: 1.0 IN DIA X 0.02 WALL
SCREEN: 2.0 IN DIA X 0.00000071 EQUIV. WALL FOR CORRECT s
E = 30 X 10^6 PSI (STEEL)

VALVE: 1-IN DIA BALL VALVE L/D = 1 ΔP = 0.003 PSI AT 0.5 LB/SEC LH_2
C_V = 34.4 VALVE OPEN/CLOSE TIME = 0.05 SEC

INJECTOR: (EQUIVALENT SAFETY FACTOR = 2.0.) C_V = 1.88

Figure 7. H672 Model for Test Cases

17.24 N/cm^2 (25 psia). The pressure downstream of the valve was 10.41 N/cm^2 (15.1 psia). The valve was assumed to be a low-loss (C_V = 34.4) ball valve with an opening time of 0.05 sec. The injector was used to simulate a regulator or higher-loss plumbing downstream. The injector C_V was chosen so that the resulting flowrate would give a screen safety factor of 2.0, in order to evaluate the performance of a screen device designed in accordance with a commonly accepted criterion. The screen device was assumed to be an unsupported tube of 325 x 2,300 dutch twill screen, 5.08 cm (2 in) in diameter by 0.305 m (1 ft) long, surrounded by gaseous helium at 22.2 K (40°R).

The second test case simulated the pressure surge caused by cryogenic boiling in a warm line. The P4557 code was used to determine the pressure surge-time history. With only 3.66 m (12 ft) of pipe, the LH_2 flowed freely out the 222 K (400°R) pipe with a pressure surge to only 11.7 N/cm^2 (16.9 psia). In order to simulate the resistance caused by a regulator or additional plumbing downstream, an additional 24.8 m (81.5 ft) of 2.5 cm (1 in) diameter line was added (giving the same resistance as the assumed test case injector), which resulted in a surge to 29.3 N/cm^2 (42.5 psia) in 0.26 sec. A "combustor" with the cryogenic pressure surge trace was added to the injector for the second test case (identical to the first case in all other respects).

Hydrodynamics Effects Test Cases

A series of 10 test cases was run to evaluate the influence of various system configurational and operational conditions on the response of the screen device and the occurrence of gas ingestion following valve opening (startup) and valve closing (shutdown). The test cases, operating conditions, and results are summarized in Table 6. Details and discussion of each case are found in the following paragraphs.

The first test case was run with the following valve operational mode: the valve was started open at 0.001 sec, was wide open at 0.051 sec, was started closed at 0.1 sec, and was completely closed at 0.15 sec. The case run time was limited to 0.2 sec to reduce computing time while adequately evaluating screen performance. The H672 code was run with the output plotting option, and the figures that follow were produced by the SC4020

Table 6

ANALYTICAL TEST CASES

Figure	Test Case	Gas Ingestion		Conditions						
		Startup	Shutdown	PØ	E	Valve Open/Close Time	Valve Dist. m	Screen Area	Screen Diameter	Screen Flowrate
8	Baseline	Moderate	Severe	0.06	E_s	Δt	0.61	A_s	D_s	w_s
9	Screen Properties (PØ)	More Severe	Very Severe	0.245	E_s	Δt	0.61	A_s	D_s	w_s
10	Screen Properties (E)	Very Severe	Extreme	0.06	$2xE_s$	Δt	0.61	A_s	D_s	w_s
11	Valve Open/Close Time	Moderate	Less Severe	0.06	E_s	$2 \times \Delta t$	0.61	A_s	D_s	w_s
12	Valve Open/Close Time	More Moderate	Much Less Severe	0.06	E_s	$5 \times \Delta t$	0.61	A_s	D_s	w_s
13	Screen-Valve Distance	Zero	Very Severe	0.06	E_s	Δt	3.05	A_s	D_s	w_s
14	Screen Area Increase (Pleating)	Zero	Moderate *	0.06	E_s	Δt	0.61	$2 \times A_s$	D_s	w_s
15	Screen Area Increase (Pleating)	Zero	Mild *	0.06	E_s	Δt	0.61	$5 \times A_s$	D_s	w_s
16	Screen Diameter	Zero	Moderate	0.06	E_s	Δt	0.61	$\sqrt{2} \times A_s$	$4\sqrt{2} \times D_s$	w_s
17	Screen Flowrate	Very Mild	Moderate	0.06	E_s	Δt	0.61	A_s	D_s	$w_s/\sqrt{2}$

*Pressure pulse reduced-gas quantity ingested increased

plotter. The screen-ullage pressure differential was chosen as being representative of screen performance for plotting purposes, although the complete H672 output was available. The baseline test case is shown in Figure 8. The tank pressure is 17.24 N/cm^2 (25 psia) and the pressure downstream of the valve is 10.41 N/cm^2 (15.1 psia), or an equivalent head differential of 99.76 m (327.3 ft) of LH_2 (compared with the screen bubble point of 0.74 m [2.42 ft] of LH_2). During opening, the screen-ullage pressure differential is seen to vary between 0 and 0.07 N/cm^2 (0.10 psi). The sharp vertical lines indicate points of ullage gas ingestion. It can be seen that relatively severe gas ingestion occurs during valve opening, but much more severe pressure surges and gas ingestion occur following valve closure. Figures 9 and 10 show the effect of screen properties on device performance. Originally, the percent open area (PØ) was input as equal to the void fraction (0.245); this may not have been accurate. The percent open area is not analytically definable for dutch twill weave screens. For square-weave screens, the open area is analytically defined, and generally is approximately equal to the void fraction squared. This may not be true for dutch twill weave screens, but use of the void fraction squared is probably closer to reality than just the void fraction. Therefore, for parametric purposes, the PØ was input as 0.06. Figure 9 shows the baseline case but with PØ = 0.245, which indicates a rather strong effect on gas ingestion — in fact, the quality in the screen device after 0.2 sec was 25.43% for PØ = 0.245 compared to 9.49% for PØ = 0.06. Similarly, Figure 10 shows the performance of the baseline case with the screen modulus of elasticity equal to twice the previously assumed value of approximately 3,860 N/cm^2 (5,600 psi). Gas ingestion is so severe that the screen device is completely full of gas (quality equals 1.0) by 0.188 sec. Clearly, screen properties can have a strong effect on screen device performance and must be accurately accounted for.

Considering the relatively slow valve operation time (0.050 sec), the severity of pressure pulse following valve closure was unexpected. Examination of the flow characteristics of the system revealed a very interesting effect. The valve does not control the flow rate in the system except to turn it "on" or "off". The flow rate is controlled by the higher resistance plumbing (injector) downstream of the valve. Hence, when the valve is only 4% open, it is at essentially full flow. This means that the effective valve opening and

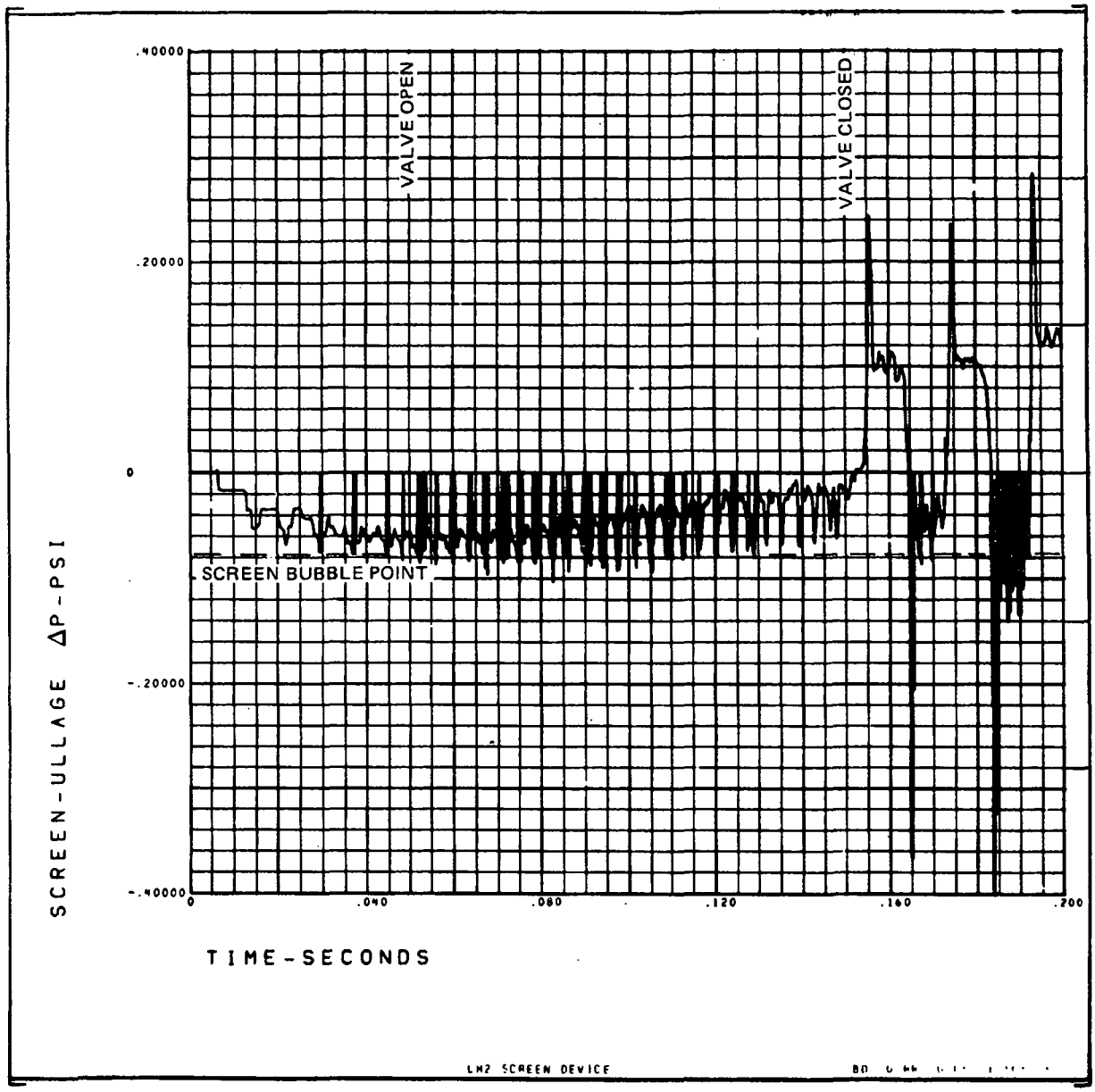

Figure 8. Baseline Screen Device Performance, Percent Open Area = 0.06

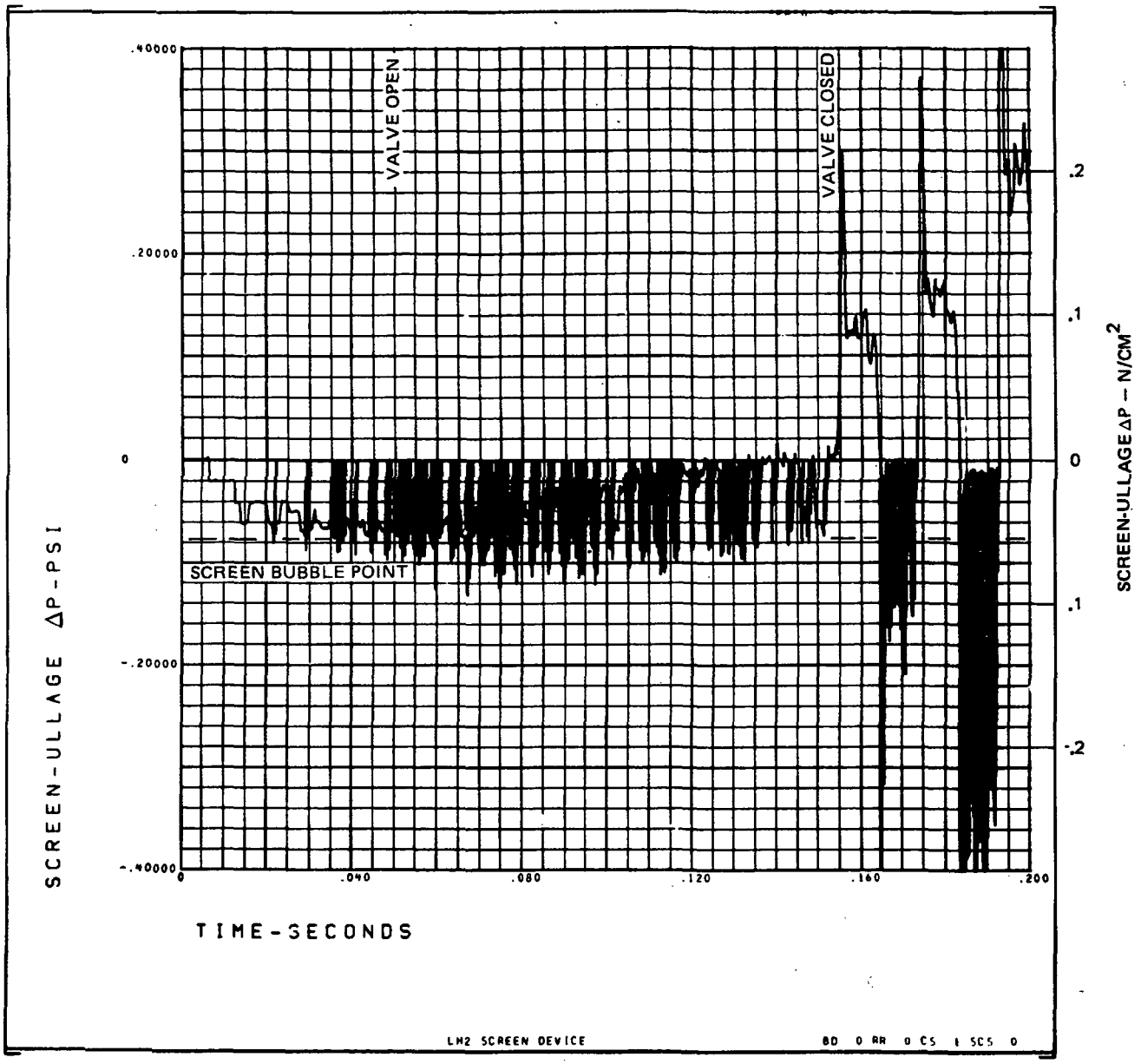

Figure 9. Screen Device Performance, Percent Open Area = 0.245

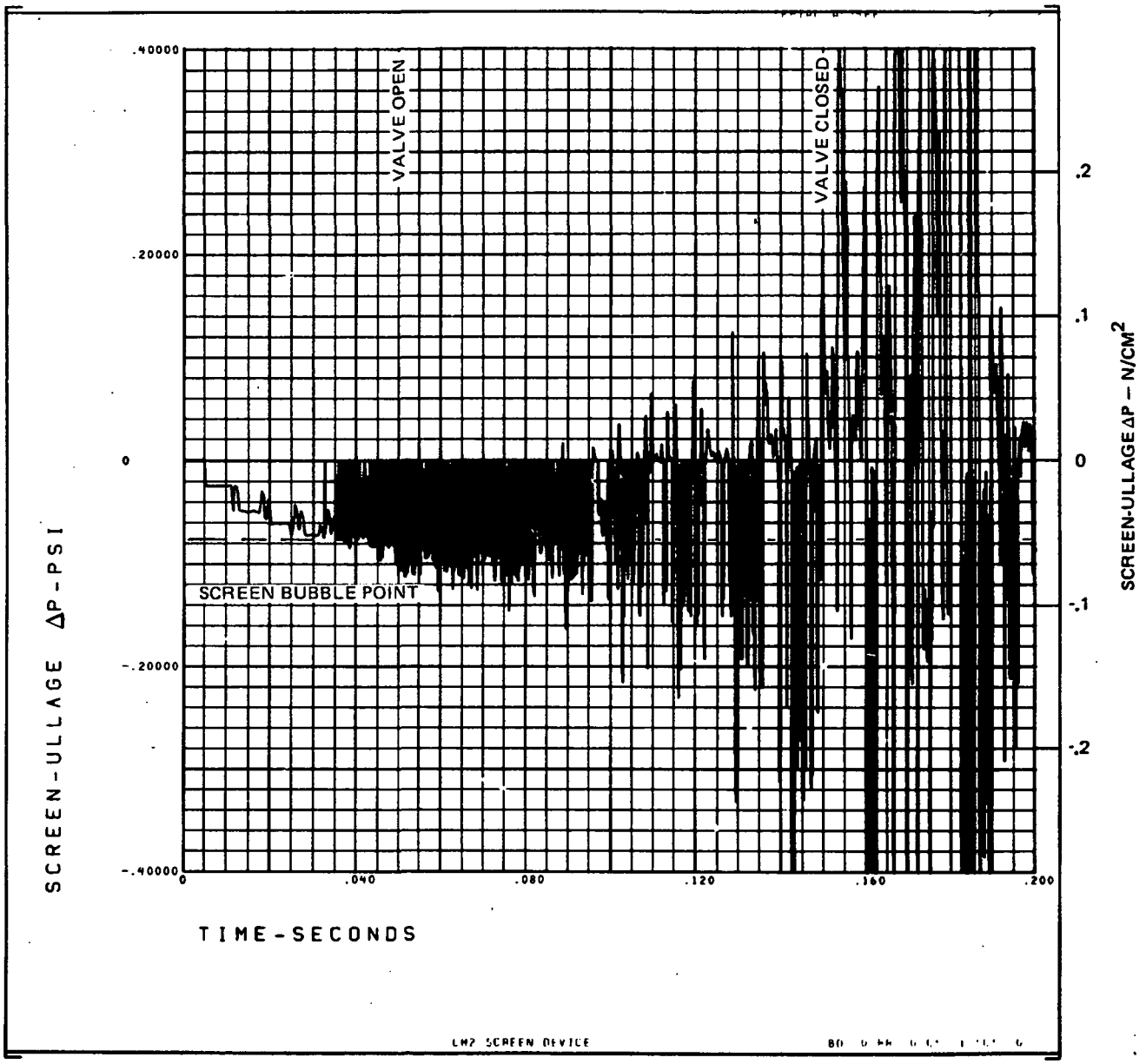

Figure 10. Screen Device Performance, 2 X Screen Modulus of Elasticity

closing time is not 0.050 sec but about 0.002 sec, which is very fast indeed. This is a real system effect and will occur whenever the primary flow rate control is not the valve, but rather the downstream system, be it a long transfer line and plumbing in the case of a propellant transfer system, or an engine injector in the case of an engine restart system. Thus, it is the effective valve operation time, relative to the total system, rather than the gross actuation time, with which the designer must concern himself.

In Figure 11 the effective valve opening/closing time was doubled. There is essentially no effect on screen performance during valve opening, but the severity of the shutdown pulses is lessened considerably. Similarly, in Figure 12, the effective valve opening/closing time was increased by a factor of 5. It can be seen that the screen performance during valve opening was improved, but some gas ingestion still occurred. At shutdown, the pressure spike was considerably attenuated, but gas ingestion still occurred. It was thought that increasing the length of pipe between the screen and valve should have the same beneficial effect on screen performance as an increase in the effective valve opening/closing time. Figure 13 shows the effect of increasing this pipe length from 0.61m (2 ft) to 3.05m (10 ft) for the baseline case: much reduced valve opening pressure surges. Hence, the effective valve opening/closing time relative to the screen device-plumbing configuration and line length are important parameters.

It was felt that increasing the screen area would allow higher inflow/outflow rates, and increased screen deflection, with consequent decrease in the screen pressure pulse. Figure 14 shows the performance of a screen device with 2 to 1 pleating (which increases screen area without increasing screen-device cross-sectional area or safety factor). Clearly, the screen-device performance is enhanced, and no gas ingestion occurs during valve opening, and in Figure 15, with 5 to 1 pleating, the pressure pulses are attenuated even more. However, it should be noted that gas ingestion still occurs during shutdown with 5 to 1 pleating, and because there is five times the screen area, even more gas volume is ingested than for the 2 to 1 pleated screen (or the baseline screen) despite the reduction in pressure pulse intensity. This assumes that gas ingestion occurs over the entire screen surface, when in fact experience indicates that there are preferential bubble

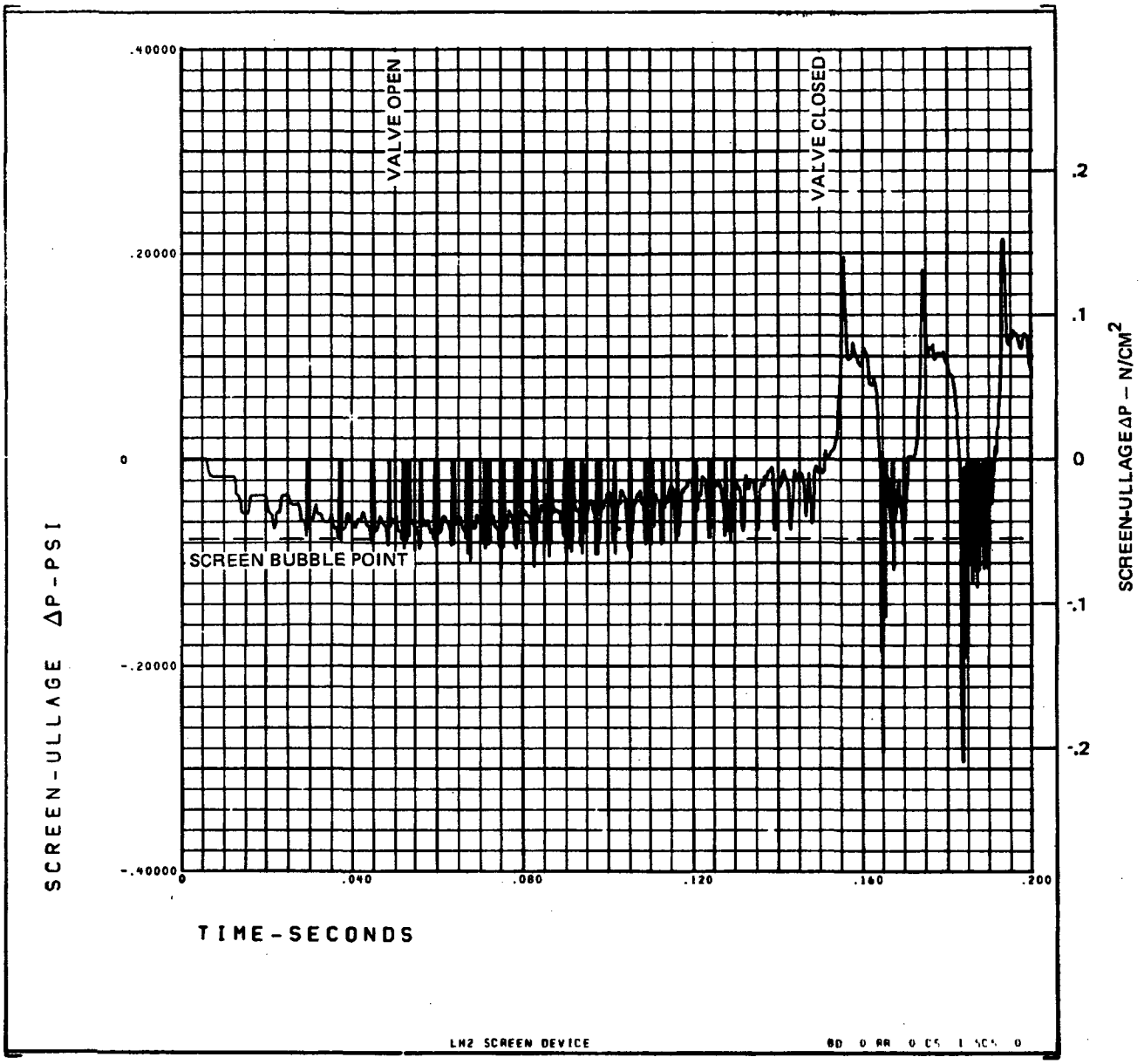

Figure 11. Screen Device Performance, 2 X Effective Valve Open/Close Time

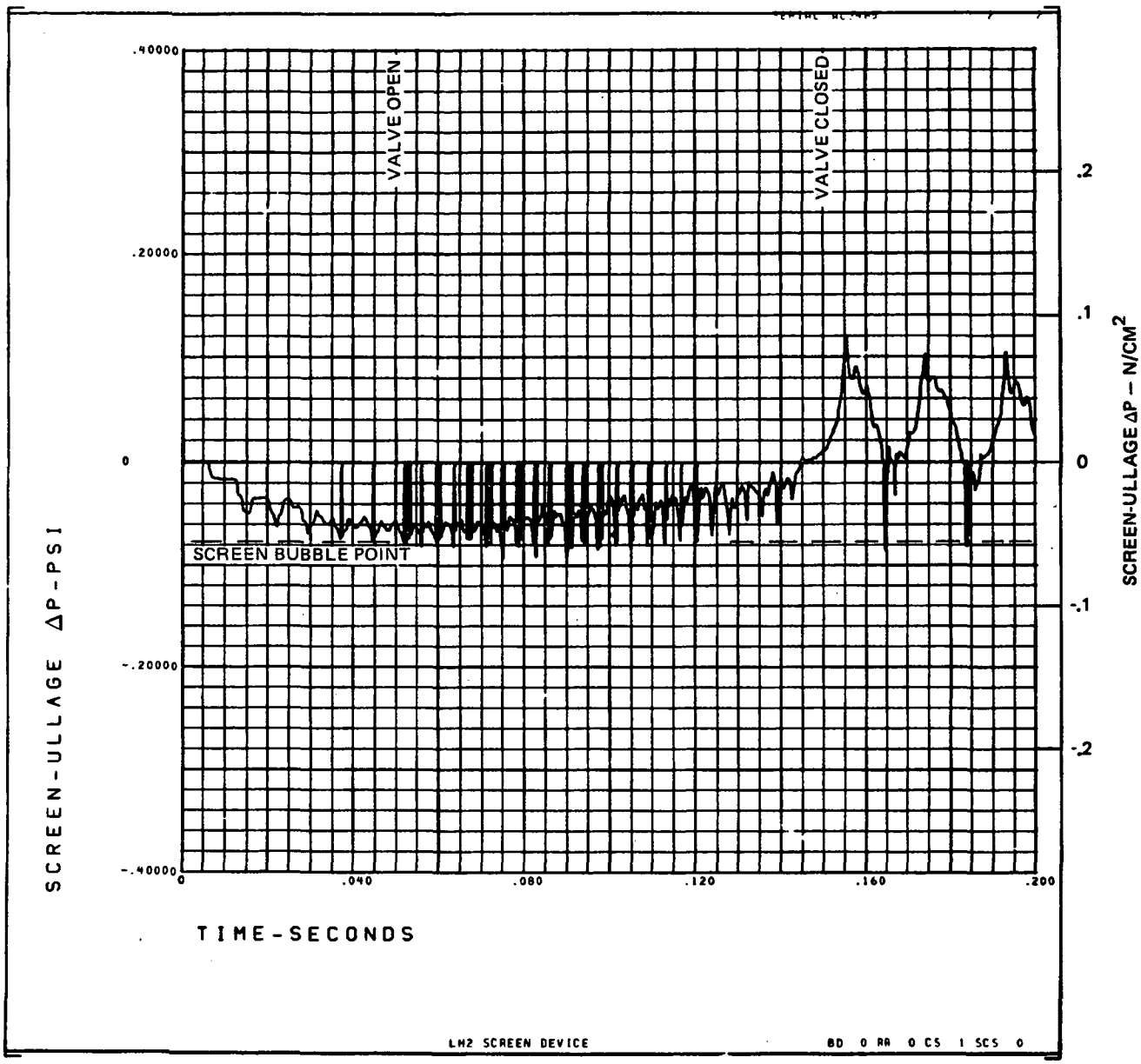

Figure 12. Screen Device Performance, 5 X Effective Valve Open/Close Time

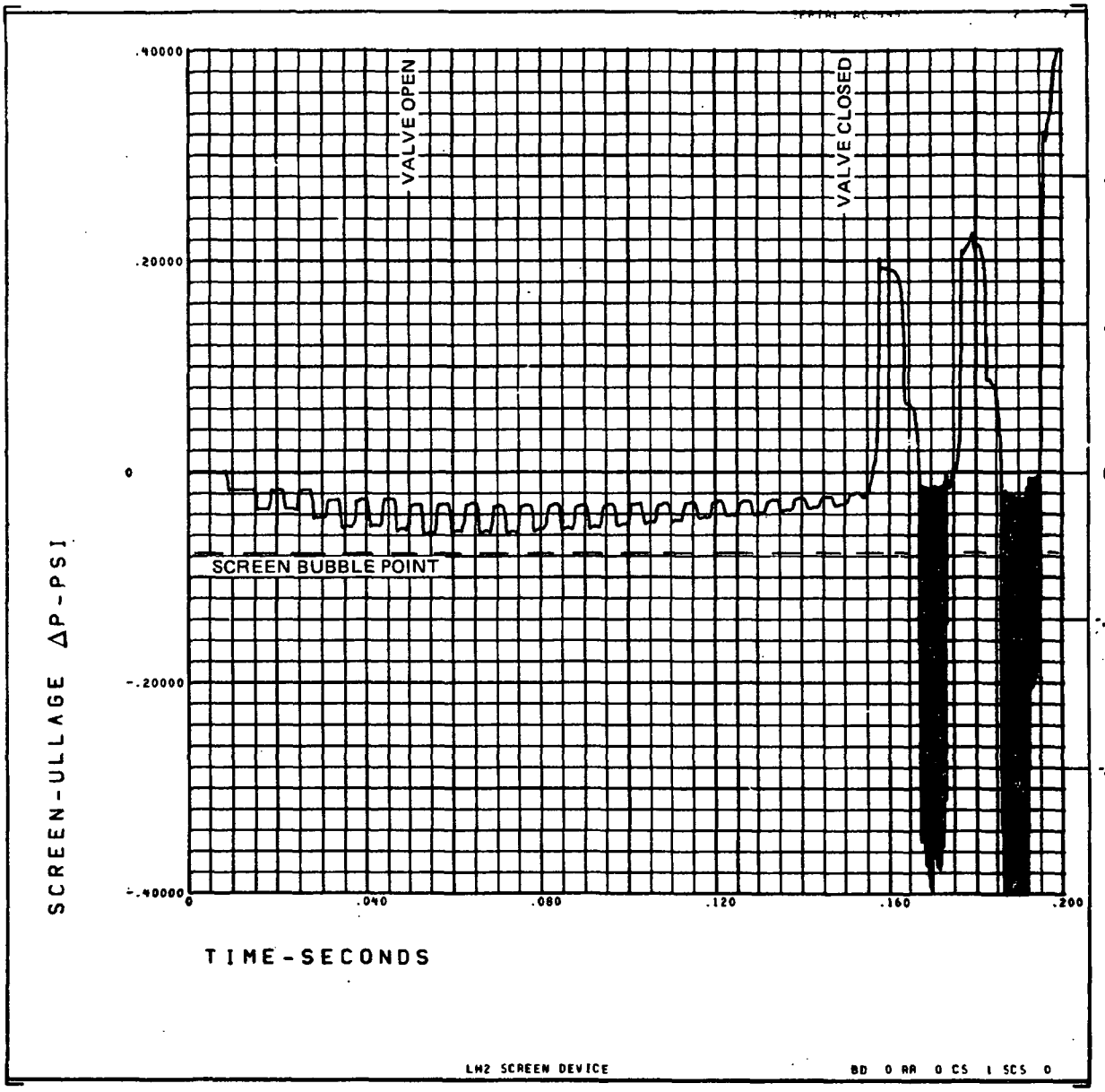

Figure 13. Screen Device Performance, Screen-Valve Distance = 3.05m (10 ft)

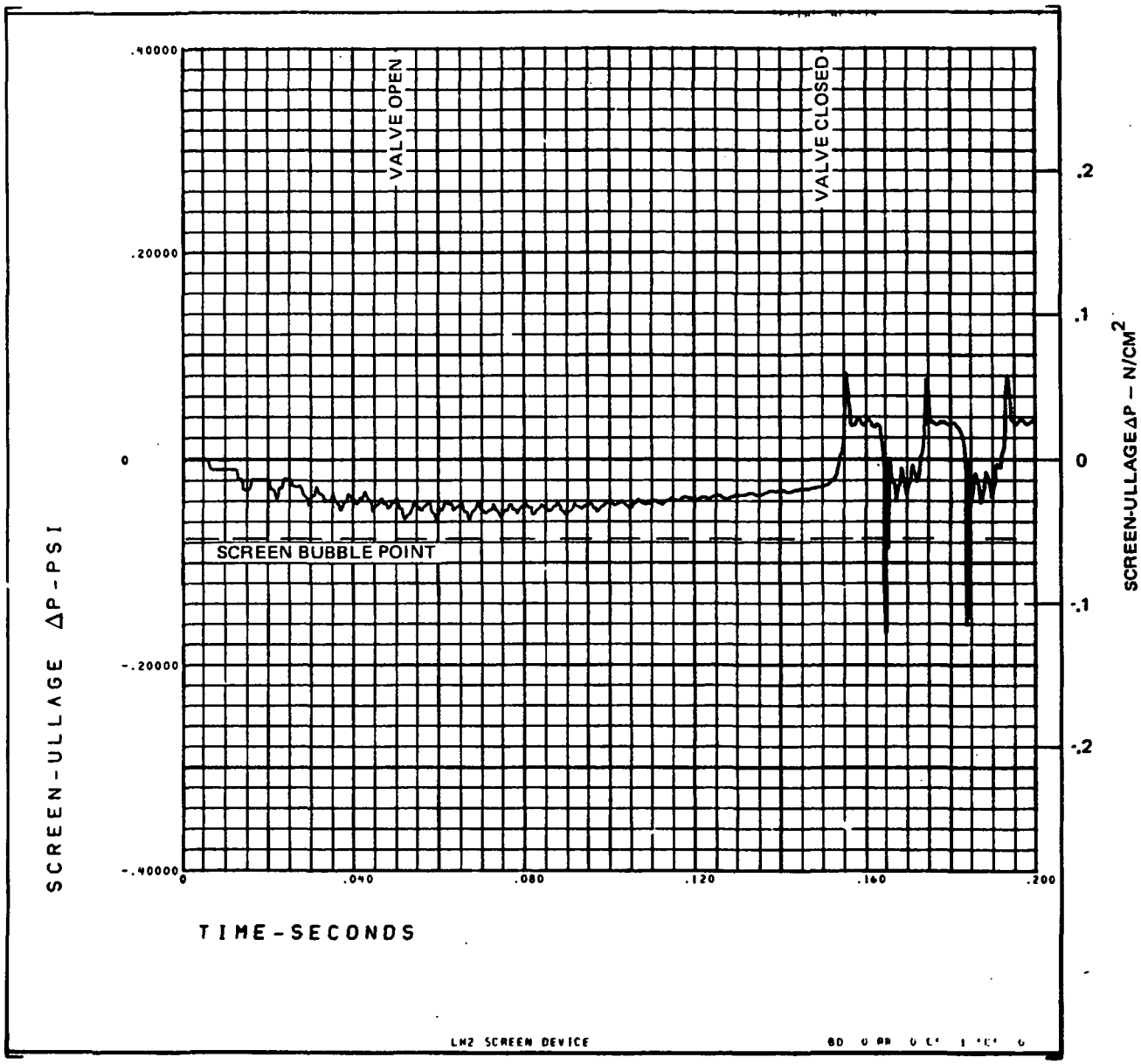

Figure 14. Screen Device Performance, 2/1 Pleated Screen Area

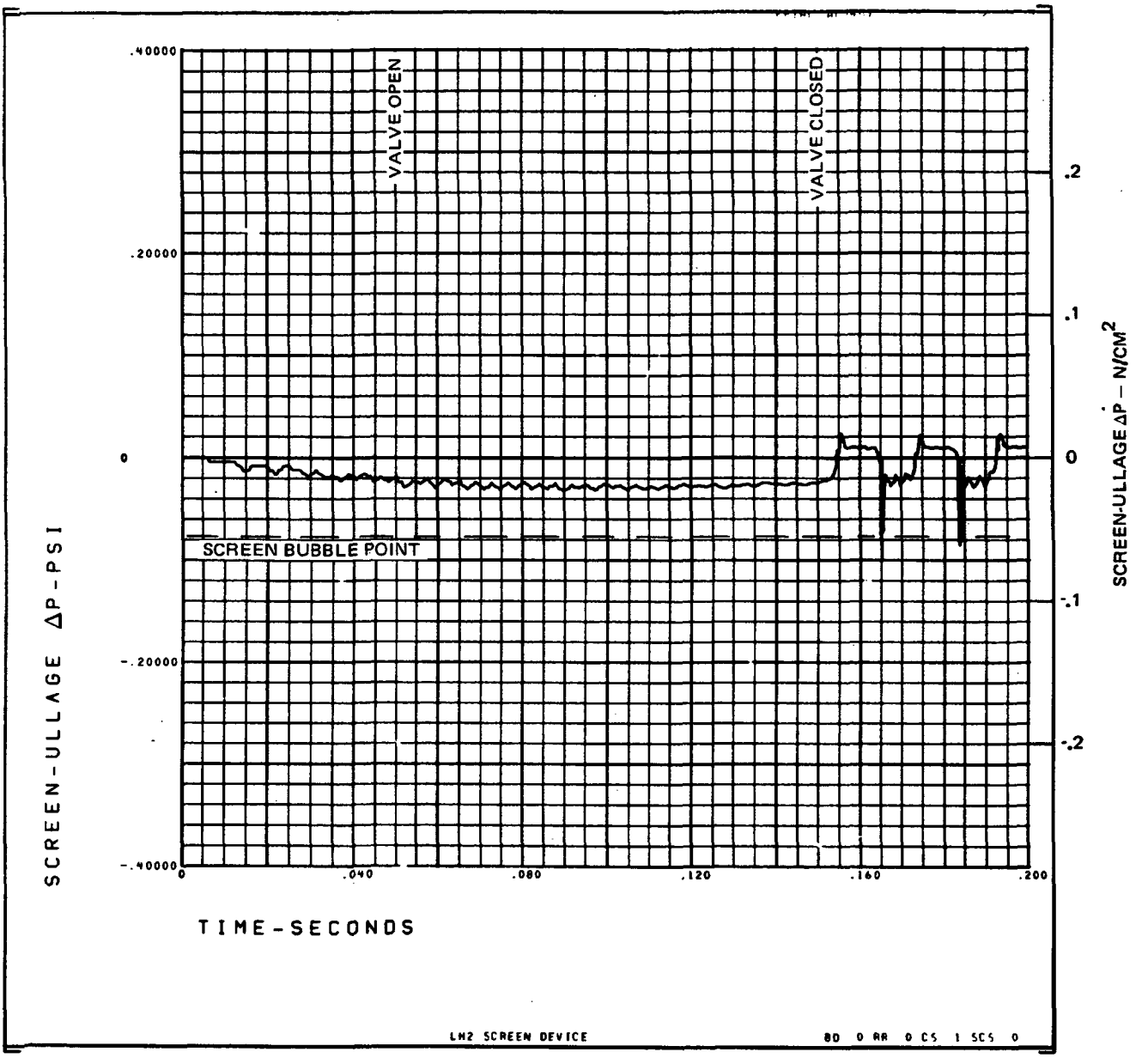

Figure 15. Screen Device Performance, 5/1 Pleated Screen Area

breakthrough locations (missing wires, pinholes, etc.) on the screen. However, the total gas ingestion required to satisfy the system flow and head balances should not be affected by whether ingestion occurs at a few points or over the entire screen surface. Because of this area effect, pleating is most effective when used in conjunction with other attenuation methods so that the pressure pulse is reduced to a value less than the bubble point and zero gas ingestion occurs.

Another method of providing increased screen area is to increase the diameter of the screen device, but this decreases the velocity and dynamic head in the device, thus increasing the screen device safety factor. Figure 16 shows the performance of the screen device with the diameter increased by the fourth root of 2, so that the safety factor is doubled to 4. Gas ingestion is eliminated during valve opening, and much reduced during shutdown. Another method of increasing safety factor, and one over which the designer may have little control, is to reduce the flow rate. Figure 17 shows the performance of the screen device with the flow reduced by the square root of 2, so that the safety factor is again doubled to 4. Note that, although gas ingestion is reduced, flow-rate reduction is not as effective as diameter increase because no increase in screen area is obtained.

Cryogenic Boiling Test Cases

The results for the second test case for cryogenic boiling pressure surge are shown in Figure 18. The magnitude of the pressure surge (to a peak of 29.3 N/cm^2 (42.5 psia) in 0.26 sec) is shown on the top of the figure. The screen-ullage pressure differential is shown on the bottom of the figure. The initial results for the first 0.06 sec (during valve opening) are essentially identical to those shown in Figure 8. It can be seen that the screen can easily accommodate the reverse flow caused by the downstream pressure surge with no problems of excessive stress or bubble ingestion.

It was thought that LO_2, with its higher surge pressure, might be a more severe case for screen device performance. However, although the pressure surged to 75.66 N/cm^2 (109.73 psia) in 4.11 sec, no gas ingestion occurred during startup, shutdown, or during the cryogenic pressure surge, because of the higher surface tension of LO_2 (compared to LH_2). Therefore, it was judged that LH_2 propellant represented a more severe test of screen device

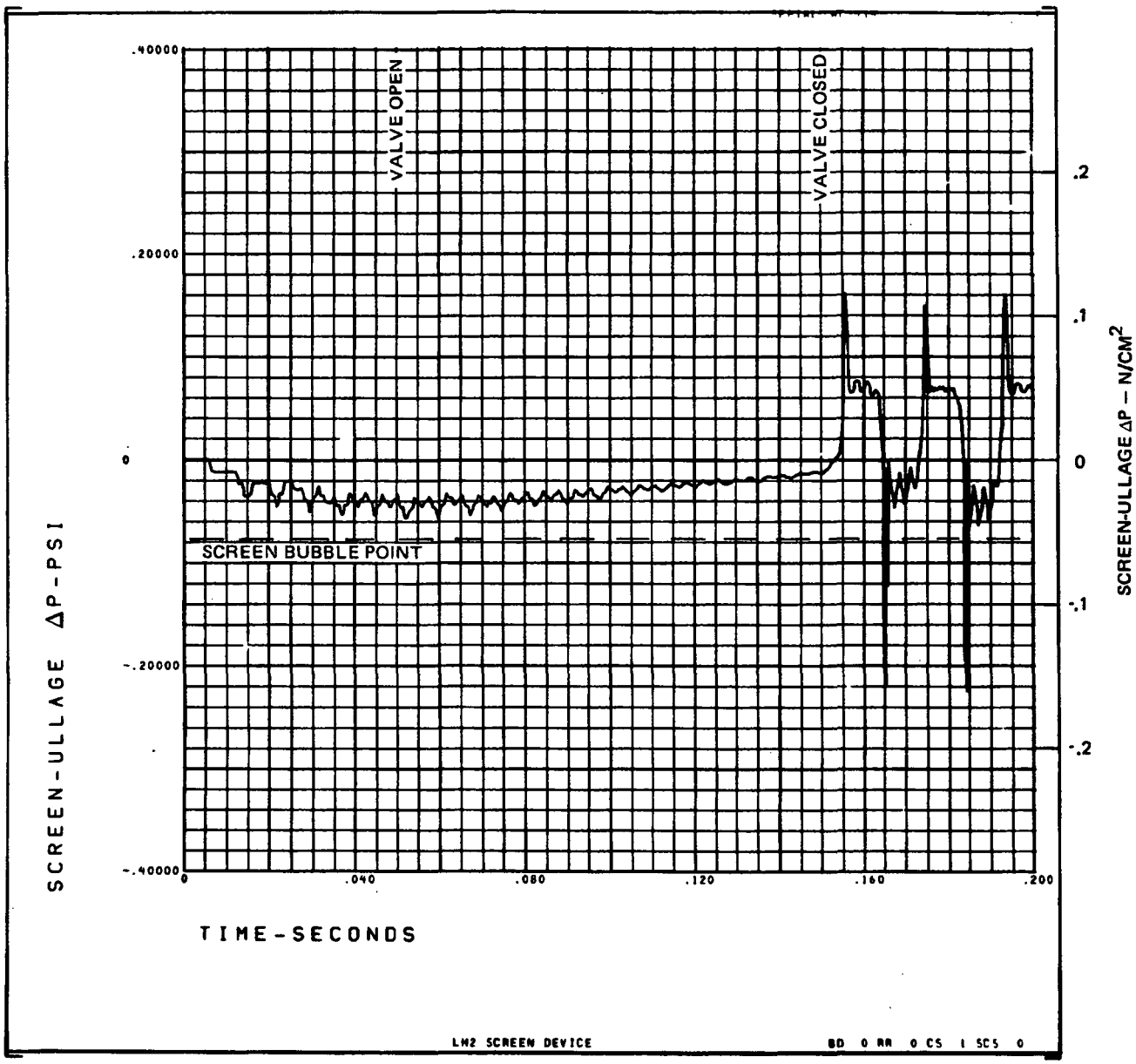

Figure 16. Screen Device Performance, Increased Screen Device Diameter

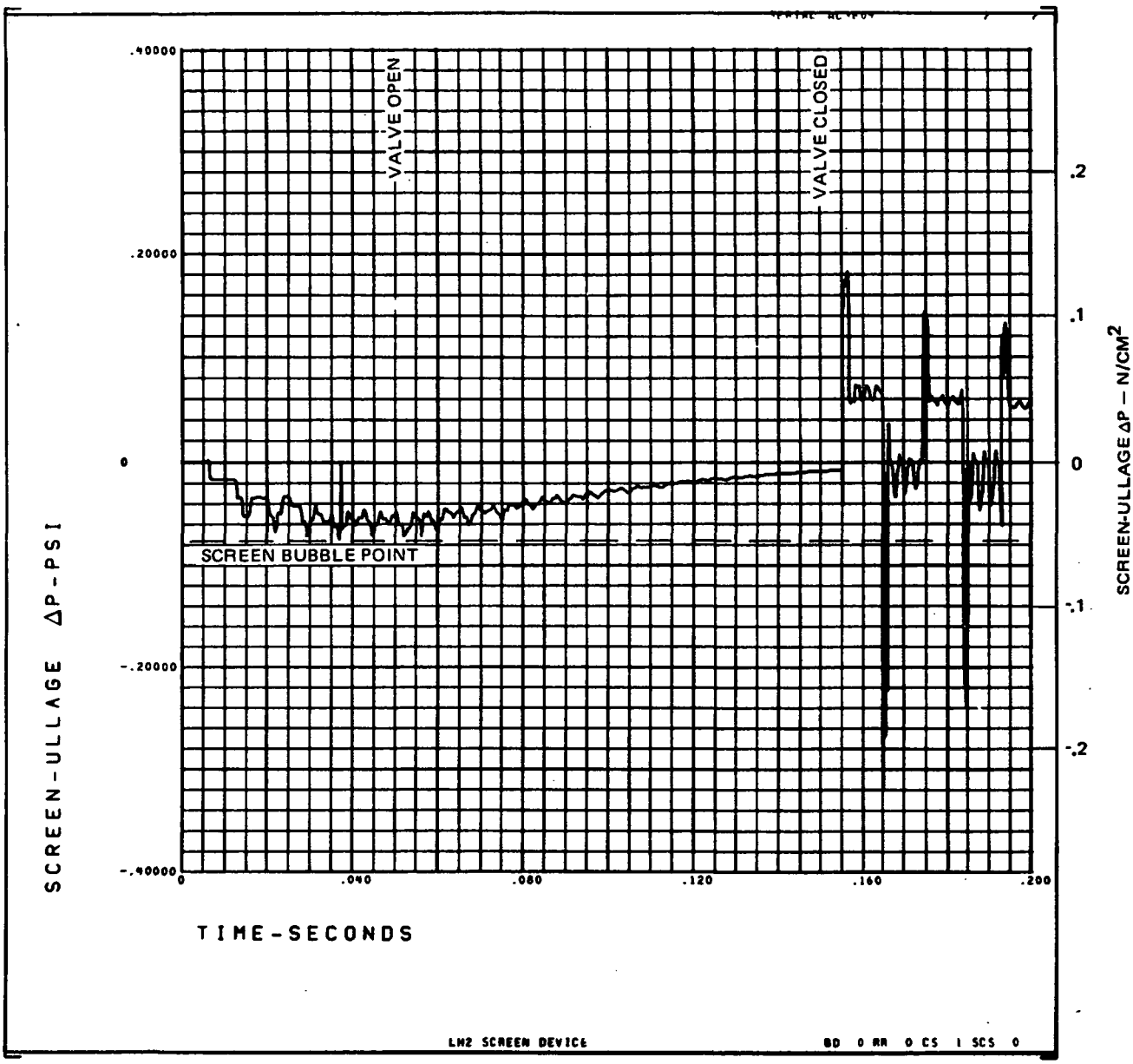

Figure 17. Screen Device Performance, Decreased Screen Device Flowrate

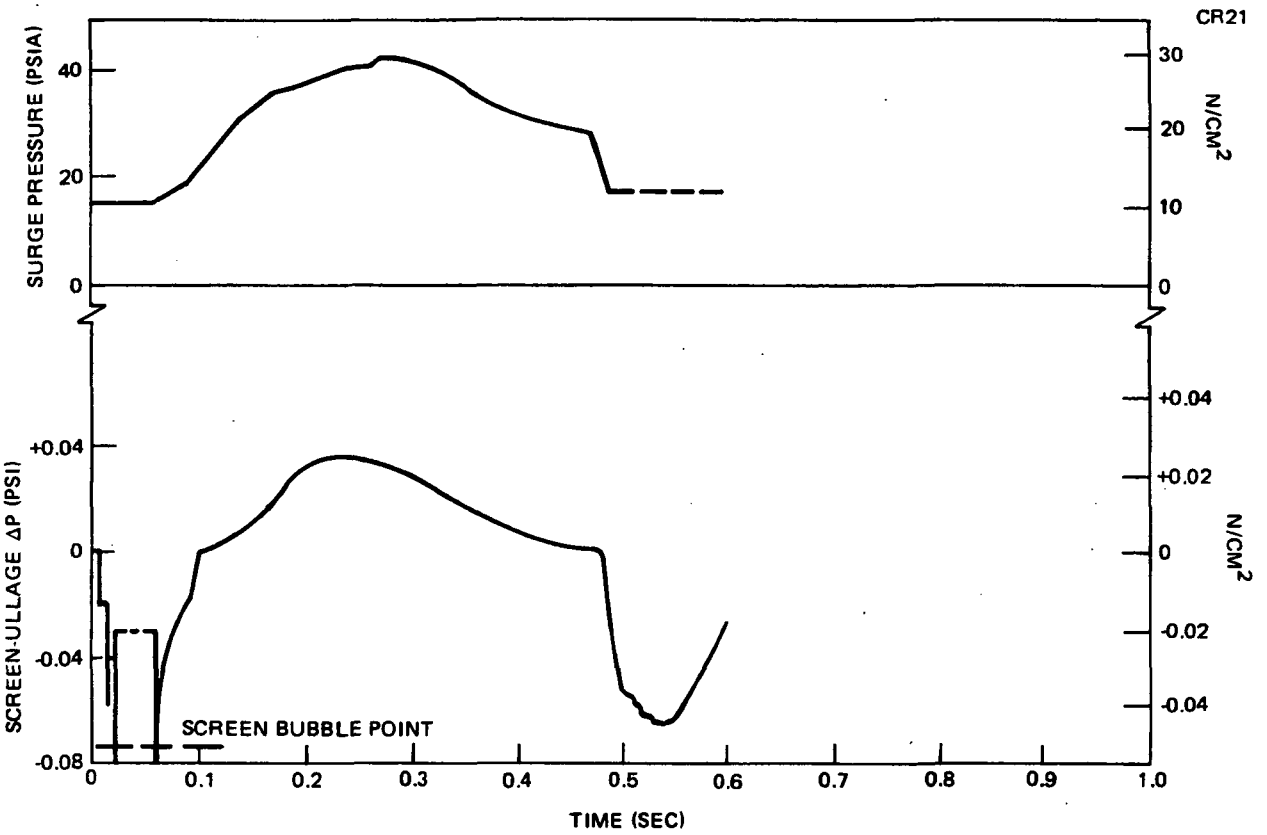

Figure 18. Cryogenic Pressure Surge – Screen Pressure Transient

performance. The screen device responded to the LO_2 cryo-surge in the same manner as for the LH_2 – it out flowed easily during the pressure surge backflow and the maximum screen-ullage pressure differential reached was only 0.0169 N/cm^2 (0.0245 psi).

These preliminary results implied that cryogenic pressure surges may not be as serious a problem as other dynamic effects. This would be investigated further in the experimental program.

Centaur D-1S Test Cases

The Centaur D-1S Acquisition System (Reference 3) was analyzed using the P4557 Cryosurge Code and the H672 Transient Analysis. A significant increase in the complexity of the model was required to simulate a screen device surrounded by both liquid and gas, the subcooler, and the branched lines to the two RL-10 engines. The model and the required parameters are shown in Appendix G for both the LH_2 and LO_2 feed systems. The P4557 Code was used to determine the cryogenic pressure surge for the two propellants. It was assumed that the worst case would be the engine chilldown

and startup with the sump and boostpump chilled and filled. The sump/pump chilldown was at very low flowrates (0.159 kg/sec (0.35 lb/sec) for LH_2 and 0.0658 kg/sec (0.145 lb/sec) for LO_2 while the engine chilldown and startup rates were much higher: 5.08 kg/sec (11.2 lb/sec) of LH_2 and 25.58 kg/sec (56.4 lb/sec) of LO_2. The temperatures of the feedlines were specified in Reference 3 as 144.4 K (260°R) for LH_2 and 150 K (270°R) for LO_2. The engine chilldown valve opening times were assumed at 0.05 sec (Reference 3). The engine feedline diameters were assumed to be 6.35 cm (2.5 in) for both the LH_2 and LO_2 systems (Appendix A) and in order to obtain the necessary restriction caused by the LO_2 valve/injection and the LH_2 chilldown valve, these large-diameter lines were made long to obtain the proper flowrate. For the LH_2 side, the pressure peaked at 14.62 N/cm^2 (21.2 psia) in 0.08 sec. compared with the tank driving pressure of 14.13 N/cm^2 (20.5 psia). This pressure surge is so small and so close to the driving pressure that it was judged to have a negligible effect on the screen dynamic performance (recall that the H672 test case surge of 29.3 N/cm^2 (42.5 psia) relative to the 17.24 N/cm^2 (25 psia) driving pressure had no adverse dynamic effect, as discussed previously). The LO_2 pressure surge case was complicated by limitations of the model: the higher-density LO_2 surged much farther into the artificially long pipe than the actual distance. The pressure surged to 18.27 N/cm^2 (26.5 psia) – relative to the 21.72 N/cm^2 (31.5 psia) driving pressure – at 0.13 sec, subsided, again reached 18.27 N/cm^2 at 3.27 sec, and continued to climb due to the increased heat transfer from the artificially long pipe surrounding the LO_2. Accordingly, the heat transfer was reduced to approximately the correct value by correcting the boiling heat flux and pipe wall temperature. This resulted in a maximum pressure of 18.75 N/cm^2 (27.2 psia) in 0.74 sec, which then subsided and did not reach the driving pressure of 21.72 N/cm^2 (31.5 psia) until 41 sec. This was longer than the engine start transient time (Reference 3); thus it was judged that cryogenic pressure surge was not a significant problem for the Centaur startup, and hence it was ignored in the Centaur dynamic simulation.

The simulation setup shown in Appendix G was run for engine valve startup and shutdown, assuming that the half of the screen device surrounded by vapor was next to the tank outlet (probably true for valve opening). The LH_2 screen device was modeled as a 16.1-cm (6.34 in) diameter tube, 2.44-m (8 ft) long with the screen fraction, f, set at 1.5 to give the proper screen

area. The four LO_2 channels were combined into one 15.2 cm (6.0 in) diameter tube, 20.8 cm (8.2 in) long, with f equal to 6.2 to give the proper screen area. For the LH_2 case, the maximum screen-ullage pressure difference during opening was 0.0234 N/cm^2 (0.034 psi) at 0.93 sec in the screen surrounded by vapor (well below the bubble point of 0.051 N/cm^2 (0.074 psi), and in the part of the screen surrounded by liquid, only 0.0022 N/cm^2 (0.0032 psi). After valve closing, three pressure pulses were strong enough to ingest vapor, with a maximum quality of 1.465%. However, this was based on the assumption that the screen was surrounded by vapor at the tank outlet; actually, at engine shutdown, the screen will almost certainly be covered with liquid at the tank outlet because of thrust settling. Therefore, the case was rerun with the screen half covered by liquid at the tank outlet. The maximum pressure differential in the screen surrounded by vapor was 0.000324 N/cm^2 (0.00047 psi).

For the case of LO_2, with the screen surrounded by vapor at the tank outlet, the maximum pressure difference during opening was 0.00331 N/cm^2 (0.0048 psi) (compared with a bubble point of 0.31 N/cm^2 (0.45 psi). At shutdown, with the same model, the difference was 0.029 N/cm^2 (0.042 psi). It therefore appears that the design of the Centaur acquisition system is more than adequate for engine startup/shutdown dynamics. Because the complex Centaur system simulation yielded little additional design information, the other system simulations were not performed.

Test Matrix Development

The Centaur D-1S simulation and the results of the LH_2 test cases were reviewed and the relevant parameters and their effects are shown in Table 7. In addition to preliminary coupon tests to determine screen properties of elastic modulus, Poissons ratio, proportional limit, and a bubble point check, the original test matrix proposed in Reference 18 included five basic horizontal specimens and two vertical specimens (see Table 2-4 of Reference 18), together with two methods of attenuation: an accumulator and a diameter-ratio attenuator. Because of the importance of screen/structure properties and pleating in their effect on device response, and in concurrence with the NASA project manager, it was decided to eliminate attenuation devices and substitute seven additional test specimens to evaluate these influences. The test specimens are shown in Table 8, and are representative

Table 7

PARAMETER SENSITIVITY ANALYSIS RESULTS

	Parameter	Effect on Screen-Ullage Pressure Difference
1.	Screen/Structure Properties, Effective E	Strong
2.	Pleating to Increase Screen Area	Strong
3.	Effective Valve Opening Time	Moderate
4.	Effective Valve Closing Time	Strong
5.	Screen-Valve Distance	Moderate
6.	Device Diameter, Increased Safety Factor	Moderate
7.	Device Flowrate, Increased Safety Factor	Moderate
8.	Saturated or Subcooled Fluid	
	A. Freon 114	None
	B. LH_2	Weak

Table 8

TEST SPECIMEN CONFIGURATIONS AND NOMENCLATURE

	Specimen					
	Vertical	Horizontal				
Screen	Plain	Plain	Pleated	Coarse Screen Backup	Perforated Sheet Backup No. 1	Perforated Sheet Backup No. 2
325 x 2300	AV	AH				
200 x 1400	BV	BH	BP	BS	BP1	BP2
720 x 140		CH				
165 x 800		DH	DP	DS	BP1	
500 x 500		EH				

of the construction methods generally employed in screen devices: plain screens, pleated screens, screens backed up with coarse screen (e.g., 14 x 14 mesh), and screens backed up with perforated sheet. It was anticipated that the degree of screen preload against the backup perforated sheet could be significant, so that two degrees of preload were evaluated, using 200 x 1400 mesh (see Table 8).

The experiment matrix covers five screens of different types. The usual fine-mesh dutch twill screens were selected, represented by 325 x 2,300 mesh and 200 x 1,400 mesh, plus the plain dutch 165 x 800 mesh. These weaves are often used for screen devices and considerable data on their properties are available. A reverse dutch weave, 720 x 140 mesh, was selected because it was anticipated that it would have a larger elastic modulus than Dutch twill screens. The fifth screen selected was 500 x 500 mesh twilled square-weave screen which probably would never be used in a screen device because it is too flimsy, but which has the advantages of equal orthotropic elastic moduli and an analytically predictable open area (which will be an advantage for later analytical correlation). All of the screens were of stainless steel because fine-mesh screens of aluminum are costly and difficult to obtain. The bubble point and flow loss coefficients of all these screens have been determined previously (Reference 1) using LH_2 at 50 psi. The screens employed for the screen/structure integration evaluation were the dutch twill 200 x 1,400 mesh and the plain Dutch 165 x 800 mesh.

From Table 7, the screen-valve distance had a moderate effect on valve opening and closing pressure surges, while the effective valves opening/closing time had a moderate to strong effect. Therefore, these were selected as additional parameters in the test matrix. Since the device diameter is fixed, the most convenient way to vary the safety factor is to vary the flowrate, again a matrix parameter. The initial value of flowrate will be set to give a safety factor of 2, the next value will be double or halve the safety factor, depending on the results of the first test.

Selection of the proper test fluids was an important consideration for the experimental program. Isopropyl alcohol, an inert fluid with known characteristics and which allows good visibility, was selected to evaluate the fluid dynamic transient effects. MDAC has had considerable experience in testing screens with isopropyl alcohol (References 1, 4, and 8) and has found it an excellent bubble point simulant for LH_2. To determine the combined fluid dynamic and boiling pressure surge transient effects, a simulant fluid with a lower boiling point was required. Freon 114, with a normal boiling point of 276.7K (38°F), was selected for this fluid. The Freons are characterized

by inertness, nonflammability, low toxicity, good transparency, and a wide range of fluid properties. The other potentially usable Freon was Freon 21, which boils at 282.2K (48°F). However, because this is a powerful solvent which dissolves plexiglass (our proposed test apparatus material, see below), it was rejected. Freon 114, while compatible with plexiglass, exhibits many other desirable properties, principally that it is an excellent simulant for LO_2. It has virtually the identical bubble point, a somewhat higher laminar flow loss coefficient (due to the low viscosity of LO_2) and only a 24% lower speed of sound than LO_2. LH_2 was selected as the third test fluid to evaluate the combined fluid dynamic and thermal pressure transient effects on screens using an actual propellant with a high probability of use in space vehicle screen acquisition systems.

It was predicted that with Freon 114, there would be essentially no effect of subcooling (or pipe temperature) on the boiling pressure surge because the Freon 114 pressure slowly converged on saturation with no pressure spike. Two data points were planned to check this nondependence on subcooling and pipe temperature using the less attenuated vertical configuration. The balance of the tests would be run at saturated conditions in a room-temperature pipe.

For LH_2, on the other hand, subcooling was predicted to be more important (but still a relatively weak effect due to the rapidity of the pressure spike), but the wall temperature was not predicted to be an effective variable. The LH_2 tests, therefore, would be run at both saturated and subcooled conditions at one wall temperature, except for one point as a check.

The final recommended test matrix is shown in Table 9 and consists of 178 tests. It was anticipated that the choice of pipe length and valve open and close time for the Freon 114 tests would be influenced by the results of the alcohol tests, considering the lower surface tension of Freon 114. For the LH_2 tests, only the short line was planned because of apparatus limitations and the requirement to keep LH_2 up to the valve. Also, because of the rapidity of the LH_2 cryogenic pressure surge, only the relatively fast valve open and close time value was planned for the matrix.

Table 9 (Page 1 of 2)

PLANNED TEST MATRIX

Fluid	Specimen	Line	Valve T	Fluid Condition	Flow Rate
Alcohol	AH	S	F		Q1, Q2
92 tests	AH	S	SL		Q1, Q2
	AH	L	F		Q1, Q2
	AH	L	SL		Q1, Q2
	AV	L	F		Q1, Q2
	AV	L	SL		Q1, Q2
	BH	S	F		Q3, Q4
	BH	S	SL		Q3, Q4
	BH	L	F		Q3, Q4
	BH	L	SL		Q3, Q4
	BV	L	F		Q3, Q4
	BV	L	SL		Q3, Q4
	BP	S	F		Q3, Q4
	BP	S	SL		Q3, Q4
	BP	L	F		Q3, Q4
	BS	S	F		Q3, Q4
	BS	S	SL		Q3, Q4
	BS	L	F		Q3, Q4
	BS	L	SL		Q3, Q4
	BP1	S	F		Q3, Q4
	BP1	S	SL		Q3, Q4
	BP1	L	F		Q3, Q4
	BP1	L	SL		Q3, Q4
	BP2	S	F/SL[1]		Q3, Q4
	BP2	L	F/SL[1]		Q3, Q4
	CH	S	F		Q5, Q6
	CH	S	SL		Q5, Q6
	CH	L	F		Q5, Q6
	CH	L	SL		Q5, Q6
	DH	S	F		Q7, Q8
	DH	S	SL		Q7, Q8
	DH	L	F		Q7, Q8
	DH	L	SL		Q7, Q8
	DP	S	F		Q7, Q8
	DP	S	SL		Q7, Q8
	DP	L	F		Q7, Q8
	DS	S	F		Q7, Q8
	DS	S/L[2]	SL/F[2]		Q7, Q8
	DS	L	F/SL[2]		Q7, Q8
	DP1	S	F		Q7, Q8
	DP1	S/L[3]	SL/F[3]		Q7, Q8
	DP1	L	F/SL[3]		Q7, Q8
	EH	S	F		Q9, Q10
	EH	S	SL		Q9, Q10
	EH	L	F		Q9, Q10
	EH	L	SL		Q9, Q10

[1] [2] Extreme case of BP1

[2] [3] Extreme Case of BS

[3] Extreme Case of DS/BPI

Specimen See Table 8

Line
S = Short
L = Long

Valve T
F = Fast
SL = Slow

Table 9 (Page 2 of 2)

PLANNED TEST MATRIX

Fluid	Specimen	Line	Valve T	Fluid Condition	Flow Rate
Freon 114	AH	S	F	SAT, T1	Q11, Q12
60 tests	AH	S/L[4]	SL/F[4]	SAT, T1	Q11, Q12
	AH	L	F/SL[4]	SAT, T1	Q11, Q12
	AV	L	F	SAT, T1	Q11, Q12
	AV	L	F	SUB, T1	Q11, Q12
	AV	L	SL	SAT, T1	Q11, Q12
	AV	L	SL	SUB, T2	Q11, Q12
	BH	S	F	SAT, T1	Q13, Q14
	BH	S/L[4]	SL/F[4]	SAT, T1	Q13, Q14
	BH	L	F/SL[4]	SAT, T1	Q13, Q14
	BV	L	F	SAT, T1	Q13, Q14
	BV	L	SL	SAT, T1	Q13, Q14
	BP	S	F	SAT, T1	Q13, Q14
	BP	S	SL	SAT, T1	Q13, Q14
	BP	L	F	SAT, T1	Q13, Q14
	BS	S	F	SAT, T1	Q13, Q14
	BS	S/L[4]	SL/F[4]	SAT, T1	Q13, Q14
	BS	L	F/SL[4]	SAT, T1	Q13, Q14
	BP1	S	F	SAT, T1	Q13, Q14
	BP1	S/L[4]	SL/F[4]	SAT, T1	Q13, Q14
	BP1/BP2[5]	L	F/SL[4]	SAT, T1	Q13, Q14
	CH	S	F	SAT, T1	Q15, Q16
	CH	S/L[4]	SL/F[4]	SAT, TI	Q15, Q16
	CH	L	F/SL[4]	SAT, T1	Q15, Q16
	DH	S	F	SAT, T1	Q17, Q18
	DH	S/L[4]	SL/F[4]	SAT, T1	Q17, Q18
	DH	L	F/SL[4]	SAT, T1	Q17, Q18
	EH	S	F	SAT, T1	Q19, Q20
	EH	S/L[4]	SL/F[4]	SAT, T1	Q19, Q20
	EH	L	F/SL[4]	SAT, T1	Q19, Q20
LH_2	AH	S	F	SAT, T1	Q21, Q22
26 tests	AH	S	F	SUB, T1	Q21, Q22
	AH	S	F	SUB, T2	Q21, Q22
	AV	S	F	SAT, T1	Q21, Q22
	AV	S	F	SUB, T1	Q21, Q22
	BH	S	F	SAT, T1	Q23, Q24
	BH	S	F	SUB, T1	Q23, Q24
	BP	S	F	SAT, T1	Q23, Q24
	BP	S	F	SUB, T1	Q23, Q24
	BS	S	F	SAT, T1	Q23, Q24
	BS	S	F	SUB, T1	Q23, Q24
	BV	S	F	SAT, T1	Q23, Q24
	BV	S	F	SUB, T1	Q23, Q24

[4]Extreme based on alcohol data

[5]If BP2 effect from alcohol data

Specimen See Table 8

Line
S = Short
L = Long

Valve T
F = Fast
SL = Slow

Fluid Condition
SAT = Saturated
SUB = Subcooled

EXPERIMENTAL PROGRAM

The experiment planning and analysis described in the previous section indicated that the screen structural properties have a profound effect on screen device response to transient pressure surges. The only data on screen structural properties (see Reference 18) are of obscure origin, and therefore the first experimental task was to determine the structural properties of the screens to be used. Following this, the test apparatus, including screen specimen configuration, instrumentation, components, and apparatus arrangement, was designed and analyzed. Exploratory tests were performed to determine valve operating characteristics and instrumentation response and define required line length parameters, and the test apparatus was fabricated and installed. Test operational philosophy and procedures were developed, and the test matrix for all three test fluids was performed. The test results are discussed in this section, but the data correlation using the H672 analysis is presented in the section entitled "Data Correlation."

SCREEN STRUCTURAL PROPERTIES

The specimen screen mechanical properties of proportional limit stress and effective elastic moduli in both the warp and shute directions were determined using an Instron tensile testing machine. The stress was determined using the load and the actual screen wire cross-sectional area, and the elastic modulus by dividing by the actual strain as determined by a 5.08-cm (2 in) Instron strain gage. The screen specimens were generally about 2.3 by 25 cm. For all five specimen screens, the load-strain curve was determined in both the warp and shute directions. For the 14 x 14 backup mesh, the curve was determined only in the shute direction (the material was too narrow to provide a specimen of sufficient length in the warp direction). For dutch weave screens, the shute direction is parallel to the shute wires, which are the fine wires bent over and under the warp wires. The warp direction is parallel to the warp wires, which are the heavier wires laid straight along the length of the screen fabric. Exceptions are the reverse dutch, 720 x 140, which has heavier shute wires that are

PRECEDING PAGE BLANK NOT FILMED

essentially straight, and finer warp wires bent over the shute wires, and the square weave, where both warp and shute wires are bent over one another. For the dutch weave screens, the load-strain curves were of different shapes in the shute and warp directions. In the shute wire direction, shown typically in Figure 19, the initial region of the curve was straight, leading to a definite inflection point. It is believed that the springiness of the bent shute wires was responsible for this initially straight section of the curve. Complete strain-free recovery was observed along this initial section of the curve. At the inflection point, the wire springiness apparently disappeared, as the wires reached full (springy) extension, and strain deformation of the wires appeared. From this point on, strain offset appeared as shown by the reversed load, and the strain increased enormously, due probably to wire displacement. In the shute direction, therefore, the proportional limit stress was assumed to be at the inflection point shown, and the effective elastic modulus as the stress over strain at the inflection point. For the warp wires, the typical load-strain curve is shown in Figure 20. Because the warp wires are essentially straight, there was no springiness, but only simple tension. The proportional limit is the point shown where permanent set begins to occur. The screen properties are shown in Table 10. For the springy shute wires, the effective elastic modulus was one-sixth to one-third of the stainless steel modulus, while for the "straight" warp wires, the effective elastic modulus was two-thirds to three-thirds of the stainless steel modulus. Why the warp wire modulus was less than the stainless modulus is not known; one explanation may be that the warp wires are not really straight, but are slightly bent during the weaving process.

For the twilled square weave 500 x 500 screen, the effective elastic modulus was nearly identical in both the warp and shute directions, as expected, but the proportional limits were somewhat different. The reason for this is unknown, but it may have been an idiosyncrasy of the weaving process; i. e., the warp wires may have been kept tighter during weaving, thus having less available spring deflection (and load) before strain deformation occurs. One specimen, the 720 x 140/shute, was stressed to failure, which occurred at a stress of 57,000 N/cm^2 (82,700 psi), which is in agreement with the textbook value of tensile strength of 304 stainless steel (Reference 19).

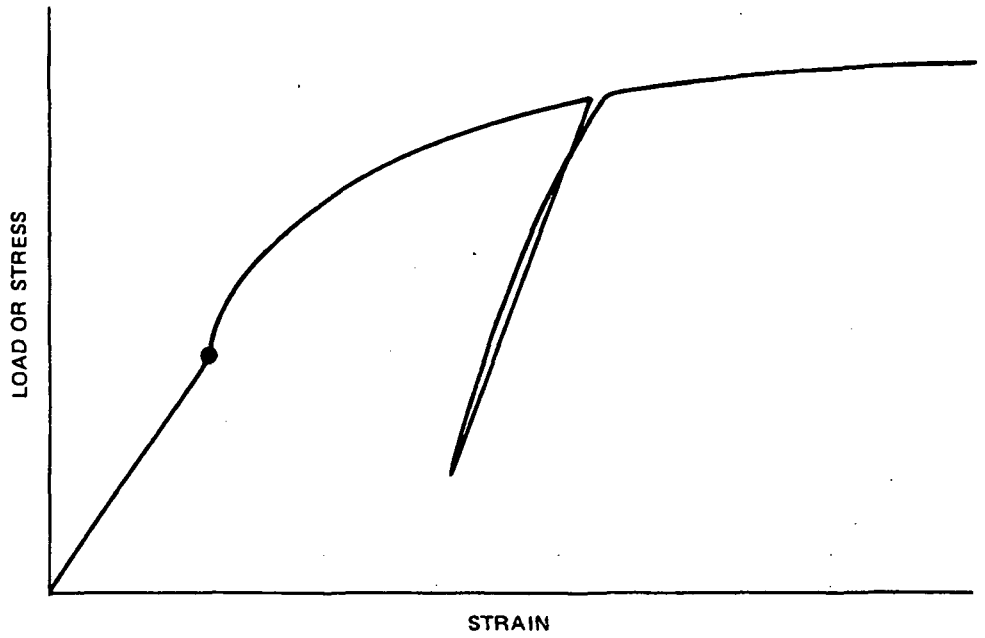

Figure 19. Load-Strain Curve for Shute Direction – Dutch Weave Screens

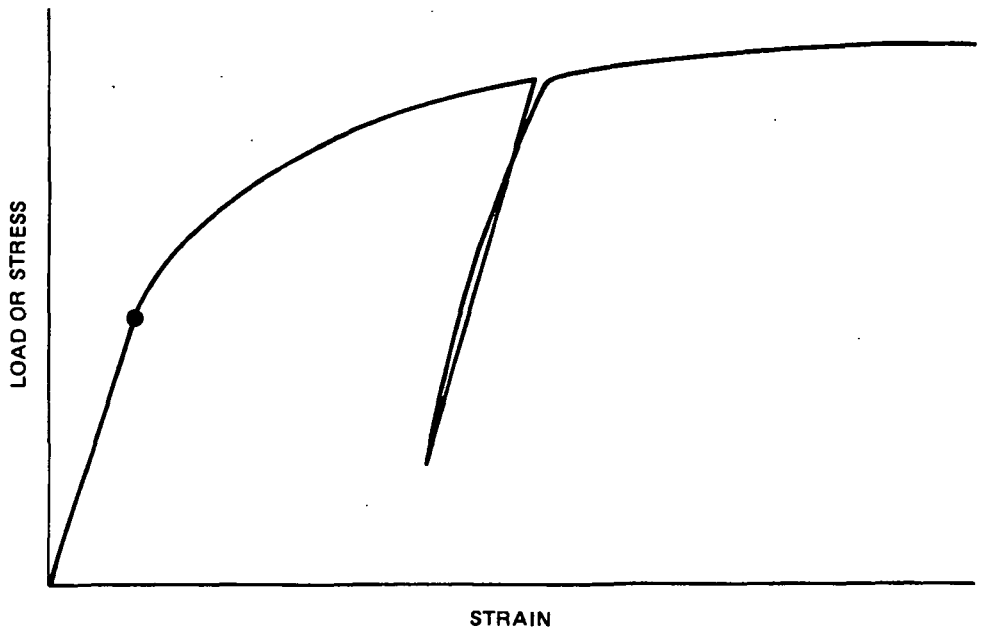

Figure 20. Load-Strain Curve for Warp Direction – Dutch Weave Screens

Table 10

SCREEN MECHANICAL PROPERTIES

Mesh	Wire Size cm (in)	Direction	Proportional Limit Stress 10^3 N/cm^2 (10^3 psi)	Effective Elastic Modulus 10^6 N/cm^2 (10^6 psi)
325 x 2300	0.00381 (0.0015)	Warp	29.1 (42.2)	22.4 (32.5)
	0.00254 (0.001)	Shute	23.0 (33.3)	5.75 (8.34)
200 x 1400	0.00711 (0.0028)	Warp	25.4 (36.8)	15.9 (23.0)
	0.00406 (0.0016)	Shute	11.4 (16.6)	4.76 (6.91)
720 x 140	0.00356 (0.0014)	Warp	16.1 (23.4)	3.23 (4.68)
	0.01092 (0.0043)	Shute	13.6 (19.7)	13.6 (19.7)
165 x 800	0.00711 (0.0028)	Warp	23.6 (34.2)	13.1 (19.0)
	0.00508 (0.002)	Shute	18.6 (26.9)	4.65 (6.74)
500 x 500	0.00254 (0.001)	Warp	15.7 (22.8)	6.04 (8.75)
	0.00254 (0.001)	Shute	21.5 (31.1)	5.96 (8.65)
14 x 14	0.0508 (0.02)	Shute	14.6 (21.2)	9.75 (14.1)

It is clear from Table 10 that the unsubstantiated data on screen elastic moduli shown in Table 2-2 of Reference 18 were completely erroneous. The implication of the much higher values of elastic moduli was that screen devices would not attenuate pressure pulses to the degree anticipated during experiment planning and may be more susceptible to breakdown.

The maximum attenuation achievable with a cylindrical screen device occurs when the minimum value of effective modulus is oriented in the circumferential direction. Therefore, the screen specimens for testing with dutch weave screens were oriented with the shute wires in the circumferential direction, the reverse dutch screen with the warp wires in the circumferential direction, and the square weave screen with the shute wires in the circumferential direction (taking advantage of the higher proportional limit stress).

TEST APPARATUS DESIGN

The basic approach to the design of the test apparatus was to design a configuration which could be used interchangeably in all three test fluids and to use the same dewar, components, lines, instrumentation, and data equipment (where possible) for all three fluids. The advantage of this approach is that random configurational variations could be eliminated and an accurate determination made of the interaction of screen properties (such as bubble point, flow loss characteristics, and moduli of elasticity) and fluid properties. The basic test tank selected was a 0.13 m^3 (35 gal) LH_2 dewar of 34.5 N/cm^2 (50 psig) working pressure which has been used by MDAC in many previous screen test programs (References 1, 2, 4, and 8). The dewar has five quartz windows which allow lighting and observation of the test specimen. Excellent viewing, even in LH_2, had been experienced in the past.

The instrumentation to be used for data acquisition during the test program may impact both the design of the screen specimen and the arrangement of the components within the test apparatus; hence, the instrumentation was evaluated and selected first. One of the most important requirements of the test program was to assure that adequate data would be obtained in order to achieve analytical correlation. The basic transient data are pressure,

gas-liquid differential pressure, and flowrate. For the isopropanol and Freon 114 tests, obtaining adequate transient pressure data was not anticipated to be a problem: available Endevco piezoelectric transducers could be used for dynamic pressure measurement, and Statham strain-gage transducers of 0-0.7 N/cm^2 (1.0 psid) could be used for screen gas-liquid pressure differential measurements. These transducers would be close-coupled to the test specimen to obtain maximum dynamic response.

However, these transducers are temperature-limited, and cannot be close-coupled (or submerged) in the LH_2 tests. In fact, there are very few pressure transducers usable at LH_2 temperature, and with these the electronics are invariably located at ambient temperature. The usual problems with these transducers are inaccuracy, zero shift, and requirement for frequent recalibration. To circumvent these difficulties, redundant pressure and ΔP transducers could be installed on long sensing lines and situated outside the dewar. During the isopropanol and Freon 114 tests, the data from these redundant transducers could be compared to the close-coupled transducer data to determine the effective lag, and this could be correlated with fluid properties. During the LH_2 tests, only the remote transducers could be used, and the data could be corrected for the lag. This technique has problems, however; variations in the predicted lag may occur because of variations in the condition of the fluid in the sensing line, and further, remote sensing lines in LH_2 are prone to purging and freezing problems.

Because of the potential problems with LH_2 pressure and ΔP measurements, dynamic flow-measurement techniques were also investigated thoroughly. Flow measurements would be required both for steady flow (to regulate the flow velocity to values consistent with screen device design requirements) and for transient flow surges and reversal in lines and screen device. Since the LH_2 tests would be the most severe, it was deemed desirable that the same flowmeter should be used for all of the tests. An exhaustive search was made to determine the basic kinds of flowmeters suitable for use with LH_2, which also promise to give reasonable dynamic response. There were only three basic kinds of flowmeters found: turbine flowmeter with magnetic pickup, turbine flowmeter with nonmagnetic pickup, and vortex-shedding flowmeter. The turbine flowmeter with magnetic pickup was found to be generally available and has been completely developed for use with LH_2.

The turbine is made of magnetic material (ferrite) and has two severe shortcomings: the magnetic drag results in a high-velocity sensing threshold for repeatable data (~35 Hz at 3 m/sec for a 2.54-cm (1.0 in) diameter meter), and the turbine is rather brittle at LH_2 temperature and is susceptible to damage from reverse flow, gas ingestion, and strong flow pulses. The vortex-shedding flowmeter has been used with LN_2, but not with LH_2. The manufacturer sees no reason why it would not be satisfactory with LH_2. To be used with all test fluids, two sets of thermistor pickups must be used: one for near-ambient temperatures, and one for LH_2-temperature. The startup vortices do occur with laminar flow, giving a frequency threshold of ~22 Hz at 0.3 m/sec for 2.54-cm diameter. Reverse flow capability is still undeveloped, although the meter is extremely rugged, and would not be damaged by reverse flow, gas ingestion, or flow surges.

The turbine flowmeter with nonmagnetic pickup was found to eliminate the problems associated with the magnetic turbine and has been completely developed for use in LH_2. The lack of magnetic drag results in high response (~500 Hz at 0.12 m/sec for 2.54-cm diameter) and the meter pickup could be configured to explicitly record reverse flow. Because of the high response, this capability may not be necessary for our system as reverse flow could be implicitly determinable. In addition, the turbine is made of high-strength material compatible with LH_2 temperature, and could handle reverse flow, gas ingestion, and severe flow pulses without damage.

Unfortunately, the nonmagnetic-pickup turbine flowmeter was found to be costly, and its procurement was not within the scope of the contract. An exhaustive search of NASA/DoD facilities to find an existing and available unit of this type was unsuccessful. For these reasons, it was decided to evaluate the performance of a magnetic-pickup turbine flowmeter in conjunction with a high-response Ramapo drag-body flowmeter in simulant (water) flow tests. At the same time, the response of remotely located (compared to close-coupled) piezoelectric pressure transducers, and the operating characteristics of the flow-control valve could be determined.

The cryogenic valve selected to start and stop the flow during the test series was a 2.54-cm (1.0 in) diameter Flowmatics ball valve with a solenoid-operated pneumatic actuator. This was a clean valve (equivalent L/D of 3)

and hence did not offer significant flow resistance. The steady-state flowrate was controlled by dewar pressure and by adjusting a CCI cryogenic hand-operated globe valve of 2.54-cm diameter. This valve, wide open, had an equivalent L/D of about 340, and thus imparted much of the flow circuit resistance.

The pneumatically actuated cryogenic Flowmatics ball valve was checked out with water-flow tests to determine the effective valve open and close time as a function of actuation pressure. Large solenoid valves were installed on the pneumatic actuator and a 0.014 m^3 (0.5 ft^3) accumulator was used to reduce actuation time. The CCI globe valve was installed downstream of the ball valve, and the steady-state flowrate was regulated to about 6.3×10^{-5} m^3/sec (1 gpm). The effective ball valve open/close time was determined by measuring the pressure rise and fall time immediately downstream of the ball valve (upstream of the control valve). The results of the tests are shown in Table 11, together with the calculated minimum flow line length (upstream of the valve) necessary to develop the maximum water-hammer pressure surge following valve closure. Isopropanol, with its high sonic velocity, would require the longest line at 9.2 m (30.2 ft), which defines the longest line used with the isopropanol (and Freon 114) test setups.

During the same tests, the flowmeter and pressure transducer response was evaluated. The instrumentation was set up with the Flowmatics cryogenic ball valve and CCI flow control valve as shown schematically in Figure 21. The tests were run with water at about 31 N/cm^2 (45 psi) and with the flow control valve set to regulate the steady-state flowrate at about 6.3×10^{-5} m^3/sec (1 gpm). The dimensions shown in Figure 21 are in centimeters.

The coding for the Endevco piezoelectric pressure transducers is: upstream-close (UC), upstream-far (UF), downstream-close (DC), and downstream-far (DF). An example of the data for flow startup is shown in Figure 22. The bottom curve is the turbine frequency and the top curve is flowrate (increasing downward) for the Foxboro magnetic turbine flowmeter. The second curve is the flowrate (increasing downward) for the Ramapo drag body flowmeter. Note that the Ramapo flow follows exactly (but inversely) the pressure traces (increasing upward) for the UC (= P_{IN}) and DC (= P_{OUT})

Table 11

VALVE OPEN/CLOSE CHARACTERISTICS

Actuation Pressure N/cm^2 (psig)	Effective* Times (sec)	Maximum Pressure Surge Line Length, m (ft)		
		Isopropanol	Freon 114	LH_2
51.7 (75)	Open: 0.019			
	Close: 0.019	11.6 (38.2)	6.3 (20.6)	9.4 (30.9)
103.4 (150)	Open: 0.015			
	Close: 0.015	9.2 (30.2)	5.0 (16.3)	7.4 (24.4)

*Flow Controlled to $\sim 6.3 \times 10^{-5}$ m^3/sec (1 gpm)

transducers only (the UF and DF transducers were not used here). This was in accordance with the flow characteristics equation:

$$\Delta H + \frac{a}{gA} \Delta Q = 0 \qquad (8)$$

Clearly, the Foxboro flowmeter did not respond to the transient flow/pressure pulses. The Endevco piezoelectric pressure transducers indicated the change in pressure, and clearly showed the pressure attenuation across the Ramapo flowmeter (both pressure transducers had about the same calibration factor). The pressure peak-to-peak time constant agreed exactly with the wave travel time from pressure transducer to pipe outlet and return.

Testing with both the close-coupled and remote (UF and DF) pressure transducers (see Figure 21) revealed the following not-unexpected results:

1. Severe pressure surges could be recorded if the long (122 cm) sensing lines were not properly bled free from gas.
2. Small sensing lines (0.32 cm, 0.125 in, diameter) attenuated the pressure signal and masked details revealed by the close-coupled transducers.

Number 1 above was anticipated to be a potentially severe problem with the LH_2 tests, since gas will of necessity be present in the sensing lines.

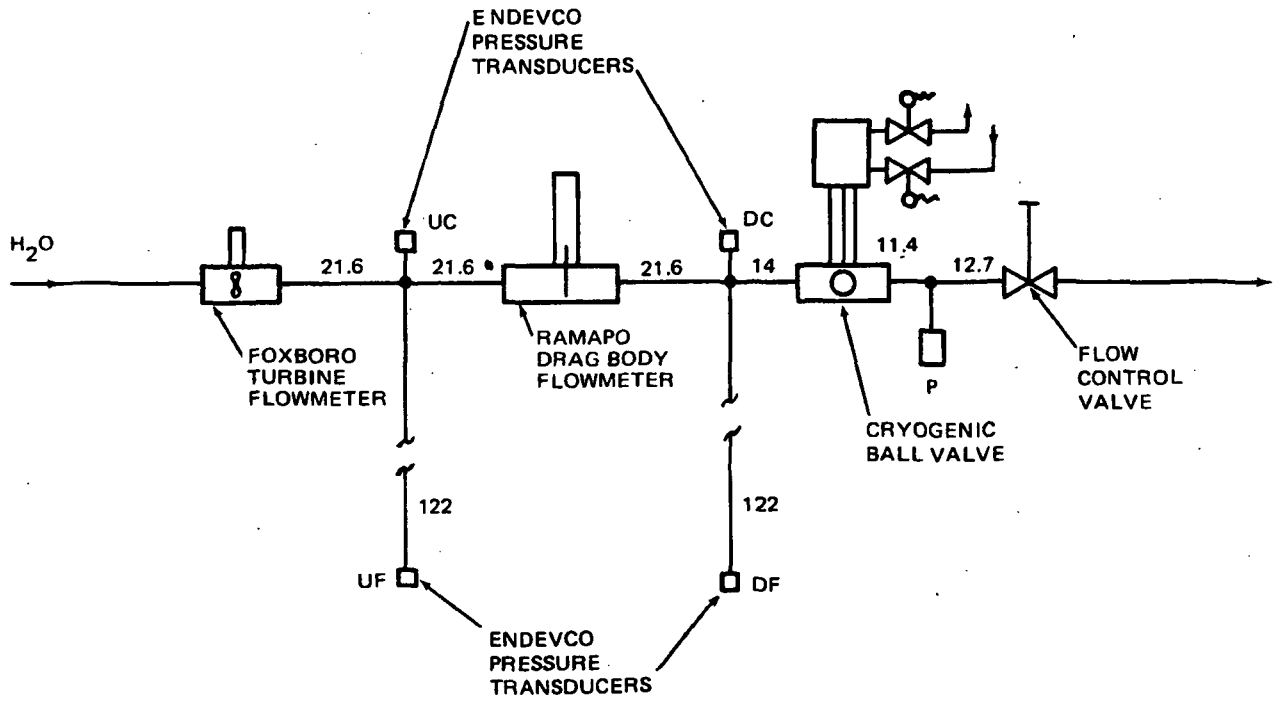

Figure 21. Flow Test Schematic

CR21

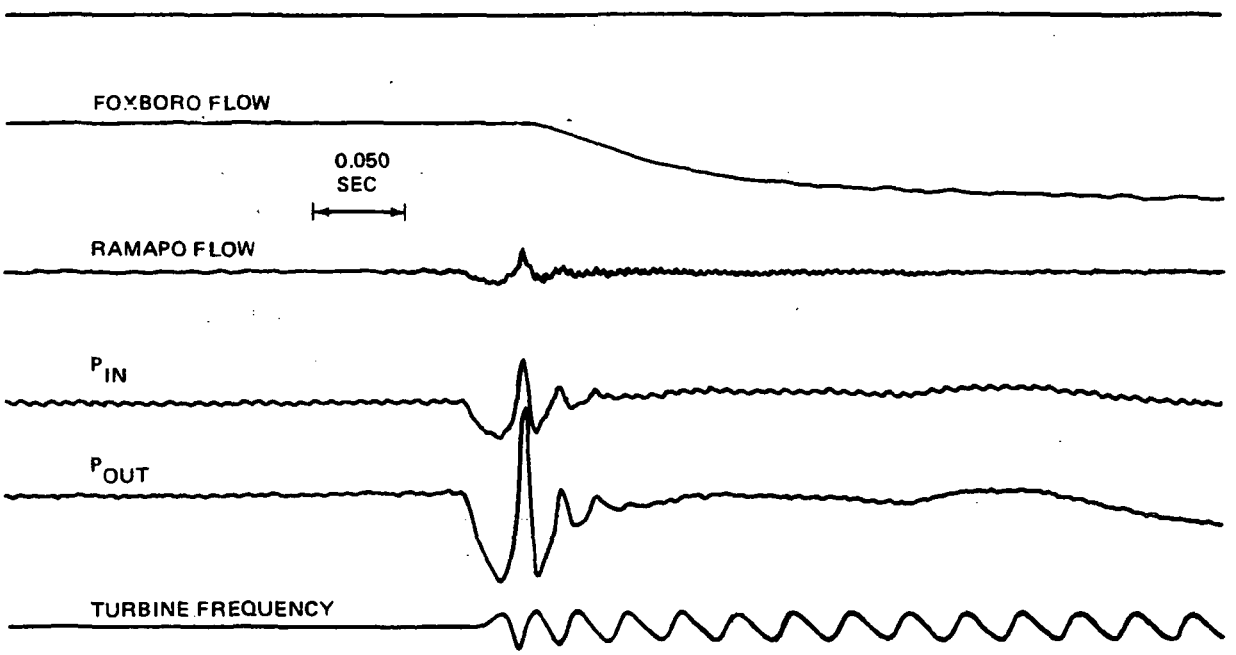

Figure 22. Flow Test Data — Valve Opening

The results of these exploratory tests, as they apply to the instrumentation design for the transient test apparatus were as follows:

1. The turbine flowmeter did not have adequate response for transient flow testing; therefore, for the isopropanol and Freon 114 tests, the Ramapo flowmeter would be used. For the LH_2 tests, a flowmeter would not be used, but pressure and differential pressure data would be acquired.
2. The close-coupled piezoelectric pressure transducers would be used for the isopropanol and Freon 114 tests, but remotely located Statham pressure and differential pressure transducers would be used for the LH_2 tests. The remote sensing lines in the LH_2 tests would be 0.64-cm (0.25 in) diameter to reduce line attenuation.

The original screen test specimen configuration proposed in Reference 18 was envisioned as a cylindrical plexiglass channel with screen bonded across an opening along the top. This configuration was reviewed and modified to provide directly correlatable data. Use of a partially cylindrical plexiglass channel with flat screen bonded on top would probably lead to correlation problems. Such a configuration may be analytically difficult to characterize, since the channel properties may dominate the screen/structure properties (see analysis section), with the result that the differences in response for different screen/structure configurations may be masked. The plexiglass channel would have the advantage of viewability, and gas ingestion may be able to be directly observed (although the quantity would still have to be determined from the bubble trap). It appeared likely that the partial-screen channel would have lower damping than a full-screen channel, so that a strong pressure pulse could crack it, especially in LH_2. Further, the channel would have a different coefficient of expansion than the screen, so that the flat-screen tension would change from the simulant fluid tests to the LH_2 tests, leading to additional correlation difficulties.

On the other hand, a cylindrical screen specimen would be a more uniform structure which could be analyzed directly. This type of specimen would provide direct correlation of the interaction of screen and structural backup and their effect on specimen response. Because the specimen would all be of the same material, contraction effects would not change screen tension. It was probable that the occurrence of gas ingestion with this specimen,

while not directly observable, could be inferred from the time of pulse travel through the specimen. Further, at shutdown, the amount of liquid spill, which would be observable, could probably be related directly to gas ingestion.

It was, however, believed to be more important to obtain response data in support of screen/structure configuration analysis, than to simply observe gas ingestion. Therefore, the recommended design for all specimens, and especially those with structural backup, was that the screens be configured as cylinders, bonded to an open tubular support frame, as shown in Figure 23. The fluid inlet would be through the screen on the right, and the gas pressure would be imposed on the screen on the left, surrounded by a plexiglass enclosure. The close-coupled bubble trap would also be made of plexiglass for direct observation of gas ingestion quantity during startup.

The plexiglass walls would be thick enough to withstand the predicted pressure surges in isopropyl alcohol and Freon 114, but there was some question as to the use of plexiglass with LH_2. MDAC has run tests in LH_2 using

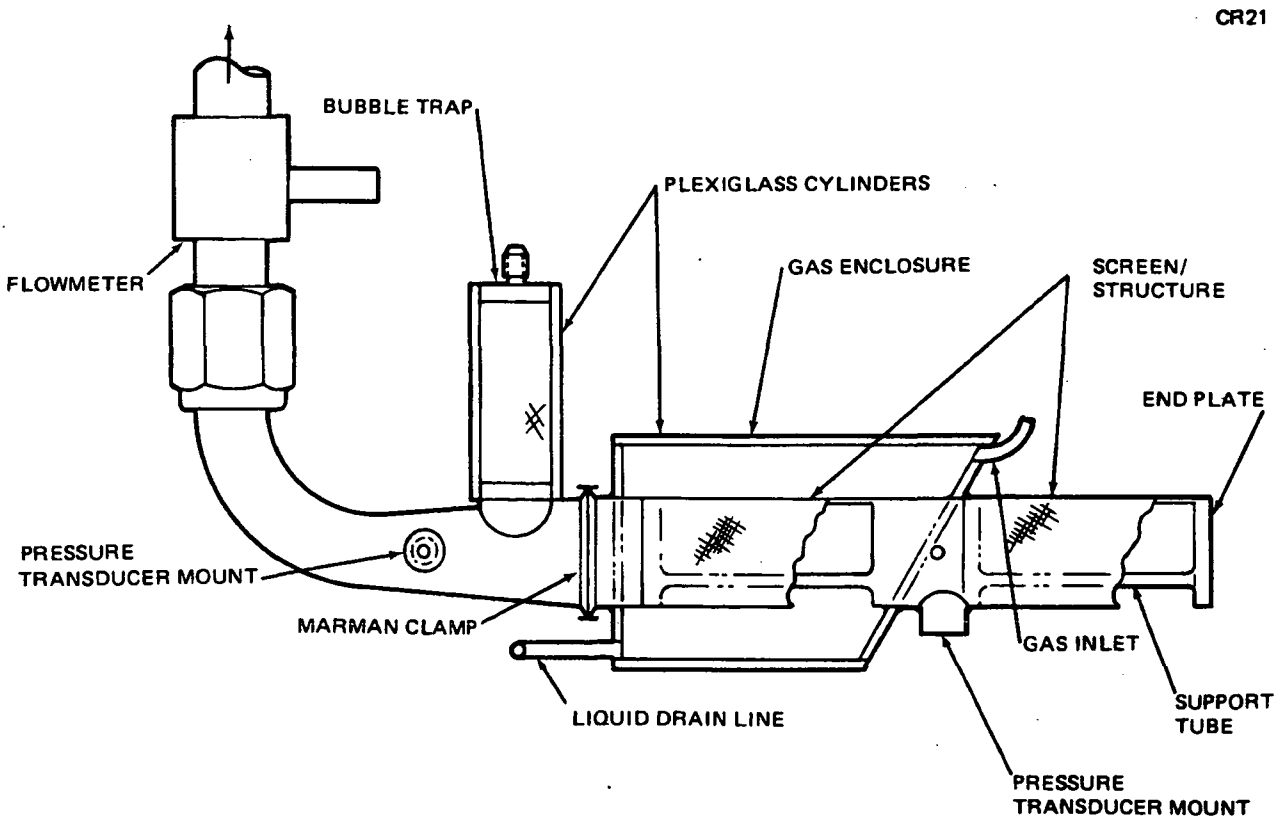

Figure 23. Screen/Structure Specimen Test Configuration

plexiglass apparatus (References 1 and 2) where it was discovered that if the plexiglass was unstressed by point loads, such as steel bolts, fittings, etc, and if the dewar was slowly filled with LH_2 to avoid sudden excessive chilling, the plexiglass survived without cracking. Both the plexiglass bubble trap and the plexiglass gas enclosure would be bonded to the specimen in a strain-free fashion, and the large gas enclosure would not be directly subjected to a pressure pulse, thus giving hope of survival in the LH_2 tests. For each specimen, the screen structure, transducer mounting base, and metal end plates would be bonded to the central tube with high-strength LH_2-compatible polyurethane adhesive. Note that the horizontal specimen shown could also be directly used for the vertical configuration tests by reversing the gas inlet and liquid drain connections.

The construction of the screen/structure specimens was straightforward: the typical plain screen specimen was a simple cylinder of screen, seam-welded longitudinally, and sized to slide over the support tube and be bonded to it. The coarse mesh backup specimen was made in the same fashion, with the coarse mesh welded first, then covered with the fine mesh screen, and TIG-welded longitudinally. The coarse mesh backup was sized to slide over the support tube, and both screens were bonded to the tube. The pleated screen specimen had approximately 3/1 area ratio pleats running in the direction of flow. The ends were coined flat and bonded to the tube.

The two perforated sheet backups were formed into open cylinders, as shown in Figure 24, with two values of angular opening, ϕ_i. The screen was seam-welded into a cylinder, and the perforated sheet cylinder was compressed, slipped inside the screen cylinder, and allowed to reopen, exerting tension on the screen, as shown in Figure 24.

The degree of tension exerted will be a function of the initial and final angular openings, as shown in Figure 25. The final angular opening was determined by examination of the specimen after installation of the perforated sheet. Both the screen and perforated sheet were bonded to the support tube. The configuration of a typical plain screen specimen, as fabricated, is shown in Figure 26.

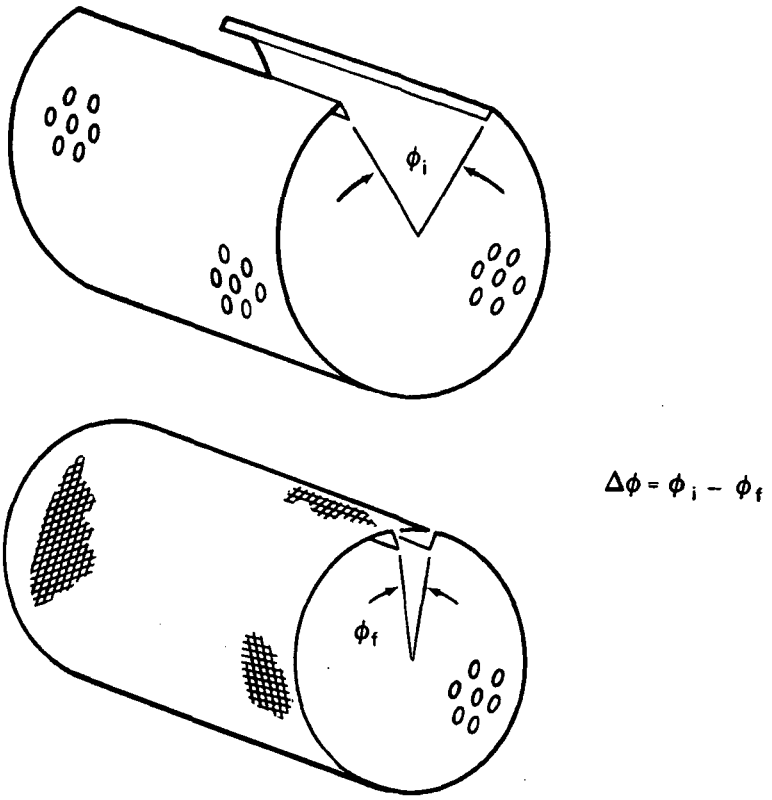

Figure 24. Screen/Perforated Sheet Construction

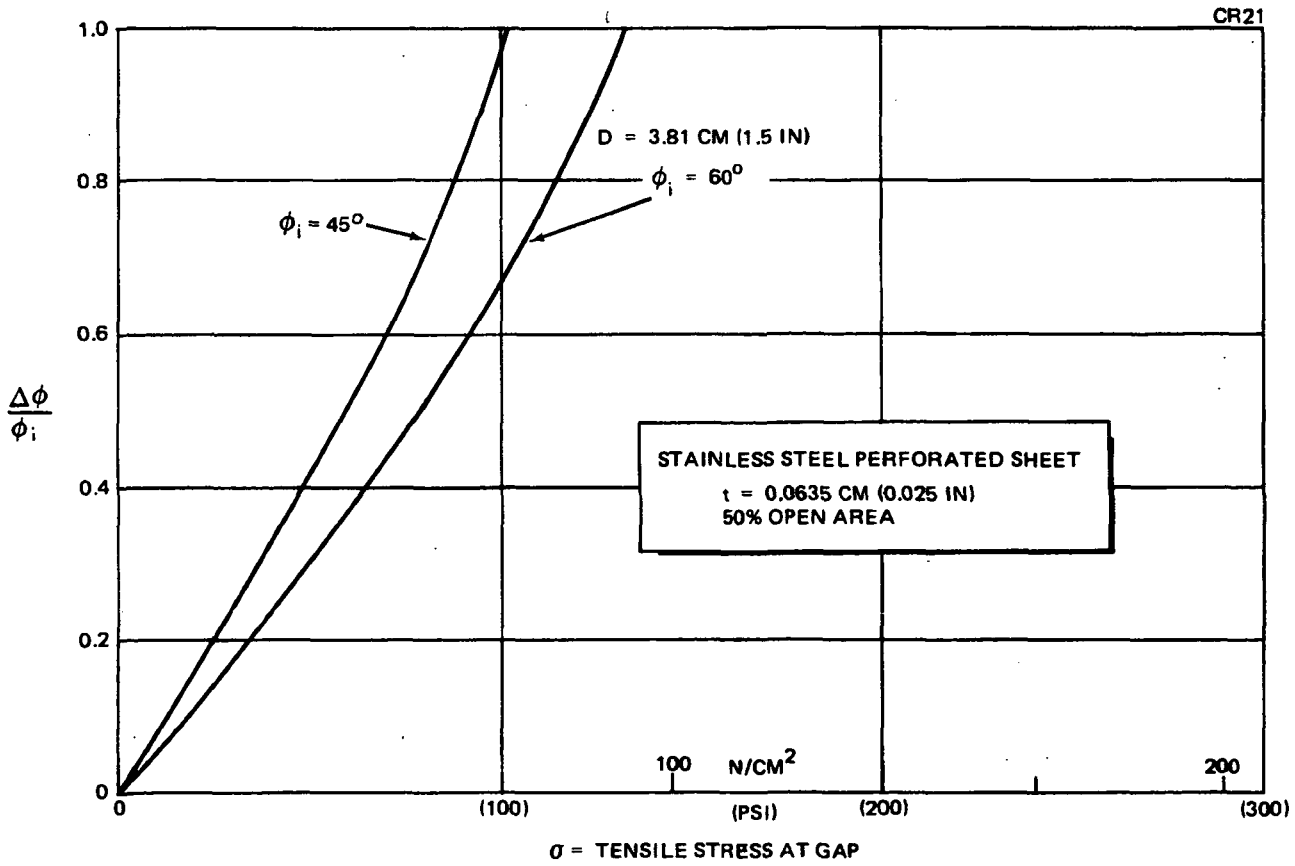

Figure 25. Tensile Stress on Deflected Perforated Sheet

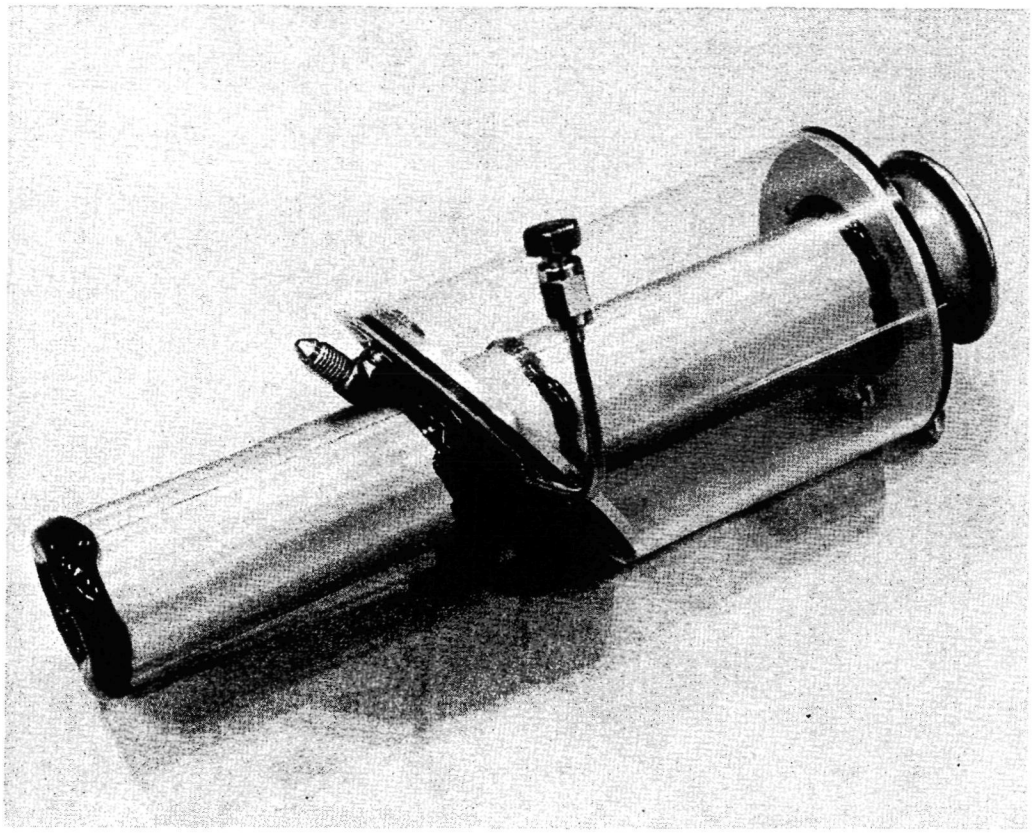

Figure 26. Plain Screen Specimen Construction

TEST APPARATUS INSTALLATION

The arrangement of the dewar, test specimen, instrumentation, lines, valves, and other components is shown schematically in Figure 27. The solid-line representation of the on/off valve and throttle valve in Figure 27 shows the "short-line" configuration; the dashed-line representation of the valves shows the valve position for the "long-line" configuration. The helium pressurization gas used to pressurize both the dewar (for outflow) and the gas enclosure around the screen specimen is cooled to fluid temperature with in-tank heat exchanger coils as shown in Figure 27.

The horizontal test apparatus (as installed within the dewar during testing) is shown in Figure 28. The dewar is in the background, and the apparatus components are identified. The apparatus configuration with the vertical specimen attitude is shown in Figure 29. The 325 x 2300 screen was also tested in the vertical position without the flowmeter installed in order to impose the minimum pressure pulse damping. Figure 30 shows the test apparatus arranged with the "short" line length of 1.2 m (4 ft), and Figure 31

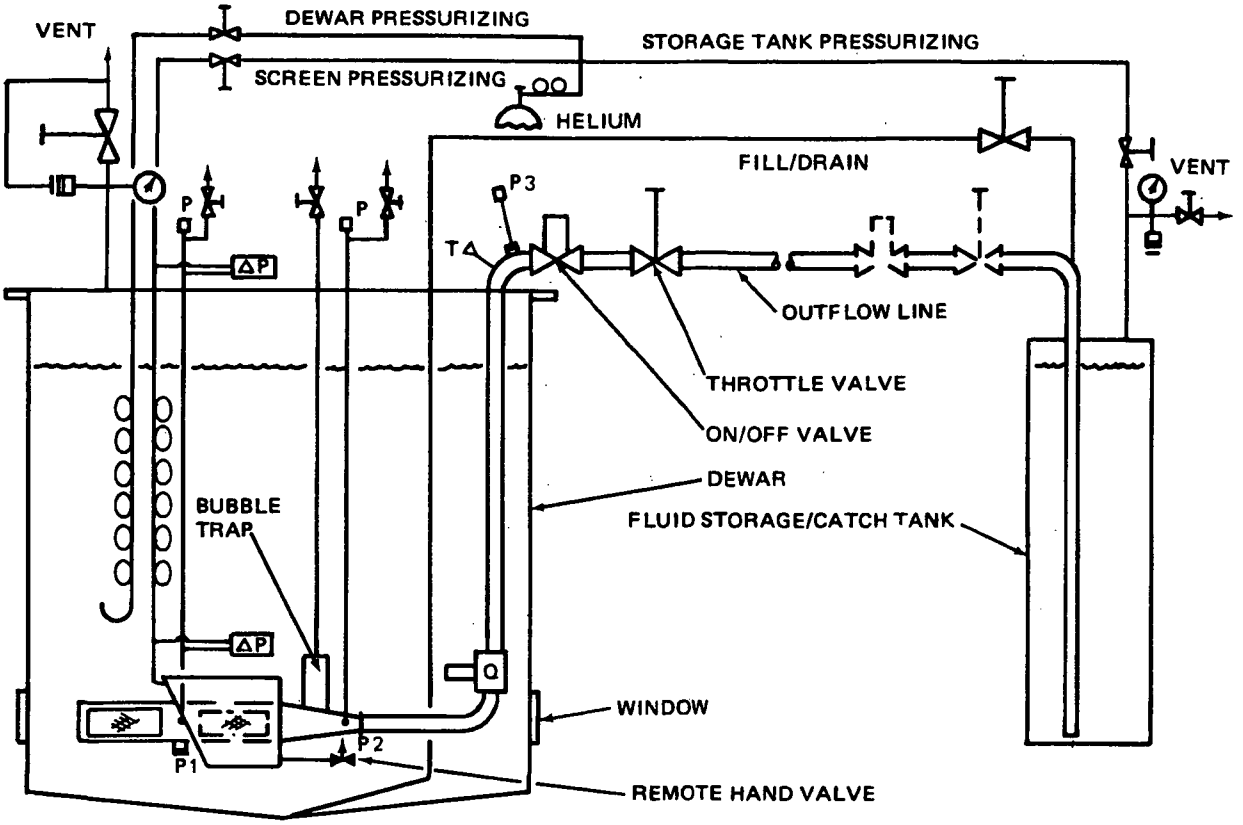

Figure 27. Test Apparatus Schematic

shows details of the valve/dewar arrangement with the 1.2 m line. The outflow line for all tests was 2.54-cm (1 in) diameter by 0.089-cm (0.035 in) wall stainless steel tubing. Figure 32 shows the test apparatus arrangement with the "long" line length of 10.4 m (34 ft). The arrangement was achieved by moving the valve complex from a position adjacent to the tank (see Figure 31) to the other end of the 9.2 m (30 ft) line, next to the supply/receiver tank. The apparatus is shown connected to a drum of isopropyl alcohol; the large horizontal cylindrical tank is Freon 114.

The apparatus configurations shown were used for the isopropyl alcohol and Freon 114 tests. For the LH_2 tests, the test apparatus was modified by removing or remoting instrumentation sensitive to low temperatures, arranging the outflow valve to provide for the "short" line and "fast" valve operation (see test matrix of Table 8), and providing for apparatus venting, purging, vacuum, and line insulation.

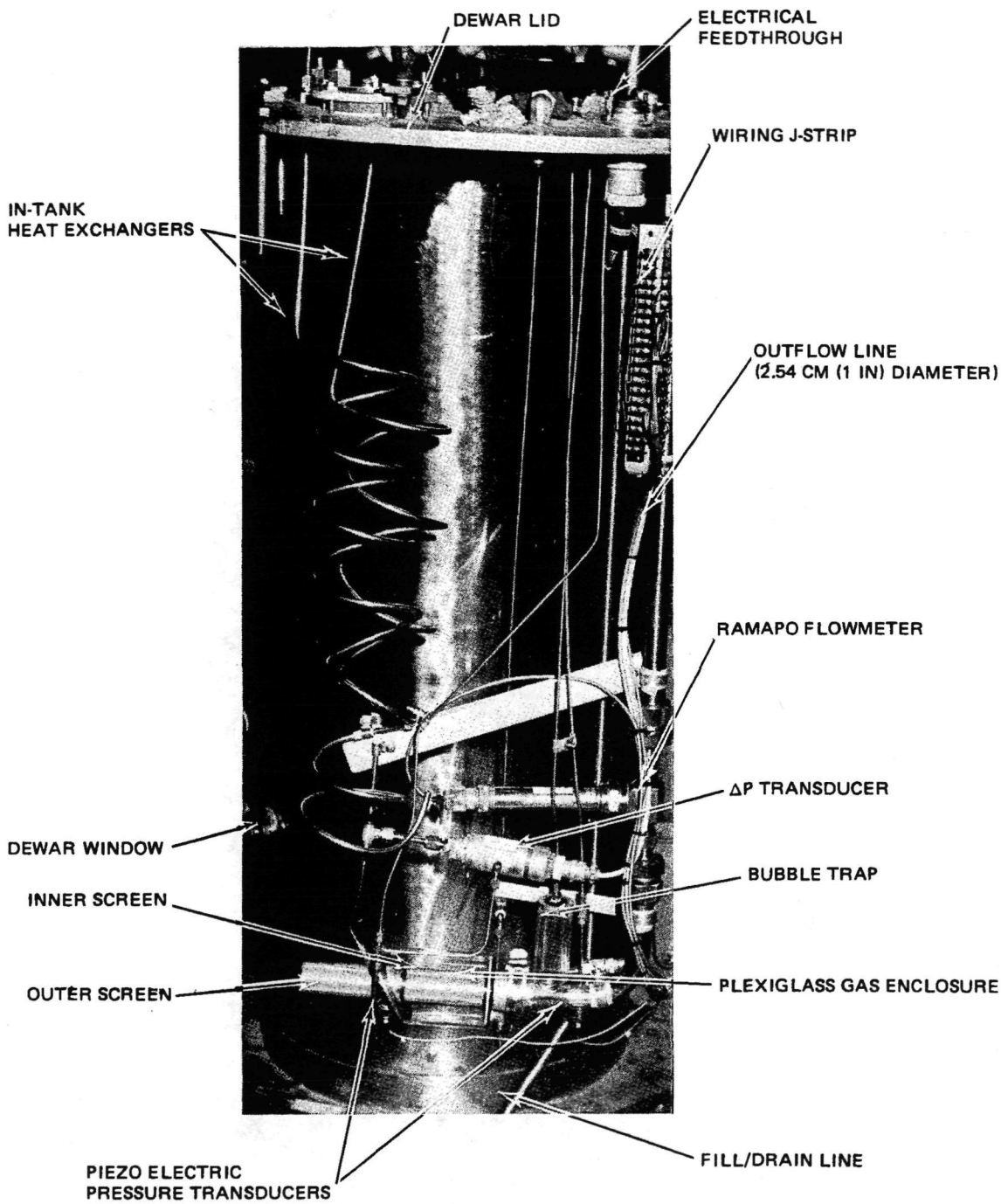

Figure 28. Horizontal Test Specimen as Installed

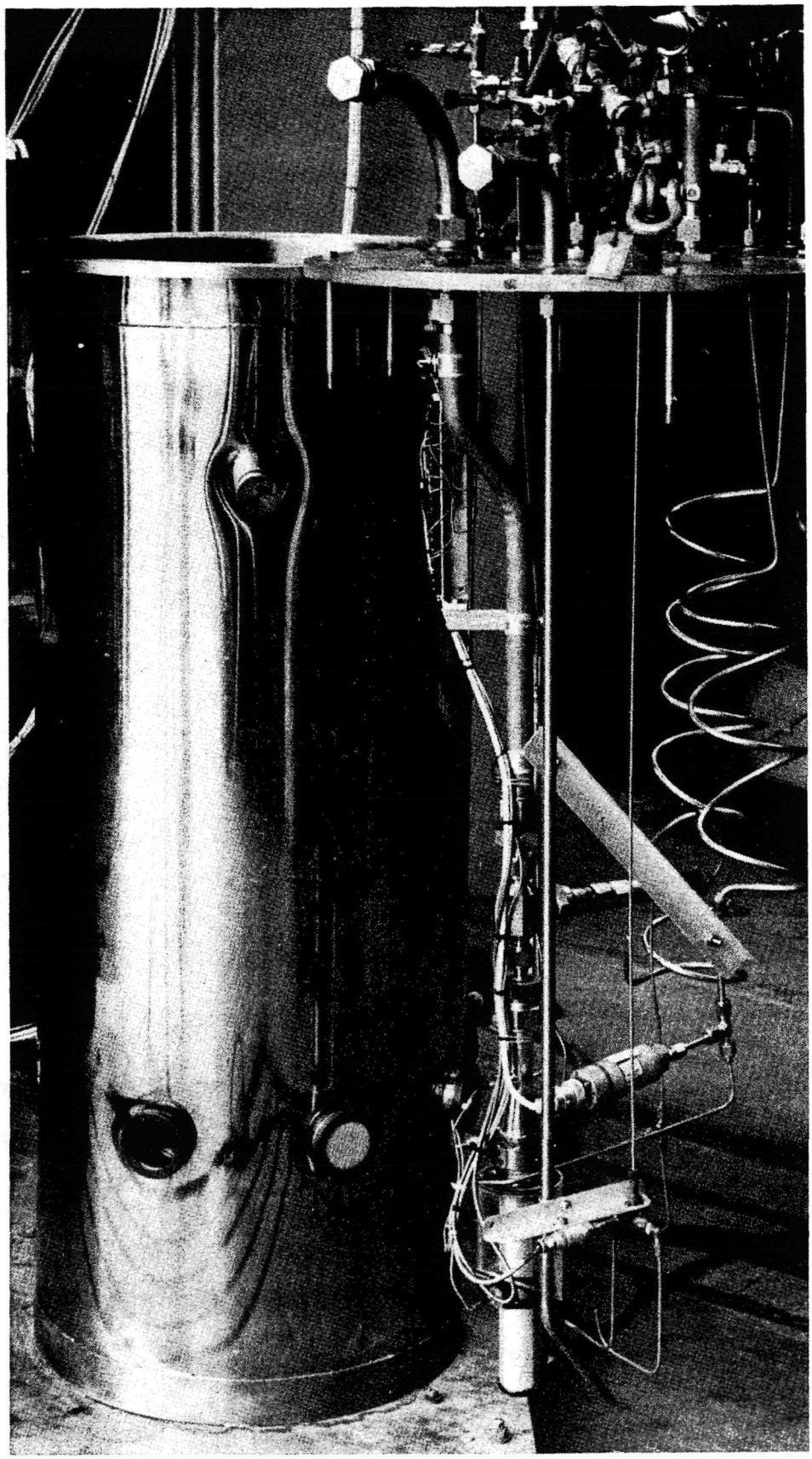

Figure 29. Vertical Test Specimen as Installed

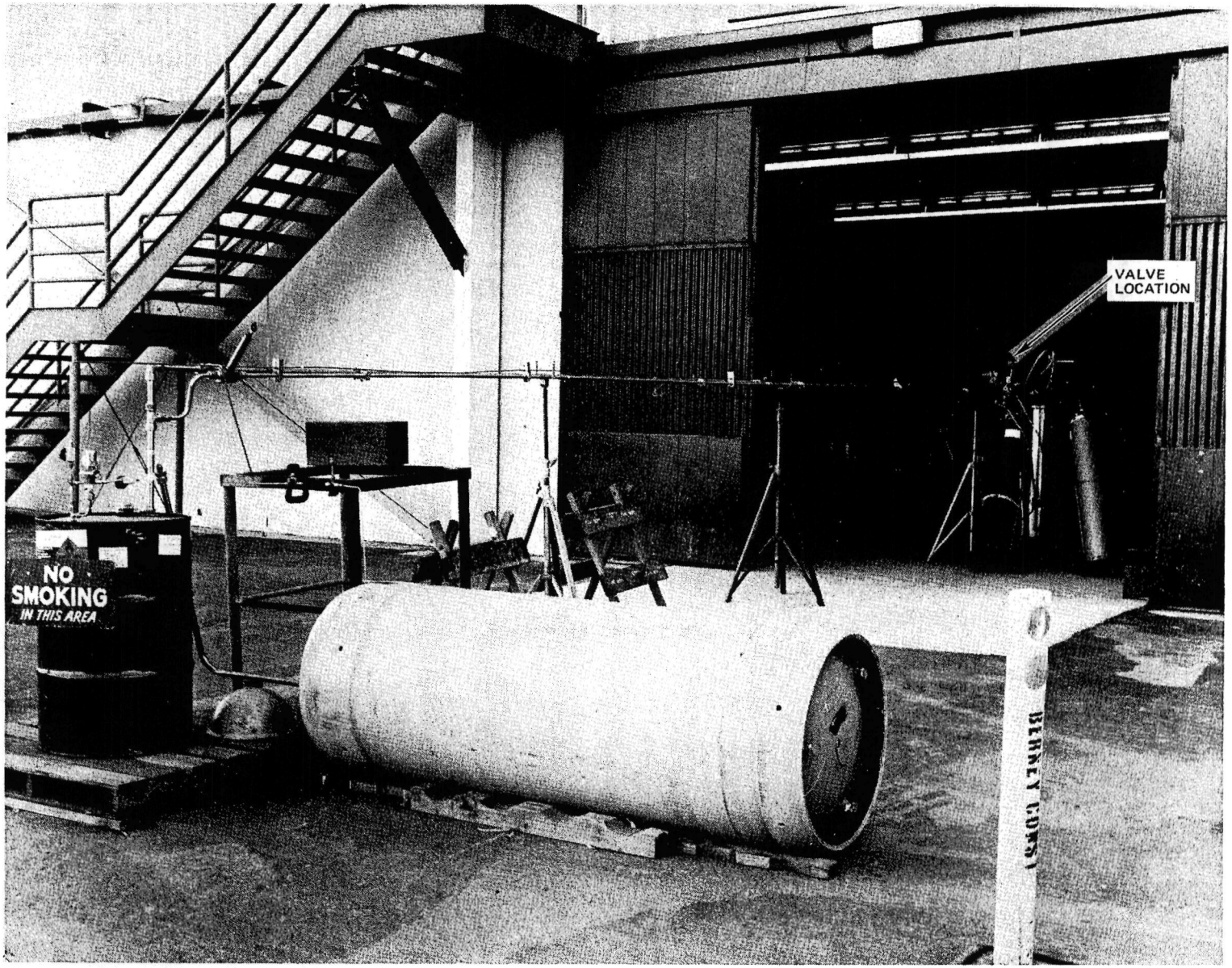

Figure 30. Short Line Apparatus Configuration

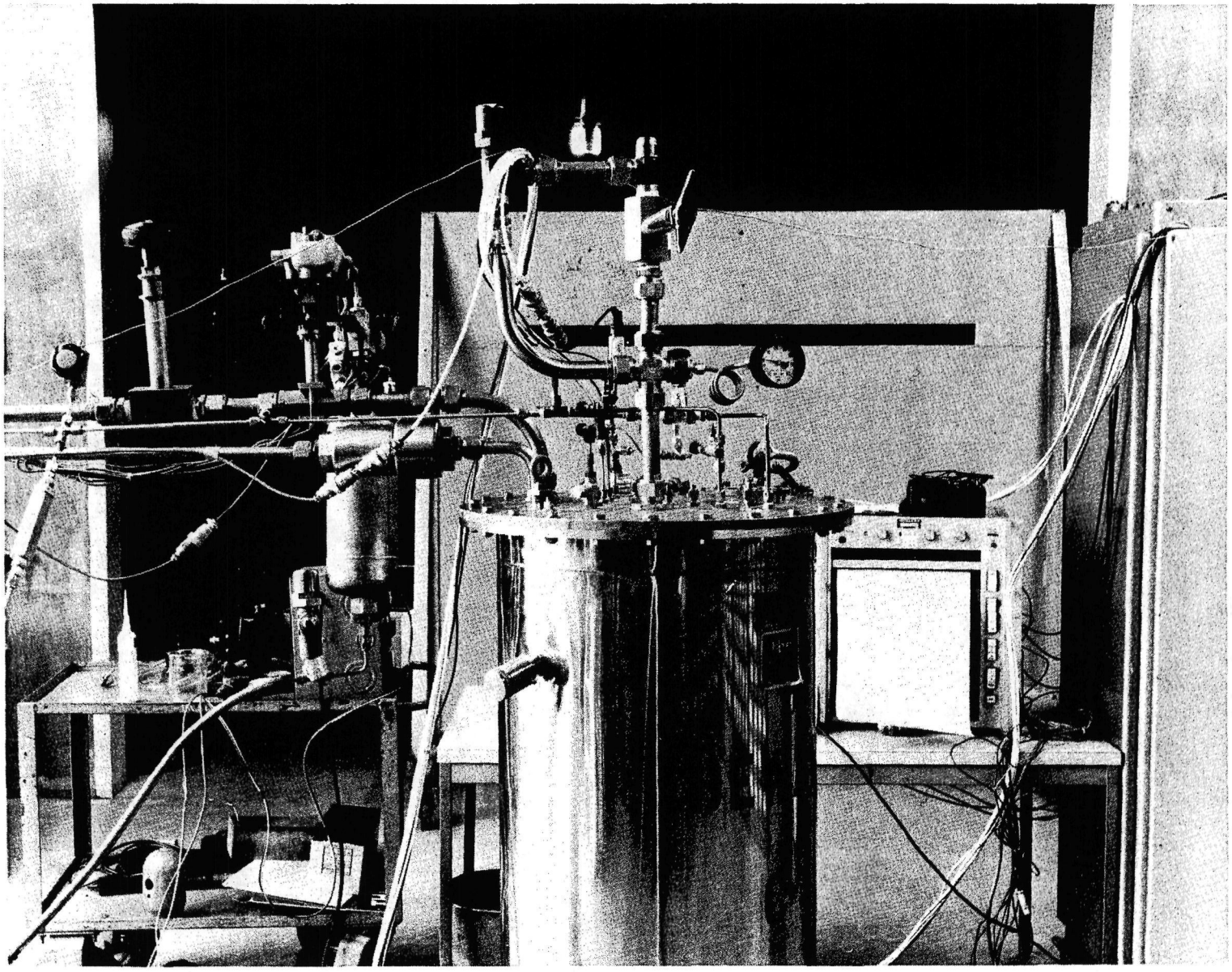

Figure 31. Valve Arrangement, Short-Line Configuration

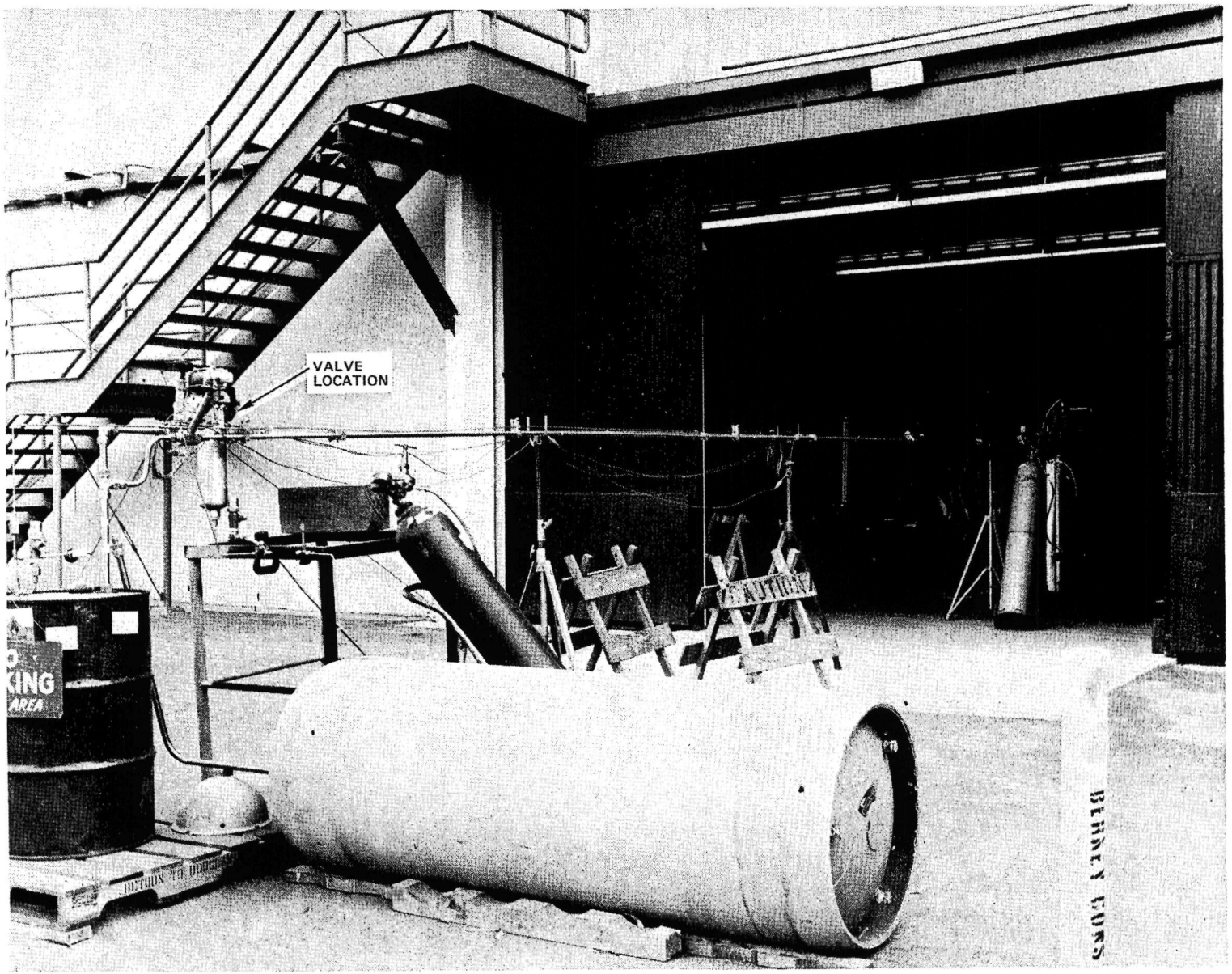

Figure 32. Long Line Apparatus Configuration

TESTING PHILOSOPHY AND PROCEDURES

For screen acquisition devices used for low-g fluid transfer, the velocity head, flow-through and friction head losses imposed by fluid flow usually constitute the bulk of the heads which must be resisted by the screen (since the gravitational hydrostatic head is usually very small). Under these conditions, the fluid flow surges will have the maximum effect on screen retention performance. In order to simulate these conditions in 1-g testing, care must be taken to minimize the imposed hydrostatic head. The cylindrical screen specimen must be surrounded by gas (to ensure that gas ingestion or liquid spillover can occur if conditions so warrant) and the surrounding gas is imposed by draining the fluid from around the specimen. Complete liquid draining was detected by the evolution of small gas bubbles, as shown in Figure 33. The maximum gas pressure imposed occurs at the top of the cylindrical specimen, and the liquid drain opening was situated (see Figure 26) so that the imposed hydrostatic head (H_{GR}) was minimized to

CR21

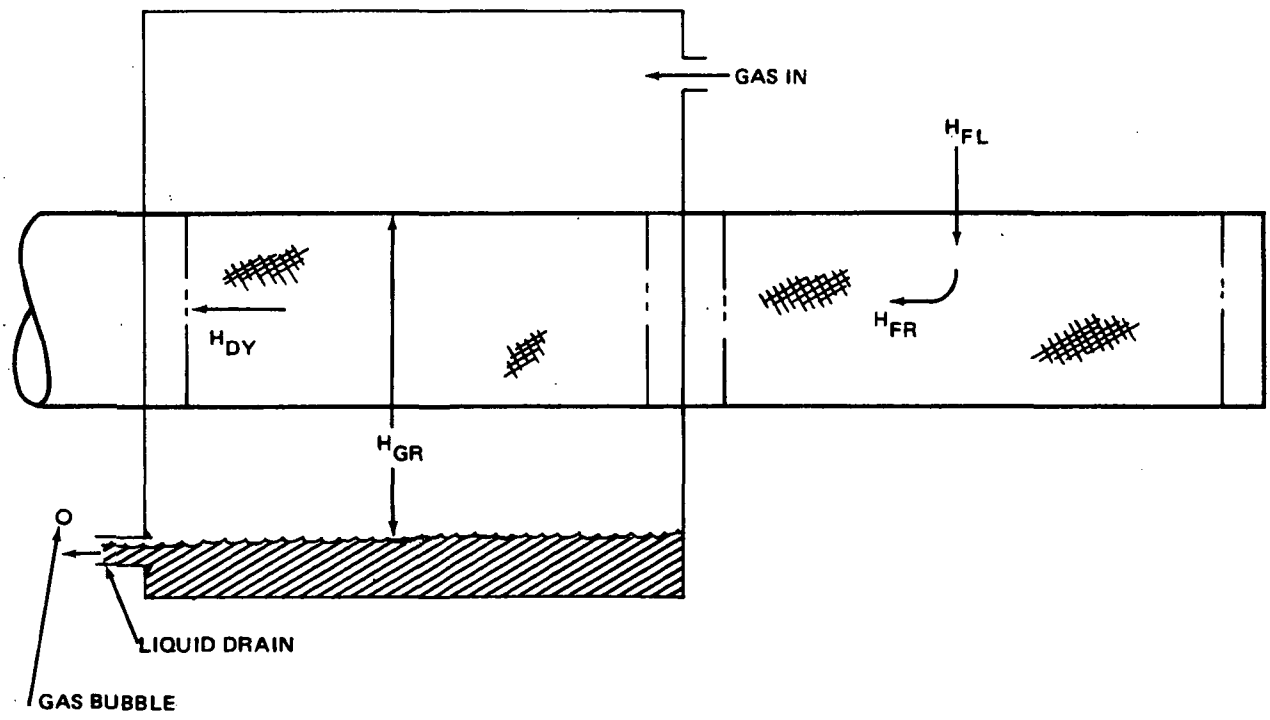

Figure 33. Screen Specimen Head Loss Nomenclature

5.1 cm (2.0 in). The head and flow losses are shown in Figure 33. The sum of imposed heads is:

$$\frac{BP}{S.F.} = H_{GR} + H_{FL} + H_{DY} + H_{FR}$$

or

$$\frac{BP}{S.F.} - H_{GR} = A' V_S + B' V_S^2 + \frac{V_P^2}{2g} + \frac{K_S V_P^2}{2g} \qquad (9)$$

where BP is the screen bubble point head capability and A' and B' are the screen liquid flow-loss coefficients defined by Equation 4. The safety factor (S.F.) is selected to give an adequate screen device design performance margin; some studies (References 1, 2, 4, and 8) have selected a safety factor of 2.0. K_S is the loss coefficient for flow turning and frictional losses. The screen approach velocity, V_S, is related to the pipe (specimen) velocity, V_P, by the ratio of screen area to cross-sectional area:

$$V_S = \frac{A_P}{A_S} V_P \qquad (10)$$

After substitution of Equation 10, Equation 9 was solved for the appropriate pipe velocity, V_P, (or baseline outflow rate) which results in a safety factor for the screen specimen of 2.0. The baseline outflow rates were imposed through a combination of dewar pressure and control valve setting. As defined previously in Table 9, the following test parameters were varied during the tests:

- Fluid; isopropyl alcohol, Freon 114, and LH_2.
- Screen device horizontal (all screens) or vertical (325 x 2300 and 200 x 1400 plain only).
- Screen weave, ranging from 325 x 2300 dutch twill to 500 x 500 square
- Screen device mounting/support method, ranging from plain and pleated screen to coarse screen and perforated sheet backup.
- Outflow line length from screen to valve of "short" (1.2 m, 4 ft) or "long" (10.4 m, 34 ft).

- Outflow rate at two baseline values; to give retention safety factors of 2.0 and 1.0, with minimum possible static gas head of about 5.1 cm (2.0 in) of alcohol imposed.
- Outflow valve open/close rate of either open/close = 0.019 sec or open/close = 0.015 sec.

The following general procedure was followed during alcohol testing for a given specimen and line-length configuration:

- With the dewar vented, the alcohol storage tank was pressurized and the dewar was filled to about 0.2 m (8 in) above the screen specimen.
- The screen specimen static bubble point was determined using a water manometer.
- The storage tank was vented and the dewar was pressurized to an appropriate pressure from about 1 to 11 N/cm^2 (1.5 to 16 psig) as required to obtain the proper steady-state outflow rate (determined by stop watch and internal scale).
- Outflow was terminated while maintaining the proper dewar pressure; the screen gas head was imposed and the bubble trap bled and filled with liquid.
- With instrumentation and oscillograph operating, outflow was initiated (valve opened) and terminated (valve closed) while the occurrence of gas ingestion or liquid spillover was observed visually through dewar windows.
- The valve actuation pressure (hence, closing speed) was changed and the test repeated.
- The dewar pressure was changed to achieve the other required steady-state outflow rate, and the test repeated, as above.

Essentially the same procedures were followed for the Freon 114 tests, except that after filling the dewar, the Freon was allowed time to saturate at atmospheric pressure. (Some early Freon 114 tests were run at saturation pressures of 2.1 N/cm^2 (3.0 psig) and 0.7 N/cm^2 (1.0 psig); see test results which follow.

Freon 114 tests performed with the long-line configuration revealed that continuous backflow occurred due to heat transfer and line boiling, and that liquid could not effectively be kept in the long line up to the valve. Therefore, most of the Freon 114 tests were run with the short-line configuration (see test results).

The same problem was anticipated with the LH_2 tests, which were all performed with the short-line configuration, and 0.015-sec valve actuation time, as planned. For the LH_2 tests, the dewar was cyclically purged to 7 N/cm^2 (10 psig) about 10 times with helium after specimen changes, before LH_2 filling took place. The LH_2 was allowed to saturate at either 1.4 N/cm^2 or 0.0 N/cm^2 (2.0 psig or 0.0 psig) except for two tests at 0.7 N/cm^2 (1.0 psig). Since there was severe line boiling and surging, it was not practical to establish a steady outflow rate; rather, all tests were run with dewar pressures of about 3.5 N/cm^2 (5 psig) or 6.9 N/cm^2 (10 psig) which were anticipated to bracket the appropriate flow rate range (see test results).

TRANSIENT TEST RESULTS

Isopropyl Alcohol Tests

As each test specimen was installed for the alcohol tests, the first test made was to determine the static alcohol bubble point of the specimen. So that gas breakthrough could be observed, the specimen, as installed, was submerged in alcohol within the dewar, and alcohol was introduced into the plexiglass gas enclosure, surrounding the inner screen. The specimen was then pressurized with gaseous helium on the inside of the screen, and the pressure increased until gas bubbles emerged from the inner or outer screen. The bubble point of the inner screen was recorded because it was the critical parameter for gas ingestion during subsequent tests. The bubble point pressure was determined with a self-calibrating water manometer, and was corrected for the depth of alcohol above the specimen. The data for each screen mesh is shown in Table 12 and for comparison previous alcohol bubble point data from Reference 1 is also shown. The bubble point pressure for each test fluid, as derived from the water manometer data, is shown.

Table 12

STATIC ALCOHOL BUBBLE POINT-SCREEN SPECIMENS

Screen	Corrected Alcohol Bubble Point (in. H_2O)	Reference 1 Alcohol Bubble Point (in. H_2O)	Bubble Point Pressure For Test Fluids					
			Alcohol		Freon 114		LH_2	
			N/cm^2	PSI	N/cm^2	PSI	N/cm^2	PSI
325 x 2300	24.8	23.9	0.618	0.896	0.411	0.596	0.052	0.076
200 x 1400	16.5	16.6	0.411	0.596	0.273	0.396	0.035	0.051
720 x 140	9.2	7.8	0.229	0.332	0.152	0.221	0.019	0.028
165 x 800	7.9	6.7	0.197	0.285	0.130	0.189	0.017	0.024
500 x 500	7.7	7.7	0.192	0.278	0.128	0.185	0.017	0.024

For the 200 x 1400 and 165 x 800 mesh screens, there were several specimens fabricated. For some of these there was minor leakage from the outer screen which made it difficult to obtain accurate bubble point data for the inner screen. This leakage was not repaired, since it was thought that it would not materially affect the inflow through the outer screen, or the gas-resistance capacity of the inner screen. All of the 200 x 1400 (and 165 x 800) mesh specimens were made from the same piece of screen, and the bubble point data which were obtained for different specimens were quite close in value; hence the bubble point shown in Table 12 for the 200 x 1400 and 165 x 800 mesh was assumed as the same for all specimens of that mesh.

The experiment matrix was set up to explore the sensitivity of the screen device response to various parameters as described in Table 7. The screen device sensitivity to some of these parameters, such as the effects of screen specimen structure (percent open area, screen fraction, effective elastic moduli, pleating, perforated sheet preload, device diameter, etc.) would be resolved by correlations with screen model simulations generated by the H672 analysis, by comparing gas ingestion, screen-ullage pressure difference, etc. in response to given conditions of initial imposed gas pressure and flowrate. Screen sensitivity to other parameters, such as valve open and close time effects, screen-valve distance, and flowrate, are responses to hydrodynamic effects which were evaluated with the alcohol tests (and to some degree with the Freon 114 tests). The screen sensitivity to parameters such as saturated or subcooled fluid conditions was anticipated to be resolvable by examination of the Freon 114 and LH_2 tests and analysis of the cryo-surge pressure pulses obtained during testing.

For each test in the matrix, both startup and shutdown occurred. Screen retention failure or gas ingestion during startup may be of prime concern for screen device design since gas could cause problems with downstream equipment (e.g., rocket engines or fuel cells) or, in low-gravity, could lead to liquid flow blockage in the screen device and complete retention failure. On the other hand, gas ingestion following shutdown may not be as severe a design problem, since the mission may have been completed (except when multiple flow cycles are required) unless complete screen destabilization

occurred (the screen device emptied completely, prohibiting further liquid flow). For the 177 tests performed, liquid spill (construed as equivalent to gas ingestion) after shutdown occurred only twice--once with Freon 114 (Run 148, Table 13) and once with LH_2 (Run 155, Table 13). In both cases, the spill was of the order of 16 cc (1.0 in^3) and gross gas overpressure had inadvertently been imposed (due to circumstances described in detail below). Complete screen destabilization never occurred, even under the most severe operating conditions imposed during testing, and therefore is believed to be an extremely unlikely occurrence.

The startup performance of the screen specimen was of particular interest because ingested gas could be trapped, observed, and measured, and because of the implications of startup gas ingestion on orbital screen device design. The startup transient and initial flow pulse data for every test are shown in Table 13. The table shows the conditions for each test, the initial gas-liquid pressure difference applied to the inner screen, the approximate steady-state flowrate as recorded by the Ramapo flowmeter, and the time and magnitude of the initial flow pulse at startup. Also shown in Table 13 is whether gas ingestion was observed, either visually into the bubble trap or by flowmeter spiking as recorded on the oscillograph. Figure 34 shows a typical oscillograph trace for flow startup with gas ingestion. The spiking of the flowmeter trace is apparently caused by springback of the dragbody when it encounters a gas bubble. (Trace ID is shown in Figure 27.)

It had been anticipated (see Table 7) that the effective valve open time would have a moderate effect on screen startup performance and potential gas ingestion. In fact, there was essentially no difference in startup performance for the 0.015-sec effective valve open time or 0.019-sec effective valve open time. This is seen by comparing the oscillograph record (Figure 35) for startup of Run 21 (0.019-sec valve, short line) with Figure 36 for startup of Run 22 (0.015-sec valve, short line). The shutdown traces for these tests were also identical. This is believed to be because the dynamics of the system are dominated by the large flow resistances which control the startup transients, rather than the effective open time differences for the low-resistance valve. The startup performance for the long line tests (e.g., Run 25; see Figure 37) was also the same for both valve actuation

Table 13

INITIAL FLOW PULSE TEST DATA

Test No.	Screen	Configuration	Line Length (m)	Valve Opening (1)	Imposed Screen-Ullage Pressure Difference N/cm²	psi	Steady Flowrate (Approx) m³/Sec x 10⁵	gpm	Time After Start (Sec)	Flow Pulse Screen-Ullage Pressure Difference N/cm²	psi	Gas Ingestion Observed: Bubble Trap	Oscillograph (Flowmeter)
Isopropyl Alcohol — Horizontal Specimen													
1	325 x 2300	Plain	1.2	F	0.26	0.38	11.1	1.8	0.57	0.41	0.60	No	Yes?
2				S	0.23	0.33	11.1	1.8	0.74	0.40	0.58	No	Yes?
3				F	0.21	0.30	10.7	1.7	0.87	0.41	0.60	No	Yes?
4			1.2	S	0.21	0.31	8.9	1.4	1.1	0.41	0.59	No	No
5			9.2	S	0.21	0.30	11.1	1.8	0.33	0.37	0.54	No	Yes?
6				F	0.17	0.24	12.2	1.9	1.75	0.51	0.74	No	No
7				F	0.08	0.11	10.2	1.6	2.30	0.42	0.61	No	No
8	325 x 2300	Plain	9.2	S	0.10	0.15	9.3	1.5	2.50	0.41	0.59	No	No
9	200 x 1400	Plain	9.2	F	0.17	0.25	11.1	1.8	2.10	0.33	0.48	No	No
10				S	0.17	0.25	11.1	1.8	2.10	0.34	0.49	No	No
11				S	0.18	0.26	10.2	1.6	1.92	0.34	0.49	Yes? (2)	No
12			9.2	F	0.19	0.27	10.2	1.6	1.92	0.34	0.49	Yes?	No
13			1.2	F	0.17	0.25	17.7	2.8	0.36	0.34	0.50	No?	Yes?
14				S	0.21	0.31	15.3	2.4	0.90	0.39	0.56	No?	No
15				S	0.17	0.25	12.5	2.0	0.90	0.34	0.49	Yes	No
16				F	0.17	0.25	13.2	2.1	0.90	0.34	0.50	Yes	No
17				F	0.17	0.25	15.6	2.5	1.10	0.38	0.55	Yes	No
18	200 x 1400	Plain	1.2	S	0.17	0.25	16.5	2.6	0.90	0.39	0.56	Yes	No
19	200 x 1400	Pleated	1.2	F	0.14	0.20	24.7	3.9	0.32	0.58	0.84 (3)	Yes?	Yes?
20				S	0.15	0.22	23.6	3.8	0.59	0.28	0.40	No	No
21				S	0.14	0.20	31.7	5.0	0.36	0.28	0.40	No	No
22				F	0.14	0.20	31.7	5.0	0.40	0.28	0.40	No	No
23			1.2	F	0.14	0.20	31.8	5.1	0.47	0.26	0.38	No	No
24			9.2	F	0.14	0.20	27.2	4.3	0.48	0.21	0.31	Yes?	Yes?
25				F	0.12	0.18	31.7	5.0	0.33	0.23	0.34	Yes?	No
26	200 x 1400	Pleated	9.2	S	0.12	0.18	31.8	5.1	0.32	0.24	0.35	No	No
27	200 x 1400	Screen Backup	9.2	F	0.21	0.30	12.5	2.0	0.92	0.34	0.49	Yes?	Yes?
28				S	0.17	0.24	12.5	2.0	0.95	0.30	0.44	Yes?	Yes?
29				S	0.15	0.22	6.3	1.0	1.55	0.27	0.39	Yes?	No
30			9.2	F	0.17	0.24	7.2	1.1	0.75	0.25	0.36	Yes?	No
31			1.2	F	0.17	0.25	14.5	2.3	0.60	0.34	0.49	Yes?	Yes?
32				S	0.15	0.22	14.2	2.2	0.89	0.33	0.48	Yes?	Yes?
33				S	0.17	0.24	11.1	1.8	0.83	0.30	0.44	Yes?	Yes?
34	200 x 1400	Screen Backup	1.2	F	0.19	0.27	12.5	2.0	0.33	0.25	0.36	Yes?	Yes
35	720 x 140	Plain	1.2	F	0.22	0.32 (5)	20.7	3.3	0.30	0.62	0.90 (3)	Yes?	Yes
36				S	0.22	0.32 (5)	19.8	3.1	0.30	0.62	0.90 (3)	Yes?	Yes
37				S	0.17	0.25	22.9	3.6	0.35	0.62	0.90 (3)	Yes?	Yes
38			1.2	F	0.19	0.27	22.9	3.6	0.35	0.62	0.90 (3)	Yes?	Yes
39			9.2	F	0.17	0.25	18.7	3.0	0.90	0.19	0.28	Yes?	Yes
40				S	0.17	0.25	19.8	3.1	0.95	0.19	0.28	Yes?	Yes
41				S	0.18	0.26	21.9	3.5	0.30	0.25	0.36	Yes?	Yes
42	720 x 140	Plain	9.2	F	0.15	0.22	21.9	3.5	0.29	0.26	0.38	Yes?	Yes
43	165 x 800	Plain	9.2	F	0.17	0.25	14.2	2.2	0.90	0.21	0.30	Yes	No
44				S	0.17	0.24	14.2	2.2	1.1	0.20	0.29	Yes	No
45				S	0.17	0.24	17.2	2.7	1.2	0.21	0.30	Yes	No
46			9.2	F	0.16	0.23	18.2	2.9	1.4	0.21	0.31	Yes	No
47			1.2	F	0.19	0.28	16.2	2.6	0.53	0.26	0.38	Yes	Yes
48				S	0.19	0.28	17.2	2.7	0.53	0.23	0.34	Yes	Yes
49				S	0.18	0.26	20.5	3.2	0.54	0.23	0.34	Yes	Yes
50	165 x 800	Plain	1.2	F	0.18	0.26	20.5	3.2	0.60	0.23	0.34	Yes	Yes
51	165 x 800	Pleated	1.2	F	0.21	0.31 (5)	30.3	4.8	0.14	0.62	0.90 (3)	Yes?	Yes
52				S	0.21	0.30 (5)	29.5	4.7	0.11	0.62	0.90	Yes?	Yes
53				S	0.17	0.24	32.2	5.1	0.11	0.62	0.90	Yes?	Yes
54			1.2	F	0.19	0.27	32.2	5.1	0.14	0.62	0.90	Yes?	Yes
55			9.2	F	0.14	0.20	30.0	4.8	0.26	0.62	0.90	Yes?	Yes
56				S	0.12	0.17	30.0	4.8	0.26	0.62	0.90	Yes?	Yes
57				S	0.13	0.19	33.4	5.3	0.30	0.62	0.90	Yes?	Yes
58	165 x 800	Pleated	9.2	F	0.08	0.11	33.4	5.3	0.23	0.62	0.90 (3)	Yes?	Yes
59	165 x 800	Screen Backup	9.2	F	0.10	0.14	14.8	2.3	1.0	0.15	0.22	No	No
60				S	0.11	0.16	14.8	2.3	1.0	0.15	0.22	No	No
61				S	0.12	0.17	17.2	2.7	1.0	0.17	0.24	Yes	No
62			9.2	F	0.11	0.16	17.2	2.7	1.5	0.17	0.24	Yes	No
63			1.2	F	0.10	0.14	17.2	2.7	0.2	0.14	0.21	No	No
64				S	0.10	0.15	17.2	2.7	0.2	0.21	0.31	Yes	No
65				S	0.10	0.15	19.2	3.0	0.38	0.21	0.31	Yes	Yes?
66	165 x 800	Screen Backup	1.2	F	0.10	0.15	19.8	3.1	0.2	0.22	0.32	Yes	Yes?
67	500 x 500	Plain	1.2	F	0.13	0.19	34.3	5.4	0.13	0.62	0.90 (3)	Yes?	Yes
68				S	0.18	0.26	32.9	5.2	0.13	0.62	0.90	Yes?	Yes
69				S	0.20	0.29 (5)	34.3	5.4	0.13	0.62	0.90	Yes?	Yes
70			1.2	F	0.12	0.17	34.3	5.4	0.37	0.62	0.90	Yes?	Yes
71			9.2	F	0.21	0.30 (5)	31.0	4.9	0.36	0.62	0.90	Yes?	Yes
72				S	0.28	0.41 (5)	31.7	5.0	0.45	0.62	0.90	Yes?	Yes
73				S	0.14	0.21	35.0	5.6	0.24	0.62	0.90 (3)	Yes?	Yes
74	500 x 500	Plain	9.2	F	0.05	0.07	35.0	5.6	0.26	0.19	0.27	Yes?	No?
75	200 x 1400	Perf. Sht. No. 1	9.2	F	0.08	0.11	10.2	1.6	1.1	0.19	0.27	No	No
76				S	0.09	0.13	9.3	1.5	1.1	0.19	0.28	No	No
77				S	0.14	0.20	7.2	1.1	1.0	0.21	0.31	No	No
78				F	0.14	0.20	8.4	1.3	1.2	0.23	0.34	No	No
79			9.2	F	0.14	0.21	10.2	1.6	1.2	0.30	0.43	No	No
80			1.2	F	0.15	0.22	7.8	1.2	1.0	0.24	0.35	No	No
81				S	0.15	0.22	7.8	1.2	1.2	0.24	0.35	No	No
82				S	0.16	0.23	7.2	1.1	1.0	0.23	0.34	No	No
83	200 x 1400	Perf. Sht. No. 1	1.2	F	0.15	0.22	8.9	1.4	1.0	0.27	0.39	No	No

Table 13

INITIAL FLOW PULSE TEST DATA (Continued)

Test No.	Screen	Configuration	Line Length (m)	Valve Opening (1)	Imposed Screen-Ullage Pressure Difference N/cm²	psi	Steady Flowrate (Approx) m³/Sec x 10⁵	gpm	Time After Start (Sec)	Flow Pulse Screen-Ullage Pressure Difference N/cm²	psi	Gas Ingestion Observed Bubble Trap	Oscillograph (Flowmeter)
84	200 x 1400	Perf. Sht.	1.2	F	0.15	0.22	5.1	0.8	0.5	0.18	0.26	Yes?	No
85	"	No. 2	"	S	0.18	0.26	5.9	0.9	0.5	0.24	0.35	Yes?	No
86	"	"	"	S	0.18	0.26	9.3	1.5	0.4	0.35	0.51	Yes?	Yes
87	200 x 1400	Perf. Sht. No. 2	1.2	F	0.18	0.26	6.6	1.0	0.4	0.28	0.41	Yes?	Yes?
88	165 x 800	Perf Sht.	1.2	F	0.62	0.90 (5)	8.9	1.4	0.20	0.62	0.90 (3)	Yes?	Yes?
89	"	No. 1	"	S	0.62	0.90 "	9.3	1.5	0.22	0.62	0.90 "	Yes?	Yes
90	"	"	"	S	0.62	0.90 "	8.4	1.3	0.18	0.62	0.90 "	Yes?	Yes
91	165 x 800	Perf. Sht. No. 1	1.2	F	0.62	0.90 (5)	7.2	1.1	0.18	0.62	0.90 (3)	Yes?	Yes
Isopropyl Alcohol – Vertical Specimen													
92	200 x 1400	Plain	9.2	F	0.18	0.26	8.9	1.4	1.75	0.27	0.39	No (4)	No
93	"	"	"	S	0.26	0.37	8.4	1.3	1.0	0.30	0.43	No "	No
94	"	"	"	S	0.21	0.30	11.1	1.8	1.6	0.37	0.53	No "	No
95	200 x 1400	Plain	9.2	F	0.19	0.28	12.2	1.9	1.9	0.37	0.53	No (4)	No
96	325 x 2300	Plain	9.2	F	0.32	0.47	9.3	1.5	1.9	0.47	0.68	No (4)	No
97	"	"	"	S	0.17	0.25	9.3	1.5	2.0	0.42	0.61	No "	No
98	"	"	"	S	0.24	0.35	14.2	2.2	1.6	0.50	0.73	No "	No
99	325 x 2300	Plain	9.2	F	0.36	0.52	10.7	1.7	1.6	0.51	0.74	No (4)	No
100	325 x 2300	Plain (5)	9.2	F	0.08	0.12	(21.9) (5)	(3.5)	1.34	0.34	0.49	No (4)	No (9)
101	"	"	"	S	0.07	0.10	(21.9) "	(3.5)	1.70	0.30	0.43	No "	No "
102	"	"	"	S	0.08	0.11	(39.1) "	(6.2)	1.45	0.47	0.68	Yes "	No "
103	"	"	"	F	0.08	0.12	(39.1) "	(6.2)	1.50	0.45	0.65	Yes "	No "
104	325 x 2300	Plain (5)	9.2	F	0.10	0.15	(39.1) (5)	(6.2)	1.50	0.46	0.66	Yes (4)	No (9)
Freon 114 (Saturated at 0.0 N/cm²) – Vertical Specimen													
105 (6)	325 x 2300	Plain	9.2	F	0.28	0.41	17.7	2.8	1.0	0.35	0.51	No (4)	No
106 (6)	"	"	"	S	0.28	0.40	17.7	2.8	1.1	0.34	0.50	No "	No
107 (6)	"	"	"	S	0.24	0.35	19.2	3.0	1.0	0.27	0.39	No "	No
108 (6)	"	"	"	F	0.27	0.39	11.8	1.9	1.0	0.29	0.42	No? "	No?
109	"	"	"	F	0.43	0.63 (8)	15.3	2.4	1.0	0.48	0.70	Yes? "	Yes?
110	"	"	"	S	0.31	0.45	11.1	1.8	0.4	0.62	0.90 (3)	No "	No?
111	"	"	"	S	0.41	0.59	18.2	2.9	0.8	0.46	0.66	No "	No?
112	325 x 2300	Plain	9.2	F	0.40	0.58	18.7	3.0	1.3	0.45	0.65	No (4)	No?
113 (7)	200 x 1400	Plain	9.2	F	0.46	0.67 (8)	20.5	3.2	0.26	0.55	0.80	Yes?(4)	Yes?
114 (7)	"	"	"	S	0.44	0.64 (8)	13.2	2.1	0.29	0.59	0.85	Yes? "	Yes?
115 (7)	"	"	"	S	0.33	0.48 (8)	18.7	3.0	0.44	0.62	0.90	No "	No?
116 (7)	200 x 1400	Plain	9.2	F	0.27	0.39	21.9	3.5	2.0	0.33	0.48	No (4)	No?
Freon 114–Horizontal Specimen													
117	325 x 2300	Plain	9.2	F	0.62	0.90 (8)	18.7	3.0	-	0.62	0.90 (3)	Yes	Yes (10)
118	"	"	"	S	0.44	0.64 (8)	20.5	3.2	0.4	0.62	0.90 "	Yes	Yes "
119	"	"	"	S	0.52	0.76 (8)	8.9	1.4	0.4	0.62	0.90 "	Yes	No? "
120	"	"	9.2	F	0.43	0.63	17.2	2.7	0.4	0.62	0.90 "	Yes	Yes "
121	"	"	1.2	F	0.50	0.72	21.9	3.5	0.15	0.62	0.90 "	No	Yes "
122	"	"	"	S	0.50	0.72	24.9	4.0	0.15	0.62	0.90 "	No	Yes "
123	"	"	"	S	0.51	0.74	20.5	3.2	0.15	0.62	0.90 "	No	Yes "
124	325 x 2300	Plain	1.2	F	0.51	0.74	20.7	3.3	0.15	0.62	0.90 (3)	No	Yes (10)
125	200 x 1400	Plain	1.2	F	0.42	0.61	20.5	3.2	0.30	0.62	0.90 (3)	No	Yes (10)
126	"	"	"	S	0.43	0.62	22.9	3.6	0.30	0.62	0.90 "	No	Yes "
127	"	"	"	S	0.34	0.50	14.8	2.3	0.30	0.62	0.90 "	No	Yes "
128	200 x 1400	Plain	1.2	F	0.43	0.62	17.7	2.8	0.36	0.62	0.90 (3)	No	Yes (10)
129	200 x 1400	Pleated	1.2	F	0.34	0.50	25.4	4.0	0.28	0.44	0.64	Yes	Yes (10)
130	"	"	"	S	0.39	0.57	25.4	4.0	0.34	0.48	0.70	Yes	Yes "
131	"	"	"	S	0.48	0.70	18.2	2.9	0.36	0.55	0.80	Yes	Yes "
132	200 x 1400	Pleated	1.2	F	0.54	0.78	17.7	2.8	0.40	0.59	0.86	Yes	Yes (10)
133	200 x 1400	Screen Backup	1.2	F	0.41	0.59 (8)	20.5	3.2	0.42	0.60	0.87	No	Yes (10)
134	"	"	"	S	0.26	0.38	25.4	4.0	0.35	0.59	0.86	No	Yes "
135	"	"	"	S	0.16	0.23	19.8	3.1	0.41	0.31	0.45	No	Yes "
136	200 x 1400	Screen Backup	1.2	F	0.19	0.27	21.7	3.4	0.41	0.34	0.50	No	Yes (10)
137	200 x 1400	Perf. Sht.	1.2	F	0.28	0.40 (8)	13.2	2.1	0.44	0.60	0.87	Yes?	Yes (10)
138	"	No. 1	"	S	0.46	0.66	11.8	1.9	0.31	0.62	0.90 (3)	Yes?	Yes (10)
139	"	"	"	S	0.34	0.50	17.2	2.7	0.60	0.47	0.68	No	No?
140	200 x 1400	Perf. Sht. No. 1	1.2	F	0.46	0.66	13.2	2.1	0.45	0.51	0.74	No	No?
141	720 x 140	Plain	1.2	F	0.53	0.77	22.9	3.6	0.26	0.62	0.90 (3)	Yes?	Yes (10)
142	"	"	"	S	0.55	0.79 (8)	21.9	3.5	0.30	0.62	0.90 "	No	Yes "
143	"	"	"	S	0.58 (5)	0.84	26.4	4.2	0.25	0.62	0.90 "	No	Yes "
144	720 x 140	Plain	1.2	F	0.62 (5)	0.90	25.4	4.0	0.23	0.62	0.90 (3)	No	Yes (10)
145	165 x 800	Plain	1.2	F	0.30 (5)	0.44	17.2	2.7	0.26	0.41	0.60	Yes	Yes (10)
146	"	"	"	S	0.52 "	0.76	13.2	2.1	0.38	0.62	0.90 (3)	No	Yes "
147	"	"	"	S	0.57 "	0.83	18.7	3.0	0.27	0.62	0.90 (3)	Yes	Yes "
148	165 x 800	Plain	1.2	F	0.62 (5)	0.90	14.8	2.3	0.25	0.62	0.90 (3)	Yes	Yes (10)
149	500 x 500	Plain	1.2	F	0.39 (5)	0.57	23.5	3.7	0.29	0.58	0.84	Yes	Yes (10)
150	"	"	"	S	0.59 "	0.85	20.7	3.3	0.25	0.62	0.90 (3)	Yes	Yes "
151	"	"	"	S	0.45 "	0.65	29.1	4.6	0.23	0.62	0.90 (3)	Yes	Yes "
152	500 x 500	Plain	1.2	F	0.46 (5)	0.66	27.2	4.3	0.24	0.62	0.90 (3)	Yes	Yes (10)

Table 13

INITIAL FLOW PULSE TEST DATA (Continued)

Test No.	Screen	Configuration	Line Length (m)	Valve Opening (1)	Imposed Screen-Ullage Pressure Difference N/cm^2	psi	Steady Flowrate (Approx) m^3/Sec x 10^5	gpm	Time After Start (Sec)	Flow Pulse Screen-Ullage Pressure Difference N/cm^2	psi	Gas Ingestion Observed Bubble Trap	Oscillograph (Flowmeter)
LH_2 – Horizontal Speciman													(9)
153	325 x 2300	Plain	1.2	F	0.03	0.04	1.4	2.0	0.16	0.32	0.46	Yes?	Yes? (10)
154					0.03	0.045	1.4	2.0	0.11	0.33	0.48	No?	Yes?
155					0.28 (5)	0.41	0.7	1.0	0.12	0.50	0.72	No?	Yes?
156					0.017	0.025	0.7	1.0	0.11	0.31	0.45	No?	No?
157					0.02	0.03	0.0	0.0	0.18	0.46	0.66	Yes?	Yes (10)
158	325 x 2300	Plain	1.2	F	0.23 (5)	0.33	0.0	0.0	0.15	0.52	0.75	Yes?	No
159	200 x 1400	Pleated	1.2	F	0.02	0.03	1.4	2.0	0.14	0.19	0.28	-	- (10)
160					0.017	0.025	1.4	2.0	0.14	0.19	0.28	-	-
161					0.05 (5)	0.07	0.0	0.0	-	-	- (11)	-	-
162	200 x 1400	Pleated	1.2	F	0.23 (5)	0.34	0.0	0.0	-	-	- (11)	-	- (10)
163	200 x 1400	Screen Backup	1.2	F	0.03	0.045	1.4	2.0	0.10	0.15	0.22	No	No
164					0.03	0.05	1.4	2.0	0.09	0.17	0.24	No	No
165					0.01	0.02	0.0	0.0	0.12	0.06	0.09	No	No
166	200 x 1400	Screen Backup	1.2	F	0.03	0.045	0.0	0.0	-	-	- (10)	No	No
167	200 x 1400	Plain	1.2	F	0.01	0.02	1.4	2.0	-	-	- (10)	No	No
168					0.05 (5)	0.07	1.4	2.0	0.11	0.01	0.02	No	No
169					0.60 (5)	0.87	0.0	0.0	-	0.60	0.87	?	?
170	200 x 1400	Plain	1.2	F	0.60 (5)	0.87	0.0	0.0	-	0.60	0.87	?	?
LH_2 – Vertical Specimen													
171	200 x 1400	Screen Backup	1.2	F	0.007	0.01	1.4	2.0	0.11	0.06	0.09	No	No
172	200 x 1400	Screen Backup	1.2	F	0.007	0.01	1.4	2.0	-	-	- (10)	No	-
173	200 x 1400	Screen Backup	1.2	F	-	- (10)	0.0	0.0	-	-	- (10)	No	-
174	325 x 2300	Plain		F	0.0	0.0	1.4	2.0	0.14	0.06	0.08	No	No
175					0.0	0.0	1.4	2.0	-	-	- (10)	No	No?
176					-	- (10)	0.0	0.0	-	-	- (10)	No	No?
177	325 x 2300	Plain	1.2	F	-	- (10)	0.0	0.0	-	-	- (10)	No	No?

(1) F = Open 0.015 Sec; Close 0.015 Sec
S = Open 0.019 Sec; Close 0.019 Sec

(2) ? = Possible Leakage Ingestion

(3) Severe ΔP Oscillation-Transducer Saturated

(4) Liquid Spill – Bubble Trap not used

(5) Flowmeter Removed (Est. Flow)

(6) Saturated at 2.1 N/cm^2 (3.0 Psig)

(7) Saturated at 0.7 N/cm^2 (1.0 Psig)

(8) Excessive ΔP Inadvertently Imposed

(9) Oscillograph – ΔP Transducer

(10) Line Boiling

(11) No ΔP Response

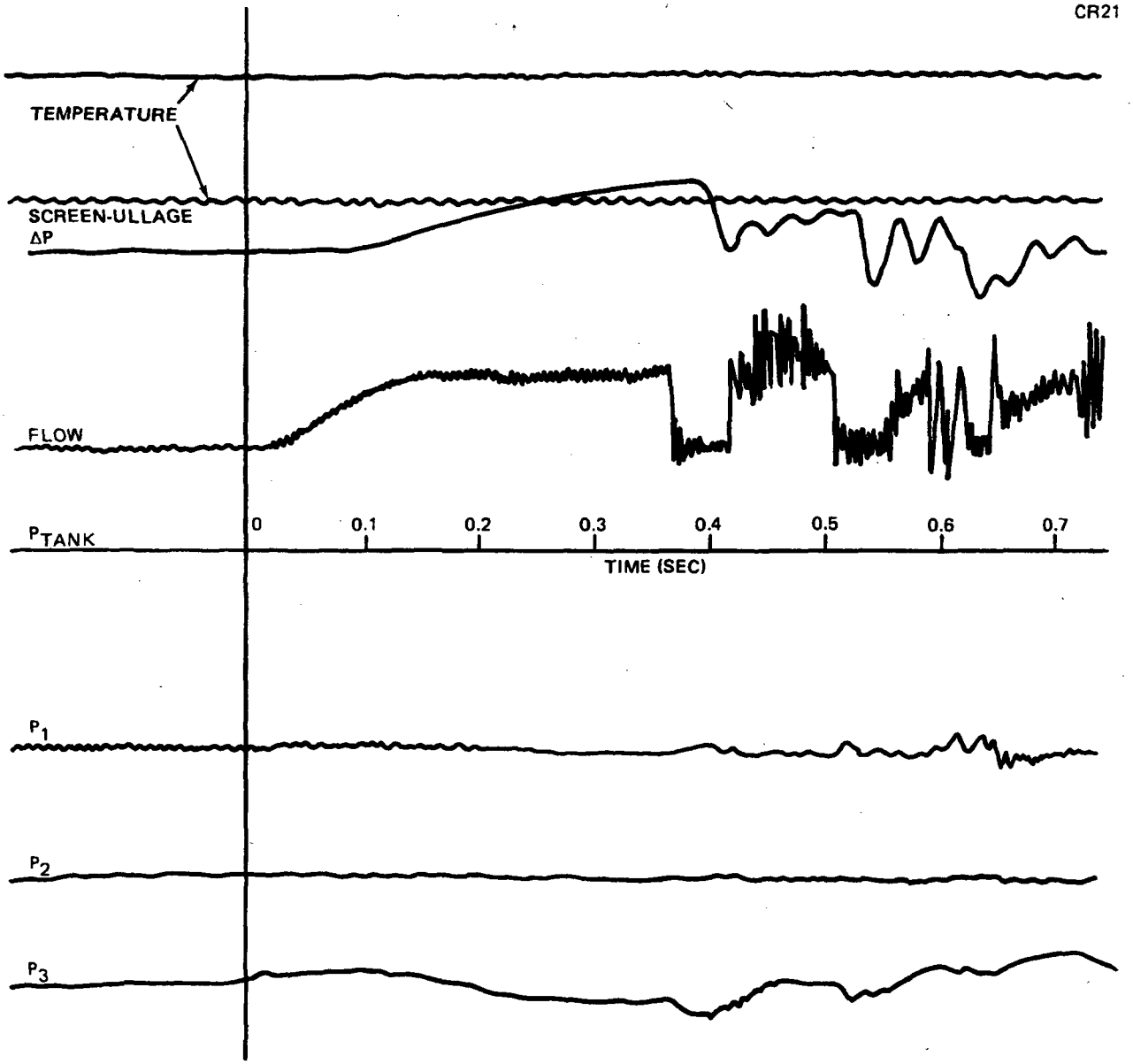

Figure 34. Oscillograph Record Showing Startup Gas Ingestion

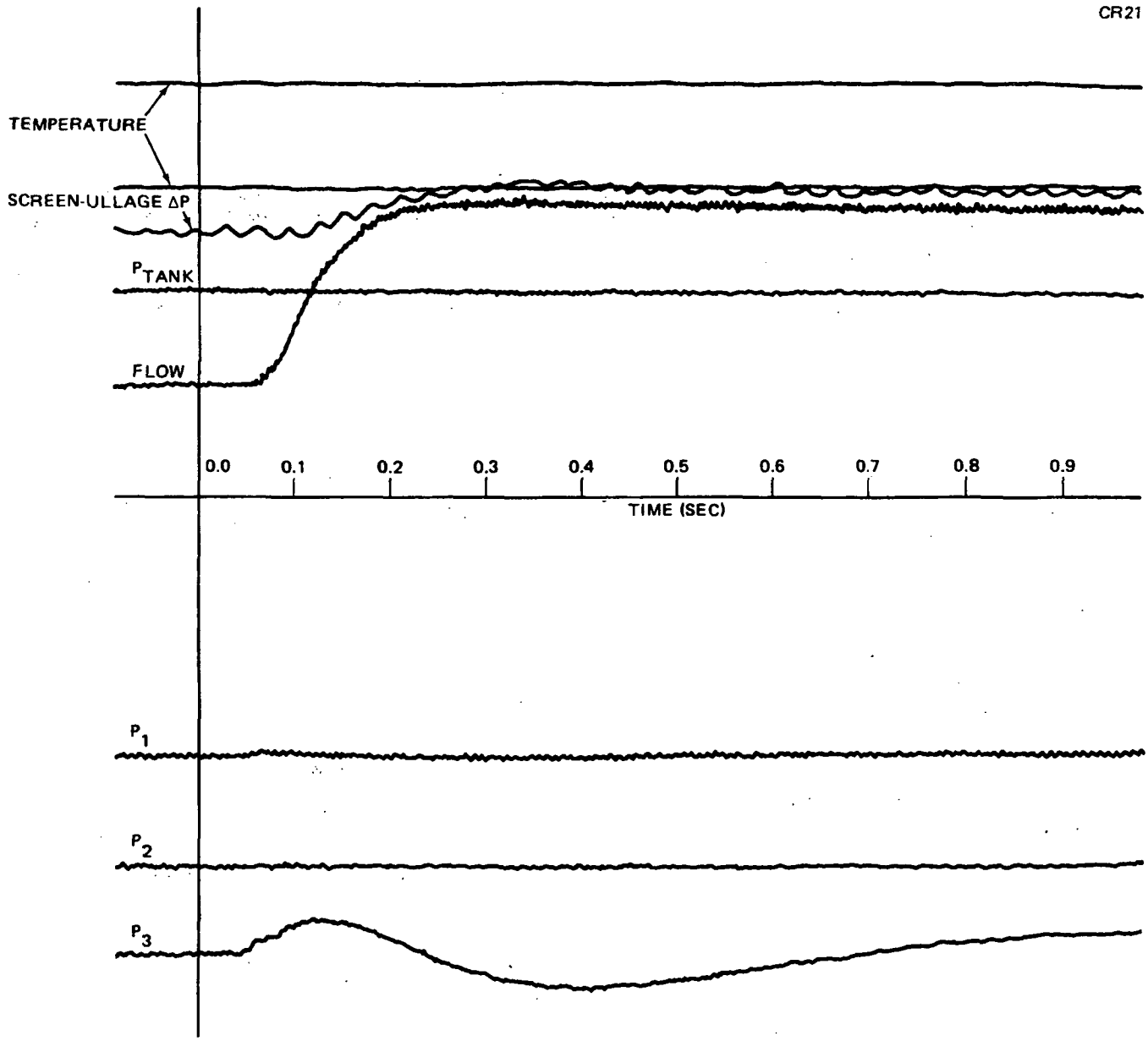

Figure 35. Run 21 Startup – 0.019 Second Valve – Short Line

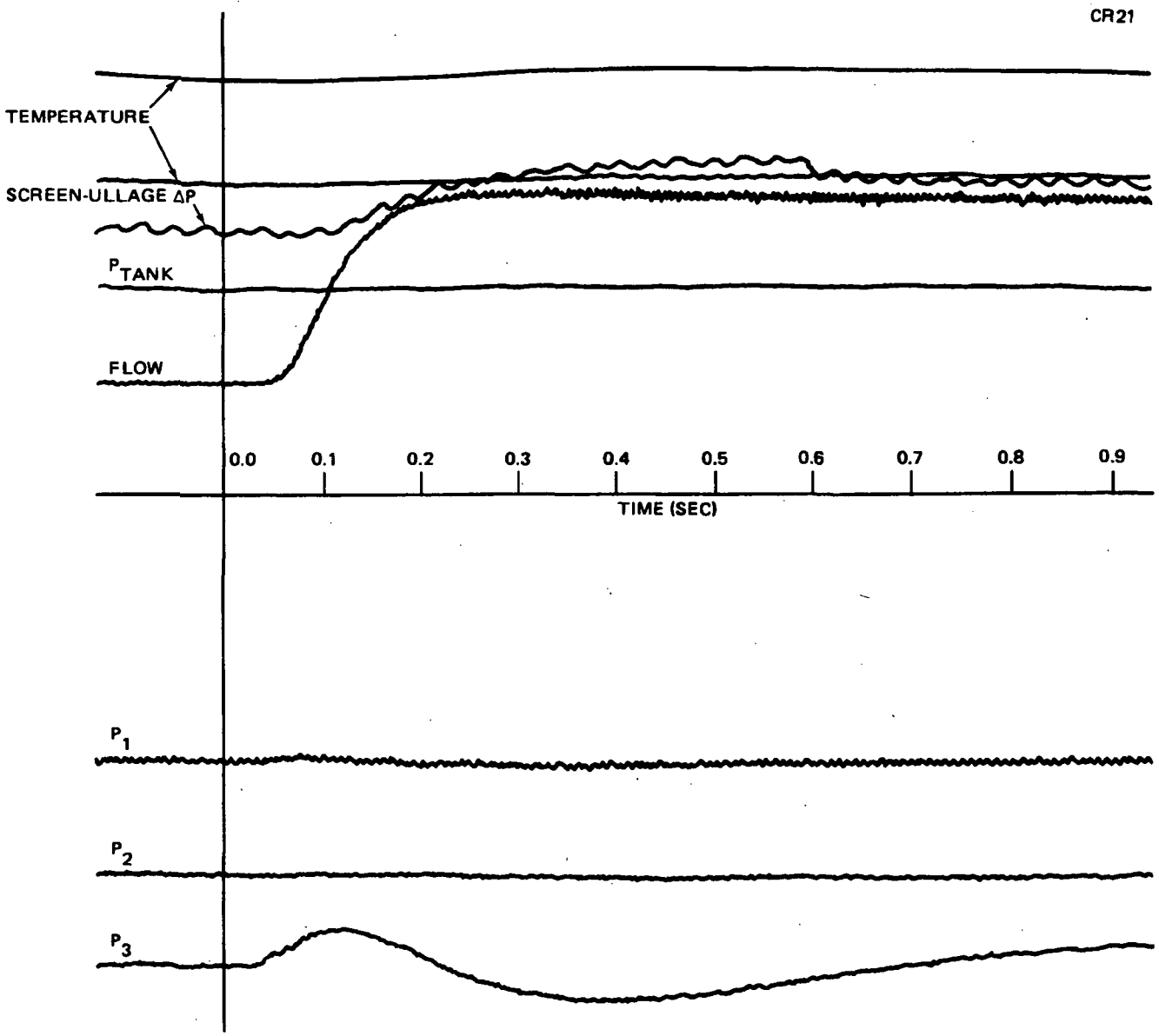

Figure 36. Run 22 Startup – 0.015 Second Valve – Short Line

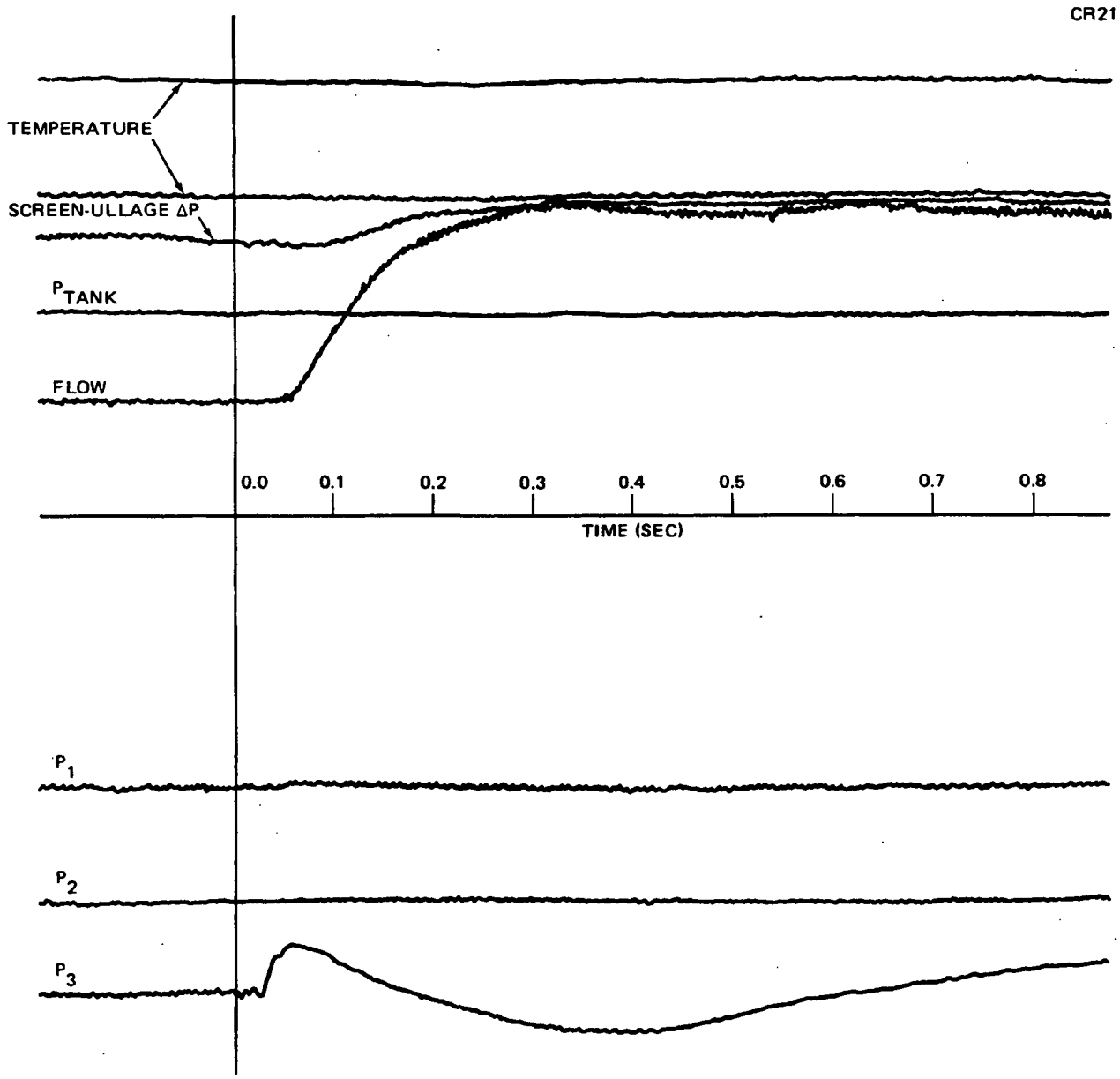

Figure 37. Run 25 Startup – 0.015 Second Valve – Long Line

times, but differed from the short-line startup trace (compare Figure 36) in taking 0.1 sec longer to reach full flow. Because the flow acceleration is slower, the screen-ullage pressure difference responds to a lower value for the long-line tests, compared to the short-line tests.

It was also anticipated that the combination of 0.015-sec valve closing time combined with the long line would result in waterhammer during shutdown. Waterhammer only occurred in seven tests and always at high flow rates. The most severe occurred with the pleated 200 x 1400 mesh (Runs 24 to 26) and happened with both valve closure times. The shutdown trace for Run 25 (0.015-sec valve closure) is shown in Figure 38, and for Run 26 (0.019-sec valve closure) in Figure 39. Although the initial pulse in both tests saturated the transducer, the magnitude of the pulse was estimated at 3.5 N/cm^2 (5 psi). The response of the screen-ullage pressure differential and flow was similar for both tests. It was not clear why the waterhammer frequency was lower for Run 25 with the 0.015-sec valve (Figure 38); the presence of an ingested gas bubble in the bubble trap for Run 25 may have contributed to the difference. Much less severe waterhammer occurred with the pleated 165 x 800 mesh (Runs 55 and 58). Although the flow rates for Runs 55 and 58 were just as high as for Runs 24 to 26, it is thought that the gas ingestion which occurred in the former runs reduced the waterhammer intensity by reducing the effective sonic velocity in the pipe. This thesis was further confirmed by the 500 x 500 mesh tests (Runs 71 to 74) where, despite high flow rates, the severe gas ingestion apparently eliminated waterhammer. The waterhammer phenomenon is further discussed in the following section on data correlation.

Except for the minimal screen response to waterhammer with the long line, neither the valve open or close time nor line length had any significant effect on screen device response beyond that expected and capable of being verified by the simulations using the H672 code with the screen model.

Examination of the initial startup flow pulse data shown in Table 13 revealed that many of the tests were subjected to excessive gas pressure, which led to gas ingestion regardless of conditions of flow, valve open/close speed, or line length.

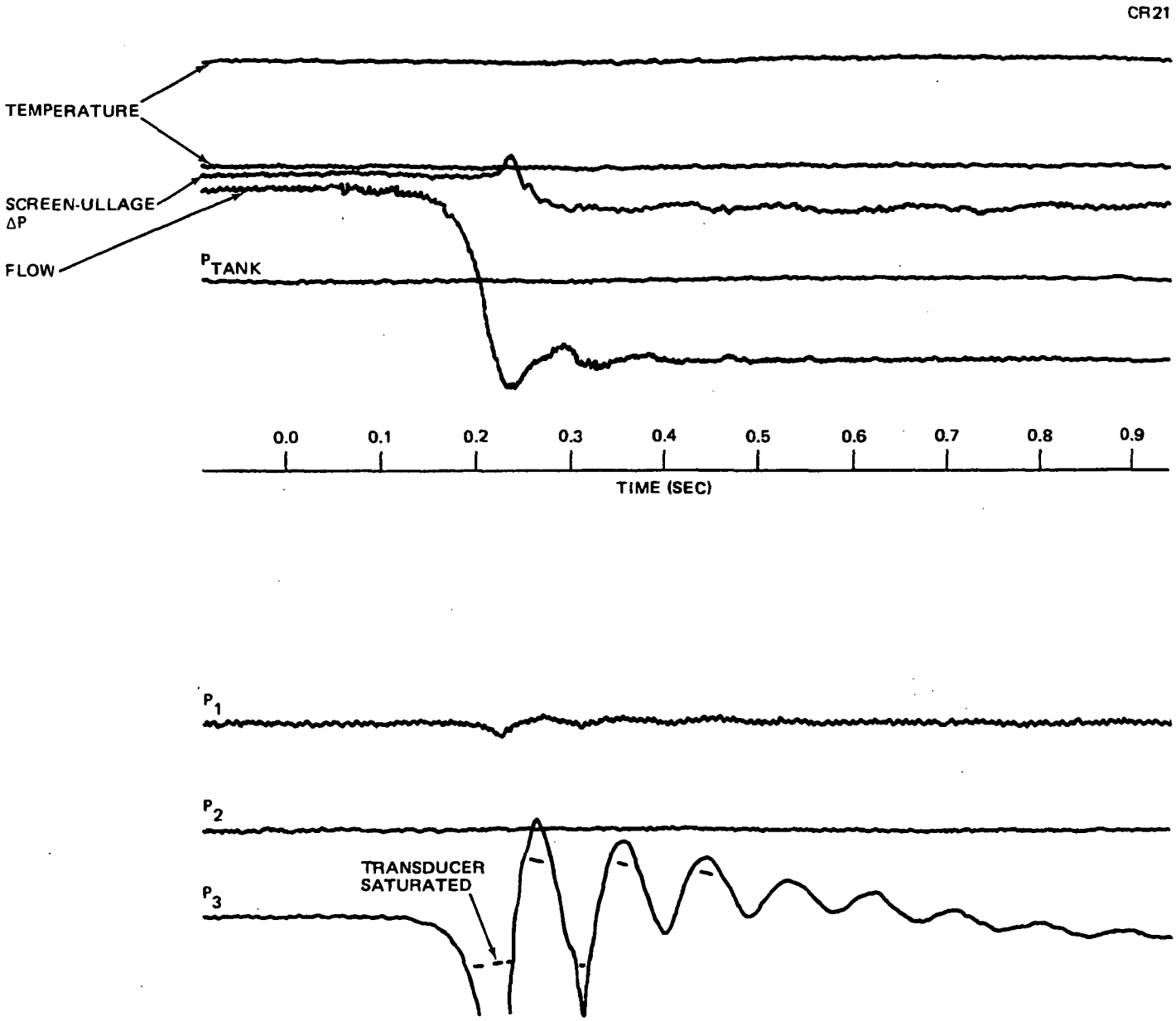

Figure 38. Run 25 Shutdown – 0.015 Second Valve – Long Line

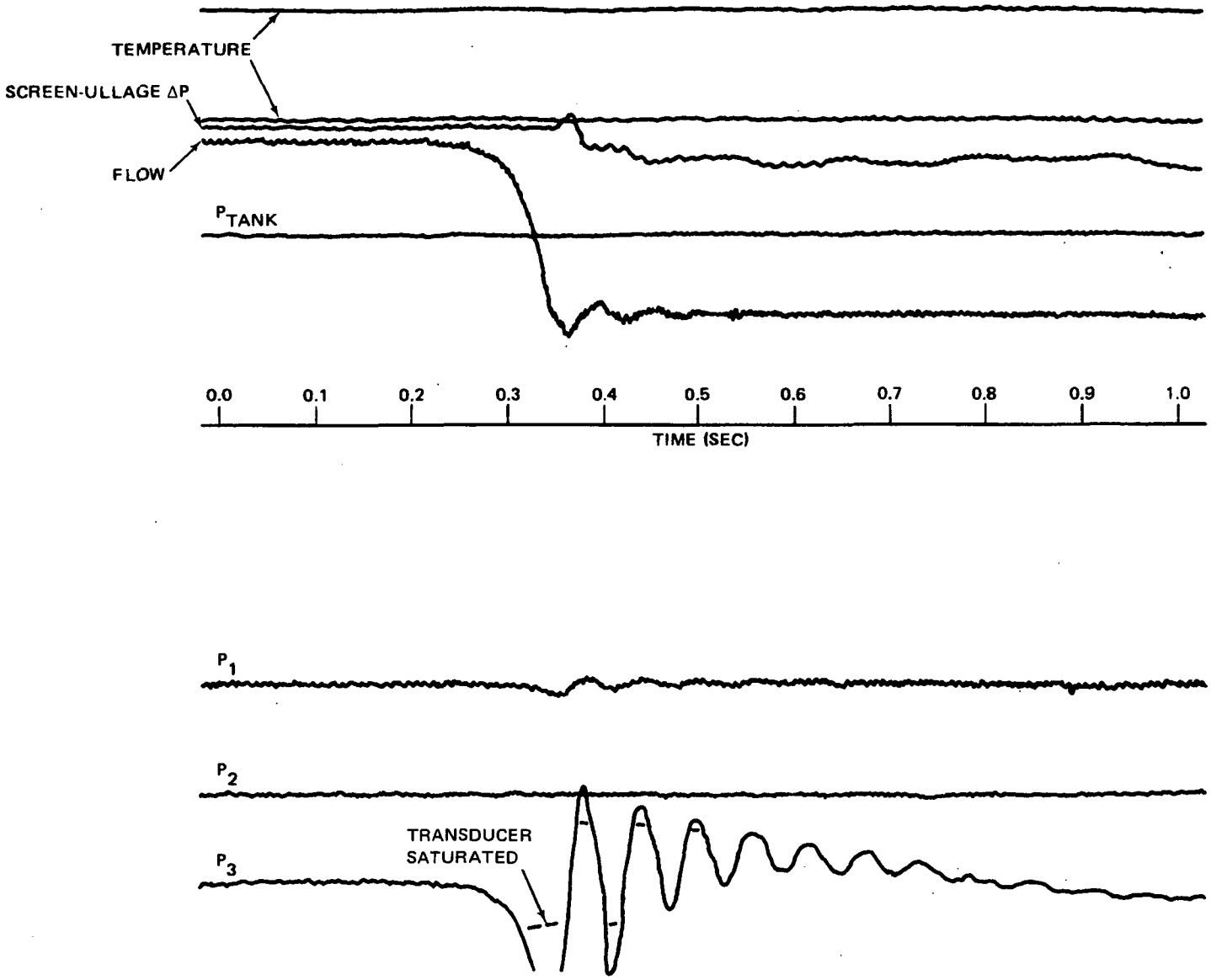

Figure 39. Run 26 Shutdown – 0.019 Second Valve – Long Line

Although it was anticipated that the minimum hydrostatic head imposed on the specimen would be about 5 cm (equivalent to 0.04 N/cm^2, or 0.06 psi), as discussed in the previous section, it was found that the minimum head which could be reliably imposed (so that bubbles were slowly and continuously emitted) was about 0.17 N/cm^2 (0.25 psi). (See Table 13.) It is thought that this may have been due to pressure drop through the very small remote-actuated bleed valve. This imposed head was quite close to the bubble point of the coarser mesh screens (see Table 12), which generally led to gas ingestion at flow startup. In addition, for some specimens there was minor leakage from the plexiglass gas enclosure which led to difficulties in clearing liquid from around the screen within the gas enclosure. When additional gas (pressure) was introduced to overcome this leakage and surround the screen with gas, the imposed pressure was inadvertently excessive (see, for example, Runs 88-91 of Table 13).

For many runs, gas ingestion occurred at startup as evidenced by gas bubbles caught in the bubble trap. Usually the quantity of gas ingestion was easily visible and readily measured. As noted from Table 13, apparently with some runs (e.g., compare Runs 24 and 25) not all gas ingestion was caught in the bubble trap and was detected by the flowmeter, as discussed previously.

Although startup gas ingestion was observed for many alcohol tests, liquid spill was never observed for horizontal specimens even at shutdown where waterhammer occurred. On the other hand, for the vertical specimens, liquid spill occurred on occasion during startup. Since the bubble trap could not be used with the vertical orientation, liquid spill was construed to indicate gas ingestion for these tests.

Despite the fact that the 104 alcohol tests were performed with all 13 test specimens listed in Table 8, the problem of inadvertent gas overpressure which occurred with many of the lower bubblepoint screens (e.g., Runs 27-58, 67-73, 88-91) effectively masked the effects of other parameters and reduced the usefulness of these tests in providing data for analysis and correlation.

Freon 114 Tests

The experiment matrix for the Freon 114 tests included 48 tests using 10 of the screen/structure specimens (the 165 x 800 mesh structural backup specimens were not tested) as shown in Table 13. The number of Freon 114 tests performed was somewhat reduced from that planned in Table 9, because it was found after about the first 16 tests (see Table 13) that it was impractical to continue testing the "long" line configuration. The reason for this was that the "long" line could not be kept wet up to the valve because heat transfer and line boiling resulted in reverse flow and emptying of the line before the run could be started. This occurred even with preflow to fill and chill the line before actual test initiation. For the same reason, it was found impossible to obtain reliable bubble point data for the specimens using Freon 114; therefore, the alcohol bubble point data were extrapolated to Freon 114 properties, as shown in Table 12. Another consequence of the line boiling was gas backflow into the bubble trap, which made if difficult to empty the bubble trap of gas prior to the run. Thus for many runs the bubble trap was nearly empty and gas ingestion could not be measured in the bubble trap but was inferred from liquid spill from the specimen (e.g., Runs 119 to 152). The partly empty bubble trap may also have contributed to gas ingestion observed by the oscillograph for Runs 119 to 152. Therefore, the most reliable runs for analysis of hydrodynamic effects were the runs with vertical orientation when the bubble trap was not used.

The first tests (Runs 105 to 108) were with the Freon 114 saturated at 2.1 N/cm^2 (3.0 psig), which is equivalent to a fluid temperature of 282.2 K (48°F). This was quite close to the line temperature, hence significant line boiling did not occur. Note that as the line got more chilled down, from Run 105 to 107, the screen-ullage pressure difference got smaller (the low flowrate of Run 108 was due to low fluid level relative to the screen at startup). For tests run with the Freon 114 saturated at 0.0 N/cm^2 (0.0 psig), the reverse flow caused by line boiling tended to fill the gas enclosure with liquid, which resulted in inadvertent gas overpressure (e.g., Run 109) that caused gas ingestion. Even when the line was chilled enough so that backflow did not cause gas overpressure, the flow into the partially empty line caused a large spike in screen-ullage pressure differential (Run 110) but inconclusive

"Page missing from available version"

page 89

encountered during the Freon 114 tests of line boiling, inadvertent overpressure in the gas enclosure, backflow, surging, and liquid spill also occurred to some degree during the LH_2 tests. Additional problems peculiar to testing with LH_2 also occurred. These included a reduced amount of instrumentation which included only platinum resistance temperature transducers, screen-ullage pressure difference, pressure upstream of the cryogenic ball valve, and a dewar pressure gage. In addition, on occasion the screen-ullage pressure differential transducer was either noisy or failed to function (see Note 11 in Table 13). The dewar vacuum was lost initially and necessitated repair of a dewar window, which resulted in good dewar performance for the balance of the test program. Although great care was taken to slowly chill and fill the dewar, apparent stress concentrations in the plexiglass gas enclosure caused them to crack and leak gas in some specimens. The gas enclosure around the 200 x 1400 pleated specimen cracked so severely that gas was not in contact with the specimen (see Runs 159 to 162 in Table 13), and for the 200 x 1400 plain specimen only partial gas coverage of the specimen was obtained (Runs 167 to 170, Table 13).

It was anticipated that the effect of saturation pressure on line boiling cryosurge could be determined; these effects were apparently masked by the degree of line chilldown which contributed more significantly to the cryosurge effect. The line downstream of the valves was insulated and became progressively more chilled with each test, and it was not practical to allow the line to warm up between tests. Since the line temperature distribution after each test was not well defined, the first test in each series was the optimum test for analysis in terms of a known temperature distribution in the downstream line.

The LH_2 dewar driving pressures of 3.5 N/cm^2 (5 psig) and 6.9 N/cm^2 (10 psig) were selected to give comparable volumetric outflow rates as for the alcohol and Freon 114 tests. Because the flowmeter resistance was not present, and the downstream resistance was reduced (the line downstream of the valve was empty), and the LH_2 density and viscosity are low, the initial LH_2 flowrate was higher than anticipated. This led to dynamic pressures which were excessive compared to the low bubble point of screens in LH_2 (see Table 12) and generally resulted in startup gas ingestion.

gas ingestion. That is, the flowmeter trace on the oscillograph showed some "noise," but not the severe spiking shown in Figure 34. The flowrate for Run 110 was probably low due to vapor choking (boiling) in the line; the next two runs showed reasonable flow rates, but because the imposed screen-ullage pressure differential was close to the screen bubble point, inconclusive gas ingestion occurred. Obvious specimen movement also occurred as a result of the line boiling and surging.

The differences in screen device performance between tests with Freon 114 saturated at 0.0 N/cm^2 or saturated at higher pressures was basically that the higher temperature (saturation pressure) fluid produced more reliable hydrodynamic effects because the effects of line boiling were minimized. On the other hand, lower temperature fluid led to line boiling, partially empty lines, and possible large flow surges and pressure spikes as described above.

Because of the erratic flowrate and pressure behavior caused by line boiling and emptying, it was decided to restrict the remaining Freon 114 tests (Runs 121-152) to the "short" line configuration in the hope that the line could be kept wet up to the valve, and the results of downstream line boiling on screen response observed under repeatable flow conditions. Unfortunately, the same problems occurring during the alcohol tests of imposing excessive screen-ullage pressure differential (above the 5.0-cm head planned) were magnified with the Freon 114 tests. Because of the increased density of Freon 114, the gas head which could be reliably imposed was of the order of 0.28 N/cm^2 (0.4 psi, compared with 0.17 N/cm^2, or 0.25 psi, for alcohol; see above) which is near the bubble point of even the 200 x 1400 mesh because of the reduced surface tension of Freon 114 compared to alcohol (see Table 12). Efforts to reduce this imposed head were not successful because of the arrangement of the gas-bleed valve, and hence general gas ingestion was observed for most of the tests with the coarser screens. This problem had been anticipated with the LH_2 tests which was why only the 325 x 2300 mesh and 200 x 1400 mesh screens were tested with LH_2.

LH_2 Tests

The experiment matrix for the LH_2 tests included 25 tests using six of the screen/structure specimens, as shown in Table 13. The problems

As was the case in the Freon 114 tests, the boiling at the valve resulted in backflow which tended to fill the bubble trap with gas, and which resulted in liquid spill as evidence of gas ingestion. Therefore, as was the case with the Freon 114 tests, the vertical specimen configuration would have produced more reliable data; unfortunately, the pressure difference transducer behaved erratically during most of these tests, as shown in Table 13. It was concluded that the first series of tests with the 325 x 2300 mesh specimen yielded the best test data and demonstrated the cleanest example of line boiling cryosurge and screen response to the cryosurge.

It was anticipated that modelling of these tests with both the P4557 cryosurge code and then with the H672 code would provide adequate verification of the screen model as well as the capability of the analyses to model test specimen response with LH_2. The modelling of the LH_2 tests is described in detail in the next section.

Page
Intentionally
Left Blank

DATA CORRELATION

In order to obtain correlation of the experimental data with the transient effects analysis, it was necessary to model the transient test apparatus and screen specimen for simulation with the H672 computer code. The objective of the data correlation was to verify important aspects of the analytical representation of the screen device. These aspects include (1) modelling of the screen device as a uniform composite structure with orthotropic structural properties based on a combination of screen and backup material properties, and (2) modelling of the gas ingestion, liquid inflow/outflow, and liquid spill characteristics of the screen device. The first aspect would be effected by comparing the performance of plain screen, pleated screen, screen backed up with coarse screen, and screen backed up with perforated plate, all of which have different screen fractions, f, and for some, different structural compliance. The second aspect leads from the first and would be verified by prediction of gas ingestion (or not) and ingested quantity under conditions which would occur experimentally. These predictions should be effected for conditions of startup, shutdown, and for all three experimental fluids.

TEST APPARATUS MODEL

In order to obtain realistic simulation, the test apparatus must be modelled accurately in order to achieve the necessary flowrates at the prescribed conditions of pressure and configuration. The test apparatus model is shown schematically in Figure 40, which identifies the heads, H_1, etc., and flows, Q_1, etc., throughout the test apparatus. The flow system starts with a tank (1), modelled by subroutine SRO5, connected to a resistance (2), modelled by SRO2. In actuality, the screen specimen is dead-ended and all outflow is through the screen, but in order to be compatible with the H672 program requirements, a very high resistance was used so that the flow through it is less than 0.1% of the screen flow. Following the resistance comes (3) the "wet" screen, (surrounded by liquid), and (4) the "dry" screen (surrounded

PRECEDING PAGE BLANK NOT FILMED

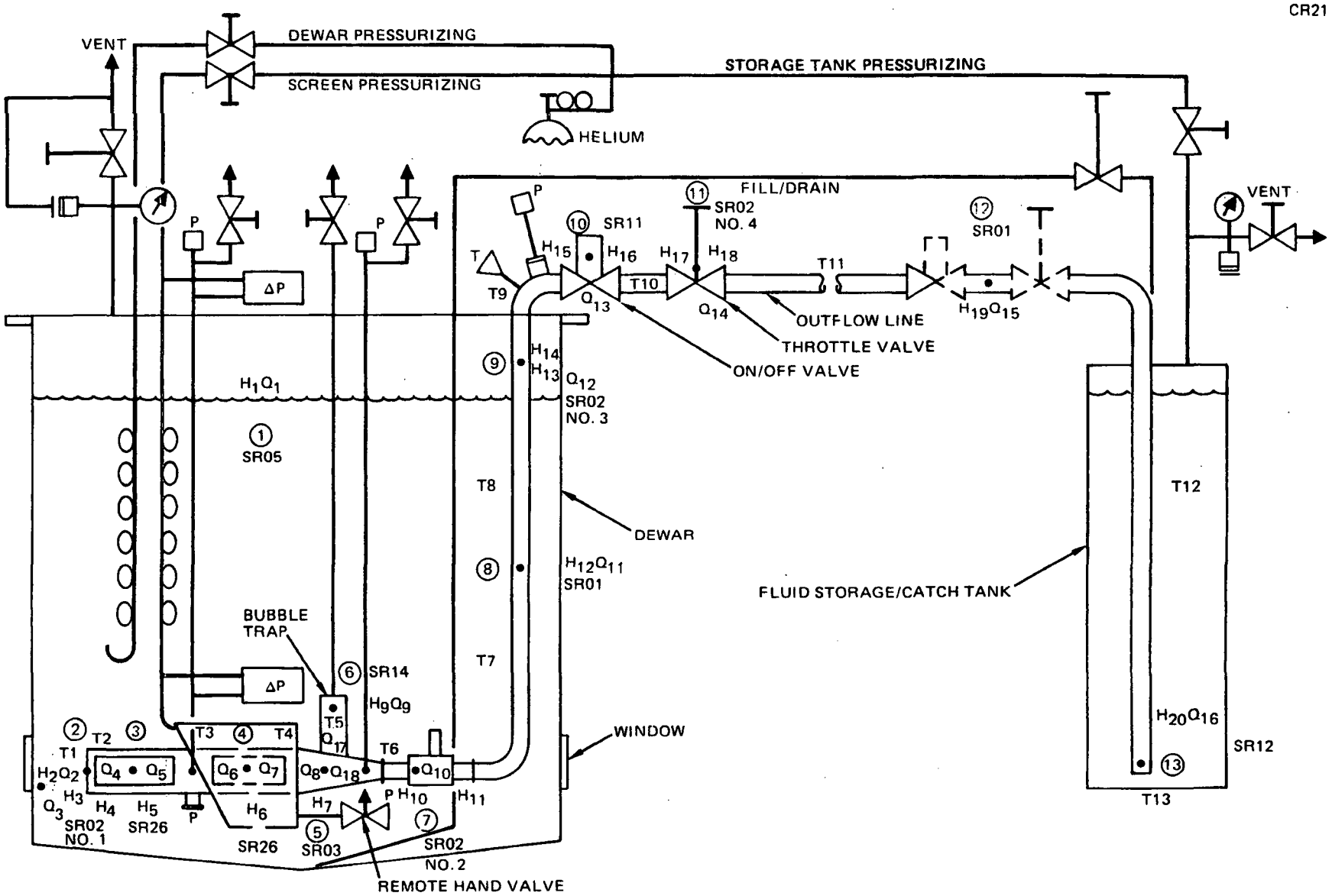

Figure 40. Test Apparatus Model Nomenclature

by gas), both modelled by SR26. Next comes a branch (5), SRO3, which leads to the bubble trap (6), modelled as a dead-ended pipe, SR14. The branch also leads to the flowmeter, (7), modelled as a resistance SRO2, then a simple pipe junction (8), modelled by SRO1. Next is another resistance (9), SRO2, which accounts for the pipe frictional resistance between the flowmeter and control valve (10) modelled by SR11. Following the control valve is the throttle valve (11), also modelled as a resistance, SRO2, which includes also the frictional resistance of the pipe downstream of the throttle valve. Finally, another simple junction (12), SRO1, connected to the outlet in the receiver tank, (13), modelled by an injector, SR12. The configurational details of each component are shown in Table 14. The actual pipe lengths and sizes were used, except for the bubble trap and screen devices, in which artificial wall thicknesses were used to make these lower modulus pipes modelled accurately by steel pipes with a common modulus of 2.07×10^7 N/cm^2 (3×10^7 psi), as required by the H672 code. The actual tank size and average ullage height were used, together with the measured initial ullage pressure. The resistance values for the flowmeter and pipes were essentially based on frictional fluid flow analysis and modified as necessary to obtain the proper baseline flowrate at a baseline tank ullage pressure. Common values of resistance were used for all simulations either with the "long" or "short" line configuration. The valve open/close characteristics were modelled as accurately as possible from the experimental data; a total valve opening time of 0.2 second was used (the effective valve opening time depended on the relative resistance values throughout the flow circuit). Details of the screen devices depend on the specimen configuration and are discussed below.

TESTS SELECTED FOR CORRELATION

To verify the screen analytical model, only certain tests were selected for detailed analysis using the H672 code. This was necessitated by the fact that H672 is quite complex to set up, and fairly costly to run; further, many of the tests were inappropriate for simulation due to experimental problems of leakage, overpressure, etc., as discussed previously.

In examining data from Table 13 to determine appropriate runs for simulation, it was noticed that, for many initial runs following specimen or line length

Table 14

TEST APPARATUS CONFIGURATION MODEL FOR H672 CODE

Components			Pipe Parameters ID	Length (ft)	Type	Datum Height (ft)
1.	SR05	Tank	T1	0.01	1	0.0
2.	SR02	Resistance	T2	0.13	1	0.0
3.	SR26	Screen (wet)	T3	0.30	1	0.0
4.	SR26	Screen (dry)	T4	0.22	1	0.0
5.	SR03	Branch	T5	0.33	3	0.0
6.	SR14	Bubble Trap	T6	0.83	2	-0.33
7.	SR02	Flowmeter	T7	1.08	4	-0.67
8.	SR01	Junction	T8	15.70 L* 0.70S*	4	-1.83
9.	SR02	Resistance	T9	15.70 L 0.70S	4	-3.50
10.	SR11	Valve	T10	0.50	4	-3.50
11.	SR02	Throttle Valve	T11	2.50 L 17.50S	4	-3.50
12.	SR01	Junction	T12	2.50 L 17.50S	4	-1.75
13.	SR12	Injector	T13	0.0	4	0.0
(14.	SR18	Cryosurge)	*L = Long S = Short			

Pipe Types	Diameter (in)	Wall Thickness (in)
1	Screen - depends on screen mesh and construction	
2	1.250	0.033
3	1.007	0.0033
4	1.000	0.035

Tank:	Dia (in)	Ullage Height (ft)	Volume (ft^3)
	16.9	3.0	5.58

Valve: 1.0 in Dia. Ball Valve, L/D = 3, C_v = 11.5, Open/Close Time = 0.20 sec.

Injector: Open pipe; C_v = 4.15; Back Pressure: 15.48 PSIA

changes, flowmeter "spiking" occurred during startup (e.g., Runs 1, 5, 13, 19, 24, etc), which may have been due to a partially empty line up to the valve. Such runs were basically not suitable for simulation since the H672 code requires liquid-filled lines up to the valve.

The first unambiguous and clearly observed and measured gas ingestion occurred with Runs 15 to 18. Run 15 was selected for analysis because it was at the lowest flowrate of the four runs (higher flowrate would increase the tendency for gas ingestion) and was also plain 200 x 1400 mesh. On the other hand, Runs 21 to 23 with pleated 200 x 1400 mesh, with 2.5 times the flowrate as Run 15 (6.25 times the velocity head) showed no tendency for gas ingestion; therefore, these runs (all at essentially identical head/flowrate conditions) were also selected for simulation.

The next several series of runs were not suitable because of either leakage or excessive initial imposed screen-ullage pressure difference. The 165 x 800 mesh with screen backup tests (Runs 60 and 61) were selected because Run 61 has a slightly higher flowrate than Run 60; thus, there was clearly observed and measured gas ingestion for Run 61, and Run 60 shows no evidence of gas ingestion.

Unfortunately, the 500 x 500 mesh screen tests generally showed gas ingestion due to a combination of unintentional gas overpressure plus possible external screen leakage. One test (Run 74) had the least ingestion (one bubble of 2.5 cm, or 1.0 in diameter, into the bubble trap, plus a minimal spiking region in the oscillograph trace for the flowmeter), so it was also selected for analysis. The previous test (Run 73) had more serious ingestion (3.8 cm, or 1.5 in, in bubble trap) plus general oscillograph spiking, but it too was selected for analysis.

All of the tests of 200 x 1400 mesh (with perforated sheet No. 1 backup) showed zero gas ingestion, and therefore the test with the maximum applied pressure differential and maximum flowrate (Run 79) was analyzed to verify that zero gas ingestion would be predicted. Similarly, all tests with 200 x 1400 mesh (with perforated sheet No. 2 backup) showed some startup gas

ingestion attributed to leakage. Run 85 ingested only a single bubble on startup which did not appear on the oscillograph, and Run 86 showed general ingestion, so these two runs were also selected.

All of the vertical specimens showed no tendency toward gas ingestion except the 325 x 2300 mesh specimen with no flowmeter. Runs 100 and 101, run at low tank (dewar) pressure, showed no ingestion, while Runs 102, 103, and 104, run at higher dewar pressure, showed clearly observed and measured liquid spill on startup, which was construed as gas ingestion. Therefore, Runs 101 and 102 were selected for simulation and comparison.

For the Freon 114 tests, there were few tests which were acceptable for simulation because of the problems of gas overpressure (due to higher density and lower surface tension of Freon 114, as discussed previously), combined with surging and the need for unambiguous determination of gas ingestion. The first three tests (Runs 105 to 107) showed no evidence of spill or oscillograph flowmeter trace spiking. Since all three runs were similar, the high flowrate test (Run 107) was selected for analysis. Nearly every screen/structure specimen was of lower bubble point and did not clearly indicate transition from zero gas ingestion to observed ingestion (as did the alcohol tests above) since general gas ingestion due to overpressure was the usual case.

For the LH_2 tests, most tests displayed problems of backflow into the bubble trap, and definite surging during outflow. The first test (Run 153) indicated a clear boiloff pressure spike at the valve, which also caused the differential pressure transducer at the screen to respond and follow the surge. Subsequent tests often did not display clear line boiloff pressure surges because the line was chilled down to some degree. For the first test in each series, the line temperature could be estimated with reasonable accuracy, unless preflow for operational reasons had chilled the line. Run 153 was unique in that it was the best example of cryogenic line boiling pressure surge, the line temperature was known, the screen specimen had maximum bubble point and reasonable initial gas pressure imposed, and all instrumentation was operating properly. Therefore, it was the only LH_2 test modeled.

The 15 tests selected for the H672 simulation, including the observed initial gas pressure imposed on the screen, flowrate, and gas ingestion, are summarized in Table 15. It is believed that the tests selected represent a comprehensive cross-section of specimens and test conditions that will allow definitive correlation of the important aspects of the model for transient behavior of screen devices as described earlier.

Table 15

TESTS SELECTED FOR H672 SIMULATION

		Experimental Observations				
		Initial ΔP		Flowrate		Gas Ingestion
Run No.	Mesh/Configuration	N/cm^2	psi	Kg/sec	lb/sec	Quality
15	200 x 1400 Plain	0.17	0.25	0.10	0.22	0.012 - 0.016
21, 22, 23	200 x 1400 Pleated	0.14	0.20	0.25	0.55	0
60	165 x 800 Screen Backup	0.11	0.16	0.12	0.26	0
61	165 x 800 Screen Backup	0.12	0.17	0.14	0.30	0.0015
73	500 x 500 Plain	0.14	0.21	0.28	0.61	0.22
74	500 x 500 Plain	0.05	0.07	0.28	0.61	0.099
79	200 x 1400 Perf. Sheet	0.14	0.21	0.08	0.18	0
85	200 x 1400 Perf. Sheet	0.18	0.26	0.05	0.10	0.148*
86	200 x 1400 Perf. Sheet	0.18	0.26	0.07	0.16	0.444*
101	325 x 2300 Plain	0.07	0.10	No flowmeter		0
102	325 x 2300 Plain	0.08	0.11	No flowmeter		0.003 - 0.012
107	325 x 2300 Plain	0.24	0.35	0.28	0.62	0
153	325 x 2300 Plain	0.03	0.04	No flowmeter		0.091

*Includes leakage

SCREEN SPECIMEN MODEL

Development of the pertinent screen specimen properties and characteristics for input to H672 requires knowledge of certain properties which are not well-defined, such as percent open area (PO) for the dutch weave screens, and effective screen fraction (f) for composite screen/structure specimens. The structural properties of the composite also depend on the screen fraction (f), as well as the structural properties of the components of the screen/structure specimen. For modelling purposes, assumptions were made for the f of each type of screen/structure specimen, depending on their construction characteristics. As shown previously in Figure 23, the screens are slipped over a support tube, which has three longitudinal struts (0.64 cm or 0.25 in wide by 7.6 cm or 3.0 in long), and are then bonded to the support tube ends. For the plain screens, it was assumed that the struts would obstruct flow through the screen, so the effective screen fraction would be the screen area less the strut area, which results in an f of 0.84. However, the struts would not materially affect the deflection of the screen (since the screen would deflect into the space between the struts) so that steel strut properties (modulus of elasticity, etc.) were ignored and only the screen properties were used in evaluating the specimen structural properties.

The pleated screen specimens were made with 0.5 cm (0.2 in) deep pleats which increased the effective specimen diameter to 4.3 cm (1.7 in), rather than the 3.8 cm (1.5 in) diameter of the plain screens. The f for the pleated screens was found by taking the actual screen circumference (number of pleats times 2.0 times 0.5 cm) and dividing by the circumference of a 4.3-cm cylinder.

The perforated sheet used as screen backup material was stainless steel 0.064 cm (0.025 in) thick with 0.478 cm (0.188 in) holes giving 50% open area. It was assumed that the 50% solid sheet kept half the screen from deflecting and obstructed half the flow area of the screen, hence the f was equal to 0.5. The perforated sheet did not contact the three struts mentioned above, so that their additional blockage was ignored. In addition, it was assumed that the structural properties of the screen/sheet composite were

made up of a 50% contribution by the screen and a 50% contribution by the solid sheet in accordance with equations (3) through (7). (See the section on Analytical Program.)

For the screen backed up with coarse-mesh screen, two different models were assumed:

1. The coarse mesh would make only point contact with the fine mesh. The fine mesh could deflect freely into the spaces of the coarse screen, giving f = 1.0 and assuming that the coarse screen properties do not contribute to the composite properties, but only the fine mesh screen properties would be used. It was also assumed that the PO for the fine mesh screen would be used since the coarse mesh screen would not materially affect the flow.
2. The second model assumed that the coarse screen rigidly supported the fine mesh screen, but that the coarse screen did not block the flow area of the fine screen, hence the screen fraction f would still equal 1.0. However the coarse screen properties would be combined with the fine mesh properties in the ratio of (1-PO) and PO, according to equations (3) through (7). For this case of the "rigidly" supported fine screen, again only the fine screen PO would be used.

The two models described above represent the two extremes of screen structural/flow behavior: the first quite compliant with minimum tendency for gas ingestion, and the second quite stiff with maximum gas ingestion tendency.

The percent open area (PO) was shown in the Analytical Program section to be important in affecting screen gas ingestion characteristics, yet it can not be analytically defined for dutch weave screens. However, for all square weave screens, PO can be analytically defined and can be related to the square weave screen void fraction, ϵ, by

$$PO = \epsilon^n$$

where the exponent n has values from 2.4 to 2.6. It was assumed that it would be conservative to use the same equation to define the value of PO for

dutch weave screens based on their ϵ (which is known), since the weaving process for the dutch weave screens could tend to reduce the PO relative to square-weave screens. The larger PO thus assumed for the dutch weave screens would have a greater tendency for gas ingestion, hence would be conservative.

The experimental proportional limit stress, elastic moduli, bubble point, and flow loss coefficients were used to define the required inputs for all of the screen/structure specimens selected for analysis that are shown in Table 16. Different models for the coarse screen backup specimens would be resolved through the results of the data correlation. The bubble points and flow loss coefficients (and gas properties) also depend on the test fluid properties; those shown in Table 16 are for isopropyl alcohol. All the units in Table 16 are British Engineering Units because these were used in the H672 code.

CORRELATION RESULTS

There are a number of problems in running the H672 code which make correlation of experimental data difficult. First, the computing time step must be kept small ($\sim$0.0005 sec) in order to be a reasonable approximation of the acoustic wave travel time through the shortest important component. On the other hand, the acoustic length of the longest component cannot exceed 40 time steps, so the system piping must be broken down into relatively short lengths. Because of the short computing time step, obtaining a reasonable time span for simulation requires many steps and results in large quantities of data. Start up of the flow process (valve opening) is straightforward, but it is not practical to start the simulation run with an existing head/flow distribution and shut down (valve closing) because the heads and flows everywhere in the system must be accurately and consistently specified. Therefore, in order to simulate shutdown, the simulation must also include startup, followed by adequate run time to achieve reasonable stability. To obtain the best compromise between total run time (and volume of data) startup flow stabilization, shutdown, and transients following shutdown, the following arbitrary event timing was used: valve starts to open at 0.001 sec, valve is wide open at 0.201 sec, valve starts to close at 0.25 sec, valve is completely closed at

Table 16

SCREEN/STRUCTURE SPECIMEN CHARACTERISTICS
(Alcohol)

Mesh	Construction	BPS*	EE	STEM	AS1	BS1	AS2	DPS	DS	DC	PO	f
325 x 2300	Plain	2.57	4473.	60.3	21.35	2.27	0.187	0.000020	1.5	0.0001035	0.027	0.84
200 x 1400	Plain	1.71	5753.	46.6	16.57	2.01	0.145	0.000033	1.5	0.0000791	0.027	0.84
200 x 1400	Pleated	1.71	3952.	46.6	16.57	2.01	0.145	0.000033	1.7	0.0000791	0.027	2.40
200 x 1400	Perf. Sht.	1.71	59430.	46.6	16.57	2.01	0.145	0.000033	1.6	0.00000582	0.027	0.50
165 x 800	Scrn. Backup Model (1)	0.82	4114.	67.25	2.023	0.264	0.0177	0.000069	1.6	0.0000920	0.11	1.00
165 x 800	Scrn. Backup Model (2)	0.82	9006.	67.25	2.023	0.264	0.0177	0.000069	1.6	0.00003954	0.11	1.00
500 x 500	Plain	0.80	1031.	12.44	1.037	0.140	0.0091	0.0000833	1.5	0.000409	0.25	0.84

*See Table 3 for nomenclature and units.
Common to all screen specimens were

LS = 3.0 in. Gamma = 1.67 RTGAS = (Depends on fluid temperature)

0.45 sec, and run terminates at 0.75 sec (the total valve open/close time was not arbitrarily selected, but was based on the experimental data). The simulations that follow show that the flow often continues to increase and/or stabilize even while the valve is closing so that usually more than 0.4 sec is available to analyze the startup transient, and about 0.3 sec to analyze the shutdown transient. However, these are rather limited times relative to the experiment operation times (~3 sec) or fluid boiling transient times (~1 to 5 sec depending on fluid), so that a certain amount of phenomenological overlap is inevitable. Generally, this problem does not arise; exceptions will be discussed below. Three basic parameters were chosen for the data correlation: (1) the screen-ullage pressure differential, (2) the outflow rate, and (3) the gas ingestion quantity (converted to effective quality in the screen device.) Correlations for this first two parameters are presented as plots generated by the H672 code and the SC4460 plotter, superimposed on which are the experimental data taken from the oscillograph records such as shown in Figures 34 to 39. The gas ingestion quantity observed in bubble trap or via liquid spill quantity is compared to the H672 prediction as a gross number (not as a plotted parameter).

The first test simulated (Run 15) had experimentally shown modest gas ingestion (equivalent quality, X, of 0.012 to 0.016) manifested as a single 1.3-cm (0.5-in) diameter bubble into the bubble trap at startup. The H672 simulation for this test, run at the proper flowrate, indicated gross, unstable gas ingestion starting at 0.436 sec, which reached X = 0.14 at 0.471 sec. The unstable pressure surges caused excessive screen stress at 0.464 sec, as shown in Figure 41, and a gross flow reversal. The apparent stabilization of the pressure surges after 0.53 sec is artificial since the code was no longer computing properly due to the gross instabilities experienced earlier. As these instabilities were not in accord with observation, the screen model was reexamined.

The model had assumed that gas ingestion was uniformly distributed through the screen device and affected the acoustic velocity in the screen device according to equation (27). It was apparent that uniformly distributed gas ingestion was not a physical reality for the screen specimen, because essentially all gas ingestion would occur at the top downstream edge of the screen (where the dynamic/friction/gravity head difference is maximum), and

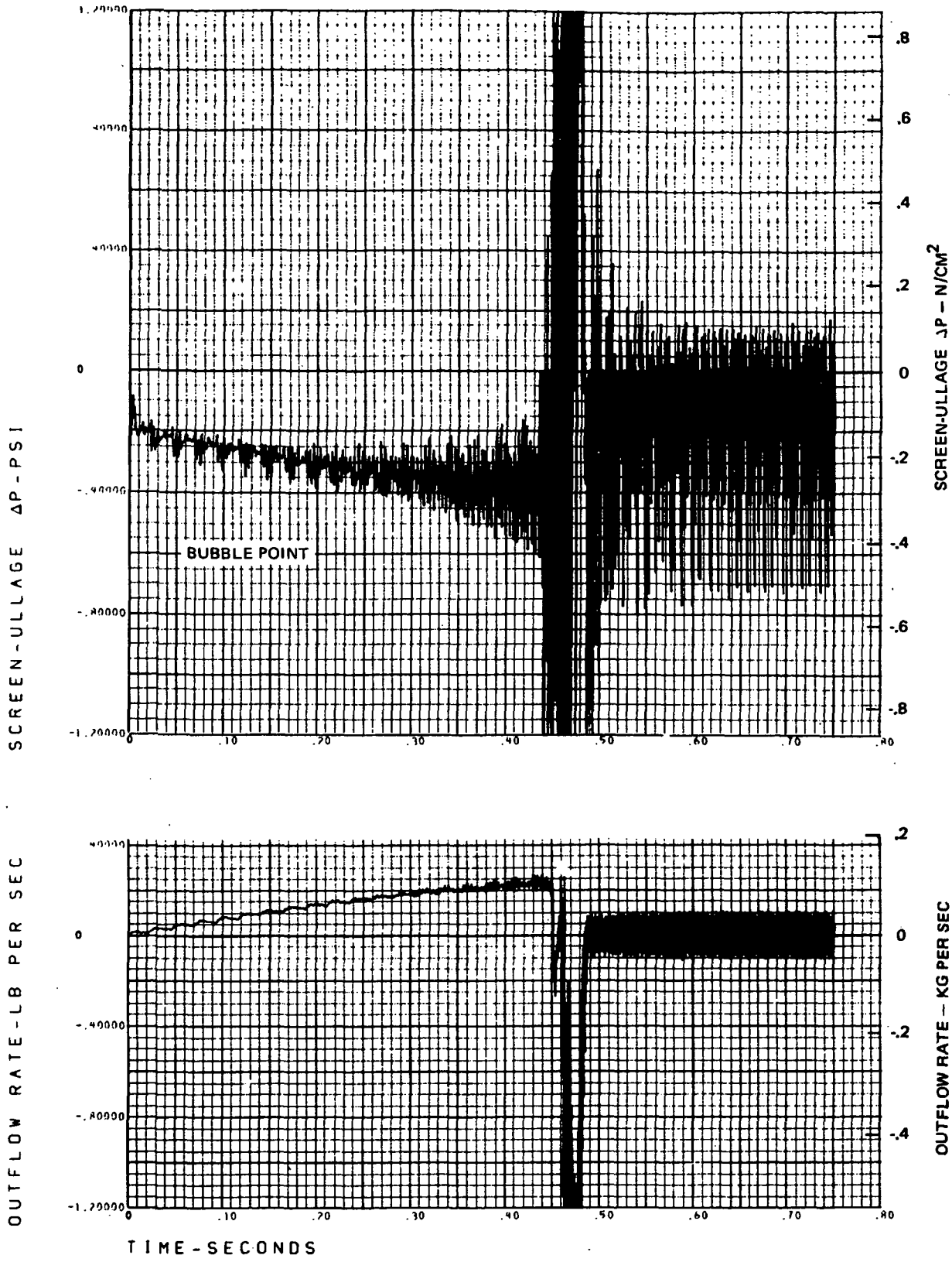

Figure 41. H672 Simulation — Run 15 — [a' = f(x)]

quickly would move into the bubble trap (see Figure 42) where it would no longer affect the screen or pipe flow or acoustic properties. Therefore, the screen model was modified so that the quality increase from gas ingestion no longer affected the acoustic velocity in the screen device. The effects of the model change on the screen-ullage pressure difference and flow for Run 15 are shown in Figure 43.

The final quality is X = 0.014, which is excellent agreement with experiment, and the pressure differential is stable and does not result in excessive stress, while the flowrate after shutdown behaves in much more reasonable fashion. Also shown in Figure 43 is the good agreement with starting experimental data, which verifies that the assumptions made in deriving PO and f were appropriate. The pressure surges occurring after shutdown were a common simulation problem which is discussed in detail below.

CR21

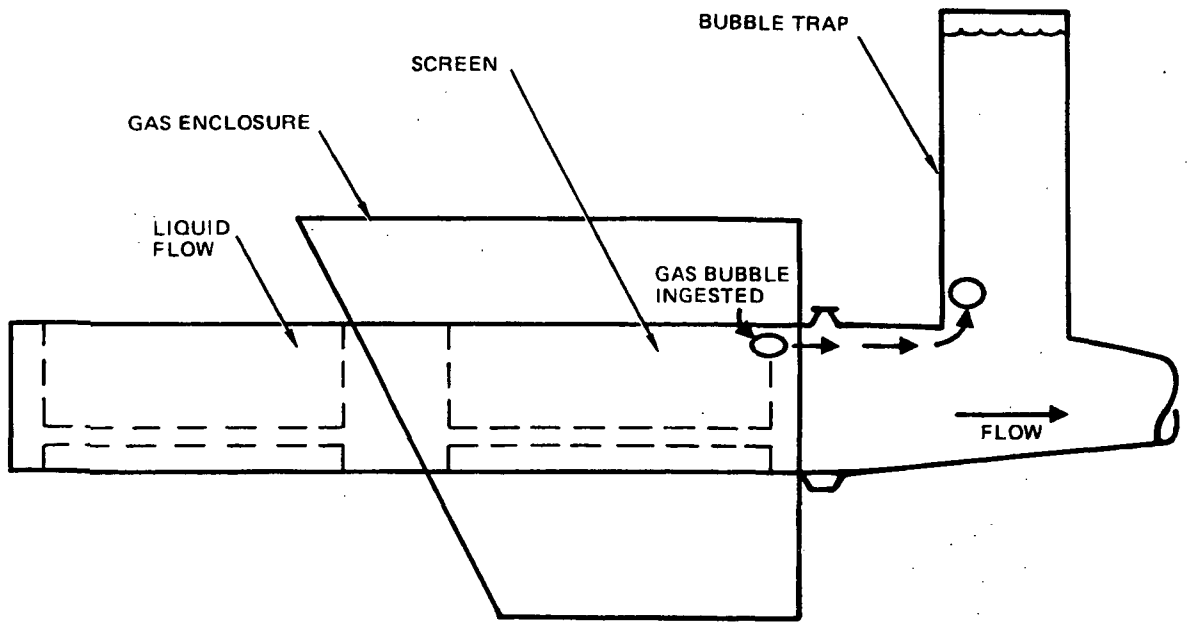

Figure 42. Bubble Ingestion Phenomenon

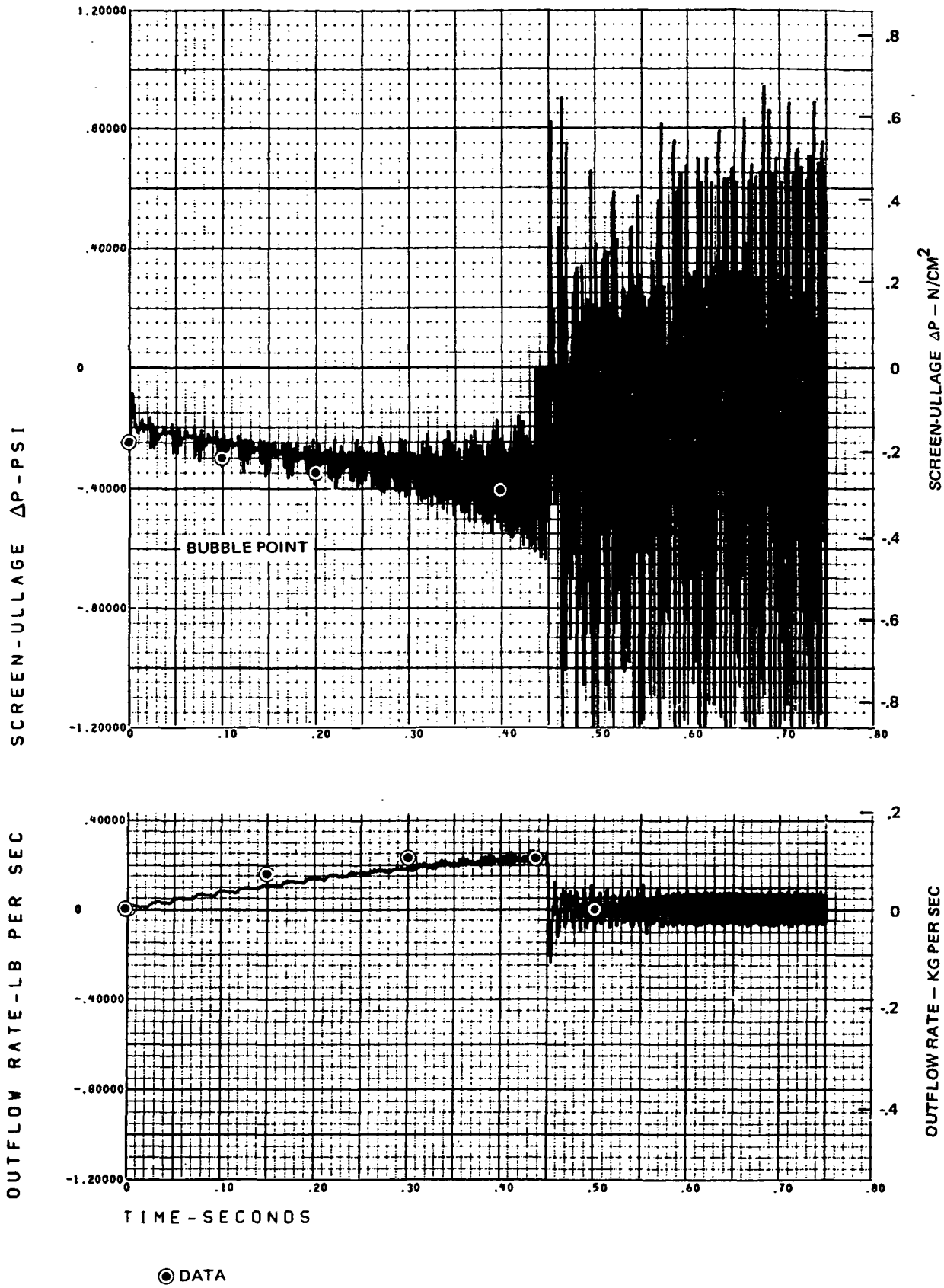

Figure 43. H672 Simulation – Run 15

For the vertical specimen orientation, where the bubble trap is not used, it was conceivable that bubble ingestion could still affect the acoustic velocity and pressure/flow relationships in the screen device. Run 102 with the 325 x 2300 screen specimen in the vertical orientation, demonstrated a very small liquid spill of 0.25 to 1.0 cc (construed to be equivalent to a gas ingestion quality of 0.003 to 0.012). When the original model (with screen acoustic velocity a function of X) was used to simulate run 102, gas ingestion started at 0.448 sec and continued until the screen stress was encountered at 0.461 sec, as shown in Figure 44. Note also in Figure 44 the gross discontinuities at about 0.5 sec. When the modified model was used to simulate run 102, the predicted quality was 0.003 at 0.448 sec, and the predicted pressure differential and flowrate are shown in Figure 45. Figure 45 also shows the agreement with the pressure differential data (flowrate data was not taken).

It was apparent that the screen model in which the quality increase due to gas ingestion does not affect the acoustic velocity within the screen device was physically more realistic and provided better correlation of the experimental data, hence this model was used for all further data correlation.

Simulation of Run 101 (companion run to Run 102) indicated that zero gas ingestion occurred, as observed experimentally. The simulations compared to experimental data for pressure difference and predicted flowrate are shown in Figure 46.

For the 200 x 1400 mesh pleated specimens (Runs 21, 22, 23), the simulation of the startup flow and pressure differential (see Figure 47) was excellent, and no gas ingestion was predicted (in agreement with the experimental data) until after the shutdown pressure spike arrived at 0.484 sec. Note that Figure 47 indicates that significant pressure surging was predicted following shutdown. In fact, the data showed no such surging. The observed shutdown behavior for virtually all tests was poorly simulated by the H672 code. The code generally predicted a very large pressure spike (over 69 N/cm^2, 100 psia, in some cases) at the valve immediately after valve closure; this was not observed by the pressure transducer at that location. In the half-dozen or so cases of waterhammer that were observed, the maximum pres-

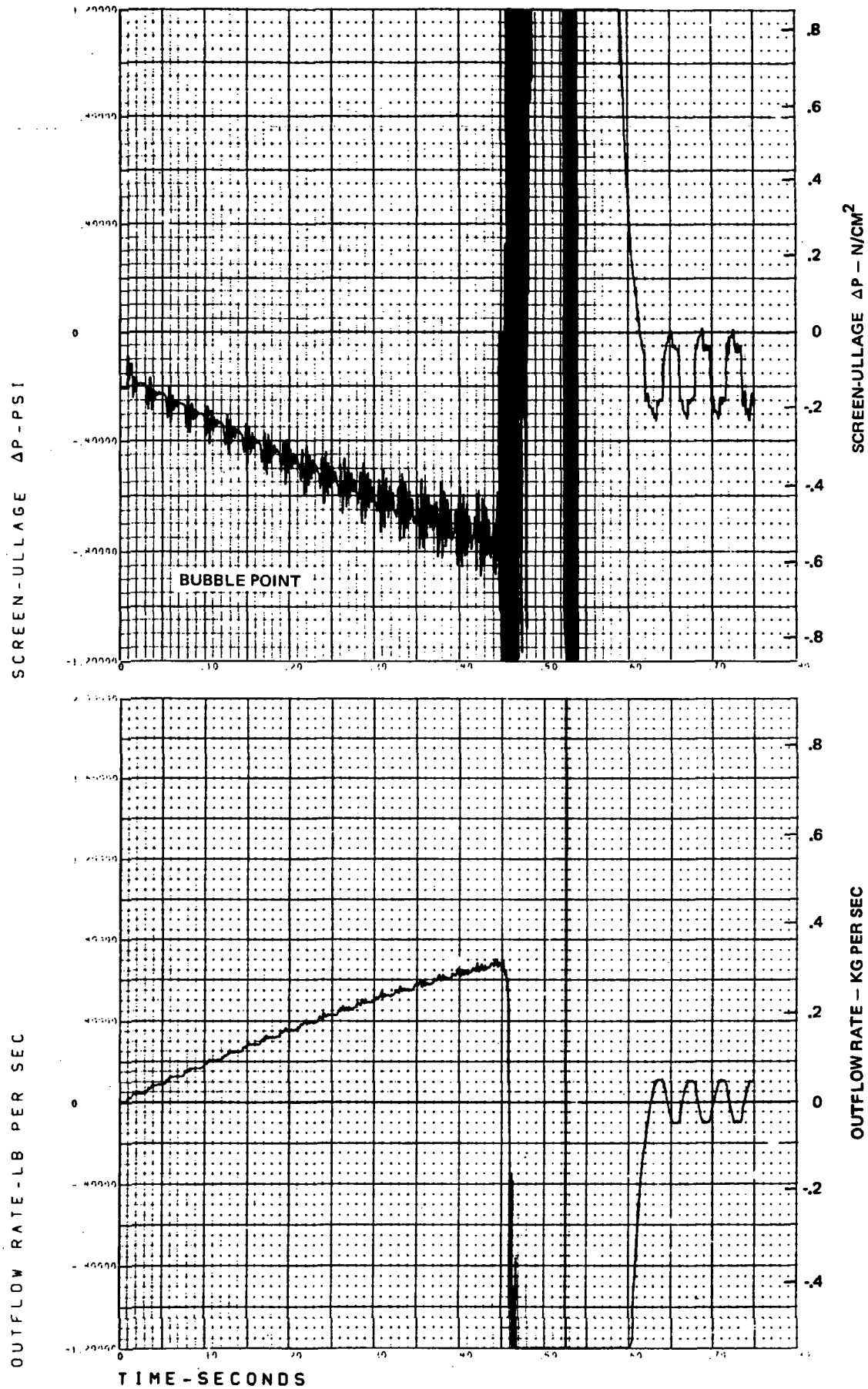

Figure 44. H672 Simulation — Run 102 — [a' = f(x)]

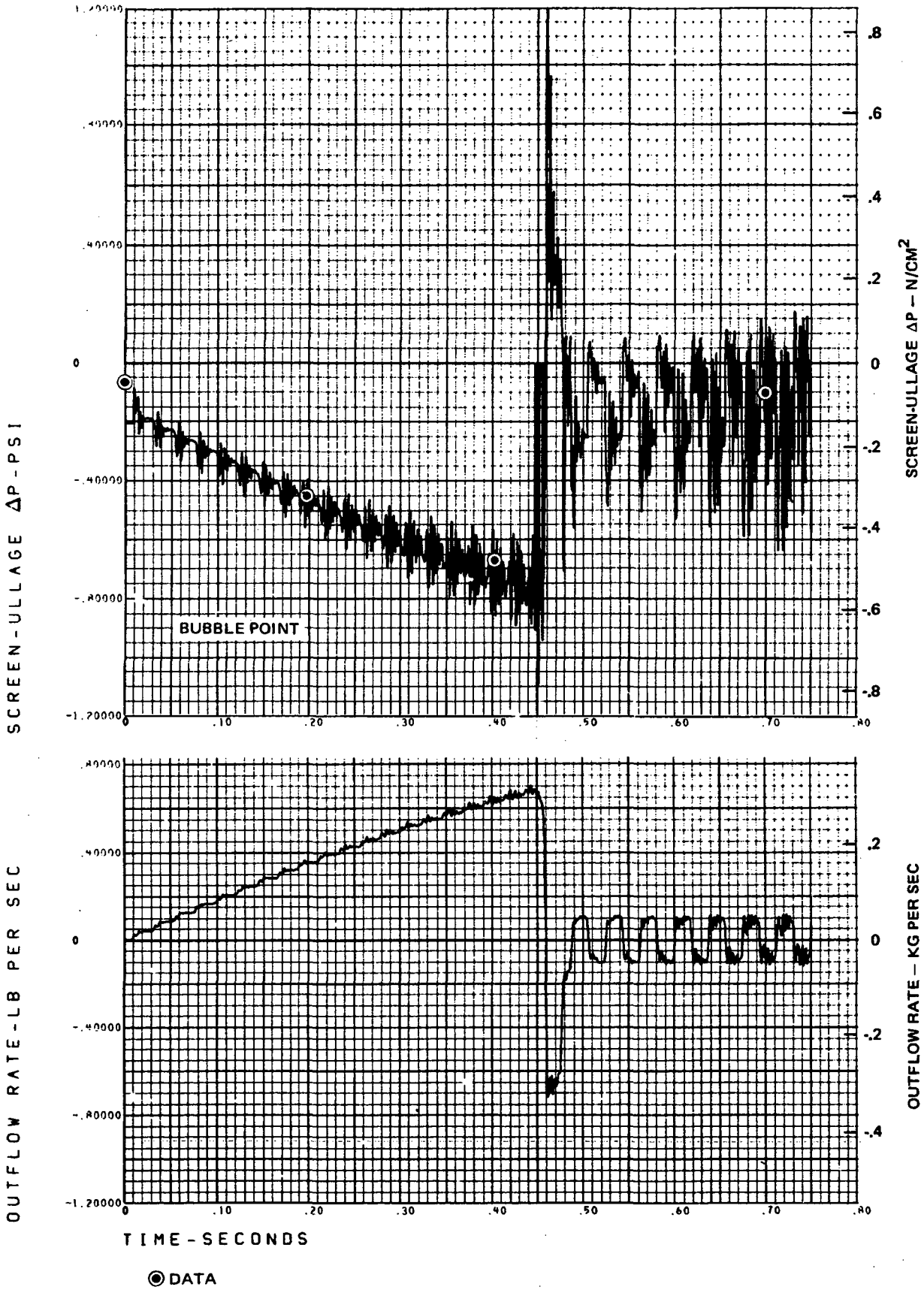

Figure 45. H672 Simulation – Run 102

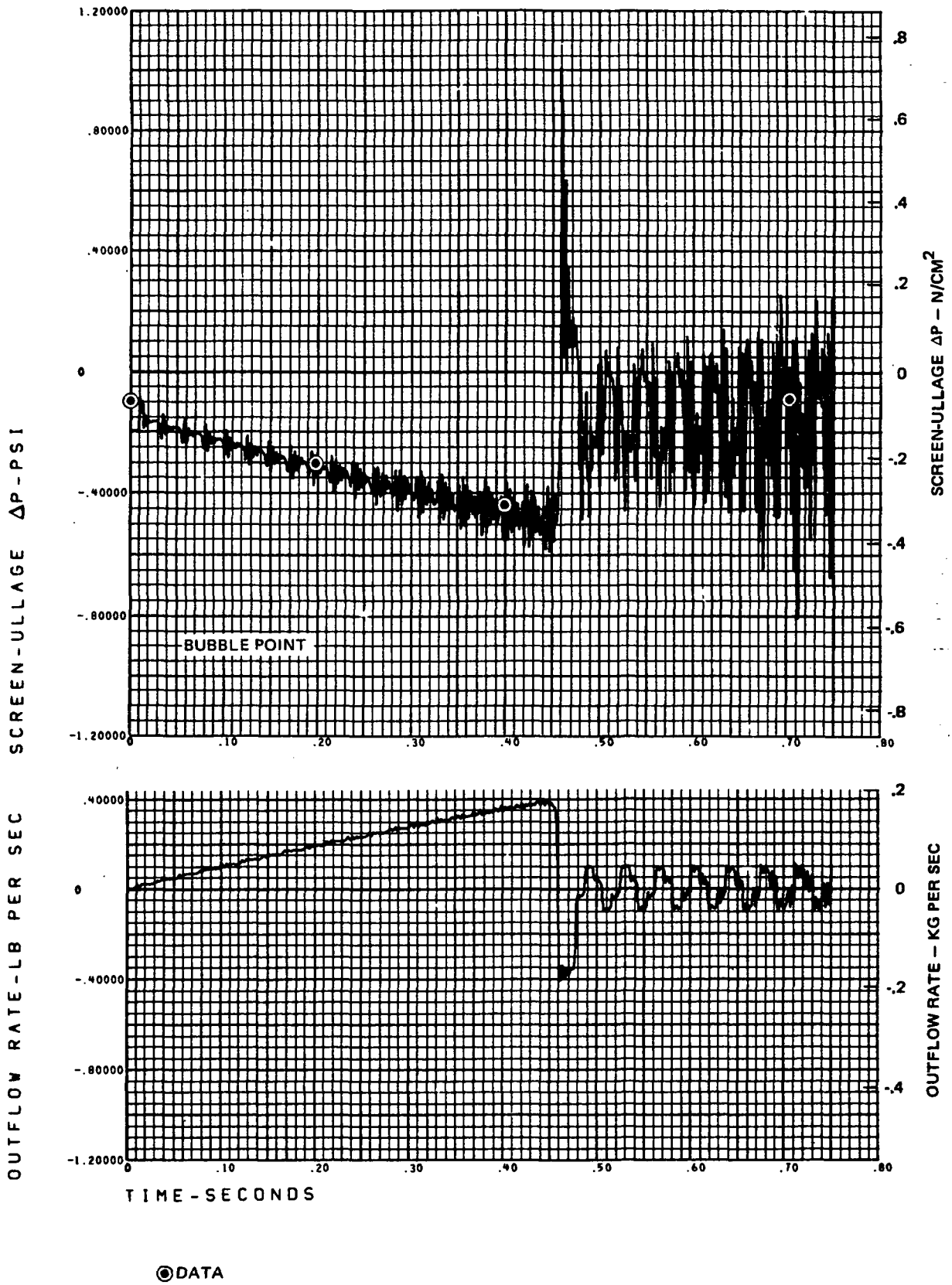

Figure 46. H672 Simulation – Run 101

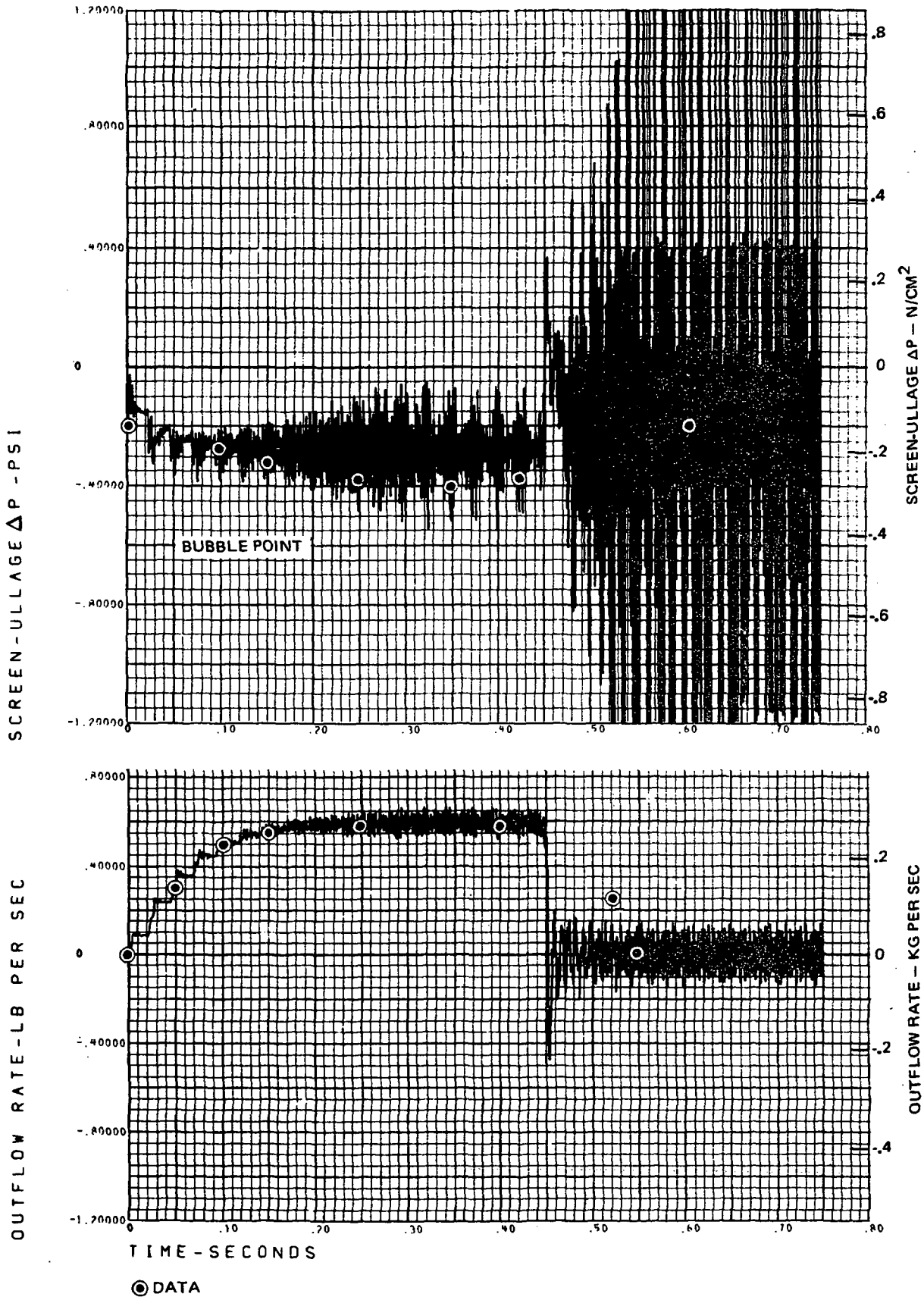

Figure 47. H672 Simulation — Runs 21, 22, 23

sure excursions at the valve were of the order of only 3.5 N/cm^2 (5 psi); (see Figures 38 and 39) and the response of the screen pressure transducers to these modest excursions were at most about 0.07 N/cm^2 (0.1 psi). Despite considerable effort investigating the reasons for this poor simulation, its cause remains unknown; possible, but unconfirmed, reasons include valve behavior at closing not in accordance with the valve model, gas bubbles in the outlet line, and leakage through the valve at closure.

When the large pulses generated by the valve closure reach the screen device, they are considerably attenuated (see Figure 47) but cause gas ingestion (negative pulse) and liquid/gas outflow (positive pulses). A potential shortcoming of the screen model is that liquid/gas outflow from a positive pulse in excess of the bubble point is in the ratio of the average quality in the screen device, assuming uniform distribution of the gas within the device. This is probably not precise; the quality near the screen may be much higher than the average quality since the gas bubbles ingested may stay near (or attached to) the screen. This is especially true for rapidly oscillating plus and minus pressure pulses, since the bubbles would not have time to migrate far from the screen. Therefore, the time required for the screen device to pump itself full of gas (while spilling liquid) may not be accurately predicted. In our tests, the observed pressure excursions were quite low; therefore, there were almost no cases of observed liquid spill following shutdown.

The simulations for the 165 x 800 mesh with coarse screen backup (Runs 60 and 61) were able to resolve the choice of the proper model for the properties of this form of construction (see previous discussion in section on Screen Specimen Model). For Run 60, where no gas ingestion was observed, the more compliant model (assuming that only the 165 x 800 mesh screen properties were appropriate) correctly predicted zero gas ingestion. For Run 61, where gas ingestion resulting in an effective quality of 0.0015 to 0.003 was observed, the same model also predicted zero gas ingestion, but the pressure pulses came within a few thousandths of a N/cm^2 (psi) of the bubble point. When the initial gas pressure around the screen was increased by only 0.007 N/cm^2 (0.01 psi), well within the possible error in recording the gas pressure, the result was gas ingestion which reached a quality of

0.089 by 0.479 sec when the shutdown pulse arrived. The less compliant model (assuming that the 165 x 800 mesh screen properties were combined with the backup screen properties) properly predicted gas ingestion (to a quality of 0.075 at 0.479 sec) for Run 61, but also predicted gas ingestion for Run 60, which had none. Reduction of the initial surrounding gas pressure by 0.007 N/cm^2 (0.01 psi) reduced the quantity of gas ingestion predicted for Run 60, but ingestion was still predicted. Therefore, it is believed that the compliant model for the screen backup structure is the model which best represents the response of this type of composite screen structure. Figures 48 and 49 indicate the good agreement with pressure differential and flow data for the simulations of Runs 60 and 61 respectively.

The simulation for Run 74 for the 500 x 500 mesh specimen also indicated that at 0.05 N/cm^2 (0.07 psi) initially imposed gas pressure, there would be zero gas ingestion, but that if the initial gas pressure were increased by only 0.007 N/cm^2 (0.01 psi), gas ingestion would occur. The predicted pressure differential and flowrate for Run 74 is compared to the data in Figure 50. Note from Figure 50 that the flowrate is somewhat underpredicted (at these high flows), which may account for discrepancy in gas ingestion prediction. The simulation for Run 73, showing general gas ingestion, as observed, is shown in Figure 51.

The final alcohol runs simulated were for the 200 x 1400 mesh backed up by perforated sheet (Runs 79, 85, 86). For the tests in which no gas ingestion was predicted (Runs 79 and 85), the pressure differential was somewhat overpredicted but the flowrate prediction was accurate (see Figures 52 and 53). For Run 86, with general gas ingestion observed, the pressure differential prediction was accurate until gas ingestion occurred (see Figure 54) when both the pressure and flow observed were erratic as was often the case for tests with general gas ingestion.

The simulation for the selected Freon 114 test (Run 107) with the 325 x 2300 mesh screen in the vertical orientation was started by using the P4557 code to predict the magnitude of the boiling pressure surge in the line. The observed startup pressure surges recorded by the pressure transducer next to the valve, were of the order of only 2 N/cm^2 ($\sim$3 psi) or less. However,

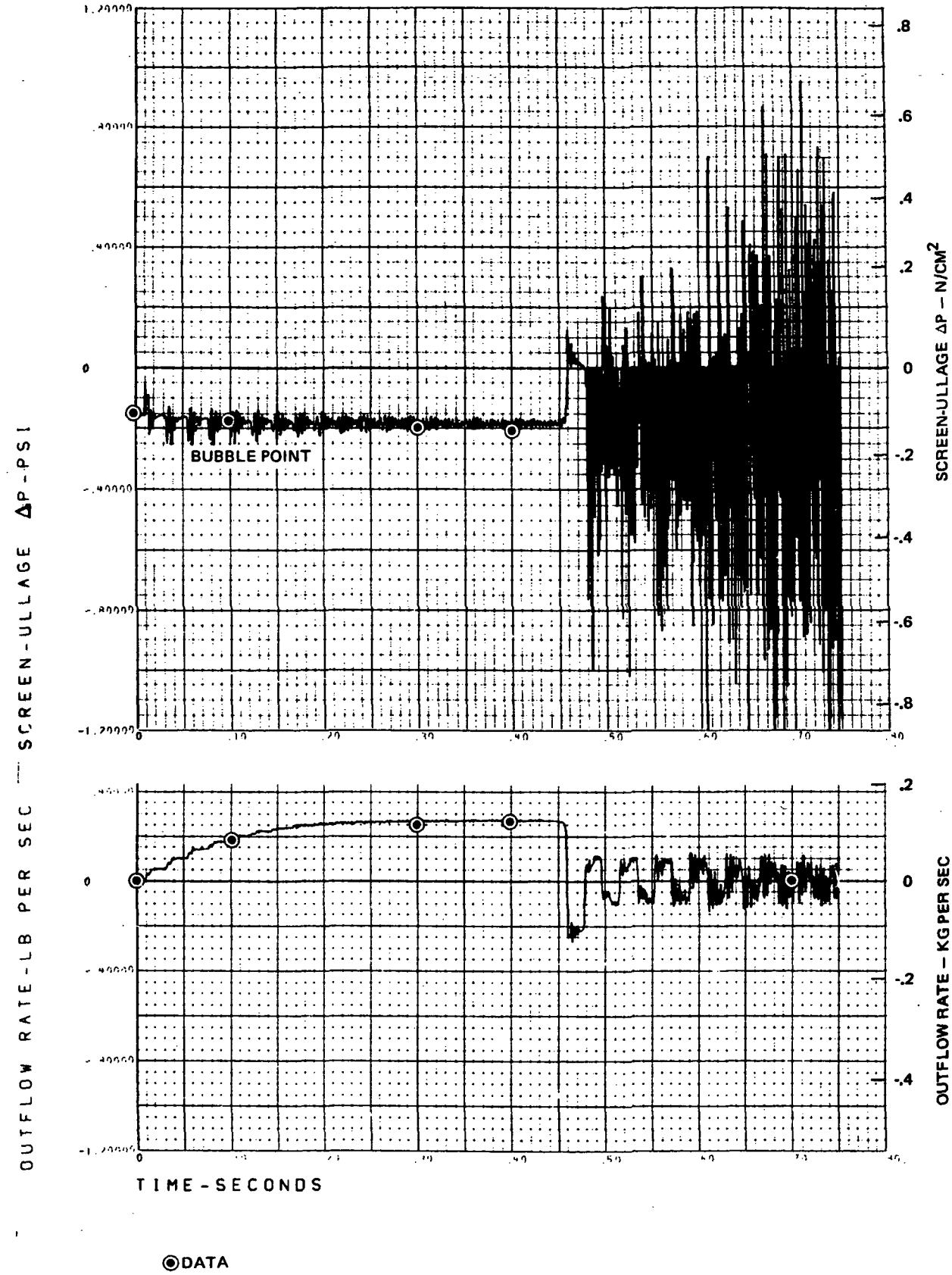

Figure 48. H672 Simulation – Run 60

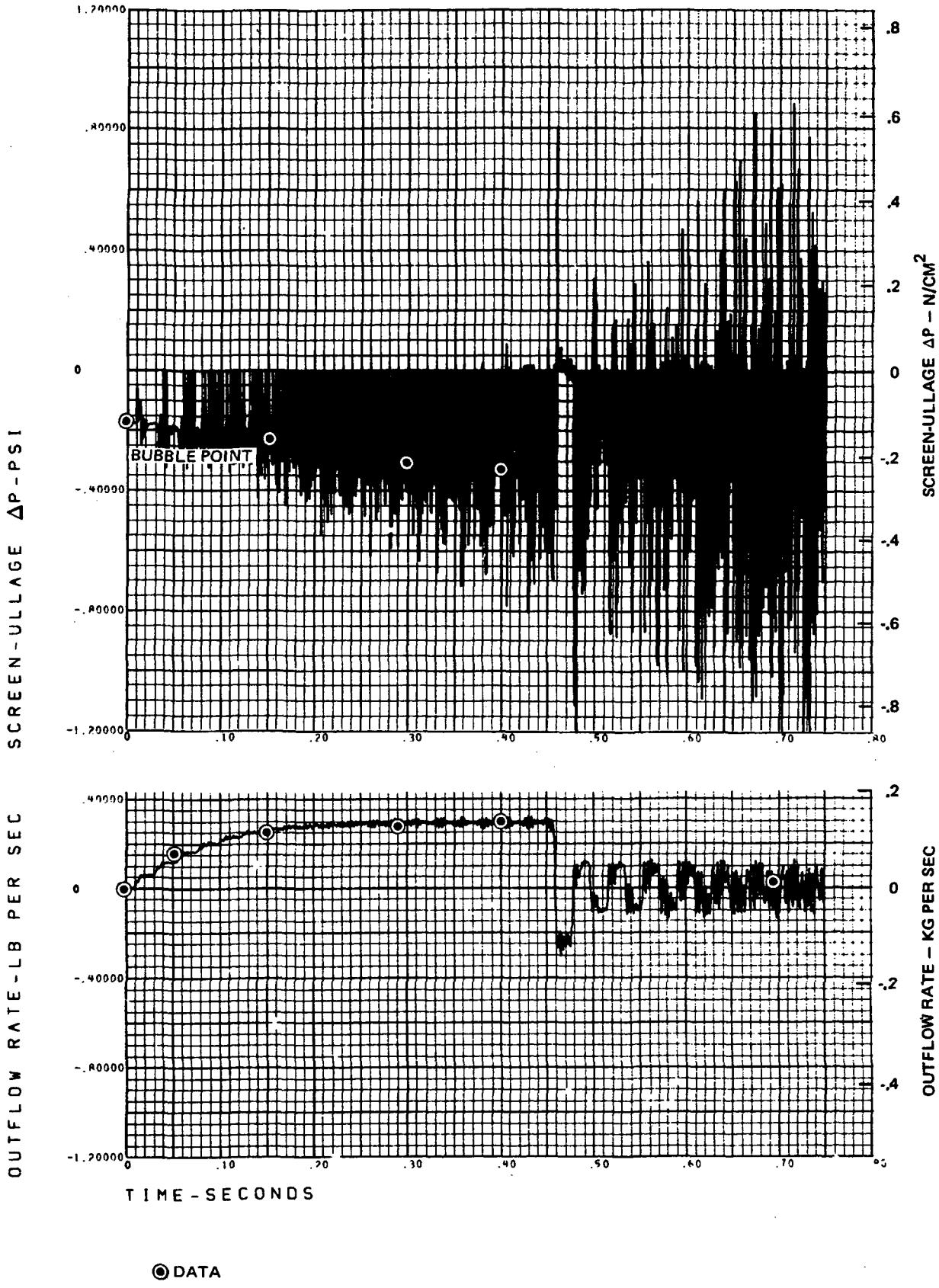

Figure 49. H672 Simulation – Run 61

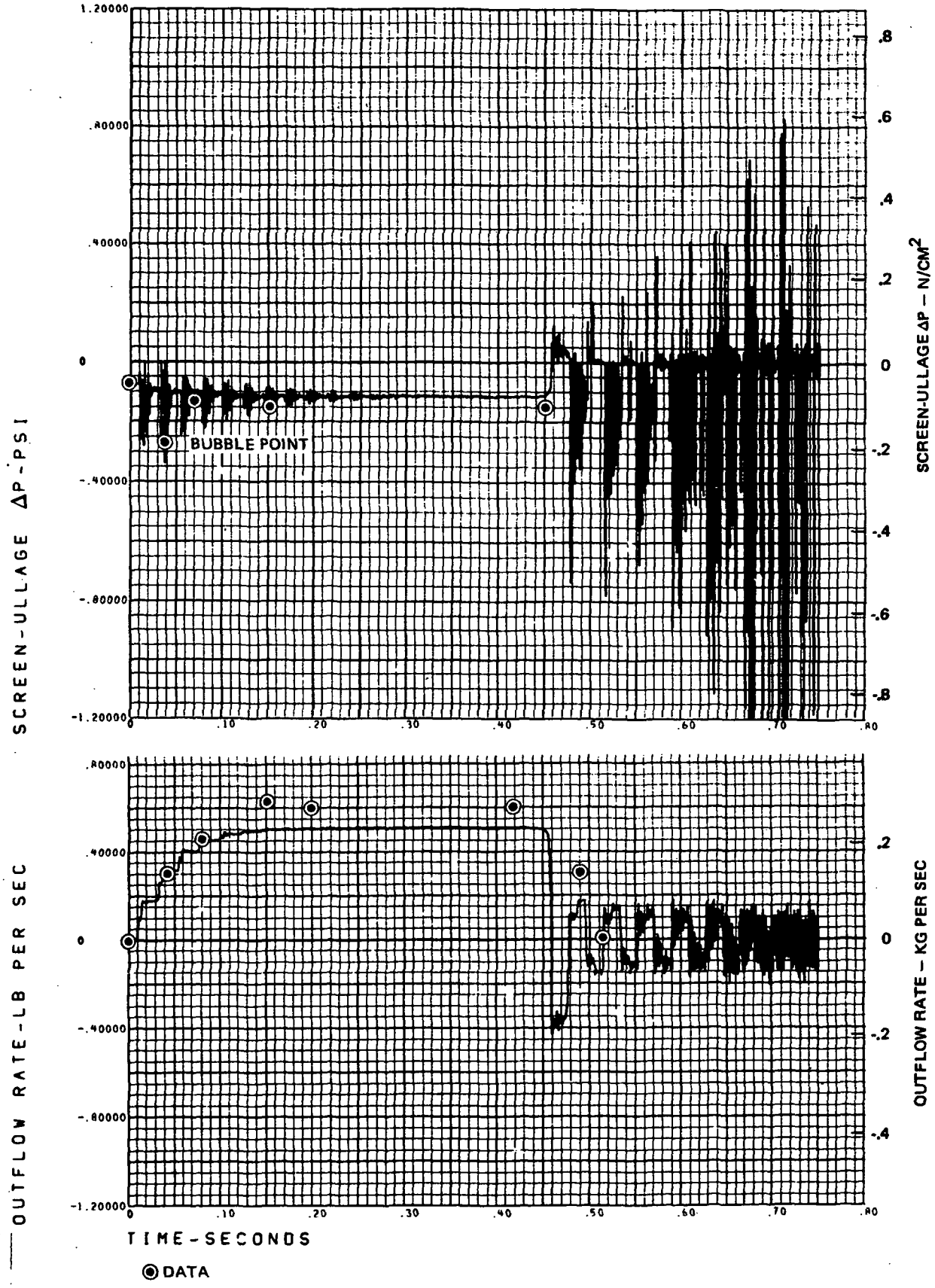

Figure 50. H672 Simulation — Run 74

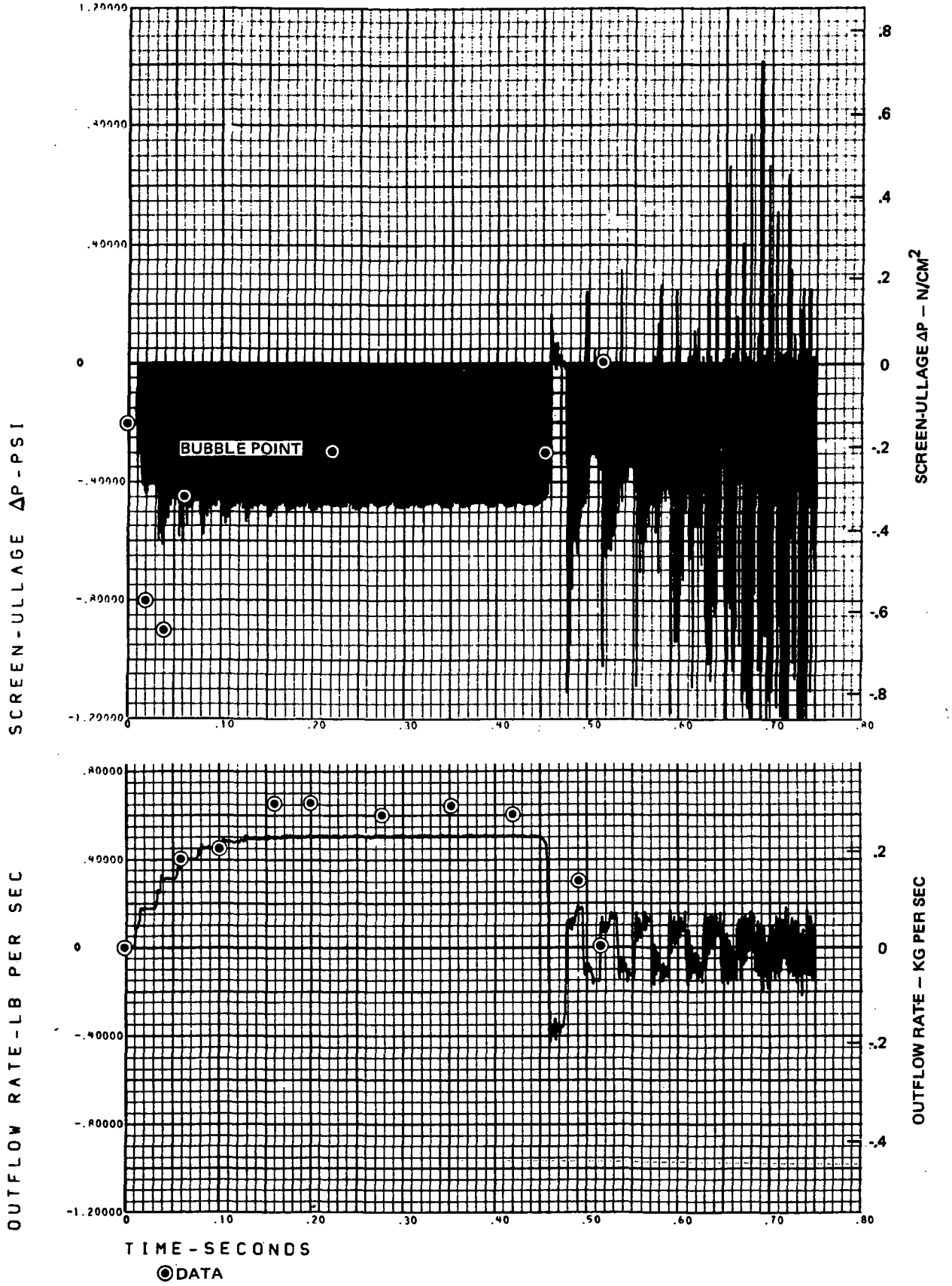

Figure 51. H672 Simulation – Run 73

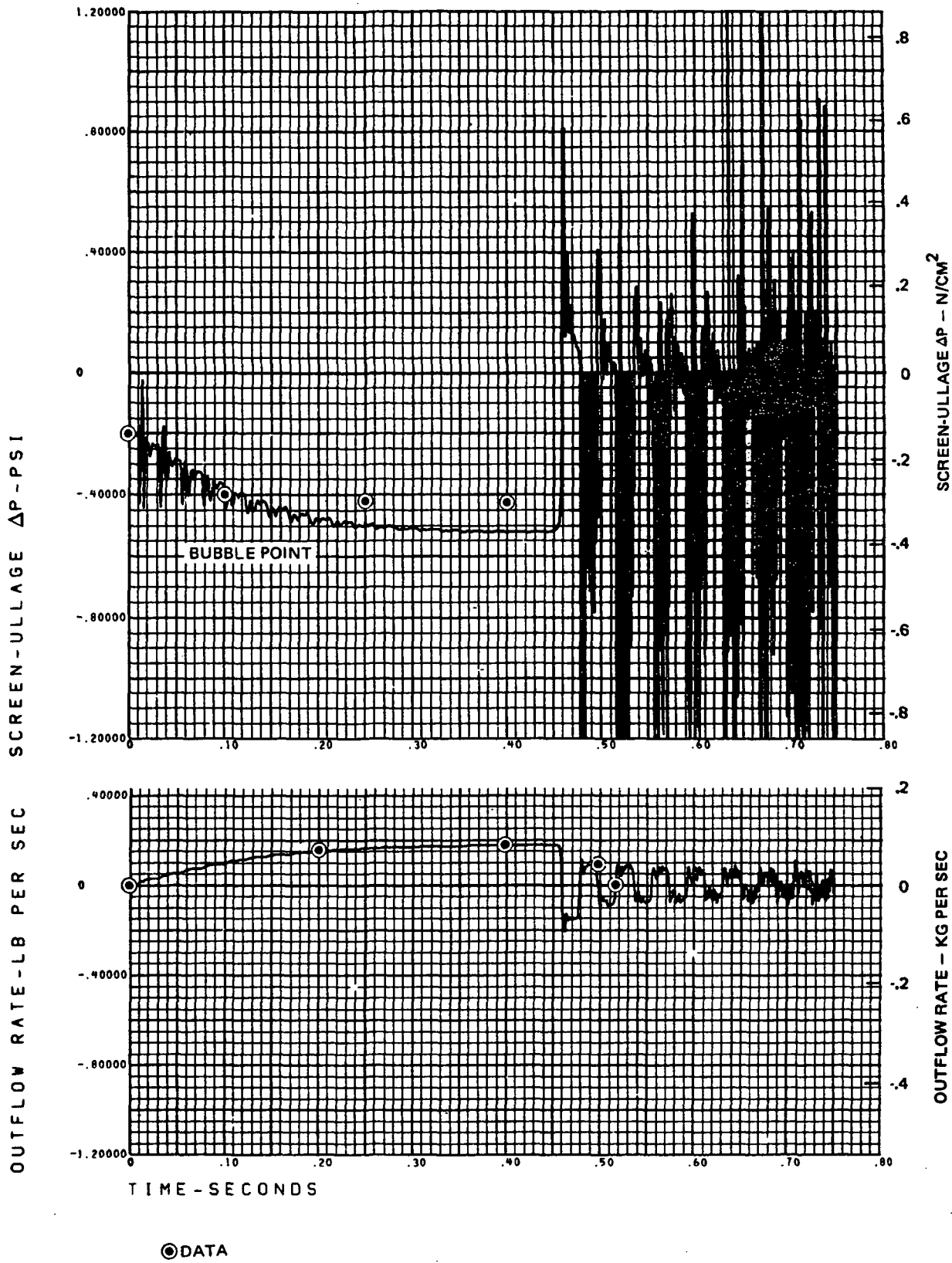

Figure 52. H672 Simulation — Run 79

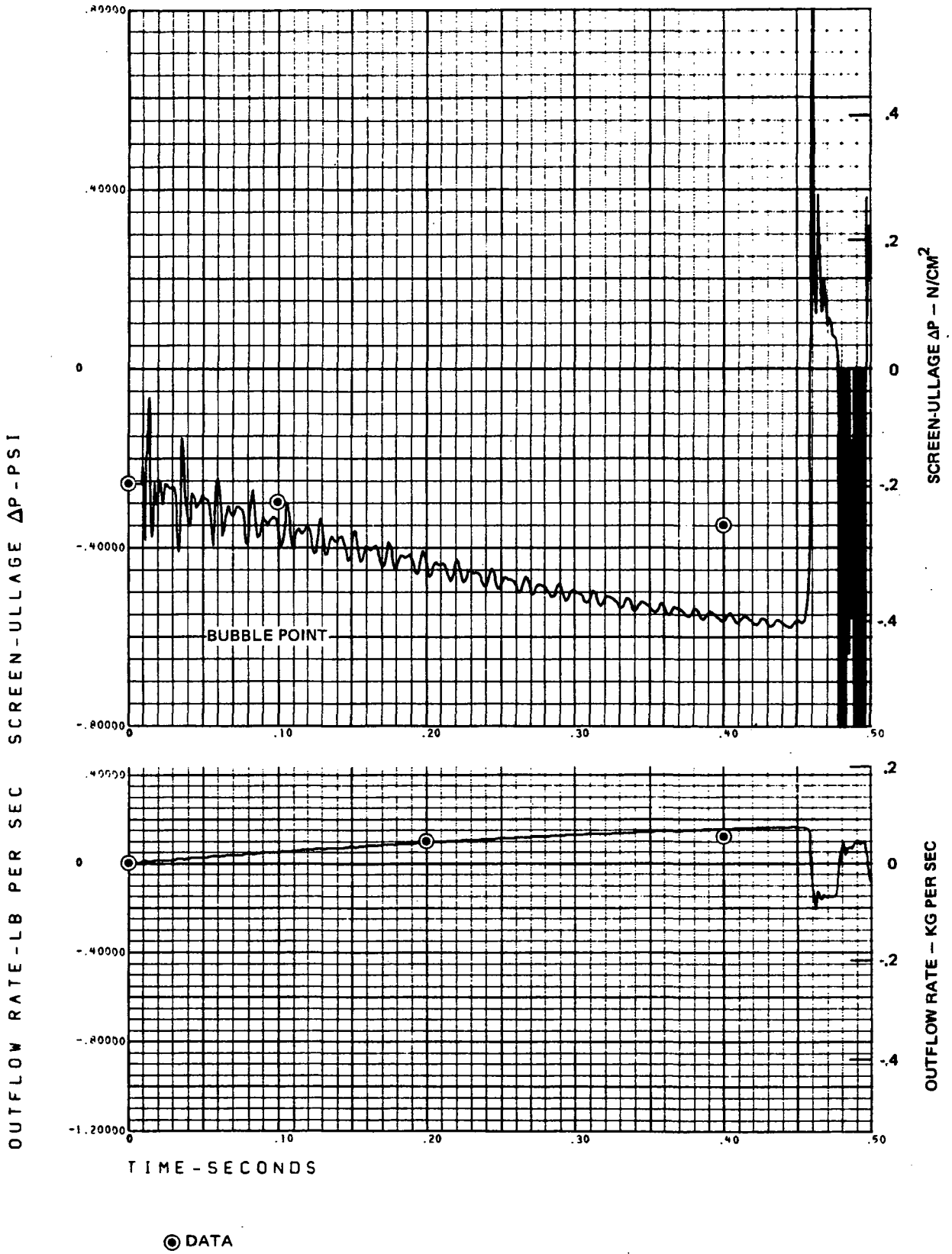

Figure 53. H672 Simulation – Run 85

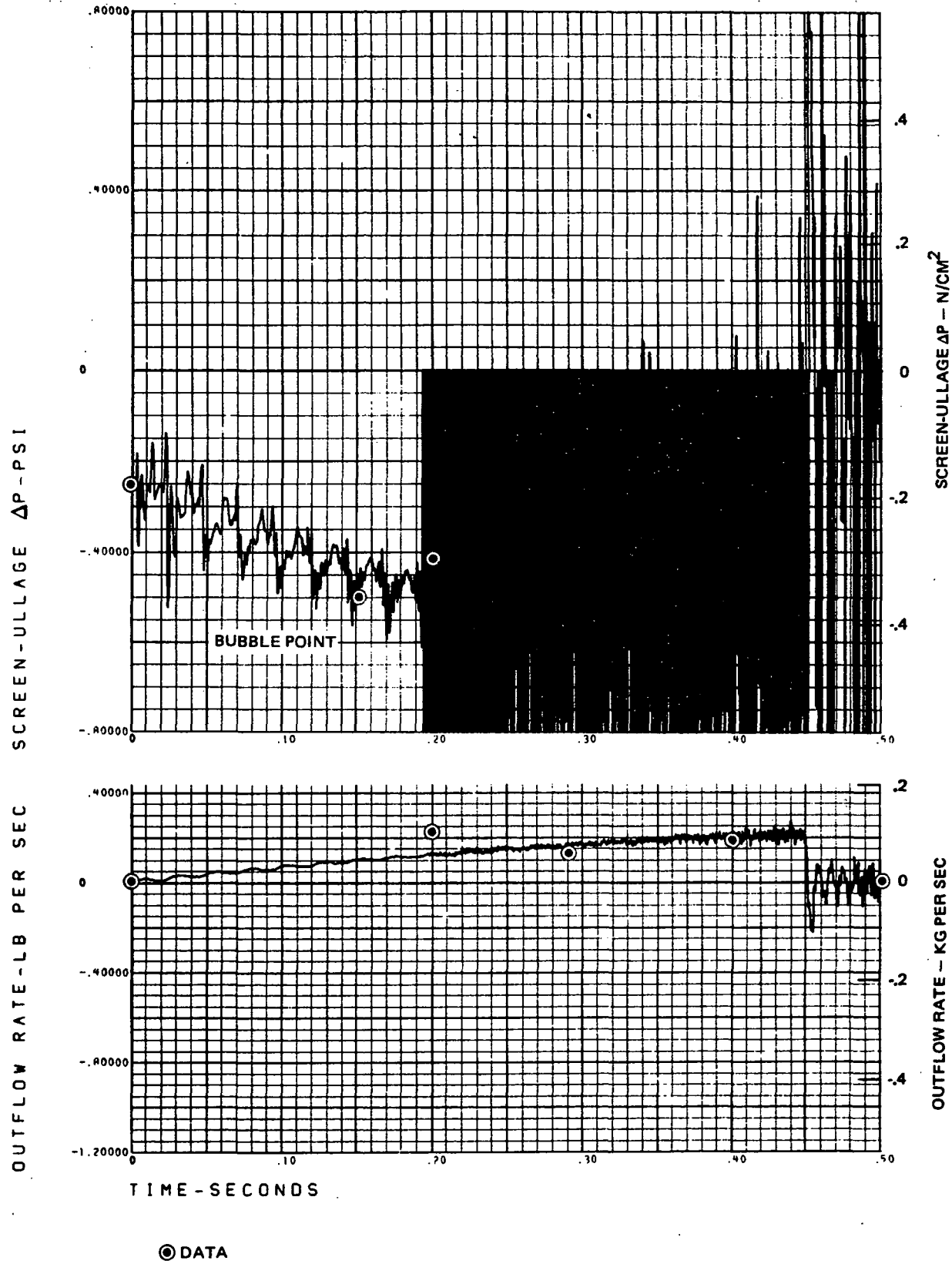

Figure 54. H672 Simulation – Run 86

the P4557 code did not predict this large a pressure pulse in the time observed (~0.1 sec), but rather a slow rise in pressure toward saturation pressure at the line temperature. It is believed that the pressure pulses observed were hydrodynamic in nature, resulting from liquid flow into a partially empty line, followed by a sudden stop at the restrictive throttle valve just downstream from the ball valve. In general, the recorded pressure differential at the screen device did not respond to the pulse recorded at the valve. The hydrodynamic simulation of Run 107, using H672 without the downstream pressure pulse input through the injector/chamber pressure spike routine, is shown in Figure 55. Both the pressure differential and flow are somewhat overpredicted, yet zero startup gas ingestion was predicted as observed.

Simulation of the LH_2 run 153 was started with modeling of the LH_2 cryosurge using the cryosurge code P4557. The modeling was complicated by the discrepancy between the P4557 code assumption of a long horizontal line downstream of the control valve, and the actual case of a high-resistance throttle valve downstream of the control valve. The long-line equivalent of the throttle valve was developed from P4557 simulations of the Freon 114 tests with the flowmeter installed, matching the predicted flowrate to the data.

The equivalent line to the LH_2 configuration was then corrected by removing the flowmeter resistance and reconfiguring the line. The resulting peak flowrate predicted by the P4557 code was close to the value predicted by the H672 code when it was run without the cyrosurge option (in order to determine the system hydrodynamic flow conditions). The experimental data for the initial valve pressure spike and differential pressure for Run 153, as traced from the oscillograph record, is shown in Figure 56. The circled points shown in Figure 56 are the interface (valve) pressure trace predicted by P4557. The peak value matches well, although the predicted rise time is somewhat slower because of the discrepancy in modeling the physical restriction of the throttle valve. The pressure pulse data was input to the H672 code through the injector/chamber pressure spike option, and the H672 simulation is shown in Figure 57 for screen ullage pressure differential and predicted flow. The reverse flow due to the pressure spike is evident from Figure 57. Gas ingestion occurs rather generally until the reverse flow

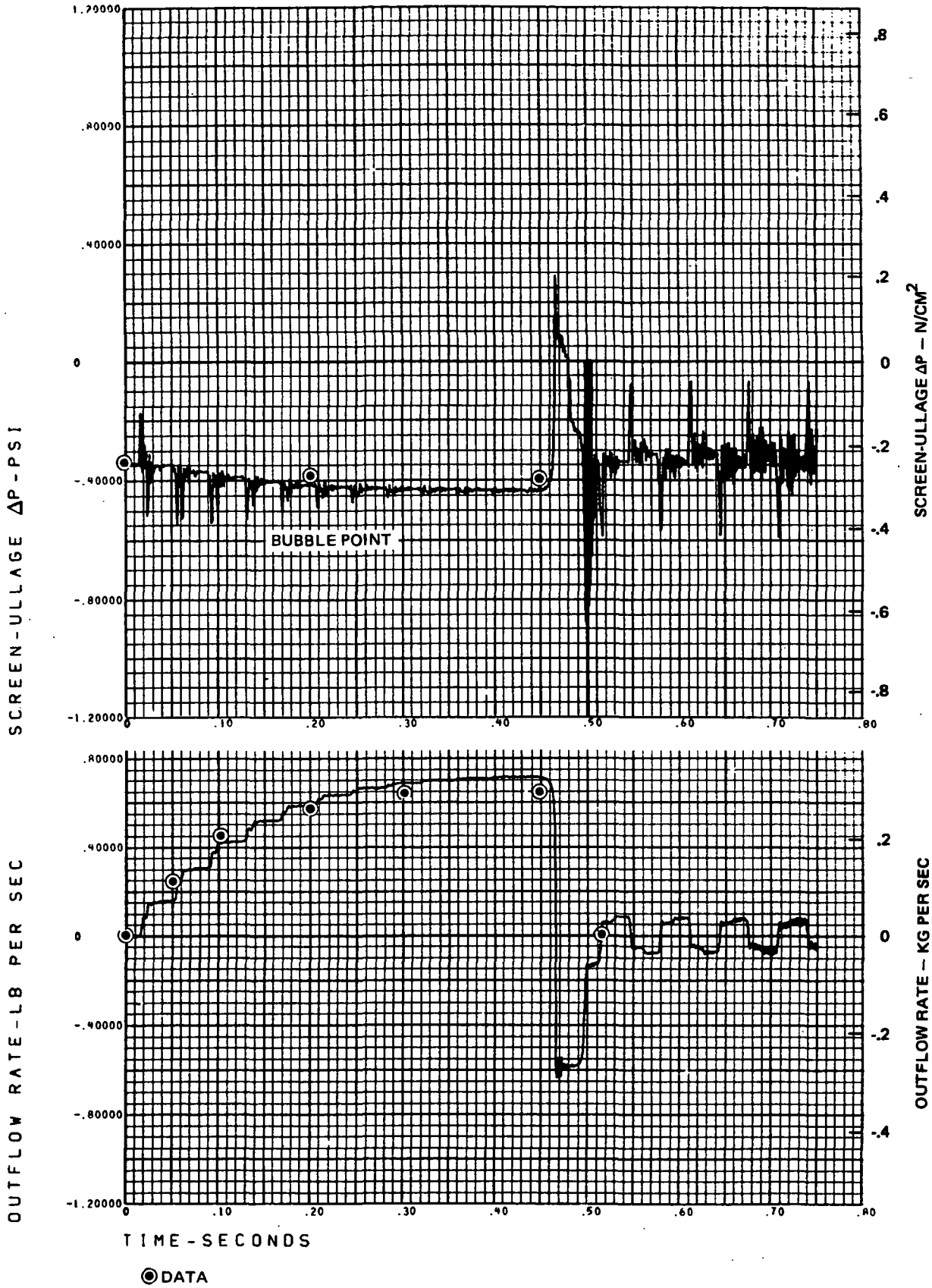

Figure 55. H672 Simulation – Run 107

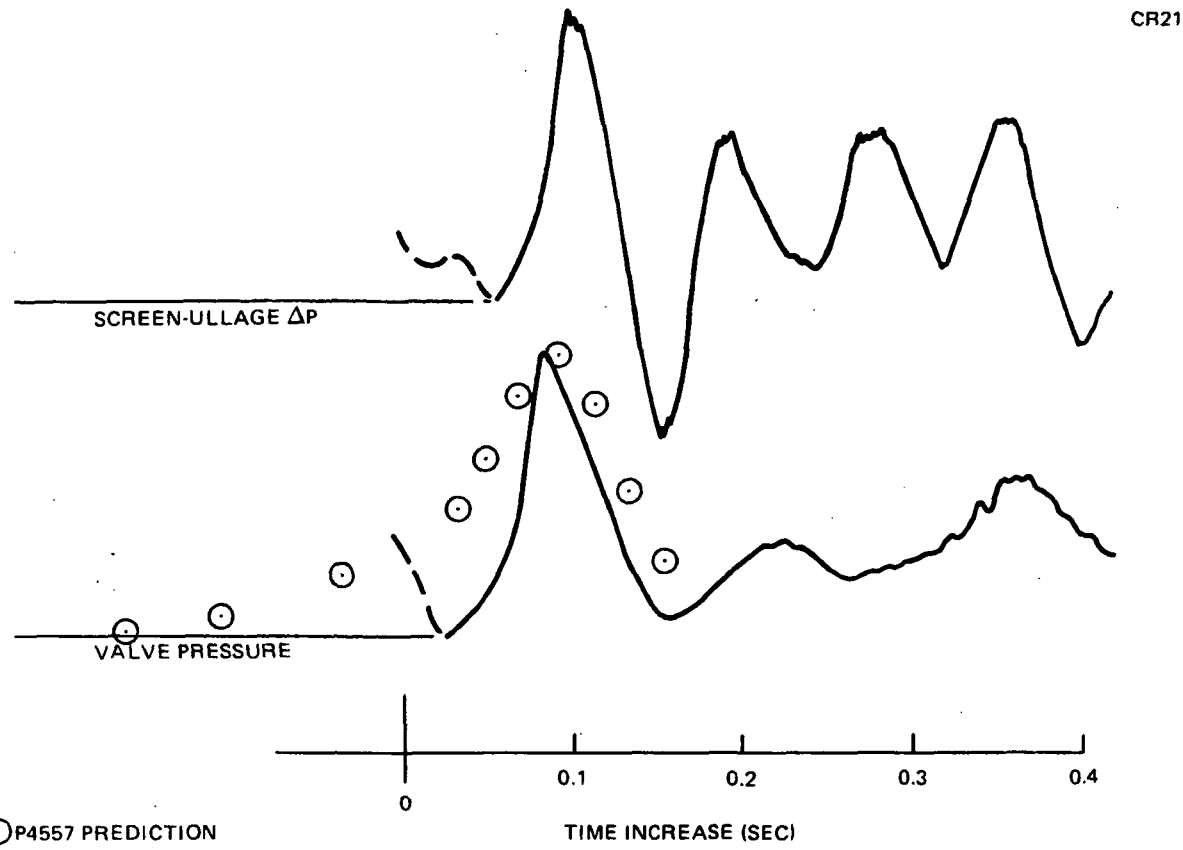

Figure 56. LH_2 Cryosurge Data

at 0.37 sec causes outflow from the screen device and cessation of ingestion, until the pressure drops below the imposed gas pressure again at 0.50 sec. The screen ullage pressure differential peaks from Figure 56 are superimposed on the H672 prediction in Figure 57 where there is fair qualitative agreement.

The results of all of the data correlation simulations are summarized in Table 17, which compares data and predictions for gas ingestion flow and screen-ullage pressure differential, and comments on the aspects of the screen model verified by the correlations.

The results of Table 17 indicate that the H672 code properly simulates flow startup and operational characteristics of a feed system, but overpredicts the shutdown pressure pulses (compared to experimental data). The SR26 subrouting modelling the screen device was shown to be an adequate representation of the characteristics of a screen device in response to pressure pulses regarding screen-ullage pressure differential, flow, and

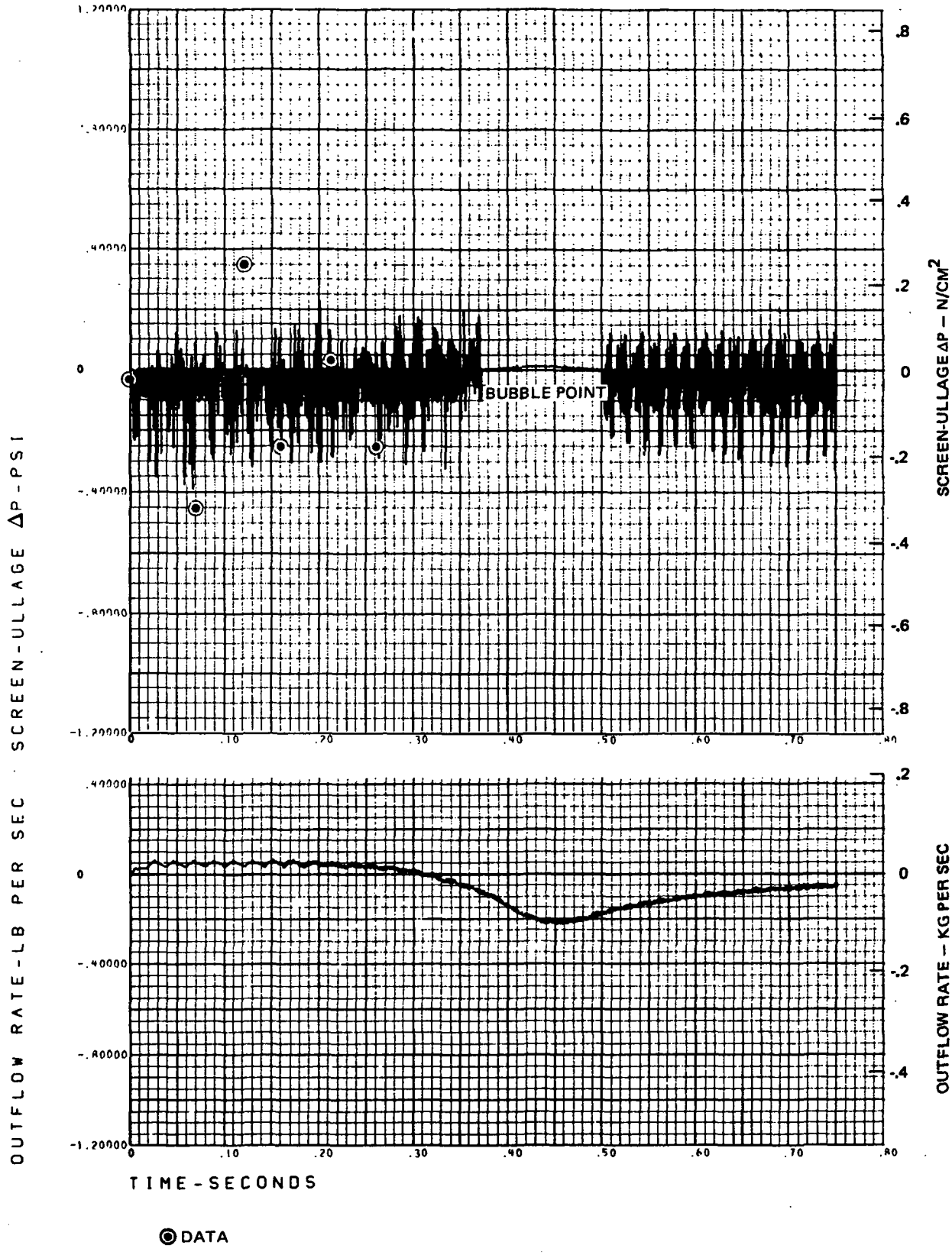

Figure 57. H672 Simulation – Run 153

Table 17

SUMMARY COMPARISON OF ANALYTICAL CORRELATIONS AND DATA

Run No.	Screen/Configuration	Gas Ingestion (Quality) Test	Gas Ingestion (Quality) Predicted	Flowrate (Kg/sec) Test	Flowrate (Kg/sec) Predicted	Pressure Differential (N/cm^2) Test	Pressure Differential (N/cm^2) Predicted	Comments
15*	200 x 1400 Plain	0.012-0.016	0.14	0.10	0.10 + surge	0.28	Unstable	Verified that a' is not a function of quality; horizontal specimen.
15	200 x 1400 Plain	0.012-0.016	0.014	0.10	0.10	0.28	~0.41	Verified PO = 0.027 f = 0.84 for dutch/plain.
102*	325 x 2300 Plain	0.003-0.012	1.0	-	0.31 + surge	0.49	Unstable	Verified that a' is not a function of quality - vertical specimen.
102	325 x 2300 Plain	0.003-0.012	0.003	-	0.31	0.49	~0.62	Verified PO = 0.027 f = 0.84 for dutch/plain.
101	325 x 2300 Plain	0	0	-	0.17	0.30	~0.34	Verified PO = 0.027 f = 0.84 for dutch/plain.
21 22 23	200 x 1400 Pleated	0	0	0.25	0.27	0.28	~0.34	Verified PO = 0.027 f = 2.4 for dutch/plain.
60	165 x 800 Screen Back	0	0	0.12	0.12	0.15	~0.14	Verified PO = 0.11 f = 1.0 Screen properties only for screen backup w/dutch.
61	165 x 800 Screen Back	0.0015	0-0.08	0.14	0.14	0.21	~0.48	Verified PO = 0.11 f = 1.0 Screen properties only for screen backup w/dutch.
73	500 x 500 Plain	0.22	0.28	0.28	0.23	0.62	~0.41	Verified PO = 0.25 f = 0.84 for square/plain.
74	500 x 500 Plain	0.099	0-0.002	0.28	0.23	0.19	~0.23	Verified PO = 0.25 f = 0.84 for square/plain.
79	200 x 1400 Perf. Sheet	0	0	0.08	0.08	0.30	0.36	Verified PO = 0.027 f = 0.50 for dutch w/perforated sheet backup; combined properties.
85	200 x 1400 Perf. Sheet	0.148**	0	0.05	0.07	0.24	~0.39	Verified PO = 0.027 f = 0.50 for dutch w/perforated sheet backup; combined properties.
86	200 x 1400 Perf. Sheet	0.444**	0.05	0.07	0.09	0.35	~0.41	Verified PO = 0.027 f = 0.50 for dutch w/perforated sheet backup; combined properties.
107	325 x 23 Plain	0	0	0.28	0.32	0.28	0.30	Verified PO, f, for F-114 for dutch/plain.
153	325 x 2300 Plain	0.091	0.11	0	0.023	0.32	~0.27	Verified PO, f, for LH_2 for dutch/plain; verified cryosurge P4557 model.

*a' = f (x)
**includes leakage

gas ingestion. The model of the screen/structure which includes screen properties and structural backup material properties as a uniformly distributed composite structure was verified for plain screen specimens, pleated screen specimens, and screen backed up by coarse screen or perforated sheet. The results indicate that pleated screen construction has maximum performance, and screen/structure methods which use only the more compliant screen properties (plain, pleated, coarse screen backup) are superior in performance to perforated sheet backup in which the less compliant backup material properties are included. The P4557 code adequately simulated the LH_2 cryosurge and, when modeled with the H672 code, produced fair agreement with experiment.

It is believed that the H672 code with screen model has been experimentally verified as a useful design tool which can predict the startup transient performance of screen devices under a wide variety of fluids and operating conditions.

Page
Intentionally
Left Blank

PRECEDING PAGE BLANK NOT FILMED

CONCLUSIONS

The conclusions reached as a result of this comprehensive analytical and experimental program to provide an analytical design tool, verified by experiment, to predict the effects of transient pressure surge on the retention performance of screen acquisition systems are as follows:

1. A detailed survey of current and potential space vehicle screen acquisition systems defined important operational and configurational aspects of twelve systems and defined appropriate categories of screen systems as (1) localized—for engine restart, and (2) distributed—for long term transfer.
2. An existing MDAC computer code, H672, for feed system transient analysis was adapted for study of screen device performance by the addition of screen model subroutines. The MDAC cryosurge analysis, P4557, was used to analyze pressure surges caused by cryogen boiling in warm lines, and provide input conditions for the H672 code.
3. The screen device model developed and programmed for inclusion into the H672 code had the following features:
   a. The screen device was treated as a uniformly-distributed composite structure incorporating orthotropic screen properties combined with backup structure properties according to the relative screen area fraction, f.
   b. The screen device flow characteristics depend on the percent open area, PO, assumed as a power function of the void fraction, and experimental flow loss characteristics as defined in Reference 1.
   c. The screen device model provides for liquid inflow/outflow; liquid leaving the screen; gas ingestion; and when resisted by the screen bubble point, no gas ingestion; screen stress analysis; and quality in the screen device due to gas ingestion.
   d. The acoustic velocity and pressure/flow balance in the screen device was assumed as a function of gas ingestion and quality.

4. A comprehensive experimental program of 177 tests using 13 screen specimen configurations; 5 meshes, 4 construction methods, and 2 orientations, together with 3 fluids; alcohol, Freon 114 and LH_2, verified the following aspects of the screen model by good agreement between analysis and experiment for gas ingestion, screen-ullage pressure difference, and flowrate:
   a. The assumption of screen device properties as a composite of screen and backup material properties was confirmed for the following structures:
      - plain screen; f = 0.84 (due to strut blockage); screen properties only
      - pleated screen; f = 2.4 (actual screen area); screen properties only
      - screen with coarse screen backup; f = 1.0; fine screen properties only
      - screen with perforated sheet backup (50% open area); f = 0.5; combined screen properties and perforated sheet properties
   b. The assumption of screen device flow characteristics as a function of the assumed percent open area functional relationship was confirmed.
   c. The screen model operational characteristics of paragraph (3c) above were confirmed.
   d. The acoustic velocity and pressure/flow balance in the screen device was shown not to be a function of quality, and the screen model was modified accordingly.
   e. The cryosurge code P4557, was shown to predict the LH_2 line boiling pressure surge with reasonable accuracy.
5. The prediction of the feed system flow shutdown transient by the H672 code did not agree well with experiment in that it tended to overpredict system pressure surges.
6. The H672 transient analysis, including the screen model, has been experimentally verified to be a useful design tool, which can accurately predict the startup transient performance of screen acquisition systems under a wide variety of fluids and operating conditions.

REFERENCES

1. E. C. Cady. Study of Thermodynamic Vent and Screen Baffle Integration for Orbital Storage and Transfer of Liquid Hydrogen. MDAC Report MDC G4798 (NASA CR-134482), August 1973.

2. E. C. Cady. Design and Evaluation of Thermodynamic Vent/Screen Baffle Cryogenic Storage System. MDAC Report MDC G5979 (NASA CR-134810), June 1975.

3. M. H. Blatt and M. D. Walter. Centaur Propellant Acquisition System Study. GDC Report CASD-NAS-75-023 (NASA CR-134811), June 1975.

4. G. W. Burge and J. B. Blackmon. Study and Design of Cryogenic Propellant Acquisition Systems - Volume I, Design Studies, Final Report, NAS8-27685. MDAC Report MDC G5038, December 1973.

5. J. Tegart. Effect of Vibration on Retention Characteristics of Screen Acquisition Systems. MMC Monthly Reports - Contract NAS3-20097, 1976-77.

6. D. F. Gluck, W. J. Hines, and R. A. Moses. Transient Flow in Capillary Systems. Report SD 73-SA-0041, March 1973.

7. R. P. Warren. Acquisition System Environmental Effects Study. MMC Report MCR-75-21, May 1975.

8. J. B. Blackmon. Design, Fabrication, Assembly, and Test of a Liquid Hydrogen Acquisition Subsystem, NAS8-27571. MDAC Report MDC G5360, May 1974.

9. M. H. Blatt, et al. Low-Gravity Propellant Control Using Capillary Devices in Large-Scale Cryogenic Vehicles - Phase I, Final Report, NAS8-21465. GDC Report GDC-DDB70-008, August 1970.

10. M. H. Blatt, et al. Low-Gravity Propellant Control Using Capillary Devices in Large-Scale Cryogenic Vehicles - Phase II, Final Report, NAS8-21465. GDC Report GDC-DDB70-008, August 1970.

11. D. A. Hess and G. F. Orton. Space Shuttle OMS Propellant Acquisition. Presented to JANNAF/AIAA Joint Propulsion Specialist Conference, Anaheim, California, June 1975.

12. SS/RCS Surface Tension Propellant Acquisition/Expulsion Tankage Technology. MMC Report No. MCR-75-171, August 1975.

13. W. Heller and E. A. Cadwallader. Positive Expulsion. CPIA Publication 210, May 1971.

14. S. C. DeBrock, et al. A Survey of Current Developments in Surface Tension Devices for Propellant Acquisition. AIAA Paper No. 70-685, June 1970.

15. W. G. Steward, R. V. Smith, and J. A. Brennan. Cooldown Transients in Cryogenic Transfer Lines. Advances in Cryogenic Engineering, Vol. 15, Plenum Press, New York, 1970. Pages 354-363.

16. W. G. Steward. Transfer Line Surge. Advances in Cryogenic Engineering, Vol. 10, Sections A-L, Plenum Press, New York, 1965. Pages 313-322.

17. E. G. Brentari, et al. Boiling Heat Transfer for Oxygen, Nitrogen, Hydrogen, and Helium. NBS Technical Note No. 317, September 1965.

18. E. C. Cady. Effect of Transient Liquid Flow on Retention Characteristics of Screen Acquisition Systems, Volume 1 - Technical Proposal. MDAC Report MDC G5910P, March 1975.

19. Materials Engineering/Materials Selector '77, Volume 84, Number 6, November 1976.

Appendix A

SCREEN ACQUISITION SYSTEM SURVEY DATA TABULATION

No. 1 Application: Cryogenic Tug

Name: Cryogenic Space Shuttle/Auxiliary Propulsion System

	LH_2 (Saturated at 17.2 N/cm^2 (25 psia))	LO_2 (Saturated at 17.2 N/cm^2 (25 psia))
Fluid:		
Quantity:	4750 KG (10,444 Lb)	17,950 KG (39,536 Lb)
Flowrate:	0-4.54 KG/Sec (0-10.0 Lb/Sec)	0-22.7 KG/Sec (0-50.0 Lb/Sec)
Environment:		
Acceleration: "g's"	On-orbit ± 0.045 (X, Y, Z) Reentry 1.25 (Z) 0.08 (X) Boost 3.00 (X)	On-orbit ± 0.045 (X, Y, Z) Reentry 1.25 (Z) 0.08 (X) Boost 3.00 (X)
Vibration:	U*	U
Thermal:	MLI Tank/Line Insulation Cold He Pressurization	MLI Tank/Line Insulation Cold He Pressurization
Valve/Pump Characteristics:	See Reference	U
Tankage and Acquisition System Configuration	See Figures A-1, A-2	Similar to Figures A-1, A-2 except 17.8-cm (7-in.) diameter channel
Transfer Line Configuration	10.2 cm dia x .05-cm wall x 3.05 m long (4-in. dia x .02-in. wall x 10 ft long) Aluminum	7.6 cm dia x .05-cm wall x 1.53 m long (3-in. dia x .02-in. wall x 5 ft long) Aluminum

Reference: G. W. Burge and J. B. Blackmon. Study and Design of Cryogenic Propellant Acquisition Systems - Volume I, Design Studies, MDAC Report MDC G5038, December 1973

* U - Unknown

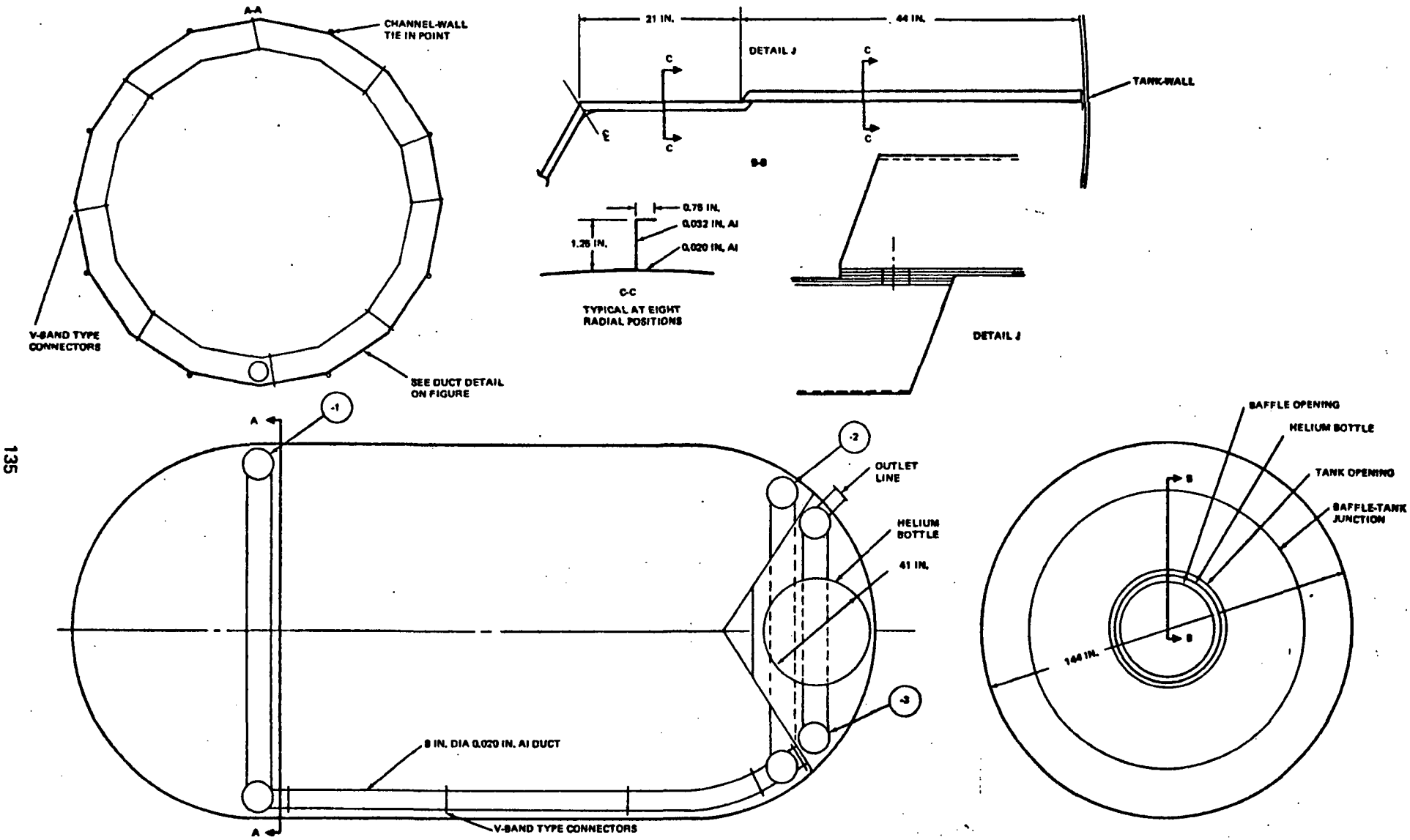

Figure A-1. LH_2 TANK AND CHANNEL CONFIGURATION

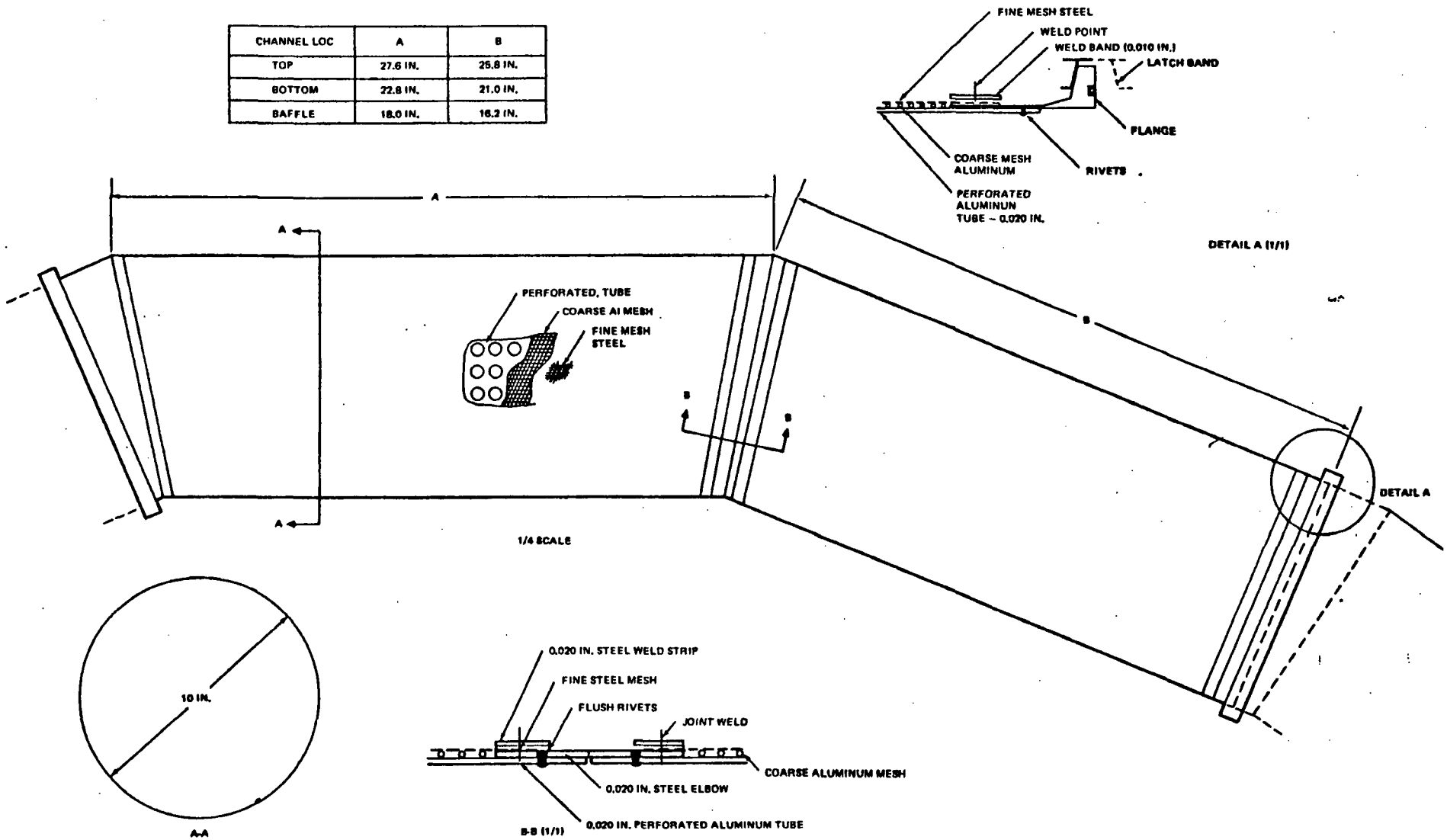

Figure A-2. LH_2 CHANNEL CONSTRUCTION DETAIL

No. 2 Application: Cryogenic Tug

Name: Advanced Space Propulsion Module

	LH_2 (Saturated at 14.7 N/cm^2 (21.3 psia))	LO_2 (Saturated at 15.9 N/cm^2 (23 psia))
Fluid:		
Quantity:	3626 KG (7,972 Lb)	21,118 KG (46,428 Lb)
Flowrate:	1.38 KG/Sec (3.04 Lb/Sec)	8.28 KG/Sec (18.24 Lb/Sec)
Environment:		
Acceleration: "g's"	0.0001-1.64	0.0001-1.64
Vibration:	U	U
Thermal:	MLI Tank/Line Insulation Cold He Pressurization	MLI Tank/Line Insulation Cold He Pressurization
Valve/Pump Characteristics:	U	U
Tankage and Acquisition System Configuration	See Figure A-3	See Figure A-4
Transfer Line Configuration	U	U

Reference: G. W. Burge and J. B. Blackmon. Study and Design of Cryogenic Propellant Acquisition Systems - Volume I, Design Studies, MDAC Report MDC G5038, December 1973

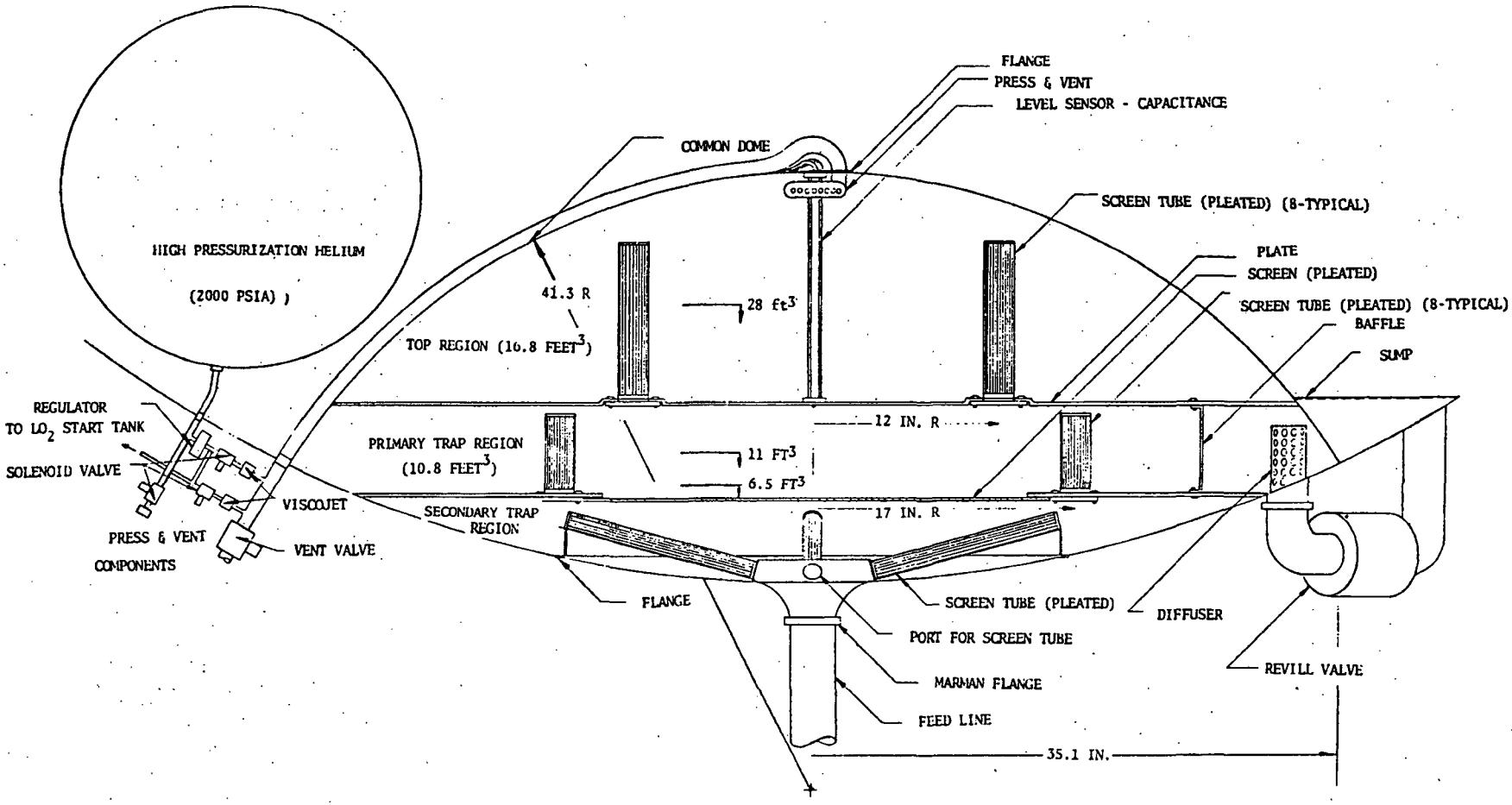

Figure A-3. ASPM LH_2 ACQUISITION SYSTEM PRELIMINARY DESIGN

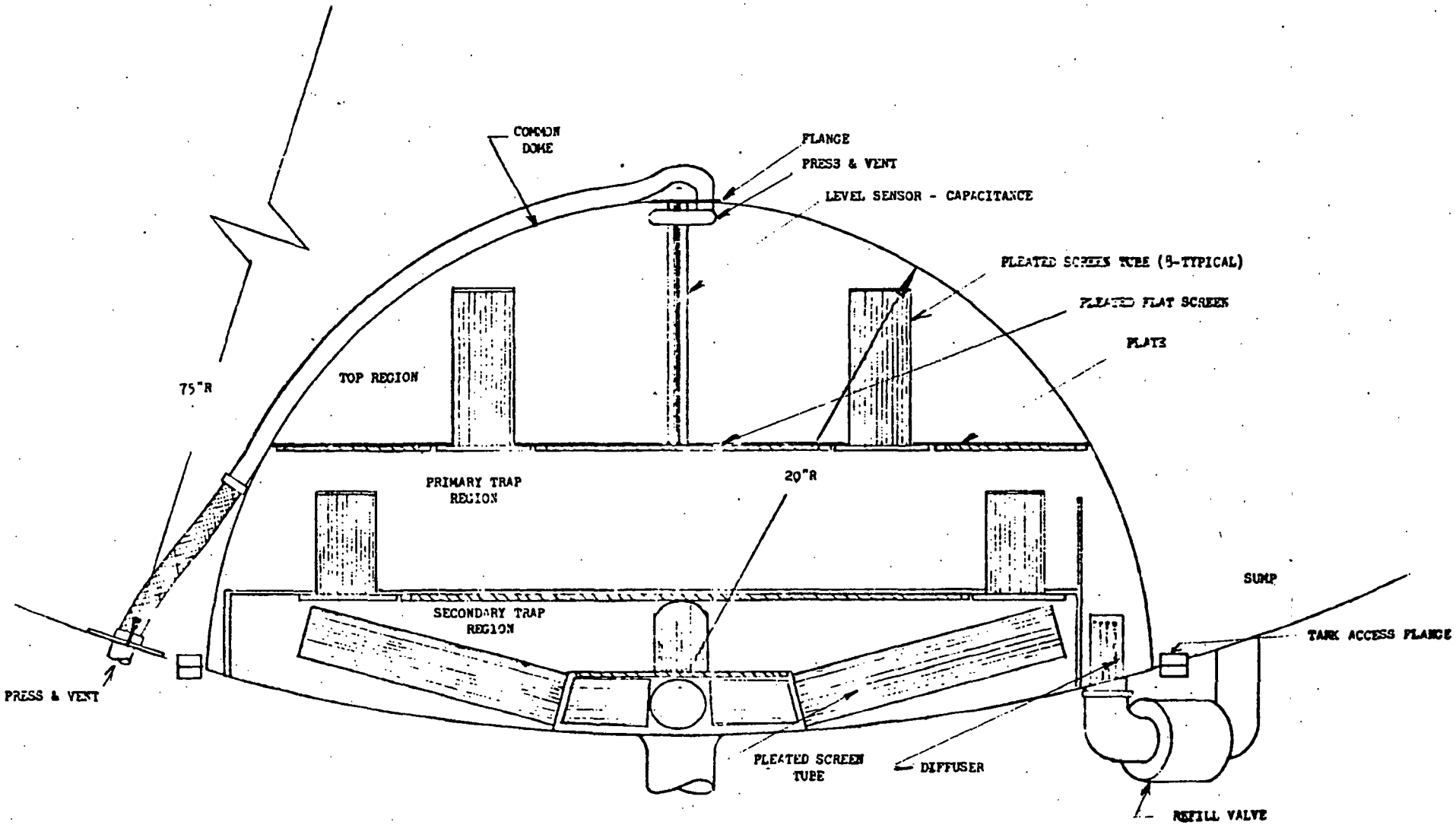

Figure A-4. ASPM LO_2 TANK ACQUISITION SYSTEM PRELIMINARY DESIGN

No. 3 Application: Cryogenic Tug

Name: Centaur D-1S

	LH_2 (Saturated at 14.1 N/cm^2 (20.5 psia))	LO_2 (Saturated at 21.4 N/cm^2 (31.0 psia))
Fluid:		
Quantity:	2397 KG (5279 Lb)	11554 KG (25450 Lb)
Flowrate:	5.1 Kg/Sec (11.2 Lb/Sec)	25.6 Kg/Sec (56.4 Lb/Sec)
Environment:		
Acceleration: "g's"	**See Reference**	**See Reference**
Vibration:	**See Reference**	**See Reference**
Thermal:	Common Bulkhead Heating Rate +19.5 W/M^2 (+6.2 B/Hr-Ft^2) Warm Helium Pressurization	-19.5 W/M^2 (-6.2 B/Hr-Ft^2) Bubbled Helium Pressurization
Valve/Pump Characteristics:	Initial Sump/Pump Chilldown See Figure A-5	Initial Sump/Pump Chilldown See Figure A-6
	Boost Pump Startup See Figure A-7	Boost Pump Startup See Figure A-8
	Engine Chilldown and Shutdown See Figure A-9	Engine Chilldown and Shutdown See Figure A-10
Tankage and Acquisition System Configuration:	**See Detailed Drawings in the Reference**	**See Detailed Drawings in the Reference**
Transfer Line Configuration:		

Reference: M. H. Blatt and M. D. Walter. Centaur Propellant Acquisition System Study. GD/C Report CASD-NAS-75-023 (NASA CR-134811), June 1975.

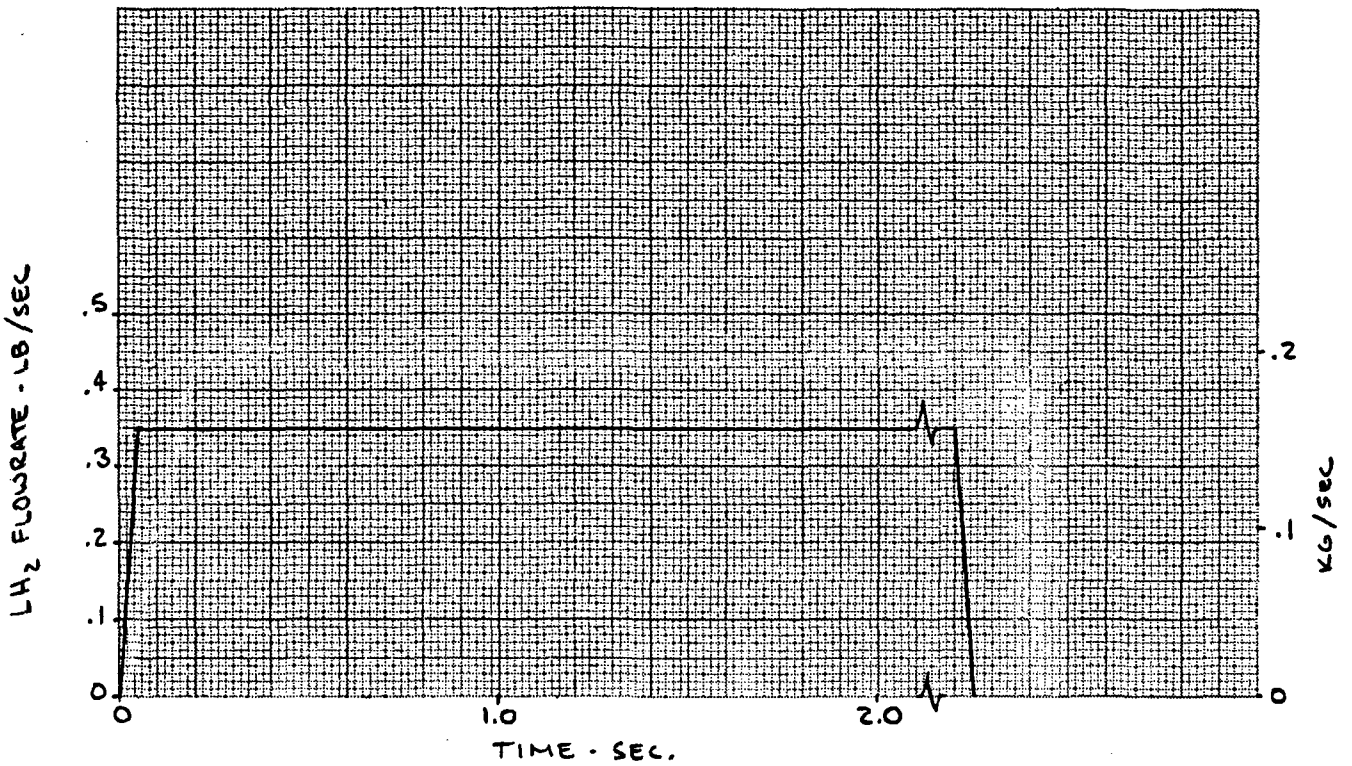

Figure A-5. LH_2 SUMP/PUMP CHILLDOWN FLOW HISTORY

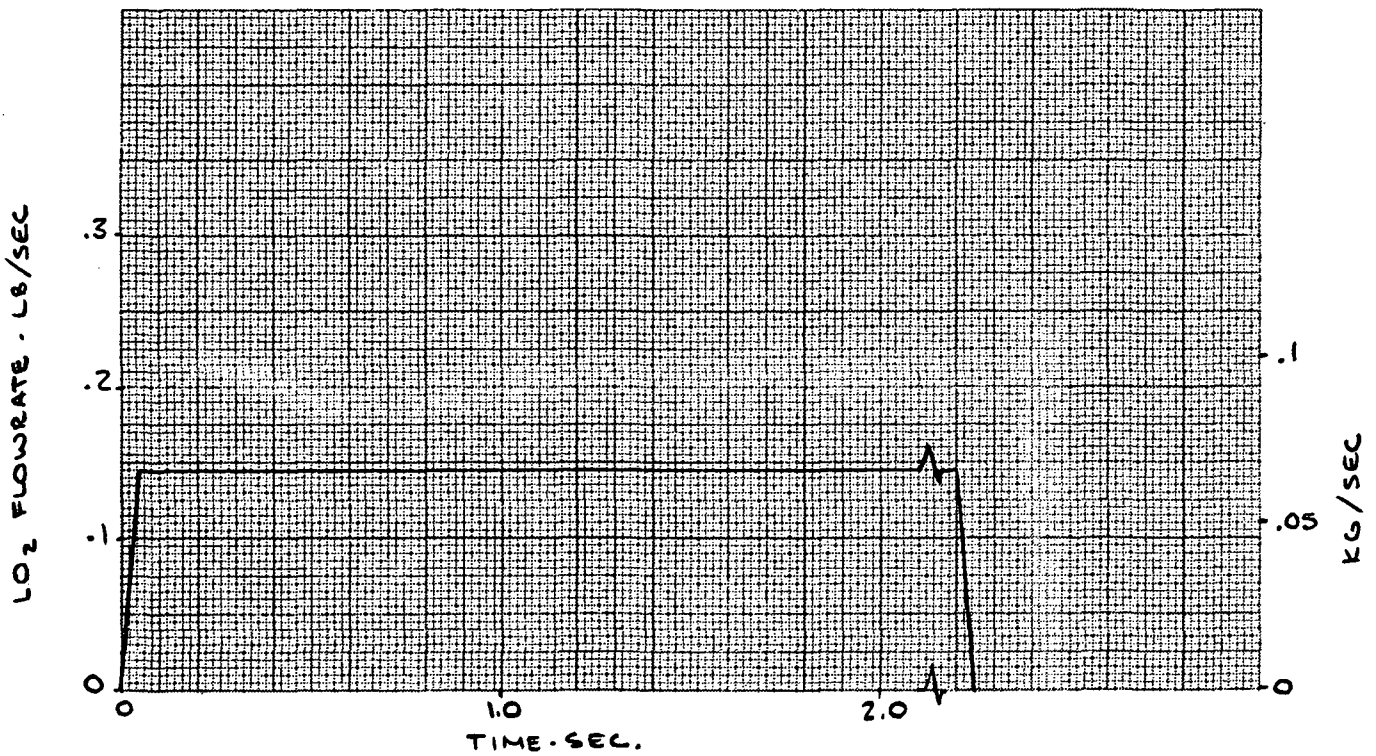

Figure A-6. LO_2 SUMP/PUMP CHILLDOWN FLOW HISTORY

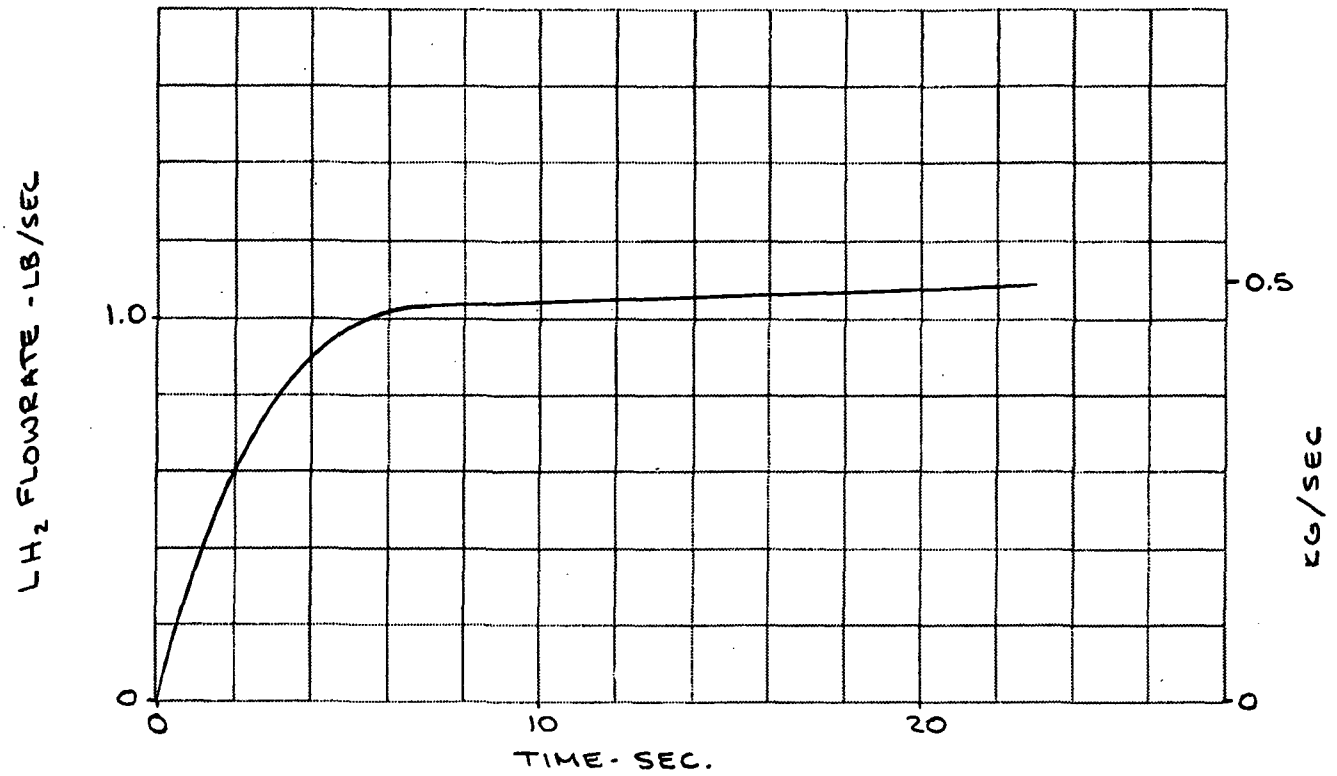

Figure A-7. LH_2 BOOST PUMP STARTUP FLOW HISTORY

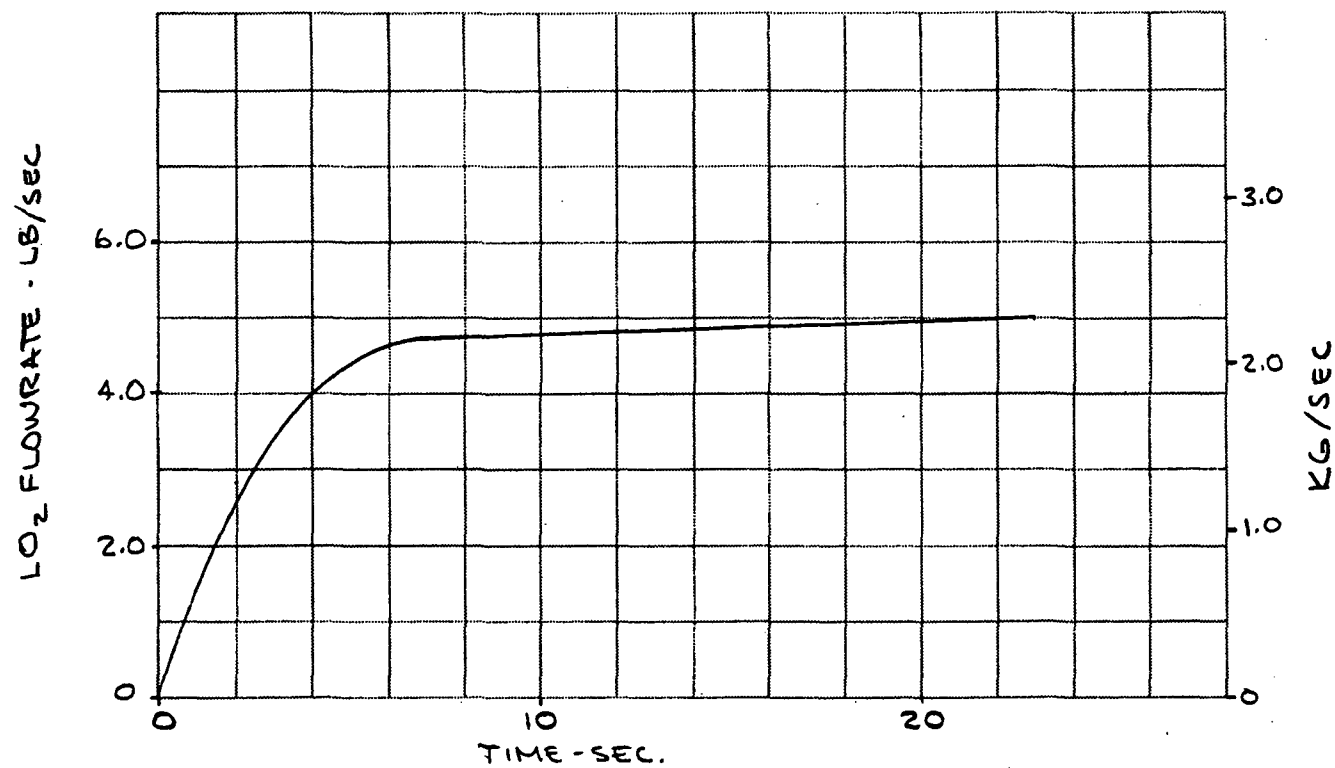

Figure A-8. LO_2 BOOST PUMP STARTUP FLOW HISTORY

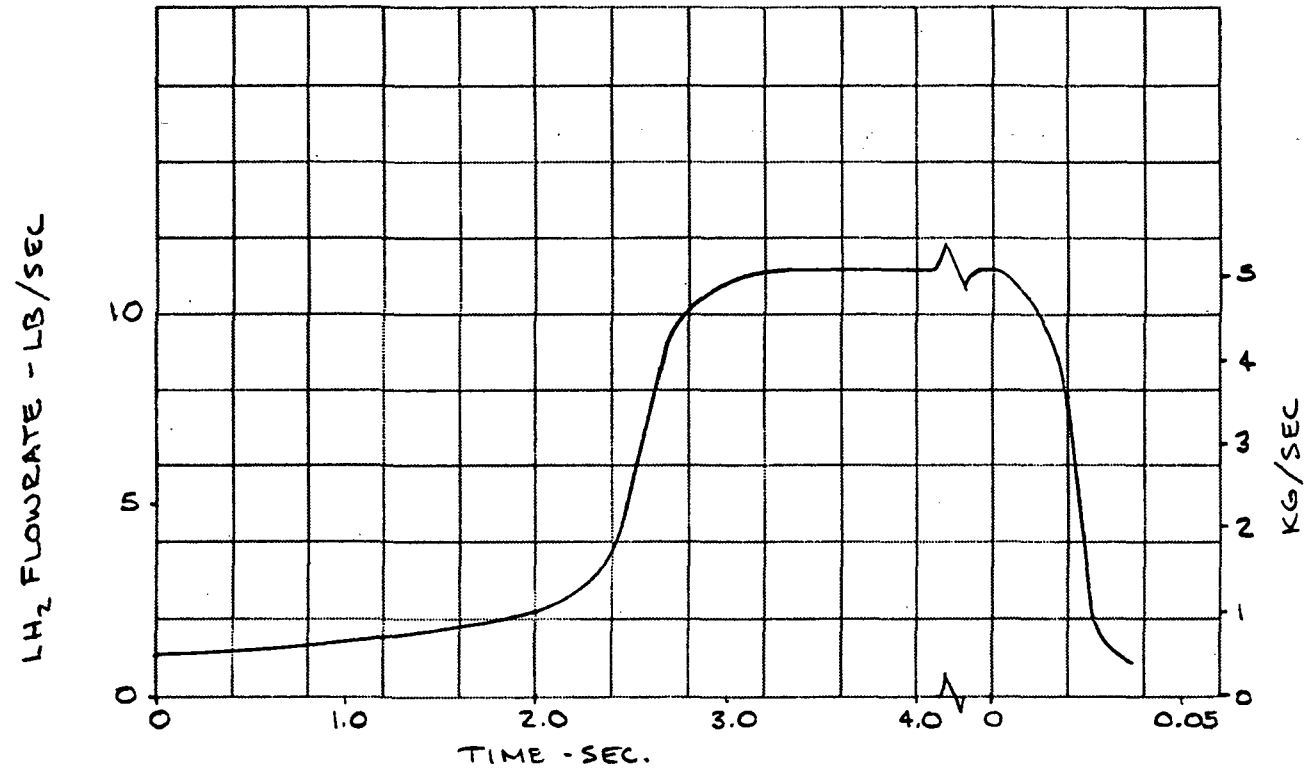

Figure A-9. ENGINE CHILLDOWN/SHUTDOWN LH_2 FLOW HISTORY

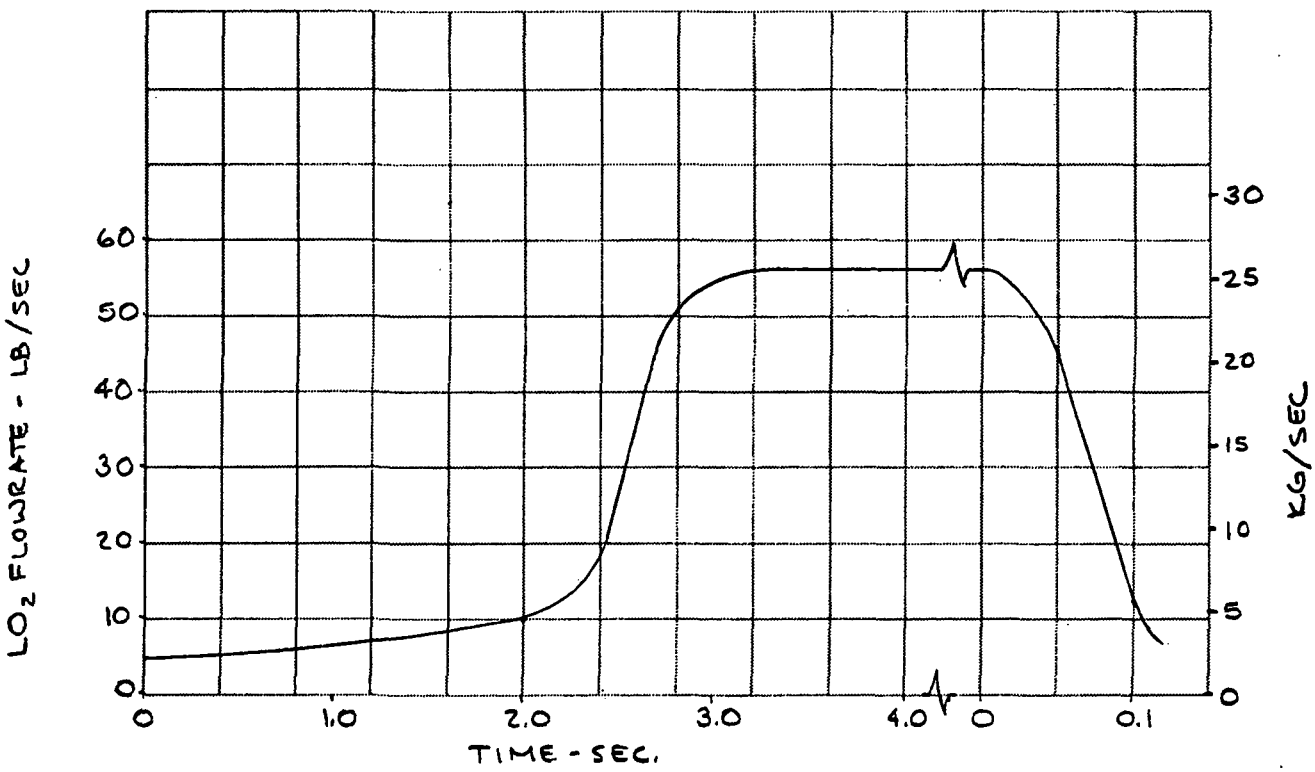

Figure A-10. ENGINE CHILLDOWN/SHUTDOWN LO_2 FLOW HISTORY

No. 4 Application: Cryogenic Tug

Name: Interface Demonstration Unit (IDU)

Fluid:	LH_2 (Saturated at 20.7 N/cm^2 (30 psia))
Quantity:	19 KG (42 Lb)
Flowrate:	3.4 KG/Sec (7.5 Lb/Sec)
Environment:	
Acceleration: "g's"	-1.0 (X)
Vibration:	U*
Thermal:	Cold and Warm, Overhead and Submerged, GHe and GH_2 Pressurization
Valve/Pump Characteristics:	U - Valve Malfunctions
Tankage and Acquisition System Configuration:	See Reference
Transfer Line Configuration:	See Reference

Reference: J. B. Blackmon. Design, Fabrication, Assembly, and Test of a Liquid Hydrogen Acquisition Subsystem. MDAC Report MDC G5360, May 1974.

* U - Unknown

No. 5 Application:	Cryogenic Tanker
Name:	S-IIB LO_2 Tanker
Fluid:	LO_2 (Saturated at 10.3 N/cm^2 (15 psia))
Quantity:	90,720 KG (200,000 Lb)
Flowrate:	16.8 Kg/Sec (37 Lb/Sec)
Environment:	
Acceleration:	Drag: -10^{-6} (X) Disturbance: $\pm 10^{-3}$ (X, YZ)
Vibration:	U
Thermal:	Cold Pressurization with Thermodynamic Vent
Valve/Pump Characteristics:	U
Tankage and Acquisition System Configuration:	See Figure A-11
Transfer Line Configuration:	U

Reference: M. H. Blatt, et. al. Low-Gravity Propellant Control Using Capillary Devices in Large-Scale Cryogenic Vehicles - Phase I, Final Report, NAS8-21465. GDC Report GDC-DDB70-007, August 1970

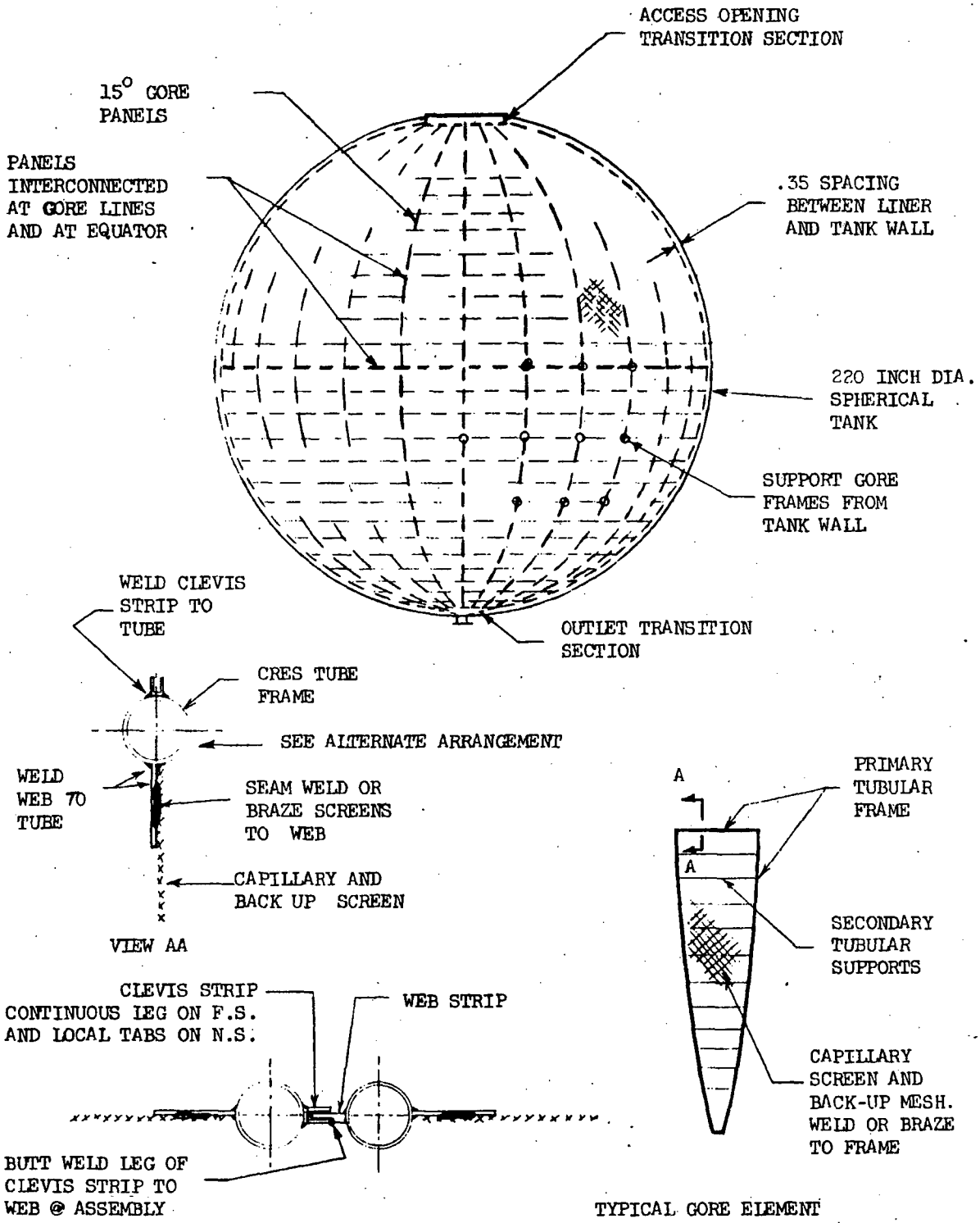

Figure A-11. Oxidizer Collector System/Full Liner Concept

No. 6 Application: Cryogenic Tanker

Name: Tug-Scale Transfer Module

	LH_2 (Saturated at 17.3 N/cm^2 (25 psia))	LO_2 (Saturated at 19.3 N/cm^2 (28 psia))
Fluid:		
Quantity:	4600 KG (10,140 Lb)	22,300 KG (49,160 Lb)
Flowrate:	.08 KG/Sec (.175 Lb/Sec)	.39 KG/Sec (.86 Lb/Sec)
Environment:		
Acceleration: "g's"	Coast: -10^{-4} (X)	-10^{-4} (X)
Vibration:	U	U
Thermal:	Cold GH_2 Pump Pressurization H_2 Thermodynamic Vent	Cold GO_2 Pump Pressurization H_2 Cooling of LO_2 Tank
Valve/Pump Characteristics:	U	U
Tankage and Acquisition System Configuration:	L/D = 2 Tank with Hemispherical Ends D = 3.78M (12.4 Ft) See Figure A-12	Spherical Tank D = 3.44M (11.3 Ft) See Figure A-12
Transfer Line Configuration:	U (3.81 cm dia. x 7.11M long) (1.5 in dia. x 282 in long)	U (3.81 cm dia. x 2.03M long) (1.5 in dia. x 80 in long)

Reference: E. C. Cady. Design and Evaluation of Thermodynamic Vent/Screen Baffle Cryogenic Storage System. MDAC Report MDC G5479 (NASA CR-134810) June 1975.

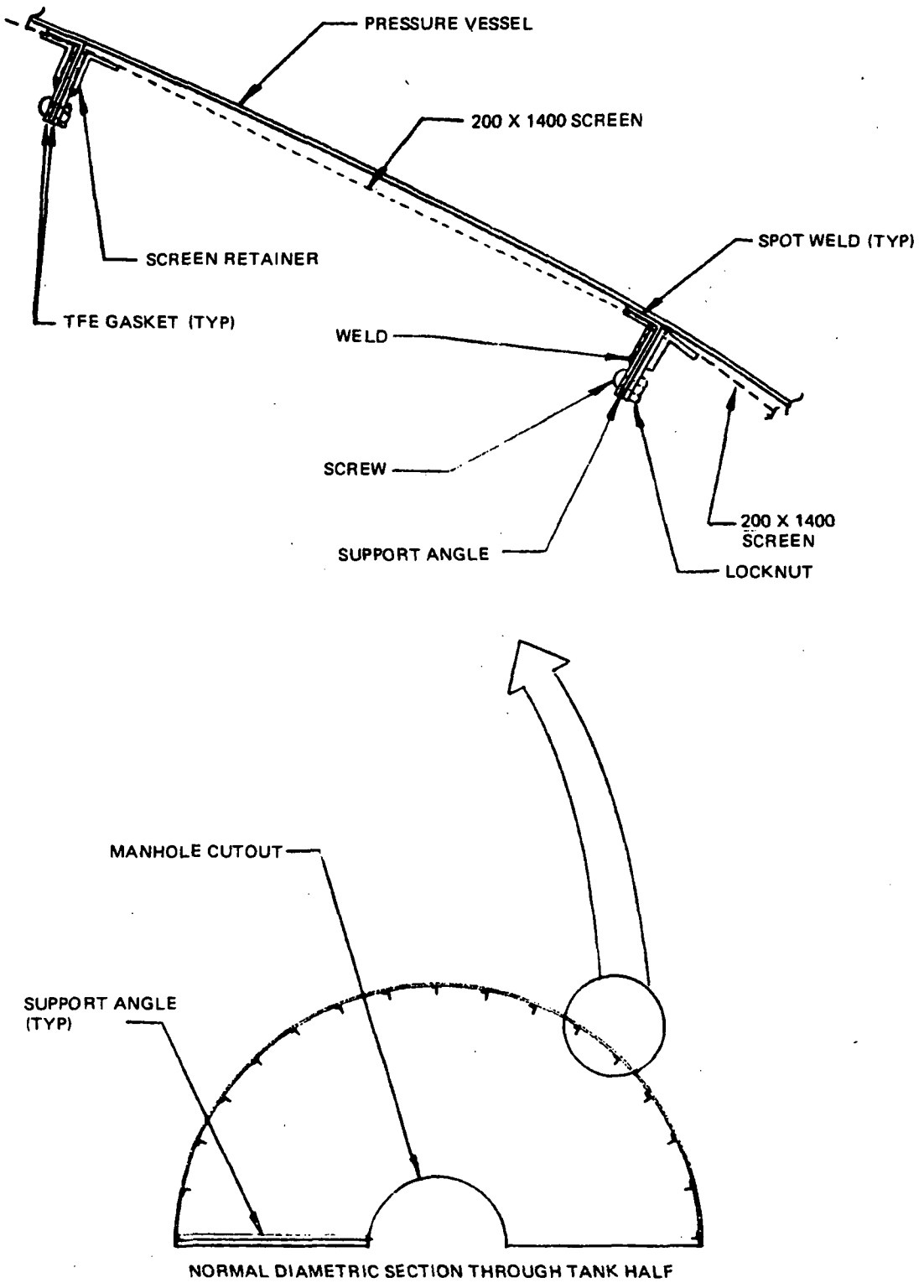

Figure A-12. SCREEN LINER MOUNTING METHOD

No. 7 Application: Cryogenic Stage

Name: S-IVC Stage Restart

	LH_2 (Saturated at 17.2 N/cm^2 (25 psia))	LO_2 (Saturated at 17.2 N/cm^2 (25 psia))
Fluid:		
Quantity:	19,500 KG (43,000 Lb) (Full) [Restart at 60% Full]	88,900 KG (196,000 Lb) (Full) [Restart at 60% Full]
Flowrate:	1.27 Kg/Sec (2.8 Lb/Sec) to 33.7 Kg/Sec (74.4 Lb/Sec)	3.7 KG/Sec (8.1 Lb/Sec) to 168.7 KG/Sec (372 Lb/Sec)
Environment:		
Acceleration: "g's"	Drag: -10^{-6} (X) Idle Mode: .00823 (X) Full Thrust: .337 (X)	Drag: -10^{-6} (X) Idle Mode: .00823 (X) Full Thrust: .337 (X)
Vibration:	U	U
Thermal:	100°K (180°R) GH_2 Pressurization Orbital Heating 627 W (2140 B/Hr)	150°K-200°K (270°R-360°R) GHe Pressurization Cooling: -381W (1300 B/Hr)
Valve/Pump Characteristics:	**See Reference**	**See Reference**
Tankage and Acquisition System Configuration:	**See Figure A-13**	**See Figure A-14**
Transfer Line Configuration:	**See Reference**	**See Reference**

Reference: M. H. Blatt, et. al. Low Gravity Propellant Control Using Capillary Devices in Large-Scale Cryogenic Vehicles - Phase II, Final Report, NAS8-21465. GDC Report GDC-DDB70-008, August 1970.

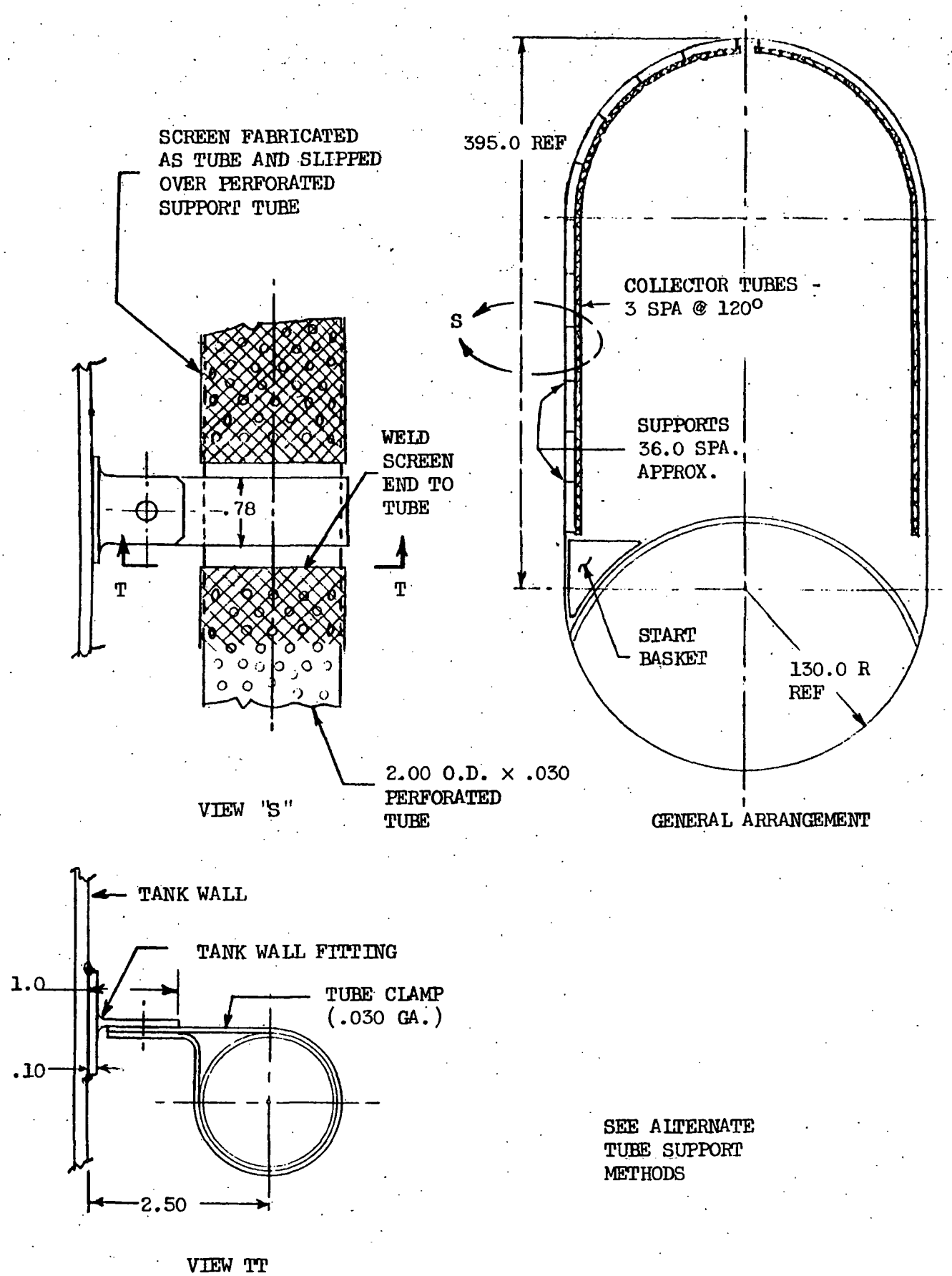

Figure A-13. Collector Tube Details

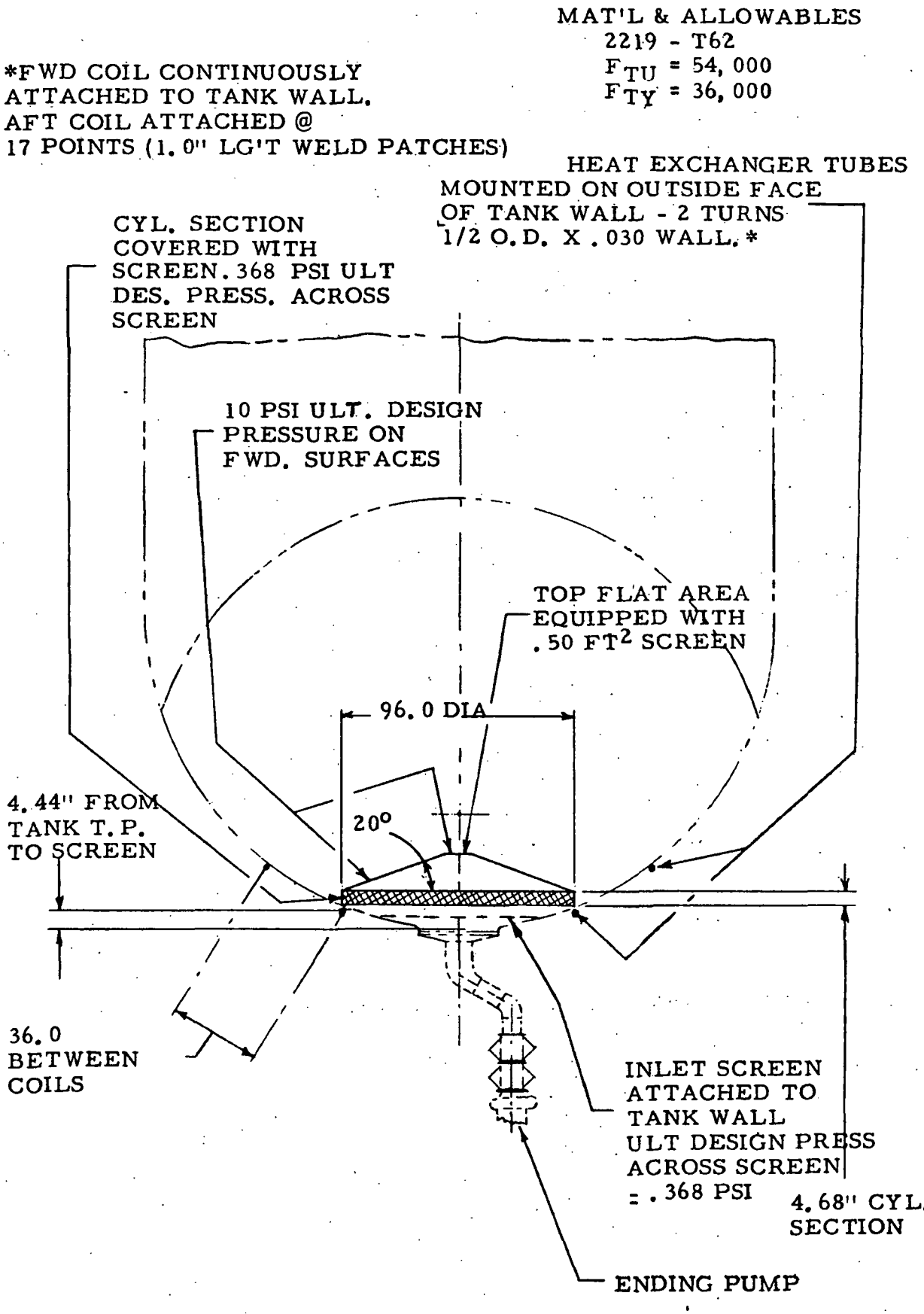

Figure A-14. Oxidizer Tank Reservoir General Arrangement and Design Ground Rules

No. 8 Application: Space Shuttle

Name: Orbital Maneuvering System (OMS)

Fluid:	N_2O_4	MMH
Quantity:	3688 KG (8130 Lb)	2221 KG (4896 Lb)
Flowrate:	Startup: 5.41 KG/Sec (11.93 Lb/Sec) Settled (Max): 10.82 KG/Sec (23.86 Lb/Sec) RCS Supply: 6.35 KG/Sec (14.00 Lb/Sec)	3.28 KG/Sec (7.23 Lb/Sec) 6.56 KG/Sec (14.46 Lb/Sec) 3.97 KG/Sec (8.75 Lb/Sec)
Environment:		
Acceleration: "g's"	Boost: +3.3 (X), =0.3 (Z) Coast: +.0767 (X), ±.04 (X,Y) -.0230 (X), (Roll, Yaw) Settling: +.024 (X) Entry: -1.6 (X), +2.5 (Z)	+3.3 (X), -0.3 (Z) +.0767 (X), ±.04 (X,Y) -.0230 (X), (Roll, Yaw) +.024 (X) -1.6 (X), +2.5 (Z)
Vibration:	See Figure A-15	See Figure A-15
Thermal:	Propellant Temperature: 4.4°C - 37.8°C (40°F - 100°F)	4.4°C - 37.8°C (40°F -100°F)
Valve/Pump Characteristics:	See Figure A-16 (Plus Additional Data)	See Figure A-16 (Plus Additional Data)
Tankage and Acquisition System Configuration:	See Figure A-17 (Plus Complete Detail Drawings*)	See Figure A-17 (Plus Complete Detail Drawings*)
Transfer Line Configuration:	Complete Detailed Drawings Available*	Complete Detailed Drawings Available*

Reference: D. A. Hess and G. F. Orton: Space Shuttle OMS Propellant Acquisition.

* MDAC-E Drawings 73T740000, 73T740010, 73J501001, 73J551001, 73J551002, 73J561001, 73A000014

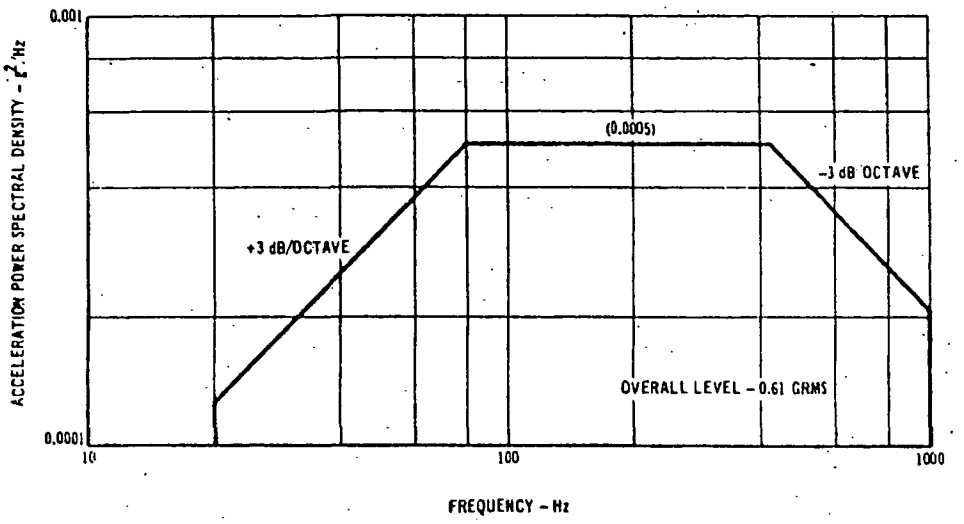

Figure A-15. ON ORBIT RANDOM VIBRATION LEVELS

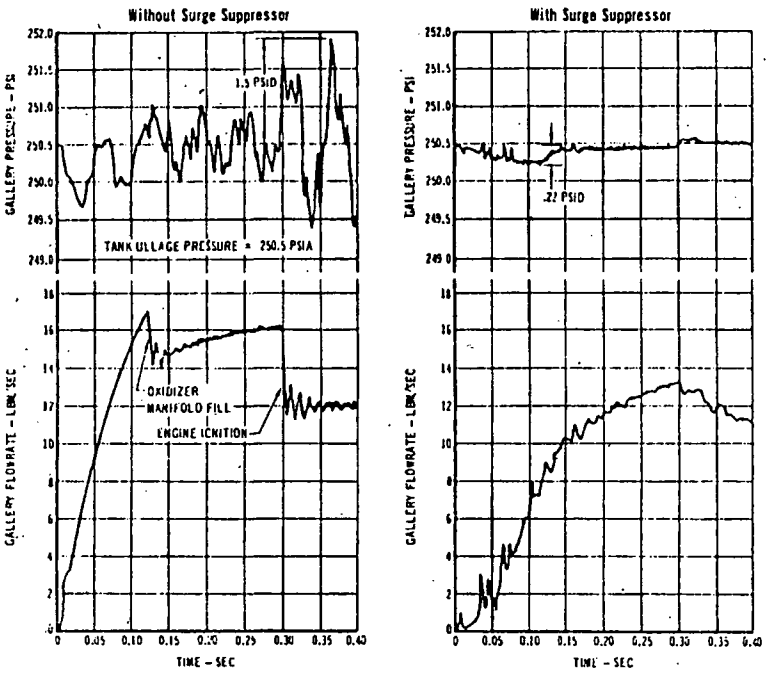

Figure A-16. GALLERY TRANSIENT PRESSURE AND FLOWRATE DURING OMS STARTUP

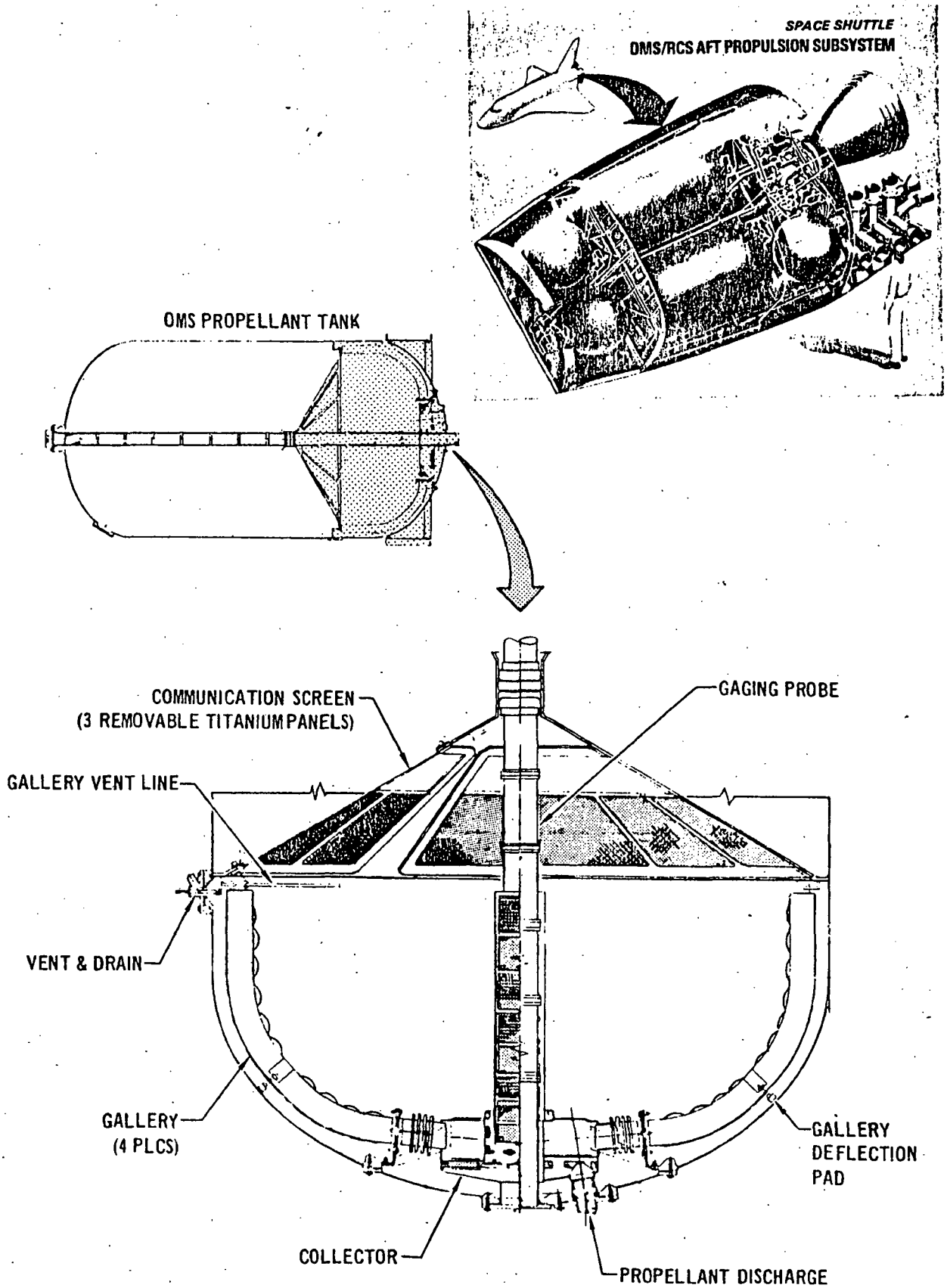

Figure A-17. OMS PROPELLANT ACQUISITION SYSTEM

No. 9 Application: Space Shuttle

Name: Orbiter Reaction Control System

Fluid:	N_2O_4	MMH
Quantity:	609 KG (1343 Lb)	381 KG (840 Lb)
Flowrate:	Per Thruster .907 KG/Sec (2 Lb/Sec)	Per Thruster .567 KG/Sec (1.25 Lb/Sec)
Environment:		
Acceleration: "g's"	Boost: +3.3 (X), -0.3 (Z) Coast: +.0767 (X), ±0.4 (X,Y) -.0230 (X), (Roll, Yaw) Settling: +.024 (X) Entry: -1.6 (X), +2.5 (Z)	+3.3 (X), -0.3 (Z) +.0767 (X), ±.04 (X,Y) -.0230 (X), (Roll, Yaw) +.024 (X) -1.6 (X), +2.5 (Z)
Vibration:	See Figure A-15	See Figure A-15
Thermal:	Propellant Temperature 4.4°C - 37.8°C (40°F - 100°F)	4.4°C - 37.8°C (40°F - 100°F)
Valve/Pump Characteristics:	U*	U*
Tankage and Acquisition System Configuration:	See Figure A-18	See Figure A-18
Transfer Line Configuration:	U*	U*

Reference: SS/RCS Surface Tension Propellant Acquisition/Expulsion Tankage Technology. MMC Report No. MCR-75-171, August 1975.

RCS Propellant Tank Design and Performance Definition. RI Supplementary Engineering Memo No. MDAC-075-104, 5 September 1975.

* Not Fully Defined to Date

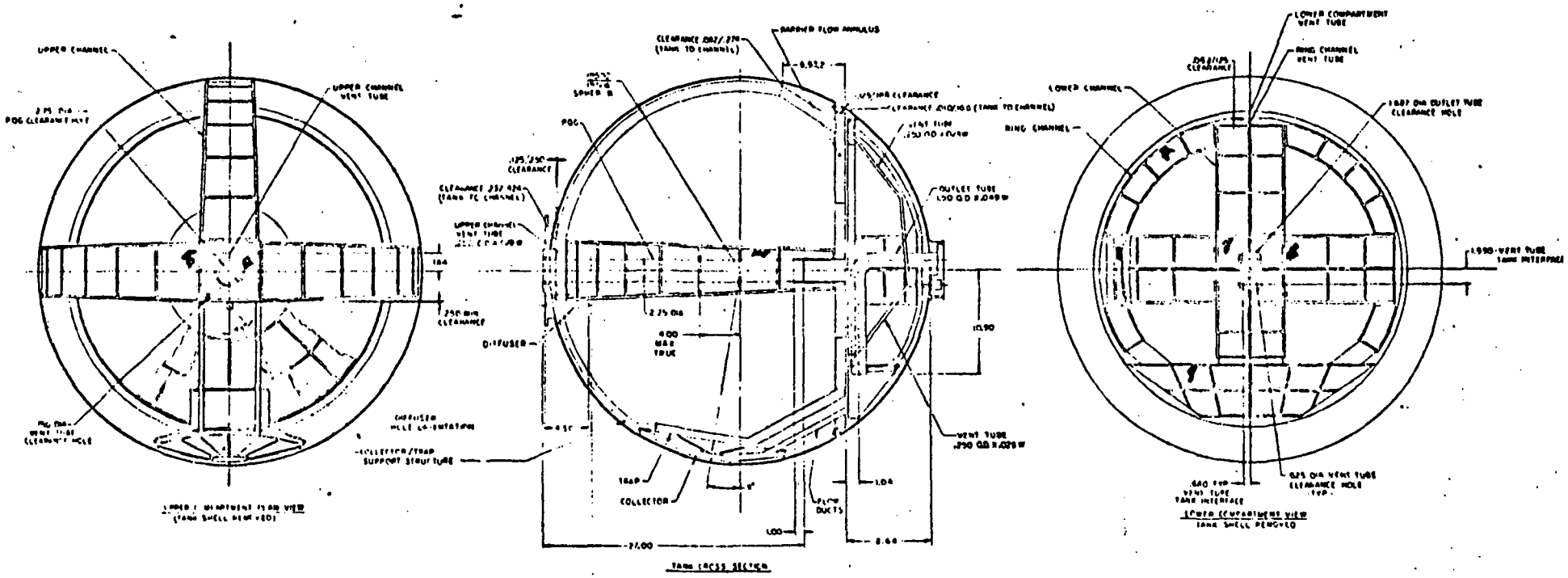

FIGURE A-18. RCS TANK ASSEMBLY

No. 10 Application: Space Shuttle

Name: Advanced Fuel Cell Reactant Supply System

	LH_2 (Saturated at 20.7 N/cm^2 (30 psia))	LO_2 (Saturated at 20.7 N/cm^2 (30 psia))
Fluid:		
Quantity: (Per Tank)	41.7 KG (92.0 Lb)	3543 KG (781.0 Lb)
Flowrate:	.032 to 1.48 Kg/Hr (.07 to 3.27 Lb/Hr)	.28 to 10.34 Kg/Hr (.618 to 22.8 Lb/HR)
Environment:		
Acceleration: "g's"	Boost: +3.3 (X), -0.2 (Z) Coast: +.0767 (X), ± .04 (X,Y) -.0230 (X), (Roll, Yaw) Settling: +.024 (X) Entry: -1.6 (X), +2.5 (Z)	+3.3 (X), -0.3 (Z) +.0767 (X), ±.04 (X,Y) -.0230 (X), (Roll, Yaw) +.024 (X) -1.6 (X), +2.5 (Z)
Vibration:	**See Figure A-15**	See Figure A-15
Thermal:	Cold GH_2 Pressurization Line Temperature 20°K - 222°K (36°R - 400°R)	Cold GO_2 Pressurization Line Temperature 98°K - 222°K (176°R - 400°R)
Valve/Pump Characteristics:	Not Applicable	Not Applicable
Tankage and Acquisition System Configuration:	**See Reference** With Full Pleated Liner	**See Reference** With Full Pleated Liner
Transfer Line Configuration:	.64 cm Dia. x .056 cm wall x 15.24M long (.25 in dia. x .022 in wall x 50 ft long) Aluminum	.64 cm Dia. x .056 cm wall x 15.24M long (.25 in Dia. x .022 in wall x 50 ft long) Aluminum

Reference: E. C. Cady. Design and Evaluation of Thermodynamic Vent/Screen Baffle Cryogenic Storage System. MDAC Report MDC G5979 (NASA CR-134810) June 1975.

No. 11 Application: Improved Agena

Name: Primary & Secondary Propulsion System

Fluid:	A-50	N_2O_4
Quantity:	1633 KG (3600 Lb)	2858 KG (6300 Lb)
Flowrate:	Primary 9.1 KG/Sec (20 Lb/Sec) Secondary .091 KG/Sec (.20 Lb/Sec)	15.9 KG/Sec (35 Lb/Sec) .159 KG/Sec (.35 Lb/Sec)
Environment:		
Acceleration: "g's"	Boost +9.0 (X) Coast -0.012 (X)	Boost +9.0 (X) Coast -0.012 (X)
Vibration:	U	U
Thermal	U	U
Valve/Pump Characteristics:	Mod. 8096 Pump - U Pneumatic Bellows Pump - U	Mod. 8096 Pump - U Pneumatic Bellows Pump - U
Tankage and Acquisition System Configuration:	**See Reference**	**See Reference**
Transfer Line Configuration:	**See Reference**	U

Reference: W. Heller and E. A. Cadwallader. Positive Expulsion. CPIA Publication 210, May 1971.

R. O. Sloma. Capillary Propellant Management System For Large Tank Orbital Propulsion Systems. CPIA Publication 190, September 1969.

No. 12 Application: Satellite

Name: Orbit Adjust System

Fluid:	N_2H_4
Quantity:	~1090 KG (2400 Lb)
Flowrate:	.25 to .47 KG/Sec (.55 to 1.032 Lb/Sec)
Environment:	
Acceleration: "g's"	+.02 (X) ± .00013 (Y,Z) -.000044 (X)
Vibration: (shock)	± .005 g-sec (X,Y,Z)
Thermal:	Propellant Temperature 4.4°C - 48.9°C (40°F - 120°F)
Valve/Pump Characteristics:	See Figure A-19
Tankage and Acquisition System Configuration:	See Figure A-19
Transfer Line Configuration:	See Figure A-19

Reference: S. C. DeBrock. Development and Flight Experience With A Capillary Propellant Management System For A Three-Axis Stabilized Vehicle.

S. C. DeBrock, et. al. A Survey of Current Developments In Surface Tension Devices For Propellant Acquisition. AIAA Paper No. 70-685. June 1970.

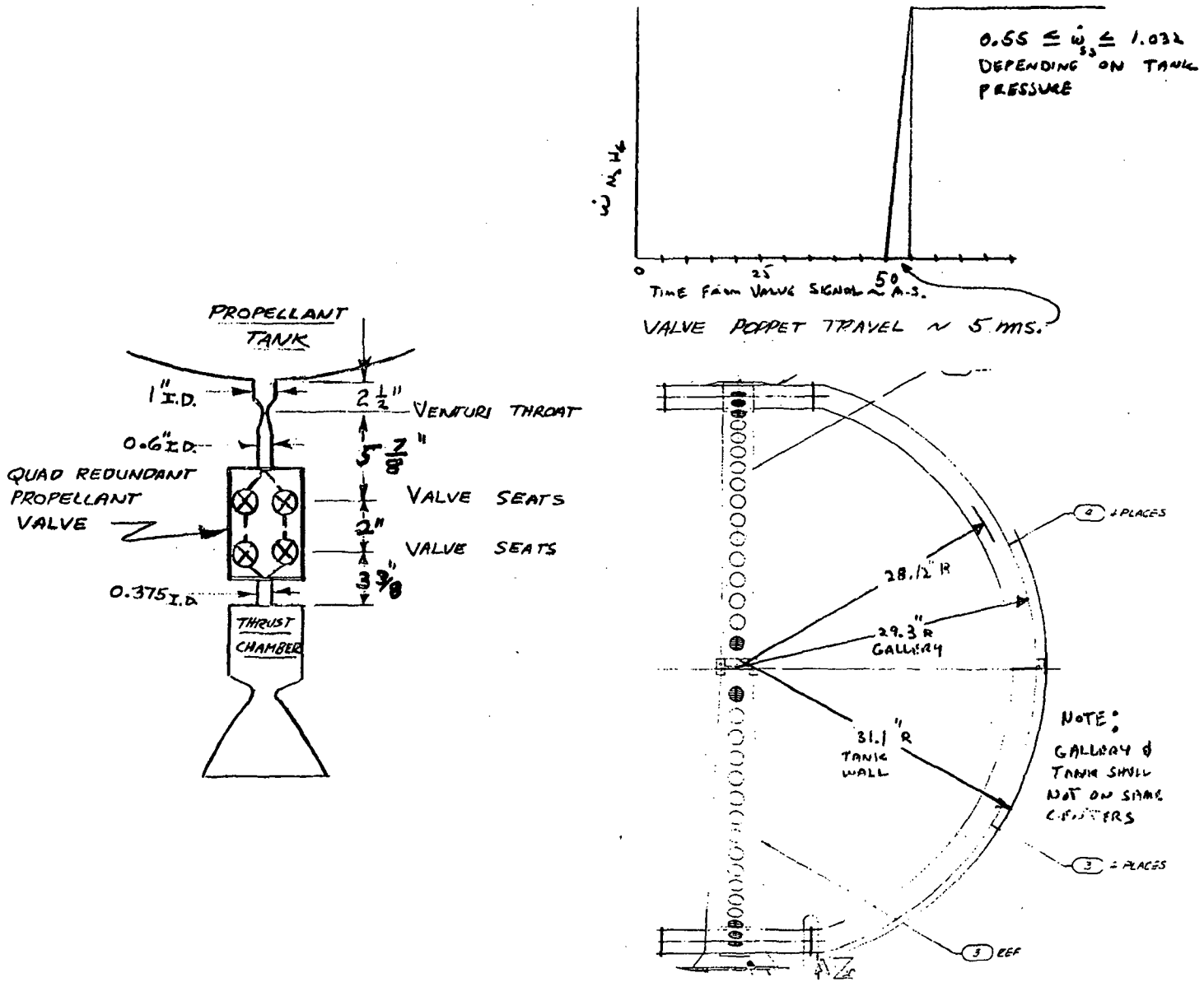

Figure A-19. SATELLITE CONTROL SECTION ORBIT ADJUST SYSTEM

Appendix B

TECHNICAL DESCRIPTION LIQUID PROPULSION FEED SYSTEM DYNAMIC ANALYSIS PROGRAM, H672

INTRODUCTION

The description of propellant feed system and rocket engine operation during severe transients inherent in startup, shutdown, pulse operation, or throttling modes has long resisted successful analytical attack. Essentially the difficulty lay in the nonlinearity of component operation during these periods, coupled with feedback effects of the individual components on the system as a whole.

Previous analytical efforts to describe engine transients are of two types. The first consists of linearizing the pertinent fluid dynamic equations and the relations that describe individual components such as valves and pumps. The linearized differential expressions are then transformed by La Place relations to a system of simultaneous equations. Solutions of these relations yield stability polars, indicating areas of operation for which the engine system may operate in a stable mode. Such solutions include component feedback effects, and generally yield a satisfactory picture of the systems operation about its design point. Unfortunately, the linear restraint placed on the pertinent equations restricts the method to small perturbations about the engine's steady-state point.

The second technique does not resort to linearization of the equations. Nonlinear properties of valves, turbines, and combusters are input in curve form, and the entire system is iterated until convergence is achieved. The engine system is treated for each time interval in a quasi steady-state manner. Valve resistances are evaluated at their current degree of opening and turbine and pump torques at their instantaneous speeds; utilizing these values the engine is steady-state balanced for this particular juncture in time.

Feedback effects are of necessity ignored, and are compensated for to some extent by continually modifying line component descriptions with observed test data. Granted the availability of sufficient experimental feedback, component modifications can be formulated which will effect an accurate simulation of the engine system. While this procedure can achieve a trustworthy simulation of a particular engine system, the results are not transferrable to new engine systems, nor can the effects of altering component parameters sensitive to liquid feedback effects such as surge tanks, valves, and injector, be assessed accurately without further experimental tests.

This appendix describes a new approach. Nonlinear description of engine components is retained at discrete junctions; however, the flow equations between components are solved by an exact technique, the method of characteristics. The result is the formulation of a pseudo wave theory. In this analysis, liquid rocket feed networks are portrayed as variable sets of components located at discrete junctions within the system. Pressure and flow information is transmitted from component to component by characteristic waves, generated and appended by perturbations and boundary conditions at the components.

The momentum and continuity equations describing the one-dimensional flow of liquids in an elastic conduit are derived and the characteristics solutions to the differential equations are developed with modifications for structural dynamic effects. These equations are then set up in finite difference form for computer solution.

The simulations of various feed system components have been developed. These include feed tanks, valves, surge tanks, spring loaded accumulators, other compliant devices such as bellows and screen channels, pumps, and liquid injectors. The component simulations were designed to use the characteristic wave equations together with the specified wave modification associated with each component to determine the pressures and flows in the system.

A general computer program was written which uses the technique described above. Emphasis was placed on overall computational flexibility; the major

result is a program in which system changes can be made by data deck modification alone.

TECHNICAL SUMMARY

The characteristic equations governing transient flow of a slightly compressible liquid in a linearly elastic conduit are derived in Reference B-1*, and listed here for convenience. (In order to simplify the following discussion, structural feedback effects and acceleration effects are neglected here.) Along a left running plus characteristic, defined as in the nominal direction of flow or as moving downstream in a piping system, the equations are:

$$\frac{dH}{dT} + \frac{a}{g}\frac{dV}{dT} = 0 \qquad (1)$$

$$\frac{dX}{dT} = a$$

For a right running minus characteristic, defined as moving against the nominal flow or upstream, the equations are:

$$\frac{dH}{dT} - \frac{a}{g}\frac{dV}{dT} = 0 \qquad (2)$$

$$\frac{dX}{dT} = -a$$

It is more convenient to handle flow in terms of volumetric flowrate Q, rather than velocity V. This has no effect on the characteristic directions, but it does modify the derivatives along the characteristic. In terms of Q, the equations along the plus and minus characteristic respectively are:

$$\frac{dH}{dT} + \frac{a}{gA}\frac{dQ}{dT} = 0 \qquad (3)$$

$$\frac{dH}{dT} - \frac{a}{gA}\frac{dQ}{dT} = 0$$

---

* B-1. W. H. Robinson. Liquid Propulsion Feed System Dynamic Analysis Program. Volume I, Technical Description Program H672. MDAC Report MDC G0451A, February 1972.

In order to get a physical picture of what Equation 3 represents, a simple pipe junction is illustrated in Figure B-1. In finite difference form, Equation 3 can be written for a plus characteristic as:

$$\Delta H + \frac{a}{gA} \cdot \Delta Q = 0 \qquad (4)$$

The speed of sound, a, is a function of liquid modulus K, considered a constant in lieu of temperature fluctuations in the line, and the wall thickness and elastic modulus of a particular pipe section. This is a constant for a single section of pipe, but may vary from section to section generally as the thickness and diameter of the pipe vary. The pipe cross-sectional area A may vary from section to section, but remains constant for any particular section. Consequently the group a/gA is a constant for any section of pipe, but is variable from segment to segment. If the

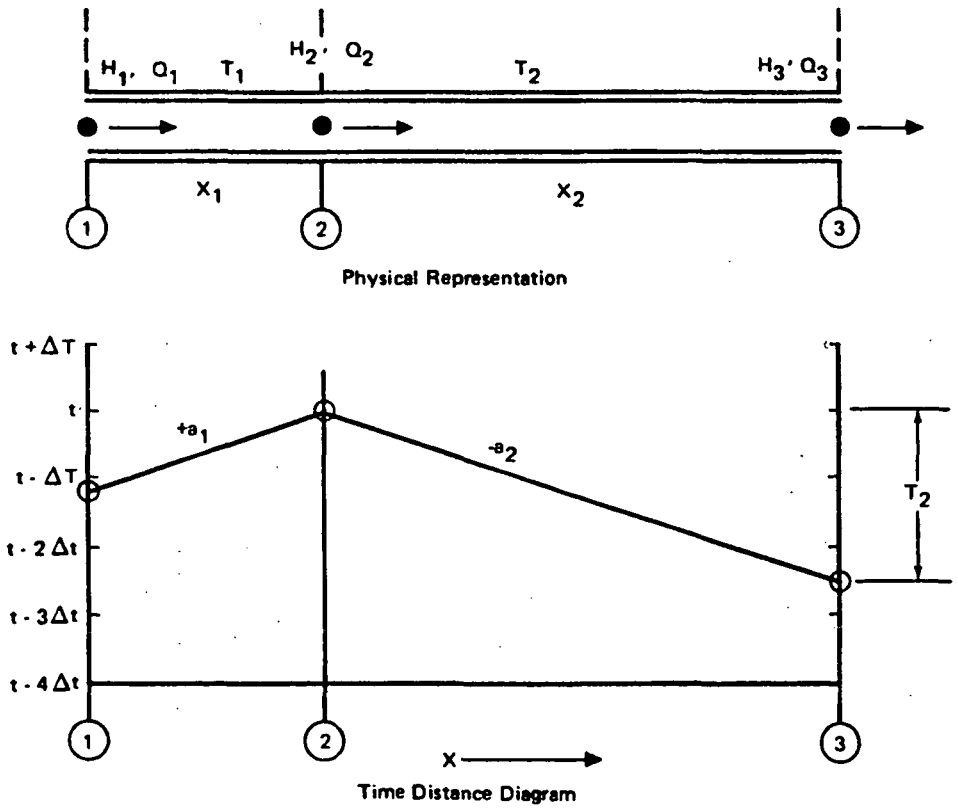

Figure B-1. Simple Pipe System

properties peculiar to waves moving with the flow are denoted by the subscript X, and those against the flow by Y, then:

$$SX = \frac{a}{gA}$$
$$SY = \frac{-a}{gA} \qquad (5)$$

Equation 4 expanded in finite difference form, and utilizing Equation 5 is:

$$H_2 - H_1 + SX\ (Q_2 - Q_1) = 0$$
$$H_2 + SX \cdot Q_2 = H_1 + SX \cdot Q_1 = CX \qquad (6)$$

Equation 6 is the basic characteristic equation for a wave traveling in the direction of flow. In like manner it can be shown that the characteristic equation moving against the flow is:

$$H_2 + SY \cdot Q_2 = H_3 + SY \cdot Q_3 = CY \qquad (7)$$

The constants CX and CY described by Equations 6 and 7 show that the waves move unmodified through a section of pipe. This result is the direct consequence of the assumptions peculiar to rocket engine systems made in the derivation. This is not to say that the waves move unchanged through the entire system; they do not. The waves are modified at discrete junctions in the system, but pass from junction to junction unmodified.

Equations 6 and 7 show no explicit time dependence. This again is the consequence of the simplifications made in the derivations. Time dependency is implicit, however, in the selection of the correct heads and flows to compute the constants CX and CY. Figure B-1 also shows the time distance diagram of the pipe system. It is assumed that the flow velocity is much less than the speed of sound. Therefore, the slope of the characteristic lines are +a for the plus characteristic, and -a for the upstream moving characteristic. The direction of flow is taken from left to right. In the diagram the pipe dimensions in Sections 1 and 2 are identical, although this is not a

prerequisite for solution. Thus both slopes are identical, but opposite in sign. These characteristics signify that wave perturbations in the system propagate with the liquid speed of sound.

In the illustration, the lengths of the pipe system are such that it requires 1.2 computing intervals for the wave to travel from Station 1 to Station 2, and 2.5 time intervals from Station 3 to Station 2. Consequently, the head and flow conditions at Station 2 at time t are a function of conditions at Station 1 at time $t-1.2\Delta t$, and Station 3 at time $t-2.5\Delta t$. The characteristic Equations 6 and 7 are computed as:

$$CX = H_1 \ (t - 1.2\Delta t) + SX \cdot Q_1 \ (t - 1.2\Delta t)$$

$$CY = H_3 \ (t - 2.5\Delta t) + SY \cdot Q_3 \ (t - 2.5\Delta t)$$

The constants CX and CY are now specified and from Equations 6 and 7, the following relations also hold:

$$CX = H_2 \ (t) + SX \cdot Q_2 \ (t)$$

$$CY = H_2 \ (t) + SY \cdot Q_2 \ (t)$$

These now are two equations for the two unknowns, H_2 and Q_2, at time t. Conditions then at Station 2 are uniquely specified at time t as:

$$Q_2 \ (t) = \frac{(CX - CY)}{(SX - SY)}$$

$$H_2 \ (t) = CX - SX \cdot Q_2 \ (t)$$

The calculation proceeds in the same manner for each junction in the pipe system, merely repeated once each time interval for each component contained in the system. The result is a lattice network of discrete points in time and space for which all the flow properties are known.

The concept of the characteristic carrying information from junction to junction, independent of all segments of the system other than those immediately adjacent to the junction under computation suggest the possibility of a modular or building block approach for the computational solution. In such an approach pieces can be added or removed from the system at will, without disturbing components not adjacent to the point of addition.

To illustrate the technique, the schematic of the pipe shown in Figure B-1 is reproduced in Figure B-2 along with a schematic showing the addition of a branch line at Station 2. For this case a third characteristic is needed; the one which runs from Station 4 to Station 2. If, for illustrative purposes, it requires 3.1 computing intervals for a wave to reach Station 2 from Station 4, the characteristic equation for this section is:

$$CZ = H_4 (t - 3.1\Delta t) + SY_{42} \cdot Q_4 (t - 3.1\Delta t)$$

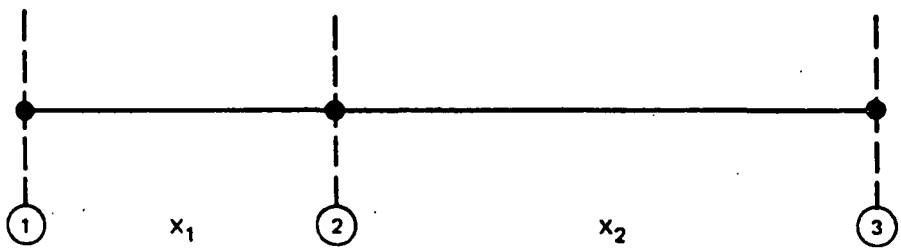

Simple Pipe System

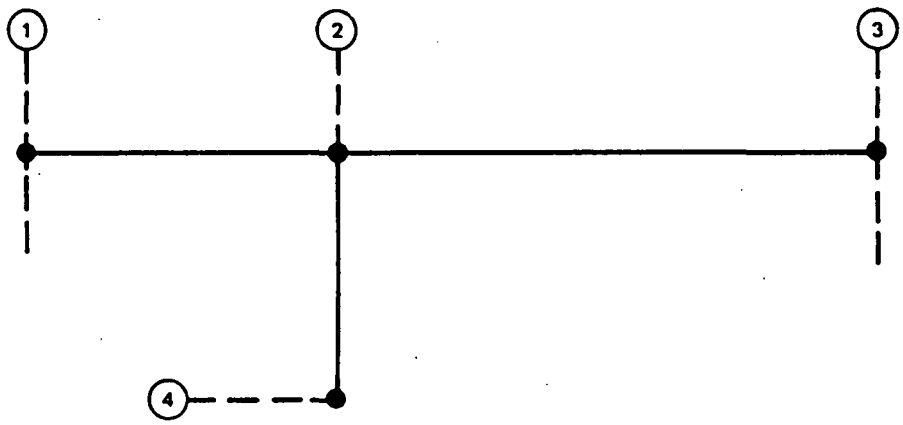

Pipe System With Tee Added at Station 2

Figure B-2. Simple Pipe Schematic

Where SY_{42} is the group -a/gA for the pipe section from Station 4 to 2. It is completely irrelevant, for this calculation, what the pipe system configuration is beyond Station 1, 3, and 4, as these regions do not contribute to the present calculation. They will of course have made significant contributions to the conditions existing at these stations, but these contingencies are assumed to be known prior to the initiation of the computation.

The conditions at Station 2 for the tee has a system of four unknowns: H_2 and the flows entering or leaving the junction at each of the pipe segments. A system of four equations is available to afford a unique, closed solution. For this discussion, the flows entering the junction are denoted by a double subscript, the first indicates the station from which the flow originated, and the second the station at which the flow is entering. Further, the flows are assumed to move from left to right, and from Station 2 towards Station 4. Using this notation, the system of equations describing the conditions at Station 2 is the three characteristic equations:

$$CX = H_2(t) + SX \cdot Q_{12}(t)$$

$$CY = H_2(t) + SY \cdot Q_{23}(t)$$

$$CZ = H_2(t) + SY_{42} \cdot Q_{24}(t)$$

Plus from continuity

$$Q_{12} = Q_{23} + Q_{24}$$

Simultaneous solution of these four equations yields:

$$H_2 = \frac{\left[\frac{CX}{SX} - \frac{CY}{SY} - \frac{CZ}{SY_{42}}\right]}{\left[\frac{1}{SX} - \frac{1}{SY} - \frac{1}{SY_{42}}\right]}$$

$$Q_{12} = (CX - H_2) / SX$$

$$Q_{23} = (CY - H_2) / SY$$

$$Q_{24} = (CZ - H_2) / SY_{42}$$

It is important to note the ease, from a computational point of view, with which the system has been radically changed. As far as Stations 1 and 3 are concerned, the system change from the simple pipe at Station 2 to a tee connection on which a great number of additional components may be connected involves only the addition of a single flow variable, Q_{23}. All other parameter designation for these stations remain the same. Only the sequence at Station 2 was changed to handle the tee connection.

The convenience with which modules may be added to or subtracted from the system allows a variety of feed configurations to be analyzed by a single computational scheme. For example, engines may be added to or deleted from a system by converting simple junctions to tees. Lines could be shortened, surge tanks or spring accumulators added, all with a minimum of inconvenience.

A computer program, H672, has been written utilizing the modular building block approach described above. The program can be conveniently subdivided into four segments for description purposes:

A. Main program — performs data initialization tasks and supervises the computational sequences.

B. Line routines – computes pressure and flow parameters in pipe segments by the characteristic method. The routines for a simple junction and tee were described previously and are representative of the routines grouped in this segment.

C. Component routines – these routines simulate various components, such as valves, tanks, pumps, injectors, and combustors, contained within the system or at its boundaries.

D. Auxiliary routines – these routines assist the line and component routines by handling such routine tasks as information retrieval, averaging, curve reading, and iteration selection.

A few additional words concerning computational features of the characteristic method are appropriate. The selection of length increments is critical to the stability of the solution. In Figure B-1, the lengths were selected such that a wave required a minimum of one computing interval in traversing the distance between stations. This procedure must be rigidly adhered to if the stability of the solution is to be insured.

The reason lies in the method of computation. For each increment in time, the flow properties are computed at each predetermined discrete junction in the system. Thus, in the example, when computing the properties at Station 2, we are assured of values at Stations 1 and 3 at times no later than $t-\Delta t$. Generally, within the system, this criteria can be assured; however, at the boundaries it may be impossible. Valves may be located less than one computing interval from an injector, and the only recourse is to shorten the computing interval, which of necessity lengthens the computational time to cover a fixed time interval. The selection of time interval of computation is then a general function of the system pipe segments.

In calculating the properties at discrete points in the system, iterations are reduced to small closed loops within a single component routine. This reduces computational time and increases the stability of the solution. A large number of check cases have been run, and stability was never a problem even when large surges due to engine ignition spikes were simulated.

APPENDIX C
SR 26 SCREEN DEVICE MODEL DEVELOPMENT

The first step in the development of the screen-channel model is the determination of the equation for acoustic velocity in the screen device (including properties of the liquid, gas bubbles, channel, or supporting structure and screen). It is assumed that initially the screen "pipe" is full of liquid. The equation for acoustic velocity in a slightly compressible liquid in an elastic pipe is well-known (Reference C-1). However, complications arise when the pipe is a nonuniform or composite structure, when the properties of the screen (hence of the pipe structure) are orthotropic, and when gas bubbles exist in the liquid. There are two kinds of screen-channel configurations which are amenable to analysis: the first is a uniformly distributed screen-channel structure which can be characterized as a pipe having properties based on the proper combination of screen and channel properties. (The second is the special case of screen only.)

Fine-mesh twilled-weave screens are basically orthotropic in nature, i.e., they have different properties in the right angle directions of the weaving axes. The properties of importance are the screen thickness, e_s, elastic modulus in the axial (E_{s_1}) and circumferential (E_{s_2}) directions, and Poisson's ratio μ_{s_1} (axially). Poisson's ratio in the circumferential direction can be derived from μ_{s_1} by:

$$\mu_{s_2} = \mu_{s_1} \frac{E_{s_2}}{E_{s_1}} \tag{1}$$

for orthotropic structures (Reference C-2). The channel support structure properties, E_p, μ_p, e_p, and the fraction of the channel area consisting of screen, f, are also necessary. It should be noted that the screen fraction, f, may not be the actual fraction but, depending on the method of screen-channel fabrication, may be an "effective" screen fraction.

C-1. J. Parmakian. Waterhammer Analysis. Dover Publications, New York, 1963.

C-2. M. H. Schneider and J. T. Hofeditz. Buckling of Fiberglass Cylinders Under External Pressure. ASME Paper No. 64-WA/UNT-12, December 1964.

Definition of the acoustic velocity in a pipe results from derivation of the continuity equation for one-dimension, unsteady flow and accounts for the elasticity of the fluid and the pipe. The pipe is shown in Figure C-1 and is assumed to be a uniformly distributed orthotropic screen-pipe structure with composite properties based on the fraction of screen area to total area:

$$f = \frac{A_s}{A_T} \tag{2}$$

and screen and pipe properties (see Figure C-1) as follows (Reference C-2):

The equivalent thickness, e, is:

$$e = e_p (1 - f) + f e_s \tag{3}$$

The longitudinal elastic modulus is:

$$E_1 = E_p (1 - f) + f E_{s_1} \tag{4}$$

and circumferential elastic modulus is:

$$E_2 = E_p (1 - f) + f E_{s_2} \tag{5}$$

Similarly, the longitudinal Poisson's Ratio is:

$$\mu_1 = \frac{\mu_p (1 - f) E_p + \mu_{s_1} f E_{s_1}}{E_p (1 - f) + f E_{s_1}} \tag{6}$$

and circumferential Poisson's ratio is:

$$\mu_2 = \frac{\mu_p (1 - f) E_p + \mu_{s_1} E_{s_2}^2 / E_{s_1} f}{E_p (1 - f) + f E_{s_2}} \tag{7}$$

It will be noted that if the screen is not constrained by or attached to the pipe f = 1, and if the screen is completely constrained by the pipe, f = 0.

Referring to Figure C-1, the deformation of the element of the composite pipe shell produced by a change in the longitudinal and circumferential stresses is

$$\Delta R = \left(R + \frac{e}{2}\right)\left(\frac{\Delta\sigma_2}{E_2} - \frac{\mu_1\,\Delta\sigma_1}{E_1}\right)$$

$$\cong R\left(\frac{\Delta\sigma_2}{E_2} - \frac{\mu_1\Delta\sigma_1}{E_1}\right) \tag{8}$$

and the change in the axial length of the element is

$$\delta x = dx\left(\frac{\Delta\sigma_1}{E_1} - \frac{\mu_2\,\Delta\sigma_2}{E_2}\right) \tag{9}$$

where $\Delta\sigma_1$ and $\Delta\sigma_2$ represent the change in the longitudinal and circumferential stresses, respectively, produced by a change in pressure. The volume enclosed by the newly stressed element is $\pi\,(R + \Delta R)^2\,(\delta x + dx)$ and the change in length compatible with the change in volume is

$$\frac{\pi\,(R + \Delta R)^2\,(\delta x + dx) - \pi R^2\,dx}{\pi R^2} \tag{10}$$

After neglecting terms which are very small when compared with those retained, the total change in length of the element is found to be

$$\delta x + \frac{2\,\Delta R}{R}dx \tag{11}$$

The change in the longitudinal stress is dependent upon the ability of the pipe to move in a longitudinal direction. Several typical cases are considered in which the movement of the pipe is restricted to varying extents

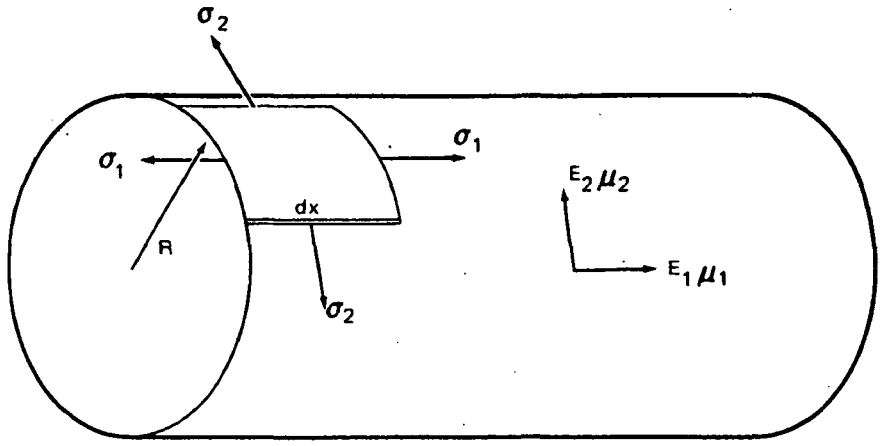

PIPE PROPERTIES	ELASTIC MODULUS, E_p
	POISSON'S RATIO, μ_p
	WALL THICKNESS, e_p
SCREEN PROPERTIES	ELASTIC MODULUS, AXIAL DIRECTION, E_{S_1}
	ELASTIC MODULUS, CIRCUMFERENTIAL, E_{S_2}
	POISSON'S RATIO, AXIAL, μ_{S_1}
	SCREEN THICKNESS, e_S

Figure C-1. Orthotropic Structure Nomenclature

A. For a pipe anchored at the upper end, free to move in a longitudinal direction throughout its lengths, and without expansion joints, the longitudinal and circumferential stresses produced by a pressure change of ρ dH are

$$\Delta\sigma_1 = \frac{\rho \, dH \, D}{4e}$$

$$\Delta\sigma_2 = \frac{\rho \, dH \, D}{2e} \qquad (12)$$

from which the change in length from (11) is

$$dx \left(\frac{\rho \, dH \, D}{4e \, E_1} - \mu_2 \frac{\rho \, dH \, D}{2e \, E_2} \right) + 2 \, dx \left(\frac{\rho \, dH \, D}{2e \, E_2} - \frac{\mu_1 \, \rho \, dH \, D}{4e \, E_1} \right)$$

$$= \left[\frac{\rho \, dH \, D}{e \, E_1} \left(\frac{1 - 2\mu_1}{4} \right) + \frac{\rho \, dH \, D}{e \, E_2} \left(1 - \frac{\mu_2}{2} \right) \right] dx \qquad (13)$$

B. For a pipe which is anchored against longitudinal movement throughout its length,

$$\Delta\sigma_1 = \mu_2 \frac{\rho\, dH\, D}{2e}$$

$$\Delta\sigma_2 = \frac{\rho\, dH\, D}{2e} \tag{14}$$

from which the change in length is

$$dx\left(\mu_2 \frac{\rho\, dH\, D}{2e\, E_1} - \mu_2 \frac{\rho\, dH\, D}{2e\, E_2}\right) + 2\, dx\left(\frac{\rho\, dH\, D}{2e\, E_2} - \mu_1\, \mu_2 \frac{\rho\, dH\, D}{2e\, E_1}\right)$$

$$= \left[\frac{\rho\, dH\, D}{e\, E_1}\left(\frac{\mu_2}{2} - \mu_1\, \mu_2\right) + \frac{\rho\, dH\, D}{e\, E_2}\left(1 - \frac{\mu_2}{2}\right)\right] dx \tag{15}$$

C. For a pipe with expansion joints between anchors (or free at both ends):

$$\Delta\sigma_1 = 0$$

$$\Delta\sigma_2 = \frac{\rho\, dH\, D}{2e} \tag{16}$$

from which the change in length is

$$dx\left(-\mu_2 \frac{\rho\, dH\, D}{2e\, E_2}\right) + 2\, dx \frac{\rho\, dH\, D}{2e\, E_2} = \frac{\rho\, dH\, D}{e\, E_2}\left(1 - \frac{\mu_2}{2}\right) dx \tag{17}$$

Therefore, the total change of length produced by the pressure change $\rho\, dH$ is:

$$\frac{\rho\, dH\, D}{e\, E_1}\, dx\, C_1 + \frac{\rho\, dH\, D}{e\, E_2}\, dx\, C_2 \tag{18}$$

where for case

A. $C_1 = \frac{1 - 2\mu_1}{4}$ $\qquad C_2 = 1 - \frac{\mu_2}{2}$

B. $C_1 = \frac{\mu_2}{2} - \mu_1 \mu_2$ $\qquad C_2 = 1 - \frac{\mu_2}{2}$

C. $C_1 = 0$ $\qquad C_2 = 1 - \frac{\mu_2}{2}$

The change in volume of the original element of fluid, dx in length, because of the elasticity of liquid under the action of a pressure change ρ dH, is:

$$\frac{\rho \pi R^2}{K} dH\, dx \tag{19}$$

and the corresponding change in length of the element of liquid is

$$\frac{\rho \pi R^2}{K \pi R^2} dH\, dx = \frac{\rho}{K} dH\, dx \tag{20}$$

The total change in length of the element of liquid caused by a pressure change ρ dH, when both the compressibility of the liquid and the deformation of the pipe are considered, reduces to

$$\rho\, dH\, dx \left(\frac{1}{K} + \frac{D C_1}{e E_1} + \frac{D C_2}{e E_2} \right) \tag{21}$$

Since H is a function of x and t, and dx/dt = V, it follows that

$$dH = \frac{\partial H}{\partial t} dt + \frac{\partial H}{\partial x} dx = \left(\frac{\partial H}{\partial t} + V \frac{\partial H}{\partial x} \right) dt \tag{22}$$

The total change in length of the element produced by a pressure change is then

$$\rho \left(\frac{1}{K} + \frac{D C_1}{e E_1} + \frac{D C_2}{e E_2} \right) \left(\frac{\partial H}{\partial t} + V \frac{\partial H}{\partial x} \right) dx\, dt \tag{23}$$

The total change in length is also

$$- \frac{\partial V}{\partial x} \, dx \, dt \tag{24}$$

so that

$$\frac{\partial V}{\partial x} = - \rho \left(\frac{1}{K} + \frac{D \, C_1}{e \, E_1} + \frac{D \, C_2}{e \, E_2} \right) \left(\frac{\partial H}{\partial t} + V \, \frac{\partial H}{\partial x} \right) \tag{25}$$

or

$$\frac{\partial H}{\partial t} + V \, \frac{\partial H}{\partial x} = - \frac{a^2}{g} \cdot \frac{\partial V}{\partial x}$$

where the acoustic velocity a is

$$a = \left(\frac{\rho}{g} \left[\frac{1}{K} + \frac{D \, C_1}{e \, E_1} + \frac{D \, C_2}{e \, E_2} \right] \right)^{-1/2} \tag{26}$$

The extension of the basic pipe analysis to liquids which include gas bubbles is given in Reference C-3. The experimental data of Reference C-3 is best correlated by assuming adiabatic bubble expansion and contraction. The final equation for the acoustic velocity in a liquid-gas mixture in a composite orthotropic pipe is:

$$a' = \left[\frac{x^2}{C_g^{\,2}} + \frac{(1 - x)^2}{C_L^{\,2}} + x \, (1 - x) \left(\frac{\rho_L}{\gamma \, P_A g} + \frac{\rho_g}{K \, g} \right) + \left\{ (1 - x) \, \frac{\rho_L}{g} + \frac{x \, \rho_g}{g} \right\} \left(\frac{D \, C_1}{e \, E_1} + \frac{D \, C_2}{e \, E_2} \right) \right]^{- 1/2} \tag{27}$$

C-3. B. R. Hanks and D. G. Stephens. Helium Injection to Reduce Resonant Frequencies in Propellant Lines. Journal of Spacecraft, Volume 6, No. 11, October 1969, pp 1202-1204.

where x is the volume fraction of gas; C_g and C_L are the acoustic velocities in the gas and liquid, respectively; ρ_g and ρ_L are the corresponding densities; P_A is the absolute pressure in the pipe; γ is the ratio of specific heats for the gas; g is the gravitational constant; K is the compressibility of the liquid; D and e are the pipe inside diameter and equivalent thickness; E_1 and E_2 are the orthotropic elastic moduli; and C_1 and C_2 are constants as given in Equation 18 depending on the form of pipe constraint.

The complete screen device will be divided into a series of sections, one of which is shown in Figure C-2. The screen area is defined by the screen fraction, and the length of the section

$$A_s = \pi \cdot D \cdot L \cdot f \tag{28}$$

The upstream and downstream conditions of head and flow are known from the previous timestep so that

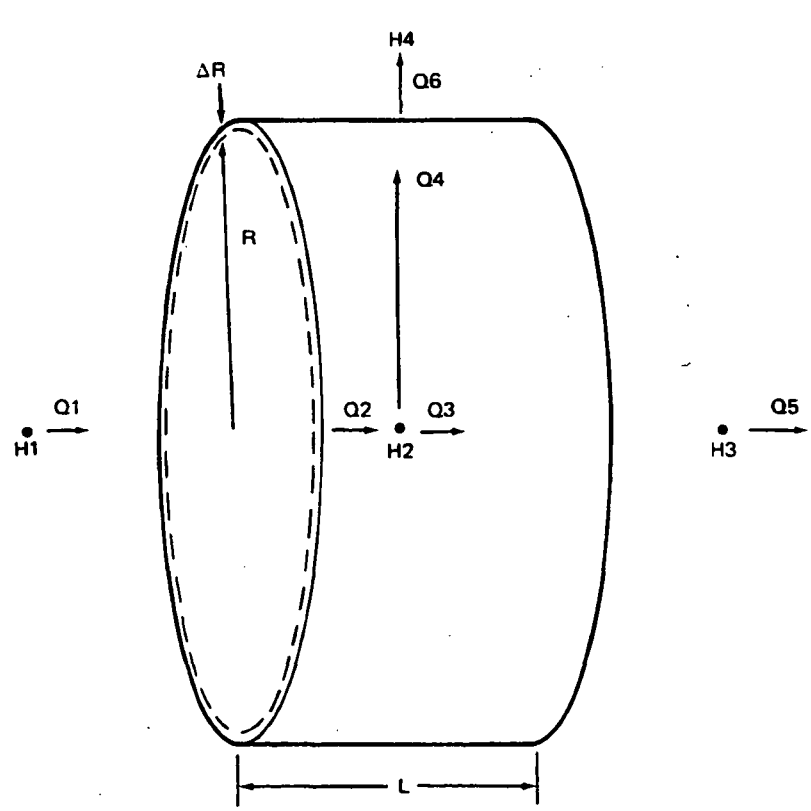

Figure C-2. Screen Device Model

$$CX = H1 + SX \cdot Q1$$

$$CY = H3 + SY \cdot Q5 \tag{29}$$

where

$$SX = \frac{a'}{g_c A_p}$$

$$SY = -\frac{a'}{g_c A_p}$$

Some of the Q4 flow, flows through the screen (Q6) because of the head difference:

$$H2 - H4 = \frac{A'Q6}{A_s} + \frac{B'(Q6)^2}{A_s^2} \tag{30}$$

where A' and B' are the experimentally determined liquid flow-loss coefficients for the screen, and H4 is the tank pressure.

The rest of the flow, Q4 - Q6, expands the pipe slightly such that the change of volume is:

$$\Delta T\ (Q4 - Q6) = L\ 2\pi R\ \Delta R \tag{31}$$

where the appropriate time increment is that required for the wave to traverse the section length:

$$\Delta T = \frac{L}{a'} \tag{32}$$

and where ΔR from Equation 9 is:

$$\Delta R = R\left(\frac{\Delta\sigma_2}{E_2} - \frac{\mu_1\ \Delta\sigma_1}{E_1}\right) \tag{33}$$

For the pipe free to move at the edges of the section,

$$\Delta\sigma_1 = 0$$

so that combining Equation 31, 32, and 33:

$$Q4 - Q6 = 2 A_p a' \frac{\Delta\sigma_2}{E_2} \tag{34}$$

Taking a pressure (force) balance on the pipe, considering the stress change in the pipe:

$$\rho_L \cdot H2 \cdot (A_s - A_o) = \rho_L H4 (A_s - A_o) + \Delta\sigma_2 e L \tag{35}$$

where A_o is the open area of the screen and $P_o = A_o/A_s$, thus

$$H2 - H4 = \frac{\Delta\sigma_2 e}{\rho_L \pi D (1 - P_o) f} \tag{36}$$

Solving for $\Delta\sigma_2$ and substituting (34) into (36) gives

$$H2 - H4 = \frac{e E_2 (Q4 - Q6)}{2 A_p a' \rho_L \pi D (1 - P_o) f} \tag{37}$$

From Figure 3 and the characteristic identities:

$$Q2 = (CX - H2)/SX$$

$$Q3 = (CY - H2)/SY$$

$$Q4 = Q2 - Q3 \tag{38}$$

Equation 38 is substituted into Equation 37 to eliminate Q4 and the result is combined with Equation 30 to eliminate H2 and give a quadratic expression in only Q6 and H4. Solving this quadratic explicitly for Q6 (flow through the screen) gives

$$Q6 = \frac{2\left(H4 - \frac{1}{ZZ}\left(H4 + \frac{c \cdot CX}{SX} - \frac{c \cdot CY}{SY}\right)\right)}{-\left(a + \frac{c}{ZZ}\right) - \left(\left(a + \frac{c}{ZZ}\right)^2 - \left(4b\left(H4 - \frac{1}{ZZ}\left(H4 + \frac{c \cdot CX}{SX} - \frac{c \cdot CY}{SY}\right)\right)\right)\right)^{1/2}} \quad (39)$$

where

$$ZZ = 1 + \frac{c}{SX} - \frac{c}{SY}$$

$$a = A'/A_s$$

$$b = B'/A_s^2$$

$$c = 2e\, E_2/a'\, \rho_L\, \pi^2\, D^3\, (1 - P_o)\, f$$

From Q6, H2 is computed from Equation 30 and the flows from Equation 38. Q3 and H2 then become the upstream values used to compute the new conditions in the next section.

With gas surrounding the screen, a negative pressure pulse in excess of the screen bubble point will result in gas ingestion with the inflow Q6' represented by a new form of equation (30):

$$H4 - H2 = \frac{A''\, Q6'}{A_s} + \frac{B''\, (Q6')^2}{A_s^2} \quad (40)$$

where A'' and B'' are the flow-loss coefficients corrected to gas properties. Q6' is found from Equation 39 with the appropriate values of a and b.

In order not to permanently deform the screen, the equivalent stress in the screen, $\Delta\sigma_2$, defined by Equation 36 for the H2 solution, must be below some critical stress, e. g., the proportional limit of the screen. Equation 36 is used to check this condition for the screen device. Another criterion which must be checked when gas surrounds the screen device is whether liquid expelled through the screen by a pressure pulse leaves the screen.

The velocity of the liquid through the screen pore is:

$$V_s = \frac{Q6}{A_s P_o} \tag{41}$$

and the velocity of the liquid globule (if $r_L > r_s$) is approximately:

$$V_L = V_s \left(\frac{r_s}{r_L}\right)^2 \tag{42}$$

where r_L is the globule radius and r_s is half the screen pore diameter, otherwise V_L equals V_s.

The globule volume is:

$$QL = \frac{4}{3} \pi r_L^3 \tag{43}$$

and for n pores where:

$$n = \frac{A_s P_o}{\pi r_s^2} \tag{44}$$

then the globule radius is:

$$r_L = \left[\frac{QLSUM}{A_s P_o} \cdot \frac{3}{4} r_s^2\right]^{1/3} \tag{45}$$

The quantity QLSUM equals QL · n and also equals $\Sigma Q6 \cdot \Delta T$ and is updated with each time step.

The liquid globule kinetic energy is

$$K.E. = \frac{4}{3} \pi r_L^3 \frac{\rho_L}{g_c} V_L^2 \tag{46}$$

and the surface tension energy is approximately

$$S.E. = \frac{\sigma \pi r_s^3}{r_L} \tag{47}$$

Assuming negligible potential energy, the criterion for liquid breakaway is for the globule kinetic energy to exceed the surface tension energy. Combining Equations 46 and 47 and solving for the critical velocity, V_{L_C}, which results in liquid globule breakaway gives:

$$V_{L_C} \simeq \left[\frac{\sigma}{\rho_L} \cdot \frac{3}{4} g_c \frac{r_s^3}{r_L^4}\right]^{1/2} \tag{48}$$

If V_L from Equation 42 is larger than V_{L_C} from Equation 48 the liquid globule will leave the screen. In addition, if the quantity of liquid outflow is sufficient to wet the entire screen surface, it was assumed that screen pore surface tension forces no longer exist, so that the liquid also leaves the screen. The quantity of liquid (QLSUM) held by the screen is kept current by correction (if any) in each time step. If QLSUM is positive, then inflow during a negative pressure pulse is liquid, until QLSUM goes to zero. This may retard gas ingestion for several time steps.

The model for gas ingestion and quality assumes that the quality in the device is uniform (i. e., the gas bubbles are not concentrated near the screen, but are distributed uniformly throughout the liquid in the screen). Throughout the H672 program, the liquid density is used to compute head, so that for gas inflow, the volumetric flow rate is corrected by the gas-liquid density ratio. The quality in the device is equal to the gas volume divided by the liquid volume (screen device volume minus gas volume). If outflow from the screen device through the downstream valve is occurring, the gas volume is diminished by the amount of entrained gas that outflows (conversely, if inflow occurs, and the downstream quality is not zero, the gas volume is similarly increased). If the quality in the device is not zero, and a positive pressure pulse in excess of the bubble point occurs, it is assumed that the gas volume

is diminished by the outflow times the current quality. The gas volume (QSUM) is kept current by correction (if any) in each time step. The acoustic velocity a', from Equation 27 is updated in each time step by the quality from the preceding time step.

APPENDIX D

```
                SUBROUTINE SCRPRP (SURX,I)
              C
              C     THIS SUBROUTINE IS USED TO PREPARE THE SURX DATA BLOCKS
              C     FOR COMPUTATIONS IN THE SR26 SCREEN DEVICE SUBROUTINE
              C
000005                DIMENSION SURX(20,4),H1(5)
000005                COMMON/A0/Z,CNST(5),RHO(2)
000005                COMMON/TURBIN/XL,THPP,WTT,XK,VO
              C
              C
000005                READ (5,100) H1,(SURX(K,I),K=1,16),N
000025                WRITE (6,101) (H1(K),K=1,5),I,(SURX(K,I),K=1,16),N
000056                SURX(3,I) = SURX(3,I)*CNST(1)
000063                SURX(5,I) = SURX(5,I)*CNST(1)*CNST(1)
000067                SURX(6,I) = SURX(6,I)*12.
000072                SURX(11,I) = SURX(11,I)/12.
000075                SURX(12,I) = SURX(12,I)/CNST(1)
000101                SURX(15,I) = SURX(15,I)/12.
000104                SURX(17,I) = SURX(3,I)/SURX(2,I)
000111                SURX(18,I) = SQRT(SURX(1,I)*CNST(4)*SURX(2,I))
000121                SURX(19,I) = RHO(N)/SURX(1,I)/SURX(3,I)/CNST(4)
000126                SURX(20,I) = SURX(17,I)/XK/CNST(4)
000131                SURX(3,I) = SURX(3,I)/RHO(N)
000134                RETURN
000134           100  FORMAT (5A4,6F10.3,/,20X,6F10.7,/,20X,4F10.7,113)
000134           101  FORMAT (1H0,//,25X,40HDESIGN DATA FOR SCREEN DEVICE LOCATED AT,1X,
                     15A4,//,54X,9HSEQUENCE ,I4,///,1X,8HGAMMA = ,F5.3,5X,8HRTGAS = ,F11
                     2.3,5X,7HPGAS = ,F8.3,5X,6HBFS = ,F6.3,5X,5HEE = ,F11.3,5X,7HSTEN =
                     3 ,F11.3,//,1X,6HAS1 = ,F9.6,5X,6HBS1 = ,F9.6,5X,6HAS2 = ,F9.6,5X,6
                     4HDPS = ,F9.7,5X,5HDS = ,F6.2,5X,5HDC = ,F9.7,//,1X,5HPO = ,F6.4,5X
                     5,4HF = ,F8.6,5X,5HLS = ,F6.2,5X,5HPW = ,F6.4,5X,4HN = ,I1)
000134                END
```

Page
Intentionally
Left Blank

APPENDIX E

```
                SUBROUTINE SP26 (SURX,J,N)
          C
          C     THIS SUBROUTINE COMPUTES THE PARAMETERS
          C     FOR A SCREEN DEVICE IN THE FEED CIRCUIT
          C
 000006           DIMENSION SURX(20,4),J(20,50),AP(20),AS(20),X(20),QLSUM(20),
                1          Q4(20),Q6(20),AAS1(20),AAS2(20),BBS1(20),CCS1(20),
                2          XL(50),THPP(30),WTT(60),XK(2),VO(2),ZZ(20),WDOT4(20),
                3          WDOT6(20),STE(20),VSUM(20),QSUM(20),RL(20),VL(20),VC(20)
 000006           COMMON/AC/Z,CNST(5),RHO(2),NPL(4),NPH(4),D(4),TIME,KPT,KPAST,
                1SX(64),SY(64),AREA(40),BLOCK(60),FV(2),F(50),K1(30),NDAT(60),
                2H(40,60),Q(40,60),PS(60),WDOT(60),HHD(60),QHD(60),T(60),TT(50),
                3DAT(50),ACL(40,50),XDOT(40,50),SIG(2)
 000006           COMMON/SEEKER/NJBLK
 000006           COMMON/LINEB/MDN(4)
 000006           COMMON/TURBIN/XL,THPP,WTT,XK,VO
 000006           EQUIVALENCE (K1(1),J1),(K1(2),J2),(K1(3),J3),(K1(4),J4),(K1(5),J5)
                1,(K1(6),J6),(K1(7),J7),(K1(8),J8),(K1(9),J9),(K1(10),J10),(K1(11),
                2J11),(K1(12),J12),(K1(13),J13),(K1(14),J14),(K1(15),J15),(K1(16),
                3J16),(K1(17),J17),(K1(18),J18),(K1(19),J19),(K1(20),J20)
                4,(K1(21),J21),(K1(22),J22),(K1(23),J23),(K1(24),J24),(K1(25),J25),
                5(K1(26),J26),(K1(27),J27),(K1(28),J28),(K1(29),J29),(K1(30),J30)
          C
          C     ***  CONTROL BLOCK CONVERSION LOOP  ***
          C
 000006           NJBLK = N
 000007           DO 50 I=1,18
 000010    50     K1(I)=J(I,N)
 000020           N2=NDAT(J2)
 000022           N4=NDAT(J4)
 000024           GO TO (11,12),J18
 000032    12     S=-1.
 000034           GO TO 13
 000034    11     S=1.
 000036    13     IF (TIME-TT(J9)) 20,30,30
          C
          C     ***SCREEN DEVICE PARAMETERS PRIOR TO WAVE ARRIVAL  ***
          C
 000041    20     GO TO (21,22),J17
 000047       21  H(KPT,J3)=HHD(J2)+ACL(KPT,J16)*DAT(J16)-ACL(KPT,N2)*DAT(N2)
 000065           Q(KPT,J6)=QHD(J5)+AREA(J14)*(XDOT(KPT,J16)-XDOT(KPT,N2))
 000101           Q(KPT,J7)=Q(KPT,J6)
 000107           GO TO 23
 000110       22  H(KPT,J3)=HHD(J4)+ACL(KPT,J16)*DAT(J16)-ACL(KPT,N4)*DAT(N4)
 000126           Q(KPT,J7)=S*QHD(J8)+AREA(J14)*(XDOT(KPT,J16)-XDOT(KPT,N4))
 000143           Q(KPT,J6)=Q(KPT,J7)
 000151    23     IF (TIME) 24,24,25
 000153    24     HHD(J3)=H(KPT,J3)
 000157           QHD(J6)=Q(KPT,J6)
 000163           QHD(J7)=QHD(J6)
 000165       25  X(J1) = 0.
 000167           VSUM(J1) = 0.0
 000170           QSUM(J1) = 0.0
 000171           QLSUM(J1) = 0.0
 000172           KPR=0
 000173           GO TO 45
          C
```


PRECEDING PAGE BLANK NOT FILMED

```
C     ***SCREEN DEVICE PARAMETERS AFTER INITIAL WAVE ARRIVAL  ***
C
000173    3) CALL PAST(TIME,T(J11),2)
000177       CALL PAST(TIME,T(J10),1)
000203       AP(J1) = WTT(J12)
000206       SXAV = SX(J12)
000207       SYAV = SY(J13)
000211       HVAP=PV(J15)*CNST(1)/RHO(J15)
000214    11) APOLD = AP(J1)
000216       AS(J1) = SURX(15,J1)*CNST(3)*SURX(11,J1)*SURX(14,J1)
000227       AAS1(J1) = SURX(7,J1)/AS(J1)
000233       AAS2(J1) = SURX(9,J1)/AS(J1)
000236       BBS1(J1) = SURX(8,J1)/AS(J1)/AS(J1)
000241       CCS1(J1) = SURX(5,J1)*2./RHO(J15)/CNST(3)/CNST(3)/(1.-SURX(13,J1))
     1                 /AP(J1)/SURX(14,J1)
000256       SXAV = SXAV*AP(J1)/APOLD
000261       SYAV = SYAV*AP(J1)/APOLD
000263       ZZ(J1) = 1. + CCS1(J1)/SXAV- CCS1(J1)/SYAV
000270       CY = RCON(H,J4,2)*SYAV*S*RCON(Q,J8,2)*ACL(KPT,J16)*DAT(J16)
     1        -RCON(ACL,N4,2)*DAT(N4)
000314       CX = RCON(H,J2,1)*SXAV*RCON(Q,J5,1)*ACL(KPT,J16)*DAT(J16)
     1        -RCON(ACL,N2,1)*DAT(N2)
C
C
C     CHECK IF SCREEN SEGMENT SURROUNDED BY LIQUID OR GAS
C
000337       IF (SURX(16,J1).GT. 0.0) GO TO 140
C
C     SCREEN SURROUNDED BY GAS
C
C     CHECK IF SCREEN PRESSURE ABOVE OR BELOW ULLAGE PRESSURE
C
000345    13) IF (H(KPAST,J3)-SURX(3,J1)) 150,150,140
C
C     CHECK IF DELTAP BELOW BUBBLE POINT
C
000354    15) IF (H(KPAST,J3)-SURX(3,J1)+SURX(4,J1)) 160,170,170
C
C     LIQUID INFLOW OR OUTFLOW
C
000366    14) Q6(J1) = 2.*(SURX(3,J1)-(SURX(3,J1)*CCS1(J1)*CX/SXAV-CCS1(J1)*CY/
     1          SYAV)/ZZ(J1))/(-AAS1(J1)*CCS1(J1)/ZZ(J1)-SQRT((AAS1(J1)
     2          *CCS1(J1)/ZZ(J1))**2+ABS(4.*BBS1(J1)*(SURX(3,J1)-(SURX
     3          (3,J1)*CCS1(J1)*CX/SXAV-CCS1(J1)*CY/SYAV)/ZZ(J1)))))
000431       IF (Q6(J1).LT. 0.0) GO TO 142
000432       H(KPT,J3) = SURX(3,J1)+AAS1(J1)*Q6(J1)+
     1                 BBS1(J1)*Q6(J1)*Q6(J1)
000444       IF (H(KPT,J3)-SURX(3,J1)-SURX(4,J1)) 145,145,146
000455    146 QSUM(J1) = QSUM(J1)*(1.-Q6(J1)*Z/SURX(15,J1)/AREA(J14)*X(J1))
000467    145 GO TO 141
000470    142 H(KPT,J3) = SURX(3,J1)+AAS1(J1)*Q6(J1)+
     1                 BBS1(J1)*Q6(J1)*Q6(J1)
000503    141 IF (H(KPT,J3).LT.HVAP) H(KPT,J3) = HVAP
000513       Q(KPT,J7) = (CY-H(KPT,J3))/SYAV
000523       Q(KPT,J6) = (CX-H(KPT,J3))/SXAV
000532       Q4(J1) = Q(KPT,J6)*Q(KPT,J7)
C
C     CHECK LIQUID LEAVING SCREEN
```

```
      C
000340        IF (SURX(16,J1).GT.0.0) GO TO 148
000344        IF (H(KPT,J3)-SURX(3,J1)-SURX(4,J1)) 147,147,151
000554   151  QLSUM(J1) = QLSUM(J1)+Q6(J1)*Z*(1.-X(J1))
000562        GO TO 152
000562   147  QLSUM(J1) = QLSUM(J1)+Q6(J1)*Z
000566   152  IF (QLSUM(J1).LE.0.0) QLSUM(J1) = 0.0
000572        IF (QLSUM(J1).GT.SURX(10,J1)/SQRT(SURX(13,J1))*AS(J1))QLSUM(J1)=0.
000610        RL(J1)=(3./16.*SURX(10,J1)*SURX(10,J1)/AS(J1)/SURX(13,J1)*
     1            QLSUM(J1))**.333
000625        IF (RL(J1).GT.SURX(10,J1)/2.) GO TO 143
000633        VL(J1) = Q6(J1)/AS(J1)/SURX(13,J1)
000636        IF (RL(J1).LE. 0.0) RL(J1) = 0.1*SURX(10,J1)/2.
000645        GO TO 144
000646   143  VL(J1) = Q6(J1)/AS(J1)/SURX(13,J1)/4.*SURX(10,J1)*SURX(10,J1)/
     1            RL(J1)/RL(J1)
000660   144  VC(J1) = SQRT(SIG(J15)*(SURX(10,J1)**3)*3./32./RHO(J15)*CNST(4)/
     1            (RL(J1)**4))
000700        IF (VL(J1).LE.VC(J1)) GO TO 148
000702        QLSUM(J1) = 0.0
      C
      C     CHECK SCREEN STRESS
      C
000703   148  STE(J1) = (H(KPT,J3)-SURX(3,J1))*RHO(J15)*CNST(3)*SURX(11,J1)*
     1            (1.-SURX(13,J1))*SURX(14,J1)
000724        IF (ABS(STE(J1)).LT.SURX(6,J1)) GO TO 149
000731        STE(J1) = STE(J1)/SURX(6,J1)
000733        WRITE (6,201) J1,STE(J1)
000742   201  FORMAT(5X,3HNO.,I3,47H SCREEN PROPORTIONAL LIMIT EXCEEDED - STRESS
     1 = ,F11.3,1X,17HTIMES MAX. STRESS)
000742   149  IF (QSUM(J1).LE.0.0) GO TO 40
000746        VSUM(J1) = VSUM(J1)+Q(KPT,J8)*Z
000754        IF (VSUM(J1)-SURX(15,J1)*AREA(J14)) 305,305,311
      C
      C     GAS INFLOW
      C
000763   161  IF (QLSUM(J1).LE.0.0) GO TO 163
000765        Q6(J1) = 2.*(SURX(3,J1)-(SURX(3,J1)+CCS1(J1)*CX/SXAV-CCS1(J1)*CY/
     1            SYAV)/ZZ(J1))/(-AAS1(J1)-CCS1(J1)/ZZ(J1)-SQRT((AAS1(J1)
     2            +CCS1(J1)/ZZ(J1))**2+ABS(4.*BBS1(J1)*(SURX(3,J1)-(SURX
     3            (3,J1)+CCS1(J1)*CX/SXAV-CCS1(J1)*CY/SYAV)/ZZ(J1)))))
001030        IF (Q6(J1).LT. 0.0) GO TO 164
001031        H(KPT,J3) = SURX(3,J1)+AAS1(J1)*CG(J1)+
     1            BBS1(J1)*Q6(J1)*Q6(J1)
001043        GO TO 161
001044   164  H(KPT,J3) = SURX(3,J1)+AAS1(J1)*CG(J1)+
     1            BBS1(J1)*Q6(J1)*Q6(J1)
001057        QLSUM(J1) = QLSUM(J1)+Q6(J1)*Z
001062        GO TO 161
001063   163  QLSUM(J1) = 0.0
001065        Q6(J1) = 2.*(SURX(3,J1)-(SURX(3,J1)+CCS1(J1)*CX/SXAV-CCS1(J1)*CY/
     1            SYAV)/ZZ(J1))/(-AAS2(J1)-CCS1(J1)/ZZ(J1)-SQRT((AAS2(J1)
     2            +CCS1(J1)/ZZ(J1))**2+ABS(4.*BBS1(J1)*(SURX(3,J1)-(SURX
     3            (3,J1)+CCS1(J1)*CX/SXAV-CCS1(J1)*CY/SYAV)/ZZ(J1))*SURX(17
     4            ,J1)/RHO(J15))))
001134        IF (Q6(J1).LT. 0.0) GO TO 162
001135        H(KPT,J3) = SURX(3,J1)+AAS2(J1)*CG(J1)+
     1            BBS1(J1)*Q6(J1)*Q6(J1)*SURX(17,J1)/RHO(J15)
```

```
001154          GO TO 161
001155      162 H(KPT,J3) = SURX(3,J1)+AAS2(J1)*Q6(J1)*
                1             BBS1(J1)*Q6(J1)*Q6(J1)+SURX(17,J1)/RHO(J15)
001176      161 IF (H(KPT,J3),LT,HVAP) H(KPT,J3) = HVAP
            C
            C       CHECK SCREEN STRESS
            C
001206      168 STE(J1) = (H(KPT,J3)-SURX(3,J1))*RHO(J15)*CNST(3)*SURX(11,J1)*
                1             (1.+SURX(13,J1))*SURX(14,J1)
001227          IF (ABS(STE(J1)),LT,SURX(6,J1)) GO TO 169
001234          STE(J1) = STE(J1)/SURX(6,J1)
001236          WRITE (6,202) J1,STE(J1)
001245      202 FORMAT(5X,3HNO.,I3,47H SCREEN PROPORTIONAL LIMIT EXCEEDED - STRESS
                1 = ,F11.3,1X,17HTIMES MAX, STRESS)
001245      169 CONTINUE
001245          Q(KPT,J7) = (CY-H(KPT,J3))/SYAV
001255          Q(KPT,J6) = (CX-H(KPT,J3))/SXAV
001264          Q4(J1) = Q(KPT,J6)+Q(KPT,J7)
001272          GO TO 180
            C
            C       NO INFLOW (RESISTED BY BUBBLE POINT)
            C
001275      175 IF (QLSUM(J1),LE,0.0) GO TO 173
001277          Q6(J1) = 2.*(SURX(3,J1)-(SURX(3,J1)*CCS1(J1)*CX/SXAV-CCS1(J1)*CY/
                1             SYAV)/ZZ(J1))/(-AAS1(J1)*CCS1(J1)/ZZ(J1)-SQRT((AAS1(J1)
                2             *CCS1(J1)/ZZ(J1))**2+ABS(4.*BBS1(J1)*(SURX(3,J1)-(SURX
                3             (3,J1)*CCS1(J1)*CX/SXAV-CCS1(J1)*CY/SYAV)/ZZ(J1)))))
001342          IF (Q6(J1),LT, 0.0) GO TO 174
001343          H(KPT,J3) = SURX(3,J1)+AAS1(J1)*Q6(J1)+
                1             BBS1(J1)*Q6(J1)*Q6(J1)
001355          GO TO 171
001356      174 H(KPT,J3) = SURX(3,J1)+AAS1(J1)*Q6(J1)+
                1             BBS1(J1)*Q6(J1)*Q6(J1)
001371          QLSUM(J1) = QLSUM(J1)+Q6(J1)*Z
001374          IF (QLSUM(J1),LE,0.0) GO TO 173
001376      171 IF (H(KPT,J3),LT,HVAP) H(KPT,J3) = HVAP
001406          Q(KPT,J7) = (CY-H(KPT,J3))/SYAV
001416          Q(KPT,J6) = (CX-H(KPT,J3))/SXAV
001425          Q4(J1) = Q(KPT,J6)+Q(KPT,J7)
001433          GO TO 180
001434      173 QLSUM(J1) = 0.0
001436          Q6(J1) = 0.
001437          H(KPT,J3) = (SURX(3,J1)+CCS1(J1)*(CX/SXAV-CY/SYAV))/(1.+CCS1(J1)/
                1             SXAV-CCS1(J1)/SYAV)
001456          IF (H(KPT,J3),LT,HVAP) H(KPT,J3) = HVAP
001465          Q(KPT,J7) = (CY-H(KPT,J3))/SYAV
001475          Q(KPT,J6) = (CX-H(KPT,J3))/SXAV
001505          Q4(J1) = Q(KPT,J6)+Q(KPT,J7)
            C
            C       QUALITY COMPUTATION
            C
001514      180 VSUM(J1) = VSUM(J1)+Q(KPT,J8)*Z
001522          IF (VSUM(J1)-SURX(15,J1)*AREA(J14)) 300,300,310
001530      300 IF (Q(KPT,J8)) 301,303,301
001534      301 IF (VSUM(J1),LE,0.5) GO TO 303
001536          IF (QLSUM(J1),GT,0.0) GO TO 305
001541          IF (QLSUM(J1),LT,0.0) GO TO 305
001542          IF (Q6(J1),GT, 0.0) GO TO 305
```

```
001545          QSUM(J1)=QSUM(J1)*(1.-Q(KPT,J8)*Z/SURX(15,J1)/AREA(J14))-G6(J1)*Z
001561          GO TO 302
001562      305 QSUM(J1) = QSUM(J1)*(1.-Q(KPT,J8)*Z/SURX(15,J1)/AREA(J14))
001575          GO TO 302
001576      303 IF (QLSUM(J1).GT.0.0) GO TO 302
001601          IF (Q6(J1).GT. 0.0) GO TO 302
001603          QSUM(J1) = QSUM(J1)-Q6(J1)*Z
001606          GO TO 302
001607      302 X(J1)=QSUM(J1)/(CNST(3)/4.*SURX(11,J1)*SURX(11,J1)*SURX(15,J1)*
               1       QSUM(J1))
001622          IF (X(J1).LE.0.0) X(J1) = 0.0
001625          IF (X(J1).LT.1.0) GO TO 40
001630          X(J1) = 1.0
001631          WRITE (6,253) J1
001637      253 FORMAT(5X,3HNO.,I3,48H SCREEN DEVICE FULL OF GAS - QUALITY EXCEEDS
               1 1.0)
001637          GO TO 40
001642      315 VSUM(J1) = Q(KPT,J8)*Z
001647          GO TO 300
001650      311 VSUM(J1) = Q(KPT,J8)*Z
001655          GO TO 305
                C
                C     ***  PRESSURE,FLOWRATE,HOLD CONVERSION SEGMENT  ***
                C
001656       40 BLOCK(J1+32) = X(J1)
001660          BLOCK(J1+36) = AP(J1)
001662          BLOCK(J1+40) = Q6(J1)
001663          IF (H(KPT,J3).LT.HVAP) H(KPT,J3) = HVAP
001673          DELTAP = (H(KPT,J3)-SURX(3,J1))*RHO(J15)/CNST(1)
001703          BLOCK(J1+44) = DELTAP
001705          BLOCK(J1+50) = QLSUM(J1)
001707          PS(J3) = H(KPT,J3)*RHO(J15)/CNST(1)
001715          WDOT(J6)=Q(KPT,J6)*RHO(J15)
001722          WDOT(J7)=Q(KPT,J7)*RHO(J15)
001726          RETURN
001727          END
*FOLLOWING VARIABLES EQUIVALENCED BUT NOT REFERENCED
J19
J20
J21
J22
J23
J24
J25
J26
J27
J28
J29
J30
```

Page
Intentionally
Left Blank

Appendix F

TECHNICAL DESCRIPTION
CRYO-LINE PRESSURE PROGRAM, P4557

When a cryogenic liquid flows into a warm transfer line, boiling of the liquid will occur until the line has been chilled to liquid temperature and liquid transfer can occur. If the liquid flow is initially rapid, an unstable situation will develop with surging flow rate and line pressure. Liquid will flow into the line due to the lag in boiling caused by a finite heat transfer rate; when boiling does occur, a relatively high velocity liquid flow will have been established. The vapor production rate will accelerate rapidly as boiling causes liquid breakup and entrainment, with an expanding heat transfer area, and will exceed the rate at which vapor can escape from the line, causing a line pressure surge which will slow and reverse the liquid flow. When the liquid has been forced back into the supply vessel and/or has boiled away, the pressure will recede and liquid flow will again enter the transfer line, repeating the process. The intensity of the flow and pressure surge will diminish as the line is cooled; the maximum pressure surge occurs on the first cycle.

The actual flow process during cooldown is very complex; however, a simple model is adequate to analyze the first cycle, which will predict the peak pressure and the time scale of the cycle. The fluid flow model assumes a uniform slug of liquid up to the liquid-vapor interface; all vapor production is concentrated at the interface with a discontinuity of density, velocity, and pressure at that point. A separate heat transfer model accounts for the expanded heat transfer area of the boiling liquid due to the expanded volume of the two-phase fluid.

Other assumptions of the model are as follows:

A. The vapor flow is adiabatic.
B. The line is horizontal, straight, and constant cross-section area.
C. The inlet valve effective area varies linearly with time from zero initially to the line area when fully open.

PRECEDING PAGE BLANK NOT FILMED

D. A step function initial temperature distribution for the line, with the initial section at liquid temperature and the downstream section at ambient temperature, is set to give approximately the same total available heat to chilldown.

E. The boiling heat flux has a constant empirical value for each fluid.

F. The wall temperature is constant.

G. Quasi-steady-state Fanno flow is assumed for the vapor stream.

The analysis describes the pressure distribution in the pipe as liquid flows in from the supply tank and gas flows out at the delivery end. The pressure on the liquid side of the liquid-vapor interface is

$$P_2 = P_o - \Delta P_L - \Delta P_f - \Delta P_v \tag{1}$$

which is the supply pressure P_o decreased by the liquid momentum pressure drop ΔP_L, the pipe friction pressure drop ΔP_f and the valve pressure drop ΔP_v. The latter two terms are given by

$$\Delta P_f = f \frac{X_2}{D} \rho_L \frac{U_L^2}{2} \tag{2}$$

where U_L is the liquid velocity, ρ_L the density, D the pipe diameter, X_2 the distance from the pipe entrance to the interface location and f the friction factor; and

$$\Delta P_v = \frac{1}{2} \rho_L U_L^2 \left[(A/A_v)^2 - 1 \right] \tag{3}$$

where A is the pipe cross-section area and A_v the valve area, which varies with time according to a specified schedule.

The liquid velocity is found from the fluid momentum equation for a constant density liquid and constant area pipe, which is integrated over a time interval from t_j to t_{j+1} with an average value of ΔP_L to give

$$U_{L_{j+1}} = \left[U_{L_j}^2 \frac{X_{2_j}}{X_{2_{j+1}}} + \left(1 - \frac{X_{2_j}}{X_{2_{j+1}}} \right) \frac{2 \Delta P_L}{\rho_L} \right]^{1/2} \tag{4}$$

which provides a time-stepped solution for the velocity when the other terms are known.

When vaporization of the liquid is occurring at the interface, a momentum pressure drop results from the velocity change, giving

$$P_3 = P_2 - \frac{W_v}{A}(U_{v3} - U_{L2}) \tag{5}$$

where W_v is the mass rate of vapor formation and U_{v3} is the vapor velocity at the interface. The pressure ratio across the vapor stream is

$$\frac{P_3}{P_4} = \frac{M_4}{M_3}\left\{\frac{1 + \left[(\gamma - 1)/2\right] M_4^2}{1 + \left[(\gamma - 1)/2\right] M_3^2}\right\}^{1/2} \tag{6}$$

where the pipe exit pressure P_4 is equal to the receiver vessel pressure P_5 for unchoked flow. To utilize the latter equation, the following expression for Fanno flow in the vapor relates the two Mach numbers:

$$\frac{f_v}{D}(X_4 - X_3) = \frac{1}{\gamma M_3^2} - \frac{1}{\gamma M_4^2} + \frac{\gamma + 1}{2\gamma} \ln\left\{\frac{M_3^2}{1 + \left[(\gamma - 1)/2\right] M_3^2} \frac{1 + \left[(\gamma - 1)/2\right] M_4^2}{M_4^2}\right\} \tag{7}$$

where f_v is the friction factor for the vapor flow. This equation is solved for M_4 when M_3 is known. The latter is found from the vapor velocity at the interface given by

$$U_{v3} = U_{L2} + \frac{W_v}{A}\left(\frac{1}{\rho_v} - \frac{1}{\rho_L}\right) \tag{8}$$

where W_v, the total mass rate of vapor production, is

$$W_v = \Sigma W_{v_j} \tag{9}$$

where ΣW_{v_j} is the sum of the vapor production rates from boiling for individual segments of the liquid from the heat transfer analysis.

The pipe and liquid are divided into small segments of equal length ΔX for the heat transfer analysis. The liquid interface travels from X_{2_j} to $X_{2_{j+1}}$ across one of these segments during each time step Δt. Since the velocity U_L is a variable, the time step also varies during the solution. The temperature T_{j+1} of each nonboiling segment is calculated from its previous temperature T_j and a forced convection heat transfer rate

$$q_{nb} = \frac{0.023}{D} (T_\omega - T_j)\, k \left(\frac{\rho U D}{\mu}\right)^{0.8} \left(\frac{C_p \mu}{k}\right)^{0.4} \tag{10}$$

in the temperature equation

$$T_{j+1} = T_j + q_{nb}\, \Delta t\, \frac{4}{C_p D \rho} \tag{11}$$

When a liquid segment reaches saturation temperature T_{sat}, determined at P_2, an empirical boiling heat flux q_b is applied to the segment with the temperature remaining at T_{sat}. The mass of fluid in a boiling segment will occupy a larger volume due to the production of vapor and will have a larger heat transfer area than a nonboiling segment. Ignoring the loss of liquid in boiling, the new heat transfer area is

$$A_{q_{j+1}} = A_{q_j} + \frac{W_{v_j}\, \Delta t\, \pi\, D}{\rho_{sv}\, A} \tag{12}$$

where ρ_{sv} is the density of saturated vapor. The vapor production rate for a segment is

$$W_{v_j} = q_b\, R_j\, \frac{\left(A_{q_{j+1}} + A_{q_j}\right)}{2\, \Delta h_v} \tag{13}$$

where the average value of A_q is used, Δh_v is the heat of vaporization and the effect of quality Y on two-phase boiling heat transfer is given by the factor R for which

$$R = \exp\left[-12.4\, (Y^{1.715} - 0.254)^2\right] \tag{14}$$

represents a fit of empirical data. A convenient expression for quality is

$$Y_j = \left(\frac{A_{q_j}}{\pi D \, \Delta X} - 1 \right) \frac{\rho_{sv}}{\rho_L} \tag{15}$$

which uses the approximation for the two-phase heat transfer area.

While the heat transfer analysis treats the expanded volume and heat transfer area of the boiling liquid segments, the preceding fluid flow analysis assumes a uniform slug of liquid from the supply vessel to the liquid vapor interface with all vapor production occurring at the interface plane.

The solution proceeds by determining the pressure distribution in the pipe for each time step, assuming a constant feed pressure P_o and iterating on ΔP_L to achieve a discharge pressure P_4 equal to the receiver vessel pressure P_5. (When the discharge flow is choked, the solution condition is $M_4 = 1$ and $P_4 \geq P_5$.) For a chosen value of ΔP_L, Equation 4 gives the liquid velocity and Equations 1 through 3 give the interface liquid-side pressure P_2. With T_{sat} determined at P_2 and the time step determined, the heat transfer Equations 9 through 15 are evaluated giving W_v. Equations 8, 7, 5, and 6, in order, then give the values of M_3, M_4, P_3, and P_4. Based on the value of P_4, the trial value of ΔP_L is corrected and the iteration repeated.

Page
Intentionally
Left Blank

Appendix G

CENTAUR SIMULATION MODEL

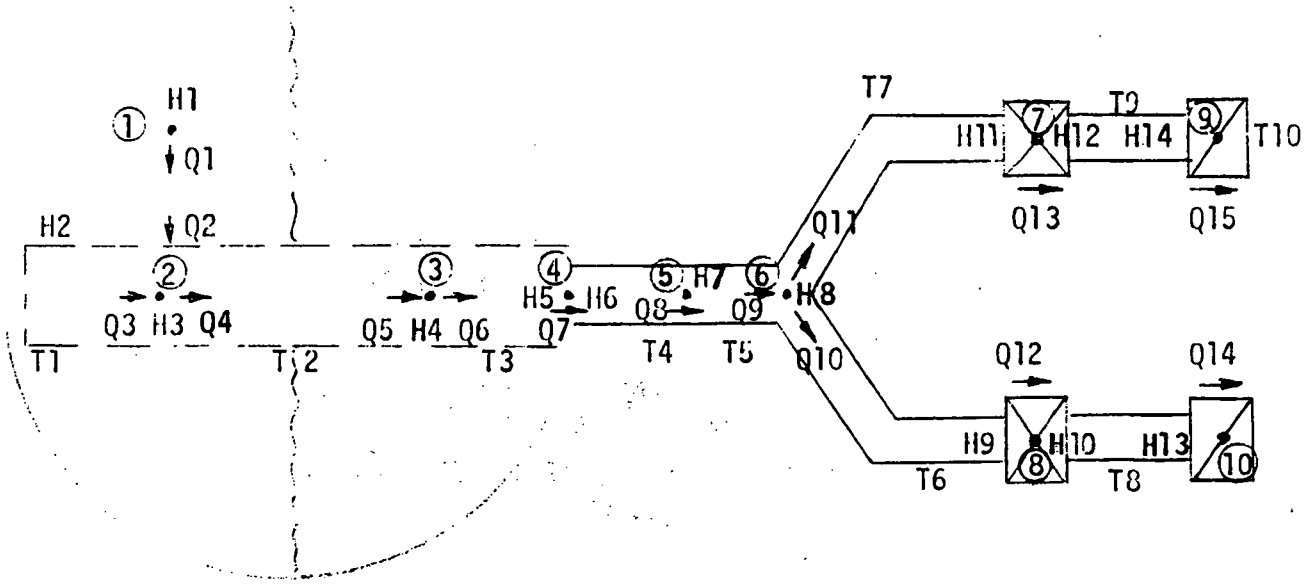

		FLUID:		
1	SR05 TANK		LH_2	LO_2
2	SR26 (WET) SCREEN	SAT P. =	19.17 PSIA	29.38 PSIA
3	SR26 (DRY) SCREEN	ρ =	4.35 LB/FT^3	68.8 LB/FT^3
4	SR02 RESISTANCE (SUBCOOLER)	K =	11558 PSI	108168 PSI
5	SR01 JUNCTION (SUMP)	σ =	1.23×10^{-4} LB/FT	8×10^{-4} LB/FT
6	SR03 BRANCH	VAPOR γ =	1.4	1.4
7	SR11 ODD VALVE	VAPOR RT =	$\frac{1545}{2} \cdot 40 = 30900$	$\frac{1545}{32} \cdot 180 = 8690$
8	SR11 EVEN VALVE			
9	SR12 ODD INJECTOR			
10	SR12 EVEN INJECTOR			

TANK:	LH_2	LO_2
VOL =	1265.4 FT^3	375.7 FT^3
DIA =	120.0 IN	120.0 IN
WALL =	.014 IN	.018 IN
ULLAGE P =	20.5 PSIA	31.5 PSIA

PRECEDING PAGE BLANK NOT FILMED

SCREEN:	LH_2	LO_2
MESH =	325 x 2300	325 x 2300
BPS =	2.29 FT	.942 FT
AS1 =	1.36	1.13
BS1 =	2.27	2.27
AS2 =	.13	.0534
DPS =	.00001 FT	.00001 FT
DS =	6.34 IN	6.0 IN
PØ =	.06	.06
DC =	.2967	.2808
LS =	48.0 IN	4.1 IN
EE =	.077	.091
STEM =	15.75	15.75
F =	1.5	6.2
PW =	1.0 or 0.0	1.0 or 0.0

PLUMBING:	LH_2	LO_2
SUMP	12-IN. DIA x .016 x 33 IN. LONG	16.7-IN. DIA x .016 x 12 IN. LONG
COMMON	3-IN. DIA x .016 x 40 IN. LONG	----
ODD BRANCH	2.5-IN. DIA x .016 x 62 IN. LONG	2.5-IN. DIA x .016 x 50 IN. LONG
EVEN BRANCH	2.5-IN. DIA x .016 x 62 IN. LONG	2.5-IN. DIA x 0.16 x 57 IN. LONG

SUBCOOLER RESISTANCE:	C_V = 38.7	45.4
	ΔP = 1.2 PSI	1.4 PSI
VALVE:	C_V = 253	242
	OPEN/CLOSE TIME = .05 SEC	.05 SEC
INJECTOR:	C_V = 61.2	31.9

DISTRIBUTION LIST

		Copies
National Aeronautics & Space Administration Lewis Research Center 21000 Brookpark Road Cleveland, OH 44135		
	M. S.	
Attn: J. R. Danicic	500-313	1
E. A. Bourke	501-5	5
TU Office	3-19	1
Report Control Off.	5-5	1
AFSC Liaison Off.	501-3	2
Library	60-3	2
R&QA Off.	500-211	1
J. Aydelott	501-7	20
T. Cochran	501-7	1
E. Symons	501-7	1
National Aeronautics & Space Administration Headquarters Washington DC 20546		
Attn: RS/Director, Manned Space Technology		1
RT/Director, Technology Utilization Off.		1
RP/F. Stephenson		1
MHE/P. N. Herr		1
RP/Director, Space Propulsion & Power		1
National Aeronautics & Space Administration Goddard Space Flight Center Greenbelt, MD 20771		
Attn: Library		1
National Aeronautics & Space Administration John F. Kennedy Space Center Cocoa Beach, FL 32931		
Attn: Library		1
DD-MDD-43/F. S. Howard		1
DD-SED-4/W. H. Boggs		1
National Aeronautics & Space Administration Ames Research Center Moffett Field, CA 94035		
Attn: Library		1
J. Vorreiter	244-7	1

			Copies
National Aeronautics & Space Administration			
Langley Research Center			
Hampton, VA 23365		M. S.	
Attn:	Library		1
	C. T. D'Aiutolo	249A	1
National Aeronautics & Space Administration			
Johnson Space Center			
Houston, TX 77001			
Attn:	Library		1
	EP2/Z. D. Kirkland		1
	EP5/W. Chandler		1
	ER/Hugh Davis		1
	EP4/Dale Connelly		1
	ER/M. Jones		1
	RM7/W. Scott		1
National Aeronautics & Space Administration			
George C. Marshall Space Flight Center			
Huntsville, AL 35812			
Attn:	Library		1
	EP43/L. Hastings		1
	EP43/G. Young		1
	EP45/Dr. Wayne Littles		1
	EP24/K. B. Chandler		1
	ES24/E. W. Urban		1
	EP43/Eric Hyde		1
Jet Propulsion Laboratory			
4800 Oak Grove Drive			
Pasadena, CA 91103			
Attn:	Library		1
	Don Young	125-224	1
NASA Scientific & Technical Information Facility			
P. O. Box 8757			
Balt/Wash. International Airport			
Attn:	Accessioning Department		10
Defense Documentation Center			
Cameron Station - Bldg. 5			
5010 Duke Street			
Alexandria, VA 22314			
Attn:	TISIA		1
National Aeronautics & Space Administration			
Flight Research Center			
P. O. Box 273			
Edwards, CA 93523			
Attn:	Library		1

	Copies
Air Force Rocket Propulsion Laboratory Edwards, CA 93523	
Attn: LKCC/J. E. Brannigan	1
LKDS/R. L. Wiswell	1
Aeronautical Systems Division Air Force Systems Command Wright Patterson Air Force Base Dayton, OH	
Attn: Library	1
Air Force Office of Scientific Research Washington, DC 20333	
Attn: Library	1
Aerospace Corporation 2400 E. El Segundo Blvd. Los Angeles, CA 90045	
Attn: Library - Documents	1
Arthur D. Little, Inc. 20 Acorn Park Cambridge, MA 02140	
Attn: Library	1
Beech Aircraft Corporation Boulder Facility Box 631 Boulder, CO	
Attn: Library	1
Bell Aerosystems, Inc. Box 1 Buffalo, NY 14240	
Attn: Library	1
L. Thompson	1
Boeing Company Space Division P. O. Box 868 Seattle, WA 98124	
Attn: Library	1
Chrysler Corporation Space Division P. O. Box 29200 New Orleans, LA 70129	
Attn: Library	1

	Copies
McDonnell Douglas Astronautics Co. 5301 Bolsa Avenue Huntington Beach, CA 92647	
Attn: Library	1
E. C. Cady	1
General Dynamics/Convair P. O. Box 1128 San Diego, CA 92112	
Attn: Library	1
R. Tatro	1
M. Blatt	1
Missiles and Space Systems Center General Electric Company Valley Forge Space Technology Center P. O. Box 8555 Philadelphia, PA 19101	
Attn: Library	1
Grumman Aircraft Engineering Corporation Bethpage, Long Island, NY	
Attn: Library	1
IIT Research Institute Technology Center Chicago, IL 60616	
Attn: Library	1
Lockheed Missiles & Space Company P. O. Box 504 Sunnyvale, CA 94087	
Attn: Library	1
G. D. Bizzell	1
S. G. DeBrock	1
Linde, Div. of Union Carbide P. O. Box 44 Tonawanda, NY 11450	
Attn: G. Nies	1
Denver Division Martin-Marietta Corporation P. O. Box 179 Denver, CO 80201	
Attn: Library	1
D. Fester	1
J. Tegart	1
A. Villars	1

	Copies
Space Division Rockwell International Corp. 12214 Lakewood Blvd. Downey, CA 90241	
Attn: Library	1
D. Gluck	1
J. Nichols	1
A. Jones	1
Northrop Space Laboratories 3401 West Broadway Hawthorne, CA	
Attn: Library	1
TRW Systems, Inc. 1 Space Park Redondo Beach, CA 90278	
Attn: Tech. Lib. Doc. Acquisitions	1
National Science Foundation, Engr. Div. 1800 G Street, NW Washington, DC 20540	
Attn: Library	1
Florida Institute of Technology Space Technology Dept. Melbourne, FL 32901	
Attn: Dr. T. E. Bowman	1
RCA/AED P. O. Box 800 Princeton, NJ 08540	
Attn: Mr. Daniel Balzer	1
Southwest Research Institute Dept. of Mechanical Sciences P. O. Drawer 28510 San Antonio, TX 78284	
Attn: H. Norman Abramson	1
Franklin Dodge	1
Tufts University Mechanical Engineering Dept. Medord, MA 02155	
Attn: Dr. Lloyd Trefethen	1
McDonnell Douglas Astronautics Co. - East P. O. Box 516 St. Louis, MO 63166	
Attn: G. Orton	1
W. Regnier	1

	Copies
Xerox Electro Optical Systems 300 North Halstead Pasadena, CA 91107 Attn: Robert Richter	1

SATISFACTION GUARANTEED

NTIS strives to provide quality products, reliable service, and fast delivery. Please contact us for a replacement within 30 days if the item you receive is defective or if we have made an error in filling your order.

- **E-mail: info@ntis.gov**
- **Phone: (888) 584-8332 or (703) 605-6050**

Reproduced by NTIS

National Technical Information Service
Springfield, VA 22161

This report was printed specifically for your order from nearly 3 million titles available in our collection.

For economy and efficiency, NTIS does not maintain stock of its vast collection of technical reports. Rather, most documents are printed for each order. Documents that are not in electronic format are reproduced from master archival copies and are the best possible reproductions available. If you have any questions concerning this document or any order you have placed with NTIS, please call our Customer Service Department at (703) 605-6050.

About NTIS

NTIS collects scientific, technical, engineering, and business related information—then organizes, maintains, and disseminates that information in a variety of format—from microfiche to online services. The NTIS collection of nearly 3 million titles includes reports describing research conducted or sponsored by federal agencies and their contractors; statistical and business information; U.S. military publications; multimedia/training products; computer software and electronic databases developed by federal agencies; training tools; and technical reports prepared by research organizations worldwide. Approximately 100,000 *new* titles are added and indexed into the NTIS collection annually.

For more information about NTIS products and services, call NTIS at 1-800-553-NTIS (6847) or (703) 605-6000 and request the free NTIS Products Catalog, PR-827LPG, or visit the NTIS Web site **http://www.ntis.gov.**

NTIS
You indispensable resource for government-sponsored information—U.S. and worldwide.

U.S. DEPARTMENT OF COMMERCE
Technology Administration
National Technical Information Service
Springfield, VA 22161 (703) 605-6000

N7728430

BA

BIN: M56 01-08-03
INVOICE: 1229995
SHIPTO: 1*85776
PAYMENT: NONE